74-21,979

KHAJAVI-NOORI, Iraj, 1945-
VISCOELASTIC PROPERTIES OF DILUTE POLYSTYRENE SOLUTIONS IN TOLUENE.

The University of Oklahoma, Ph.D., 1974
Engineering, chemical

University Microfilms, A XEROX Company, Ann Arbor, Michigan

THIS DISSERTATION HAS BEEN MICROFILMED EXACTLY AS RECEIVED.

Downloaded from SHAREOK. Persistent Handle URL: https://hdl.handle.net/11244/3756

THE UNIVERSITY OF OKLAHOMA

GRADUATE COLLEGE

VISCOELASTIC PROPERTIES OF DILUTE POLYSTYRENE SOLUTIONS IN TOLUENE

A DISSERTATION

SUBMITTED TO THE GRADUATE FACULTY

in partial fulfillment of the requirements for the

degree of

DOCTOR OF PHILOSOPHY

BY

IRAJ KHAJAVI-NOORI

Norman, Oklahoma

1974

VISCOELASTIC PROPERTIES OF DILUTE POLYSTYRENE

SOLUTIONS IN TOLUENE

APPROVED BY

DISSERTATION COMMITTEE

ABSTRACT

Measurements of dynamic shear viscosity, η', and elastic shear modulus, G', are reported for solutions of polystyrene in toluene. The polymers had sharp molecular weight distributions, $\bar{M}_w/\bar{M}_n = 1.08$, and molecular weights of 1.93×10^5 and 2.67×10^5. One, two and three weight percent solutions of polymer dissolved in toluene were used.

A torsionally oscillating quartz crystal with a fundamental frequency of 59 kHz was used as a viscometer. This viscometer was calibrated in five Newtonian liquids.

Data were taken at 77° and 100°F, over a pressure range of atmospheric to 120,000 psig. Thus, the effects of pressure and concentration on viscoelastic properties of the polymer solutions were determined at two temperatures and for two molecular weights.

Variation of the dynamic viscosity of each polymer solution with concentration was studied. A linear relationship between viscosity and concentration was observed at each particular pressure and temperature.

The method of reduced variables was used to convert the information obtained at various pressures and temperatures to a reference state (atmospheric pressure and room

temperature) over an equivalent frequency range of 3×10^5 to 2×10^7 sec^{-1}. The effect of reduced frequency on η' and G' was also determined and the results were compared with the predictions of Rouse and Zimm theories. It is concluded that the data of this investigation are in better agreement with the Zimm theory.

ACKNOWLEDGMENTS

I would like to express my sincere gratitude to Dr. R. G. Rein, Jr., Dr. S. E. Babb, Professor W. J. Ewbank, and Professor G. Tuma, the members of my doctoral committee, for the guidance and support they have provided during this research. I am especially grateful to the chairman of my committee, Dr. C. M. Sliepcevich, for his interest, direction and support, and to Dr. Rein, for his continual guidance, constructive suggestions and stimulating discussions.

There are certain individuals to whom the author is indebted for their aid and assistance:

My colleague, Dr. T. T. Charng, for his assistance in taking part of the data.

Professor W. J. Ewbank, of the Aerospace and Mechanical Engineering Department, for providing the necessary equipment and his permission to use his laboratory in taking density and low shear rate viscosity data on some of the test liquids.

Dr. R. J. Block, of the School of Chemical Engineering and Materials Science, for plating the electrodes on the quartz crystal.

Dr. D. van der Helm, of the Chemistry Department, for determining the orientation of the quartz crystal.

Mr. G. J. Scott, of the Physics Instrument Shop, for his technical suggestions and assistance in the repair and machining of parts of the high pressure apparatus and crystal holder.

Dr. J. P. Flynn, of the Dow Chemical Company, for providing the crystals of polystyrene polymers used in this work.

Mr. John Ice for proofreading the manuscript.

Ms. Bobbie Everidge for her efforts in preparing the manuscript, Mrs. Carlotta Wood for her assistance in typing, and Ms. Mary Ann Matthews for handling part of the graphical work.

The National Science Foundation for providing the financial support of this project.

My parents who have always valued and encouraged education.

Lastly, my wife, Mercede, to whom I am dedicating this work, and without whose understanding, sacrifice and constant encouragement this work could not materialize.

TABLE OF CONTENTS

		Page
LIST OF TABLES		ix
LIST OF ILLUSTRATIONS		xi
Chapter		
I.	INTRODUCTION	1
II.	BACKGROUND AND THEORY	5
	Origin of Viscoelastic Behavior in Polymer Solutions	5
	General Response of Viscoelastic Systems to Transient and Dynamic Testings	8
	Molecular Theory for Dilute Polymer Solutions	29
III.	ULTRASONIC TECHNIQUE FOR MEASURING MECHANICAL PROPERTIES OF VISCOELASTIC LIQUIDS	39
	Torsional Quartz Crystal	39
	The Effect of Temperature and Pressure and the Method of Reduced Variables	45
IV.	DESCRIPTION OF EQUIPMENT AND MATERIAL	51
	Pressure Cell	51
	Pressure Generating System	53
	Pressure Measurement	59
	Quartz Crystal	63
	Oscillator	68
	Impedence Bridge	68
	Detector	69
	Frequency Counter	70
	Temperature Controller	71
	Auxiliaries	74
	Materials	75

Chapter Page

V. EXPERIMENTAL PROCEDURE 83

Preliminary Preparation and Cleaning of the System 83
Pressurization of the System 85
Calibration of the Viscometer. 91

VI. RESULTS AND DISCUSSION 97

Calibration Parameters 97
Measurement of the Viscoelastic Properties of Polymer Solutions 115

VII. CONCLUSIONS. 170

NOMENCLATURE. 172

REFERENCES. 176

APPENDICES. 181

A. DENSITY DATA OF CALIBRATION LIQUIDS 182

B. VISCOSITY DATA OF CALIBRATION LIQUIDS . . . 188

C. REDUCED AND DIMENSIONLESS VISCOELASTIC PROPERTIES OF S-108 AND S-109 POLYSTYRENE SOLUTIONS 194

D. VISCOELASTIC PROPERTIES OF S-108 AND S-109 POLYSTYRENE SOLUTIONS AS PREDICTED BY ROUSE AND ZIMM THEORIES 201

LIST OF TABLES

Table		Page
1.	Comparison of $(\Delta L)_o^P$ of Toluene and 1, 2 and 3 Weight Percent Solutions of S-108 in Toluene at 77°F and 100°F.	78
2.	Comparison of $(\Delta L)_o^P$ of Toluene and 1, 2 and 3 Weight Percent Solutions of S-109 in Toluene at 77°F and 100°F.	79
3.	Low Shear Rate Viscosities of 1, 2 and 3 Weight Percent S-108 and S-109 Polystyrenes in Toluene at 77°F and 100°F	81
4.	Resonant Frequency and Resistance at Resonant Frequency of the Quartz Crystal in Various Calibration Liquids at 77°F.	99
5.	Resonant Frequency and Resistance at Resonant Frequency of the Quartz Crystal in Various Calibration Liquids at 100°F	101
6.	Values of Calibration Constants for the Quartz Crystal at 77°F and at Various Pressures.	103
7.	Values of Calibration Constants for the Quartz Crystal at 100°F and at Various Pressures.	104
8.	Means and Standard Deviations of K_f and R_{E_o}	105
9.	Comparison of Parabolic Constants of $\Delta f_o/f_o = a_o \times 10^{-6} + a_1 \times 10^{-9}P + a_2 \times 10^{-14}P^2$	108
10.	Values of $c[\eta]$ of S-108 and S-109 Polymer Solutions at 77°F and 100°F.	169
11.	Reduced and Dimensionless Viscoelastic Properties of 1 Percent S-108 Polystyrene in Toluene	195

Table Page

12. Reduced and Dimensionless Viscoelastic Properties of 2 Percent S-108 Polystyrene in Toluene 196

13. Reduced and Dimensionless Viscoelastic Properties of 3 Percent S-108 Polystyrene in Toluene 197

14. Reduced and Dimensionless Viscoelastic Properties of 1 Percent S-109 Polystyrene in Toluene 198

15. Reduced and Dimensionless Viscoelastic Properties of 2 Percent S-109 Polystyrene in Toluene 199

16. Reduced and Dimensionless Viscoelastic Properties of 3 Percent S-109 Polystyrene in Toluene 200

17. Viscoelastic Properties of 1 Percent S-108 Polystyrene in Toluene as a Function of Angular Frequency at 77°F. Predicted by Rouse and Zimm Theories. 202

18. Viscoelastic Properties of 2 Percent S-108 Polystyrene in Toluene as a Function of Angular Frequency at 77°F. Predicted by Rouse and Zimm Theories. 203

19. Viscoelastic Properties of 3 Percent S-108 Polystyrene in Toluene as a Function of Angular Frequency at 77°F. Predicted by Rouse and Zimm Theories. 204

20. Viscoelastic Properties of 1 Percent S-109 Polystyrene in Toluene as a Function of Angular Frequency at 77°F. Predicted by Rouse and Zimm Theories. 205

21. Viscoelastic Properties of 2 Percent S-109 Polystyrene in Toluene as a Function of Angular Frequency at 77°F. Predicted by Rouse and Zimm Theories. 207

22. Viscoelastic Properties of 3 Percent S-109 Polystyrene in Toluene as a Function of Angular Frequency at 77°F. Predicted by Rouse and Zimm Theories. 207

LIST OF ILLUSTRATIONS

Figure		Page
1.	Schematic Diagram of Cooperative Modes of Motion of a Polymer Molecule	8
2.	Response of a Perfectly Elastic Material to Pure Shear Stress	9
3.	Response of a Perfectly Elastic Material to Oscillatory Shear Stress	10
4.	Response of a Purely Viscous Material to Constant Shear Stress	10
5.	Response of a Purely Viscous Material to Oscillatory Shear Stress	12
6.	Response of a Viscoelastic Material to a Sinusoidally Varying Shear Strain	13
7.	Maxwell Model	17
8.	Creep Response of Maxwell Model	20
9.	Stress Relaxation of Maxwell Model	20
10.	Frequency Dependence of Maxwell Model . . .	23
11.	Voigt Model and Its Response to the Creep Test	25
12.	a. Generalized Maxwell Model; b. Generalized Voigt Model	26
13.	Representation of a Polymer Molecule by the Bead-Spring Model	30
14.	Dimensionless Elastic Modulus versus Dimensionless Angular Frequency for Rouse and Zimm Theories	34

Figure		Page
15.	Dimensionless Dynamic Viscosity versus Dimensionless Angular Frequency for Rouse and Zimm Theories	35
16.	Electrode Arrangement for Torsionally Vibrating Quartz Crystal	40
17.	The Assembly Diagram of the 150,000 psig High Pressure Vessel	52
18.	Bottom Cover of the Pressure Cell	54
19.	Schematic Diagram of the Pressure System . .	56
20.	Design and Specifications of the Free Piston in Separator Number 1	57
21.	The Assembly Diagram of High Pressure Intensifier	60
22.	Schematic Diagram of the Pressure Measuring Equipment	61
23.	Details of an Improved Crystal Mounting . .	66
24.	Electronic Equipment Required for Measurements	67
25.	Damaged Crystal and Crystal Holder	90
26.	Typical Data for Determining Resonant Frequency (Data for Methyl Cyclohexane at 20,000 psig and 77°F)	93
27.	Typical Plot of R_E and f as a Function of $(\pi f \rho \eta)^{1/2}$. Measurements at 77°F and 110,000 psig	95
28.	Effect of Pressure on Δf_o at 77°F	106
29.	Effect of Pressure on Δf_o at 100°F	107
30.	Comparison of the Pressure Effect on $\Delta f_o/f_o$ for Various Investigations	109
31.	Effect of Pressure on K_R at 77°F	111
32.	Effect of Pressure on K_R at 100°F	112

Figure Page

33. Effect of Pressure on Dynamic Viscosity of S-108 Polystyrene ($\bar{M}_W = 2.67 \times 10^5$) Solutions at 77°F 117

34. Effect of Pressure on Dynamic Viscosity of S-109 Polystyrene ($\bar{M}_W = 1.93 \times 10^5$) Solutions at 77°F 118

35. Effect of Pressure on Dynamic Viscosity of S-108 Polystyrene ($\bar{M}_W = 2.67 \times 10^5$) Solutions at 100°F 119

36. Effect of Pressure on Dynamic Viscosity of S-109 Polystyrene ($\bar{M}_W = 1.93 \times 10^5$) Solutions at 100°F 120

37. Effect of Pressure on Dynamic Viscosity of S-108 Polystyrene ($\bar{M}_W = 2.67 \times 10^5$) Solutions at 77° and 100°F 122

38. Effect of Pressure on Dynamic Viscosity of S-109 Polystyrene ($\bar{M}_W = 1.93 \times 10^5$) Solutions at 77° and 100°F 123

39. Effect of Pressure on Elastic Shear Modulus of S-108 Polystyrene ($\bar{M}_W = 2.67 \times 10^5$) Solution at 77°F 125

40. Effect of Pressure on Elastic Shear Modulus of S-109 Polystyrene ($\bar{M}_W = 1.93 \times 10^5$) Solutions at 77°F 126

41. Effect of Pressure on Elastic Shear Modulus of S-108 Polystyrene ($\bar{M}_W = 2.67 \times 10^5$) Solutions at 100°F 127

42. Effect of Pressure on Elastic Shear Modulus of S-109 Polystyrene ($\bar{M}_W = 1.93 \times 10^5$) Solutions at 100°F 128

43. Effect of Pressure on Elastic Shear Modulus of S-108 Polystyrene ($\bar{M}_W = 2.67 \times 10^5$) Solutions at 77° and 100°F 129

44. Effect of Pressure on Elastic Shear Modulus of S-109 Polystyrene ($\bar{M}_W = 1.93 \times 10^5$) Solutions at 77° and 100°F 130

Figure Page

45. Effect of Polymer Molecular Weight on Elastic Shear Modulus at 77°F 132

46. Effect of Polymer Molecular Weight on Elastic Shear Modulus at 100°F 133

47. Effect of Concentration on Viscosity of S-108 Polystyrene ($\bar{M}_W = 2.67 \times 10^5$) Solutions at 77°F and Various Pressures . 134

48. Effect of Concentration on Viscosity of S-109 Polystyrene ($\bar{M}_W = 1.93 \times 10^5$) Solutions at 77°F and Various Pressures 135

49. Effect of Concentration on Viscosity of S-108 Polystyrene ($\bar{M}_W = 2.67 \times 10^5$) Solutions at 100°F and Various Pressures 136

50. Effect of Concentration on Viscosity of S-109 Polystyrene ($\bar{M}_W = 1.93 \times 10^5$) Solutions at 100°F and Various Pressures 137

51. Effect of Pressure and Temperature on the Rate of Increase of Viscosity with Concentration for S-108 ($\bar{M}_W = 2.67 \times 10^5$) and S-109 ($\bar{M}_W = 1.93 \times 10^5$) Polystyrene . . . 139

52. Effect of Pressure on $a_{T,P}$ of S-109 Solutions at 77°F and 1 percent S-109 Solution at 100°F 142

53. Effect of Pressure on α and $\rho_o T_o/\rho T$ of S-109 Solutions at 77°F and 1 Percent S-109 Solution at 100°F 144

54. Effect of Reduced Angular Frequency on Reduced Dynamic Viscosity of 1 Percent S-108 Solution at 77° and 100°F 145

55. Effect of Reduced Angular Frequency on Reduced Dynamic Viscosity of 2 Percent S-108 Solution at 77° and 100°F 146

56. Effect of Reduced Angular Frequency on Reduced Dynamic Viscosity of 3 Percent S-108 Solution at 77° and 100°F 147

Figure Page

57. Effect of Reduced Angular Frequency on Reduced Dynamic Viscosity of 1 Percent S-109 Solution at 77° and 100°F 148

58. Effect of Reduced Angular Frequency on Reduced Dynamic Viscosity of 2 Percent S-109 Solution at 77° and 100°F 149

59. Effect of Reduced Angular Frequency on Reduced Dynamic Viscosity of 3 Percent S-109 Solution at 77° and 100°F 150

60. Reduced Elastic Modulus versus Reduced Angular Frequency of 1 Percent S-108 Solution 151

61. Reduced Elastic Modulus versus Reduced Angular Frequency of 2 Percent S-108 Solution 152

62. Reduced Elastic Modulus versus Reduced Angular Frequency of 3 Percent S-108 Solution 153

63. Reduced Elastic Modulus versus Reduced Angular Frequency of 1 Percent S-109 Solution 154

64. Reduced Elastic Modulus versus Reduced Angular Frequency of 2 Percent S-109 Solution 155

65. Reduced Elastic Modulus versus Reduced Angular Frequency of 3 Percent S-109 Solution 156

66. Reduced Dimensionless Dynamic Viscosity of 1, 2 and 3 Weight Percent S-108 Solutions as a Function of Reduced Dimensionless Angular Frequency at 77° and 100°F 162

67. Reduced Dimensionless Dynamic Viscosity of 1, 2 and 3 Weight Percent S-109 Solutions as a Function of Reduced Dimensionless Angular Frequency at 77° and 100°F 163

68. Reduced Dimensionless Elastic Modulus of 1, 2 and 3 Weight Percent S-108 Solutions as a Function of Reduced Dimensionless Angular Frequency at 77° and 100°F 164

Figure Page

69. Reduced Dimensionless Elastic Modulus of 1, 2 and 3 Weight Percent S-109 Solutions as a Function of Reduced Dimensionless Angular Frequency at 77° and 100°F 165

70. Effect of Pressure and Temperature on the Density of Normal Pentane 183

71. Effect of Pressure and Temperature on the Density of Normal Octane 184

72. Effect of Pressure and Temperature on the Density of Toluene 185

73. Effect of Pressure and Temperature on the Density of Methyl Cyclohexane. 186

74. Effect of Pressure and Temperature on the Density of Di(2-Ethylhexyl) Sebacate . . . 187

75. Effect of Pressure and Temperature on the Viscosity of Normal Pentane 189

76. Effect of Pressure and Temperature on the Viscosity of Normal Octane 190

77. Effect of Pressure and Temperature on the Viscosity of Toluene 191

78. Effect of Pressure and Temperature on the Viscosity of Methyl Cyclohexane 192

79. Effect of Pressure and Temperature on the Viscosity of Di(2-Ethylhexyl) Sebacate . . 193

CHAPTER I

INTRODUCTION

There are various theories which describe the mechanical behavior and properties of perfect solids and perfect liquids. The classical theory of elasticity and the theory of hydrodynamics are two of the oldest theories describing the behavior of these materials. The theory of elasticity describes the behavior of solids for which stress is directly proportional to strain but is independent of rate of strain. This class of solids is known as perfectly elastic or Hookean solids. On the other hand, hydrodynamics deals with behavior of liquids for which stress is directly proportional to the rate of strain and not the strain itself. These liquids are called perfectly viscous or Newtonian liquids.

However, these two categories represent only the extremes of a very broad spectrum of behavior of materials, and it is observed that the behavior of many materials, especially the polymeric systems, cannot be described by any of the classical theories. The materials which show a combination of elastic and viscous behavior are therefore called viscoelastic.

The deviations observed in mechanical behavior of viscoelastic materials from predictions of classical theories of elasticity and hydrodynamics may be due to various reasons. For instance, the strain in a solid or the rate of strain in a liquid might not be directly proportional to stress, but may depend on the stress in a more complicated manner. An example of this behavior is usually observed in solids when they are stressed past their elastic range or when the deformation is so large that the relation between stress and strain becomes non-linear. A second type of deviation which can again exist in either solids or liquids is observed when the behavior of materials depends on the strain, the rate of strain, and even higher time derivatives of strain. In some experiments a material may show both of the above deviations. However, if the deviation is limited only to the second type, the behavior of the material is considered to be linearly viscoelastic. In other words, in a linear viscoelastic response, the ratio of overall stress to overall strain (i.e., the overall modulus) is a function of time only and not of the magnitudes of stress or strain.

Many books and papers on the mathematical structure and phenomenological theories of linear viscoelasticity have been published. These theories are useful in predicting and describing the mechanical behavior of many viscoelastic materials. They have also been used for interrelating different

types of experimental measurements and calculating one parameter from measurement of another.

Viscoelastic behavior is manifest in many different ways. One way of observing viscoelastic behavior is through dynamic mechanical testing. When a perfectly elastic material is subjected to a sinusoidally varying stress, the strain will also vary sinusoidally and will always be in phase with the stress. The work done on a perfectly elastic material can be completely recovered after the stress is removed. In contrast with perfectly elastic materials, when a purely viscous liquid is subjected to dynamic tests, the strain will be ninety degrees out of phase with the stress, and all of the input energy is dissipated as heat. However, in viscoelastic materials, the phase angle between stress and strain usually falls somewhere between zero and ninety degrees; part of the energy input is stored and can be recovered, and some is dissipated as heat. As will be shown in the next chapter, the results of dynamic tests enable one to calculate an elastic modulus and a mechanical damping or loss modulus for the material.

The dynamic mechanical testing has proven useful (especially at ultrasonic frequencies) for many purposes such as investigating the behavior of lubricants at high shear rates. Suitable ultrasonic tests enable one to investigate material behavior without any appreciable generation of heat which is the main limiting factor in steady-state, continuous high-shear rate measurements. Oscillatory techniques can be

used to simulate the behavior of lubricants at high shear rates because the imposed oscillatory drive is similar to the rapidly changing tensile and compression stresses experienced by the liquid in actual practice.

Dynamic oscillatory testing is also useful in studies of chemical and molecular structure of polymer systems. Many molecular theories of polymer systems have been confirmed by studying the response of polymers to dynamic oscillatory measurements. These molecular theories usually apply to very dilute solutions of linear polymers in which the molecules can be assumed to be isolated from each other. Most of the experiments used to investigate these theories are carried out at atmospheric pressure with various ranges of frequency and temperature. However, the theories have not been evaluated with data obtained under high hydrostatic pressure.

This work presents measurements of the dynamic viscoelastic properties of dilute solutions of two different molecular weight polystyrenes in toluene at two temperatures (77° and 100°F) and high pressures (atmospheric pressure to 120,000 psig). An oscillating quartz crystal, resonant at its fundamental frequency (about 59 kHz) is used. The quantities of interest are the dynamic storage modulus, G', and the dynamic loss modulus, G" (or $\eta' = G''/\omega$, where ω is the angular frequency), which are measures of energy storage and loss, respectively. The results of this investigation are compared with the existing molecular theories for dilute polymer solutions.

CHAPTER II

BACKGROUND AND THEORY

In this chapter the origin of viscoelastic behavior in polymer solutions, the general response of viscoelastic materials in transient and dynamic experiments, and finally the molecular theories related to dilute polymer solutions are discussed.

Origin of Viscoelastic Behavior in Polymer Solutions

It is known that the presence of relatively small amounts of dissolved polymers can cause a tremendous increase in the viscosity of solvents. This effect was first quantitatively discussed by Einstein for a suspension of rigid, non-interacting spheres; he showed that

$$\eta_{rel} = \frac{\eta}{\eta_s} = 1 + 2.5\phi \qquad (1)$$

where η = viscosity of the suspension

η_s = viscosity of the solvent

η_{rel} = relative viscosity

ϕ = volume fraction of spheres

The polymer molecules in a solution are of course neither rigid nor spherical, and at finite concentrations

they interact and entangle with one another. Therefore, the increase in the relative viscosity of polymer solutions is usually much higher than the value predicted by Einstein's equation. Subsequent investigations on the viscosity of dilute polymer solutions ($\mu_{rel} < 2$), led to the Huggins equation (22):

$$\eta_{sp}/c = [\eta] + k'[\eta]^2 c \qquad (2)$$

where k' = constant for the specific polymer-solvent system

c = polymer concentration, gm/dl

η_{sp} = specific viscosity = $\eta_{rel} - 1$

$[\eta]$ = intrinsic viscosity = $\lim_{c \to 0} (\eta_{sp}/c)$

The concept of elasticity of polymer solutions is not as well known as the contribution of the polymer to the solution viscosity, but usually the elasticity is considered in terms of the thermal motions and orientations of polymer molecules. When a mechanical stress is applied to a polymer solution, the polymer chains start going through a deformation process, and they acquire a less probable distribution and conformation. The net result is a decrease in the entropy of the system and a corresponding increase in the free energy, and therefore storage of elastic energy. If the sample is kept in this deformed condition, the random thermal motion of the molecules will tend to return the system to its uniform and most probable distribution. As a result, stress relaxation takes place, and the stored energy in the system is

dissipated as heat. The change in free energy is expressed by Wall (53) as

$$\text{Free Energy} = kT \ln \left(\frac{P}{P_o}\right) = T\Delta s \qquad (3)$$

where P_o = probability of finding molecules in their most probable distribution

P = probability of finding molecules in the deformed state

Δs = change in the entropy of the system

k = Boltzmann constant

T = absolute temperature, °K

The free energy can be equated to elastic energy $\sigma^2/2G$ (σ being the shear stress and G the elastic modulus), and thus G is calculated. The above phenomenon is therefore usually called the "entropy elasticity."

The complex motions of flexible threadlike macromolecules can be expressed as a series of characteristic modes which require various degrees of cooperation among the segments of the molecule. Figure 1 shows the various cooperative modes of motion of a polymer molecule. The first mode corresponds to the translation of the entire molecule which requires the maximum cooperation from all segments. The second corresponds to the motion of the two ends in opposite direction in which the cooperation is less than the first mode, and so on. The relaxation time is defined as the ratio of viscosity to shear rigidity:

$$\tau = \eta/G \qquad (4)$$

It is a measure of time necessary for stress relaxation. It is apparent that each one of the above modes is associated with a relaxation time. It is also apparent that there is such a vast number of different modes that the relaxation times can be easily approximated to a continuous distribution over the time scale. The relaxation times and their distributions play an important role in determining the response of a polymer system to transient and dynamic experiments, as will be discussed later.

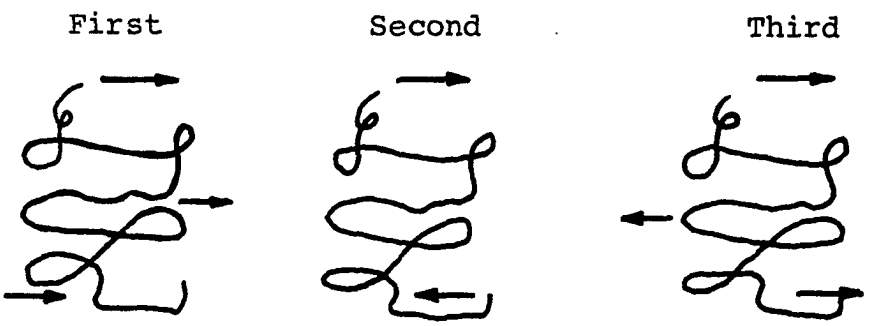

Figure 1. Schematic Diagram of Cooperative Modes of Motion of a Polymer Molecule (Adopted from Ferry, Reference 16).

General Response of Viscoelastic Systems to Transient and Dynamic Testings

In any experiment on viscoelastic systems, there are certain quantities in terms of which the response of the system can be best described. These quantities will now be

discussed in relation to purely elastic solids, purely viscous liquids, and viscoelastic materials.

Purely Elastic Materials

Figure 2 represents an element of a purely elastic material under pure shear; pure shear is the kind of deformation which produces a change in shape with no change in volume.

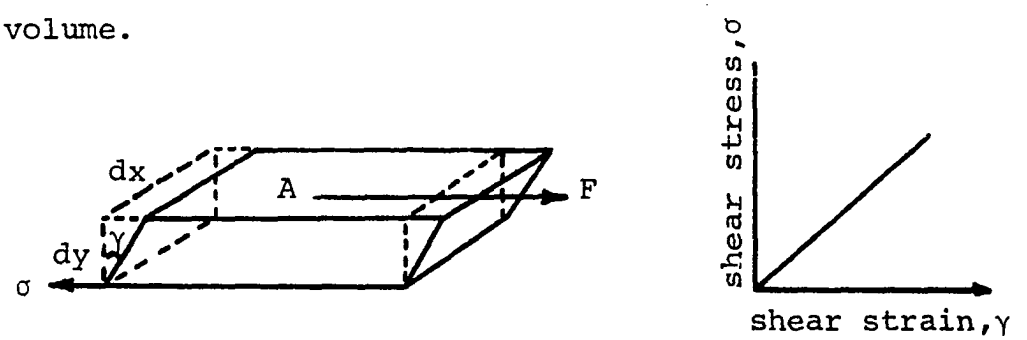

Figure 2. Response of a Perfectly Elastic Material to Pure Shear Stress.

The element shown in Figure 2 will therefore obey Hooke's law for a perfectly elastic material from which all the applied mechanical energy can be recovered. The shear modulus or modulus of elasticity is

$$G = \frac{\text{stress}}{\text{strain}} = \frac{F/A}{dx/dy} = \frac{\sigma}{\tan \gamma} \qquad (5)$$

$$= \frac{\sigma}{\gamma} \quad \text{for small strains}$$

Now if the same element of material is subjected to a sinusoidally varying stress, the strain would go through a sinusoidal variation which will always be in phase with the stress, as shown in Figure 3.

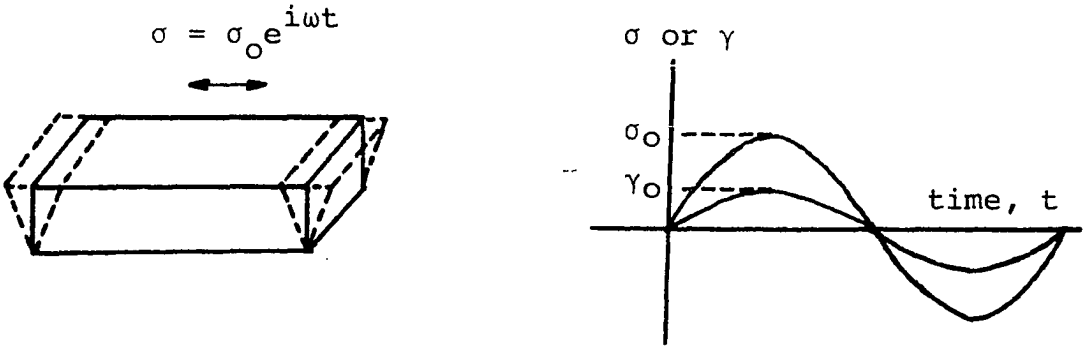

Figure 3. Response of a Perfectly Elastic Material to Oscillatory Shear Stress.

Therefore, in a sinusoidal deformation, with applied stress $\sigma(t) = \sigma_o e^{i\omega t}$, the strain will be $\gamma(t) = \gamma_o e^{i\omega t}$, where ω is the angular frequency. Again, G will be a constant defined by $G = \sigma_o / \gamma_o$. The mechanical analog of such a material is a linear spring.

Purely Viscous Liquids

This term applies to the class of materials which obey Newton's law for flow in which all the applied mechanical energy is non-recoverably dissipated as heat in the material. Figure 4 shows such liquid contained between two large parallel plates of area A which are everywhere separated by a very small distance y.

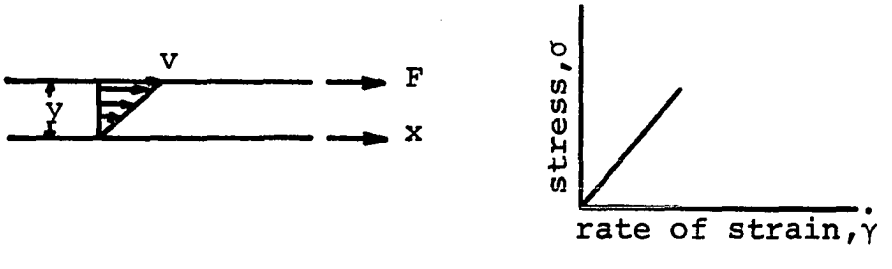

Figure 4. Response of a Purely Viscous Material to Constant Shear Stress.

If a constant force F is applied to the upper plate, the plate starts moving, and after some time it reaches a certain velocity, v. Provided the flow is laminar, the force F and the velocity v can be related by

$$F/A = \eta(v/y) \quad \text{or} \quad \eta = \sigma/\dot{\gamma} \tag{6}$$

Equation 6 states that the force per unit area is proportional to the ratio of the velocity v and the distance y, i.e., the rate of shear $\dot{\gamma}$. The constant of proportionality η is called viscosity and is a measure of the resistance of liquid to the flow. The above relation is known as Newton's law of viscosity.

Now if a sinusoidally varying force is applied to the upper surface, the rate of strain will also vary sinusoidally and will always be in phase with the stress, as shown in Figure 5 (the strain itself will be 90° out of phase with the stress).

Therefore, for a sinusoidal stress, $\sigma(t) = \sigma_o e^{i\omega t}$, the rate of strain will be $\dot{\gamma}(t) = \dot{\gamma}_o e^{i\omega t}$, and $\eta = \sigma_o/\dot{\gamma}_o$ would remain a constant. The behavior of purely viscous liquids can be compared with a linear dashpot.

Viscoelastic Materials

As it was mentioned before, neither Hooke's law nor Newton's law alone can describe the response of a viscoelastic material to an applied stress or strain. In case of a viscoelastic solid, the material does not keep a constant deformation

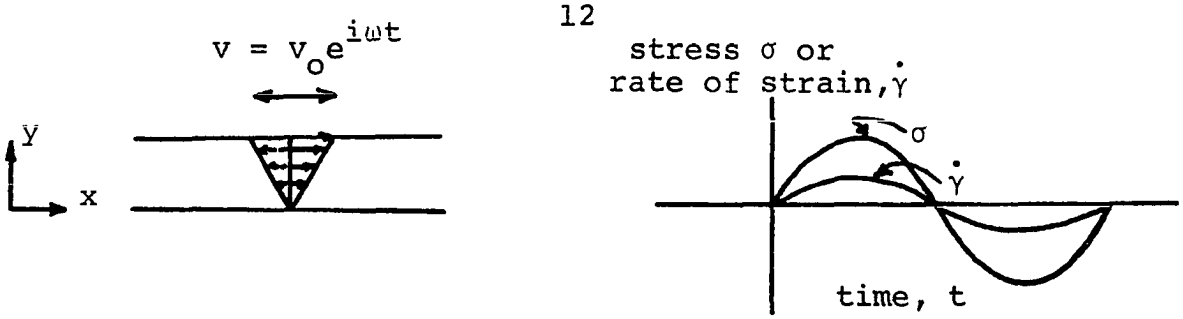

Figure 5. Response of a Purely Viscous Material to Oscillating Shear Stress.

under a constant stress, and it gradually goes through further deformation with time. This phenomenon is called creep. Also, when the material is suddenly brought to a certain deformation, the stress required to maintain this deformation gradually decreases with time or relaxes. Similarly, a viscoelastic liquid when flowing under certain stress does not dissipate all the input energy as heat since it stores some of that energy. When a viscoelastic solid or a viscoelastic liquid is subjected to a sinusoidally varying stress, the strain (in solids) or the rate of strain (in liquids) is not in phase with the applied stress.

Consider the sinusoidally varying strain $\gamma = \gamma_o e^{i\omega t}$ applied to the upper surface of an element of a viscoelastic material, as shown in Figure 6a. The deformation will cause a stress such as $\sigma = \sigma_o e^{i(\omega t+\delta)}$ which will be out of phase with the applied strain by a phase angle equal to δ (Figure 6b or 6c). Figure 6c can be assumed as being generated by the projection of two vectors, σ^* and γ^*, rotating in a complex plane. It is customary to resolve the vector representing the dependent variable (in this example σ^*) into two components:

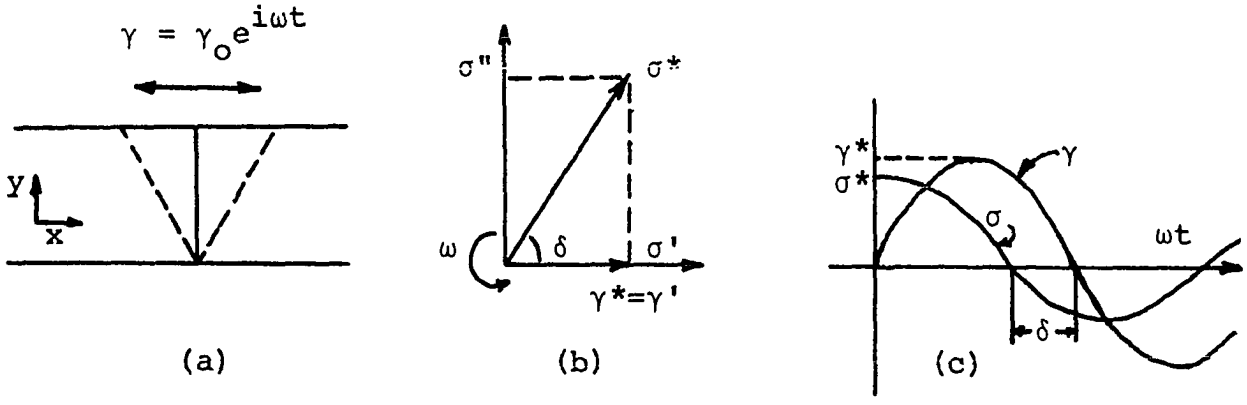

Figure 6. Response of a Viscoelastic Material to a Sinusoidally Varying Shear Strain.

in phase and 90 degrees out-of-phase with the independent variable (γ) as shown in Figure 6b. The in-phase and out-of phase components are designated by prime and double prime, respectively. Noticing that $\gamma^* = \gamma'$ and $\gamma'' = 0$, an in-phase or storage modulus and an out-of-phase or loss modulus can be defined by

$$G' = \frac{\sigma'}{\gamma'} \quad \text{storage modulus} \tag{7}$$

$$G'' = \frac{\sigma''}{\gamma'} \quad \text{loss modulus} \tag{8}$$

Consequently, a complex modulus G* can be defined as the vector sum of the in-phase and out-of-phase moduli, given by

$$G^* = G' + iG'' = \frac{\sigma' + i\sigma''}{\gamma'} = \frac{\sigma^*}{\gamma^*} \tag{9}$$

$$|G^*| = \sqrt{G'^2 + G''^2} = \sigma_o/\gamma_o \tag{10}$$

From Figure 6b the phase angle δ between the stress and strain can be defined as

$$\tan \delta = \frac{\sigma''}{\sigma'} = \frac{G''}{G'} \tag{11}$$

Tan δ is normally called the loss-tangent.

From the above discussion it is clear that each dynamic measurement at any particular angular frequency provides simultaneously two independent quantities G' and G", or equivalently, the loss tangent, tan δ, and the ratio of the peak stress to peak strain, σ_o/γ_o.

Recalling Newton's law, that stress is proportional to the rate of strain, we can similarly define a complex viscosity η^* by

$$\eta^* = \sigma^*/\dot{\gamma}^* \tag{12}$$

where $\dot{\gamma}^*$ is the rate of strain as defined by

$$\dot{\gamma}^* = \frac{d\gamma^*}{dt} = i\omega\gamma_o e^{i\omega t} = i\omega\gamma^* \tag{13}$$

Therefore, from Equations 9, 12 and 13

$$\eta^* = \frac{\sigma^*}{i\omega\gamma^*} = \frac{G^*}{i\omega} = \eta' - i\eta'' \tag{14}$$

where η' and η'' are the real and imaginary parts of the complex viscosity η^*. The components of the complex viscosity and complex modulus can be easily related by equating the real and imaginary parts in Equation 14 which gives

$$\eta' = \frac{G''}{\omega} \quad \text{and} \quad \eta'' = \frac{G'}{\omega} \tag{15}$$

Boltzmann Principle of Superposition

The Boltzmann superposition principle is a generalized principle of linearity. It states that the effect of the sum

of causes is equal to the sum of the effects of each of these causes.

Application of the Boltzmann principle of superposition in rheology can be described as follows. When a shear stress $\sigma_o(t)$ is applied at time zero to an unloaded body, a deformation will take place which can be described by the following equation.

$$\gamma(t) = J(t) \cdot \sigma_o(t) \tag{16}$$

where $J(t)$ is a time dependent compliance defined as the ratio of shear strain to shear stress. If at the same zero time another shear stress $\sigma_1(t)$ is applied to the body, the shear strain will then be proportionally larger and can be expressed by

$$\gamma(t) = J(t)[\sigma_o(t) + \sigma_1(t)] \tag{17}$$

However, if the stress $\sigma_o(t)$ is applied at time $t = 0$ and stress $\sigma_1(t)$ is applied at a later time $t = t_1$, the total strain at any time $t > t_1$ will be the sum of the respective strains at the respective times:

$$\gamma(t) = \sigma_o(t)\ J(t) + \sigma_1(t)\ J(t-t_1) \tag{18}$$

For a continuous variation of loading, the Boltzmann superposition principle states that the deformation at any time t is equal to the summation of all deformations which would have been observed at that time if each of the loads had been

applied independently. In the integral form this relation is given by

$$\gamma(t) = J(0)\ \sigma(t) + \int_0^\infty \sigma(t-\theta)\ \frac{dJ(\theta)}{d\theta}\ d\theta \qquad (19)$$

By similar reasoning, the shear stress $\sigma(t)$ can be easily obtained as a function of a time dependent shear strain, and the following equation will result.

$$\sigma(t) = G(0)\ \gamma(t) + \int_0^\infty \gamma(t-\theta)\ \frac{dG(\theta)}{d\theta}\ d\theta \qquad (20)$$

The last two equations serve as a mathematical representation of the Boltzmann superposition principle. Further discussion and examples of application of this principle have been given by Leaderman (26) and Ferry (16).

There are two restrictions on the application of the Boltzmann principle of superposition. First, the strain must be directly proportional to stress at any time, t, after the application of stress or strain. In other words, the response of a material to a sum of inputs is equal to the sum of responses. Second, the strain that results from a load currently applied should be independent from previously applied loads. This condition requires that the response of a material to an input load be independent of the chronology of applying the loads. For a material to be linearly viscoelastic, both of the above conditions must be satisfied. In many of the experiments with the polymer systems, especially in high frequency

dynamic testings, the amplitude is so small that the above conditions are readily satisfied.

Mechanical Models

Application of mechanical analogs to simulate the behavior of viscoelastic materials is desirable in visualizing the behavior of these materials. The complexity of mechanical models varies enormously from one model to another. These models start from a single combination of a spring and a dashpot, and then the number of elements increases for more complicated behaviors.

The most preliminary way of representing the mechanical properties of a viscoelastic material is by using one dashpot with a viscosity η and one spring with a shear modulus G. It is possible to combine these elements either in series or parallel which gives rise to the Maxwell and the Voigt models, respectively. Both of these models introduce a relaxation time τ as was defined by Equation 4.

Maxwell Model: Maxwell presented his model as a series combination of a spring and a dashpot as shown in Figure 7.

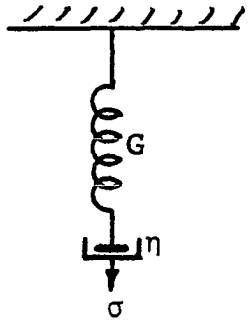

Figure 7. Maxwell Model.

The applied shear stress σ acts with equal magnitude on both the spring and dashpot, while the deformation will be the sum of the two deformations, i.e.,

$$\sigma = \sigma_s = \sigma_d \tag{21}$$

$$\gamma = \gamma_s + \gamma_d \tag{22}$$

Equation 22 can be differentiated with respect to time.

$$\dot{\gamma} = \dot{\gamma}_s + \dot{\gamma}_d \tag{23}$$

Realizing that $\dot{\gamma}_s = \dot{\sigma}/G$ and $\dot{\gamma}_d = \sigma/\eta$, and substituting these values in Equation 23 gives

$$\dot{\gamma} = \frac{\dot{\sigma}}{G} + \frac{\sigma}{\eta} = \frac{\dot{\sigma}}{G} + \frac{\sigma}{\tau G} \tag{24}$$

Equation 24 is the differential equation of motion of a Maxwell model. This equation can also be rearranged to give

$$\sigma = \eta\dot{\gamma} - (\frac{\eta}{G})\dot{\sigma} = \eta\dot{\gamma} - \tau\dot{\sigma} \tag{25}$$

There are two important mechanical tests commonly applied to polymers: First a creep test in which a constant stress is instantaneously applied to the material and the variations of the resulting strain as a function of time are followed. Deformation of material after removing the stress is called creep recovery. The second mechanical test is a stress relaxation test, in which a strain is suddenly applied to the material and held constant, and the changes in the resulting stress as a function of time are observed.

The response of a Maxwell model to creep and stress relaxation experiments can be described as follows. When a stress is suddenly applied to a Maxwell model, it will cause an instantaneous stretching of the spring to its equilibrium condition as determined by $\gamma_s = \sigma/G$. The dashpot will extend linearly with time at a rate of σ/η and will continue to flow as long as the stress is maintained. When the stress is removed the spring will immediately contract by an amount equal to its original extension, and the dashpot will stop flowing with a permanent set equal to $(\sigma/\eta)t$, where t is the duration of the experiment (Figure 8). Thus, in a creep test the Maxwell model exhibits elastic strain, creep, elastic recovery and permanent set which are the usual phenomena observed in a viscoelastic material.

Similarly in the stress relaxation experiment, when the Maxwell model is strained suddenly by a constant value equal to γ, the resistance of the dashpot will initially be infinite, and the spring will be stressed by an amount equal to $G\gamma$. The spring then starts to contract, but the contraction is resisted by the dashpot. The more the spring contracts, the less its restoring force becomes, and therefore the rate of contraction continuously drops. Solution of Equation 25 with $\dot{\gamma} = 0$ and the boundary condition $\sigma = G\gamma$ at $t = 0$ will give

$$\sigma = G\gamma e^{-t/\tau} \qquad (26)$$

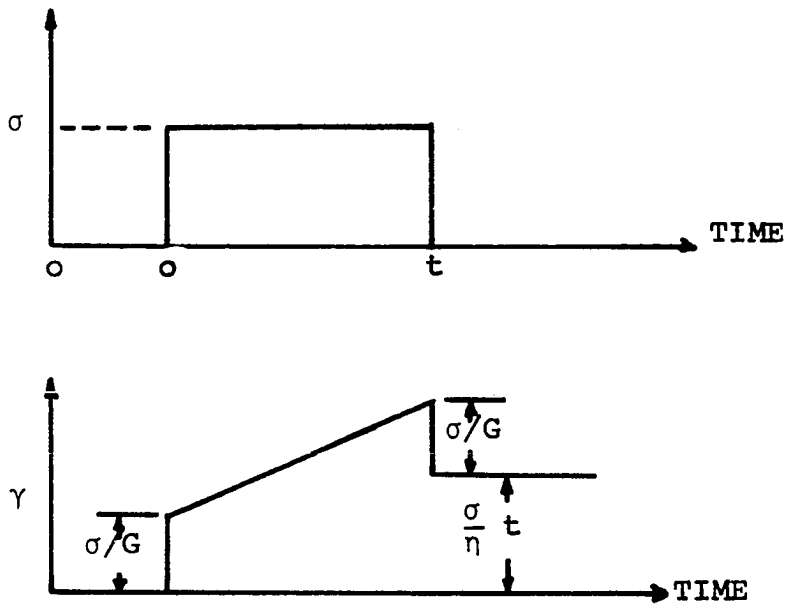

Figure 8. Creep Response of Maxwell Model.

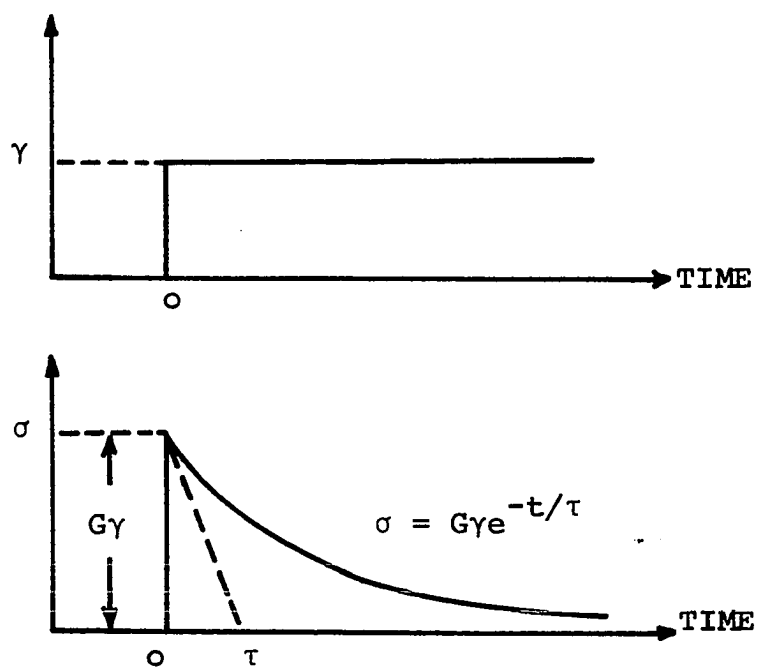

Figure 9. Stress Relaxation of Maxwell Model.

Thus, the relaxation time, τ, serves as the time constant for the exponential decay. In other words, the stress will decrease by 1/e or 37 percent in a period of time equal to τ, as shown in Figure 9. The stress relaxation data of most polymers qualitatively follow the same shape as a Maxwell model, but they cannot be fitted quantitatively with a single G and η.

To investigate the dynamic mechanical behavior of a Maxwell model, assume that the stress and strain can be presented as complex oscillatory functions of the form (32)

$$\gamma^* = \gamma_o e^{i\omega t} \tag{27}$$

$$\sigma^* = \sigma_o e^{i\omega t} \tag{28}$$

Substituting Equations 27 and 28 into Equation 24 gives

$$i\omega \gamma_o = \frac{i\omega\sigma_o}{G} + \frac{\sigma_o}{\tau G} \tag{29}$$

Recalling that $G^* = G' + iG'' = \sigma_o/\gamma_o$, it follows that

$$i\omega = \frac{i\omega G^*}{G} + \frac{G^*}{\tau G} \tag{30}$$

Expanding Equation 30 and separating it into real and imaginary parts gives

$$G' = \omega\tau G'' \tag{31}$$

$$\omega = \frac{\omega G'}{G} + \frac{G''}{\tau G} \tag{32}$$

Substituting Equation 31 into Equation 32 and considering the relations in Equation 15, the final solution for the dynamic behavior of a Maxwell model as a function of frequency is obtained.

$$G'(\omega) = \frac{\omega^2\tau^2 G}{1 + \omega^2\tau^2} = \omega\eta'' \tag{33}$$

$$G''(\omega) = \frac{\omega\tau G}{1 + \omega^2\tau^2} = \omega\eta' \tag{34}$$

$$G''/G' = \frac{1}{\omega\tau} = \frac{\eta'}{\eta''} \tag{35}$$

Equations 33 and 34 indicate that under dynamic testing both an elasticity G' and a viscosity η' will appear, and as ω approaches infinity, the viscosity η' tends to zero. The dependence of a Maxwell model to the changes in frequency is shown in Figure 10.

Voigt Model: The Voigt model is a parallel combination of a spring with shear modulus G and a dashpot with viscosity η. In the Voigt model, the applied strain acts with equal magnitude on both the spring and dashpot.

$$\gamma = \gamma_s = \gamma_d \tag{36}$$

The resulting stress supported by the model is the sum of the stress supported by spring and dashpot.

$$\sigma = \sigma_s + \sigma_d \tag{37}$$

Combining Equation 37 with equations describing deformation

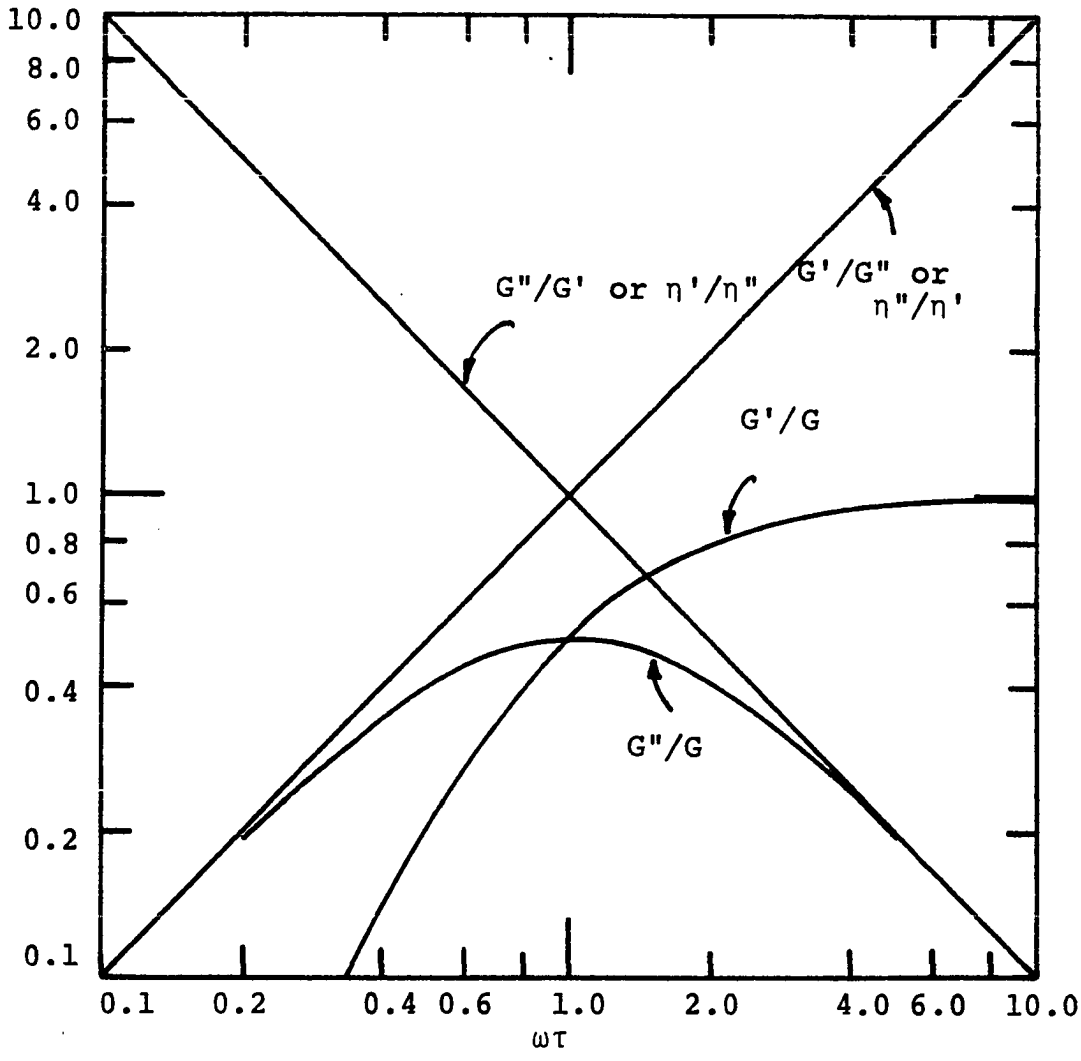

Figure 10. Frequency Dependence of Maxwell Model.

of spring and dashpot, the differential equation of motion of the Voigt model is obtained.

$$\sigma = G\gamma_s + \eta\dot{\gamma}_d \tag{38}$$

When a sudden stress is applied to a Voigt model, as in a creep test, only the dashpot will show an initial resistance to deformation. Therefore the strain versus time curve would initially have a slope of σ/η. As the extension of the element continues, the resistance provided by the spring increases continuously, and as a result the rate of creep decreases. Finally, after sufficient time, the model reaches the equilibrium stage with only the spring supporting the load; the equilibrium strain will be equal to σ/G. The response of the model can therefore be represented by

$$\gamma = \frac{\sigma}{G}\left(1 - e^{-t/\tau}\right) \tag{39}$$

Now if the stress is removed after the equilibrium stage has been reached, the strain decreases exponentially according to

$$\gamma = \frac{\sigma}{G} e^{-t/\tau} \tag{40}$$

It should be noted that a Voigt model, in contrast to the Maxwell model, does not flow indefinitely under a constant stress and also would not show a permanent set. Therefore, the Voigt model is usually used to represent a viscoelastic solid, while the Maxwell model is generally used for viscoelastic liquids.

The Voigt model cannot be used successfully for stress relaxation experiments because application of a sudden strain will meet the infinite resistance of the dashpot, and therefore infinite stress is required. Figure 11 shows a Voigt model and its response to creep test.

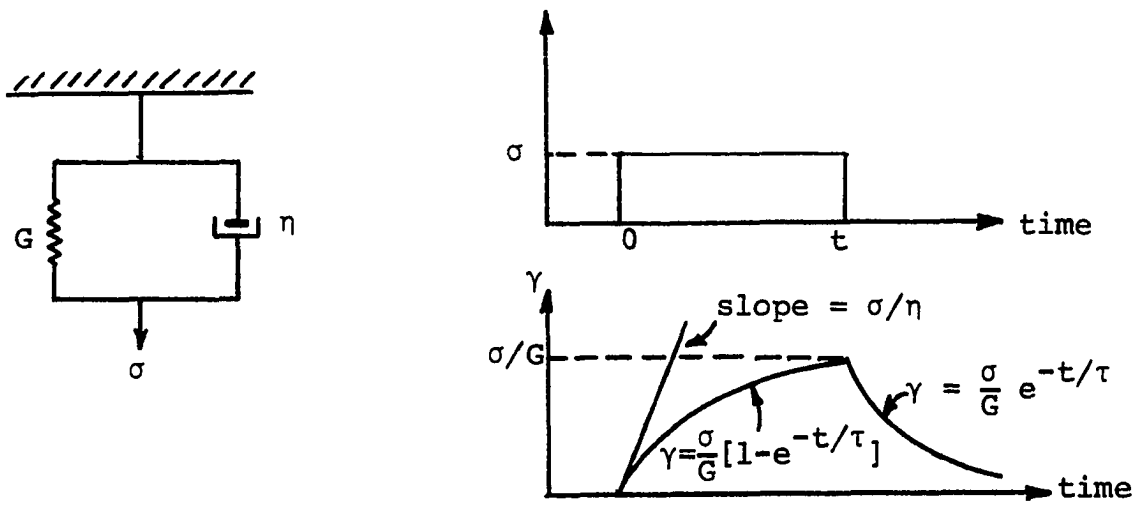

Figure 11. Voigt Model and Its Response to the Creep Test.

The dynamic mechanical behavior of a Voigt model can also be derived by following a procedure similar to the one for a Maxwell model. The following equations will result:

$$G' = G = \omega\eta'' \tag{41}$$

$$G'' = G\omega\tau = \omega\eta' \tag{42}$$

Distribution of Relaxation Times

Although Maxwell and Voigt models give a qualitative presentation of the behavior of viscoelastic materials, they cannot quantitatively describe the behavior of such systems. Therefore, a variety of different models with increasing number of elements have come into existance. Two of the models more commonly used are the generalized Maxwell model and the generalized Voigt model. These models consist of a parallel combination of N Maxwell elements and a series combination of N Voigt elements, respectively. Each element has a different relaxation time τ, as shown in Figure 12.

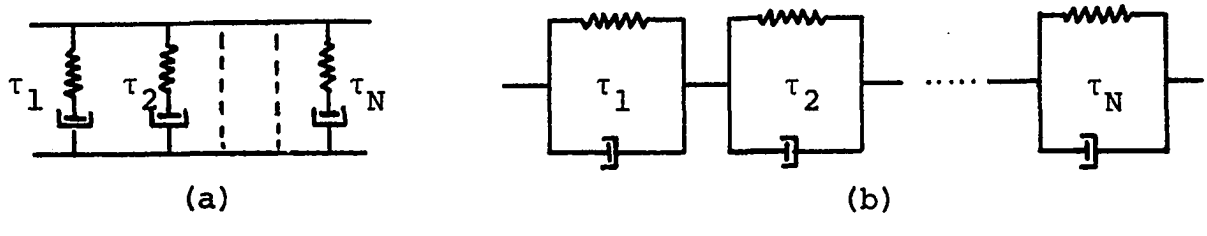

Figure 12. a. Generalized Maxwell Model.
b. Generalized Voigt Model.

In the generalized Maxwell model, each Maxwell element will contribute a stress which is given by an expression such as Equation 25. The total stress is simply the addition of all the individual stresses. Therefore, the overall $G'(\omega)$ and $G''(\omega)$ can be obtained simply by summing their respective values for each element. From Equations 33 and 34

$$G'(\omega) = \sum_{i=1}^{N} \frac{\omega^2 \tau_i^2 G_i}{1 + \omega^2 \tau_i^2} = \omega \eta'' \qquad (43)$$

$$G''(\omega) = \sum_{i=1}^{N} \frac{\omega \tau_i G_i}{1 + \omega^2 \tau_i^2} = \omega \eta' \qquad (44)$$

Incorporation of several Maxwell elements in parallel has proved to be effective to improve the qualitative prediction of the behavior of the polymer systems over narrow ranges of frequencies and at one particular temperature. However, the model still fails when used over the extremely large ranges of frequencies in which G' and G" change. Furthermore, as was mentioned earlier, the enormous number of relaxation times corresponding to the different modes of motion of a macromolecule necessitates an infinite number of Maxwell elements in a generalized Maxwell model. Thus the relaxation times will be so closely spaced that the sums in Equation 43 and 44 can simply be replaced by integrals, i.e.,

$$G'(\omega) = \int_{-\infty}^{\infty} [H(\tau)\ \omega^2\tau^2/(1 + \omega^2\tau^2)]\ d(\ln \tau) \qquad (45)$$

$$G''(\omega) = \int_{-\infty}^{\infty} [H(\tau)\omega\tau/(1 + \omega^2\tau^2)]\ d(\ln \tau) \qquad (46)$$

where $H(\tau) = \tau G(\tau)$. The quantity $H(\tau)$ is known as the "relaxation time function" or the "relaxation spectrum" (12, 16, 32). Due to the broad distribution of the relaxation times, it is

more convenient to represent the distribution as a function of ln τ rather than as a function of τ itself.

As Equations 34, 44 and 46 suggest, the value of $G''(\omega)$, and therefore $\eta'(\omega)$, tend to zero as ω approaches infinity. This condition is not true for a dilute polymer solution because both solvent and polymer contribute to the solution viscosity. Therefore, for polymer solutions another parameter $\omega\eta_s$, where η_s is the solvent viscosity, is added to each of the above mentioned equations.

$$G''(\omega) = \omega\eta_s + \frac{\omega\tau G}{1 + \omega^2\tau^2} \tag{34-a}$$

$$G''(\omega) = \omega\eta_s + \sum_{i=1}^{N} \frac{\omega\tau_i G_i}{1 + \omega^2\tau_i^2} = \omega\eta' \tag{44-a}$$

$$G''(\omega) = \omega\eta_s + \int_{-\infty}^{\infty} [H(\tau)\omega\tau/(1 + \omega^2\tau^2)]\, d(\ln \tau) \tag{46-a}$$

These equations indicate that the viscosity of the solution approaches the solvent viscosity as ω takes very large values (16, 19).

In an analogous manner, a "retardation-time function" or "retardation spectrum" can be defined for the generalized Voigt model when the number of Voigt elements becomes infinitely large (12, 16). Ferry (16), Gross (19), and Tobolsky (50) have given the interrelationship between the relaxation and retardation spectra, as well as the exact and approximate relations to calculate these functions from experimentally determined viscoelastic functions.

Molecular Theory for Dilute Polymer Solutions

It was mentioned earlier that the elasticity of a polymer solution can be described in terms of thermal (Brownian) motion and changes in the orientation of polymer molecules. It was also mentioned that many different relaxation times will be present in a dynamic experiment because of the large number of different configurations a long polymer molecule can assume. This fact was shown by the dynamic measurements of Baker (5) on dilute solutions of several polymers. He tried to express his data in terms of a modified Maxwell element (a single Maxwell element in parallel with a second dashpot) and calculated the spring and the dashpot constants at each particular frequency. He found that the calculated values were functions of frequency of measurement. Only by using a model consisting of several elements could he fit his data for more than one frequency. Later Rouse (44) and Zimm (54) developed theories which predicted a series of relaxation times associated with changes in configuration of polymer molecules in dilute solutions. In these theories a polymer molecule is considered to be N equal submolecules, each of which is long enough for the separation of its ends to obey a Gaussian probability function (17).

In both models the molecule is considered as a series of beads connected by springs, such that each bead and spring represent a segment of the polymer chain (Figure 13). Only beads offer viscous resistance to the flow of solvent; any

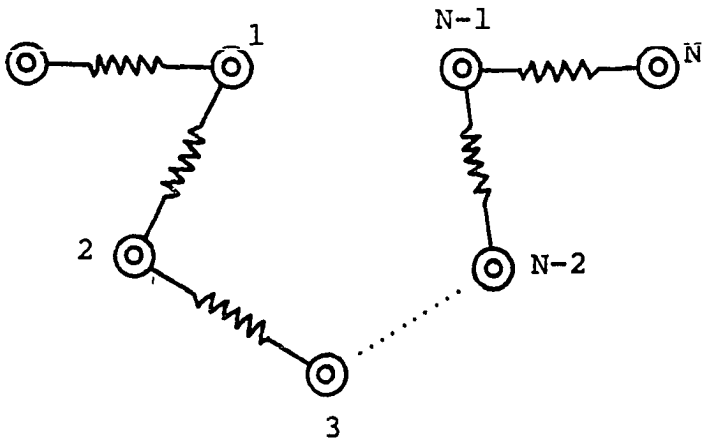

Figure 13. Representation of a Polymer Molecule by the Bead-Spring Model.

energy stored in the system is accounted for by motion of the springs away from their equilibrium. Assigning the loss of energy to the interaction of beads with the surrounding environment is only an approximation because the energy dissipation takes place along the entire length of the polymer chain. The justification for including the springs in the model is due to the fact that when a flexible polymer molecule is stretched (due to any applied shear stress or other disturbances), the number of configurations the polymer segment can assume decreases rapidly with increasing end-to-end separation. Therefore the entropy decreases, and an entropic restoring force will be created which acts in the same manner as a spring.

The essential difference between the Rouse (44) and Zimm (54) theories is in the way the polymer molecule and the surrounding solvent interact. In the Rouse theory the velocity of solvent through the molecule is not affected by the

presence of the molecule, and the flow field of the solvent around a particular bead is not altered by the presence of other beads of the same molecule. This concept is known as the "free draining" assumption (17). On the other hand, the Zimm theory assumes a hydrodynamic interaction between the beads using the method discussed by Kirkwood and Riseman (23); this concept is referred to as the "non-free draining" case.

In both the Rouse and Zimm theories, the expressions for G' and G" and the dynamic viscosity η' of the polymer solution are given by (16):

$$G' = nkT \sum_{p=1}^{N} \frac{\omega^2 \tau_p^2}{1 + \omega^2 \tau_p^2} \tag{47}$$

$$G'' = \omega \eta_s + nkT \sum_{p=1}^{N} \frac{\omega \tau_p}{1 + \omega^2 \tau_p^2} \tag{48}$$

and

$$\eta' = \frac{G''}{\omega} = \eta_s + nkT \sum_{p=1}^{N} \frac{\tau_p}{1 + \omega^2 \tau_p^2} \tag{49}$$

where n is the number of the polymer molecules per cubic centimeter, k the Boltzmann's constant, T the absolute temperature, $\omega = 2\pi f$ the angular frequency, η_s the solvent viscosity and N the number of submolecules. In the theory of Rouse, the relaxation times are

$$\tau_p = \frac{6(\eta - \eta_s)}{\pi^2 p^2 nkT} \tag{50}$$

where η is the static viscosity of the solution and p = 1, 2, 3 ... represents the different modes of motion of the polymer. The relaxation times in the Zimm theory are

$$\tau_p = \frac{1.71(\eta - \eta_s)}{\lambda_p' \, nkT} \tag{51}$$

where λ_p' is a numerical coefficient (55) whose first few values (p = 1, 2, 3, 4) are 4.04, 12.79, 24.2, and 37.9. These quantities are the eigenvalues resulting from solution of the equation of motion of the polymer chain. Noting that nkT = cRT/M, where c is the concentration of polymer in the solution in grams of polymer per cubic centimeter of solution, R is the gas constant and M is the molecular weight of the polymer, Equations 47 through 51 become

$$G' = \frac{cRT}{M} \sum_{p=1}^{N} \frac{\omega^2 \tau_p^2}{1 + \omega^2 \tau_p^2} \tag{52}$$

$$G'' = \omega \eta_s + \frac{cRT}{M} \sum_{p=1}^{N} \frac{\omega \tau_p}{1 + \omega^2 \tau_p^2} \tag{53}$$

$$\eta' = \frac{G''}{\omega} = \eta_s + \frac{cRT}{M} \sum_{p=1}^{N} \frac{\tau_p}{1 + \omega^2 \tau_p^2} \tag{54}$$

$$\tau_p = \frac{6(\eta - \eta_s)M}{\pi^2 p^2 cRT} \qquad \text{(Rouse Theory)} \tag{55}$$

$$\tau_p = \frac{1.71(\eta - \eta_s)M}{\lambda_p' \, cRT} \qquad \text{(Zimm Theory)} \tag{56}$$

It is apparent that the above frequency-dependent properties can be completely predicted from the steady flow viscosity of the solution and solvent, the concentration, and the molecular weight of the polymer. Equations 52 and 53 indicate that both G' and G" - $\omega\eta_s$ are proportional to cRT/M; also, Equations 55 and 56 predict that the relaxation times in the Rouse and Zimm theories are both proportional to $(\eta - \eta_s)M/cRT$. Hence it is possible to reduce the results for different concentrations of polymers and different molecular weights to two dimensionless curves by plotting the dimensionless variables G'M/cRT and $(G" - \omega\eta_s)M/cRT$ versus the dimensionless angular frequency $\omega(\eta - \eta_s)M/cRT$. Similarly in Equation 54, $\eta' - \eta_s$, the contribution of the polymer to the solution dynamic viscosity, can be normalized by dividing by $\eta - \eta_s$, the contribution of the polymer to the static viscosity of the solution. These values are then plotted against $\omega(\eta - \eta_s)M/cRT$ to give a dimensionless plot of dynamic viscosity against angular frequency. Figures 14 and 15 show these plots for the Rouse and Zimm theories.

It should be realized that both the Rouse and Zimm theories assume that Gaussian statistics apply to the distribution of molecular configurations; that is, the root-mean-square distance of the ends of the molecule as well as the root-mean-square distance between the ends of each chain segment are proportional to $M^{1/2}$, where M is the molecular weight of the polymer. For this reason these theories are applicable in a

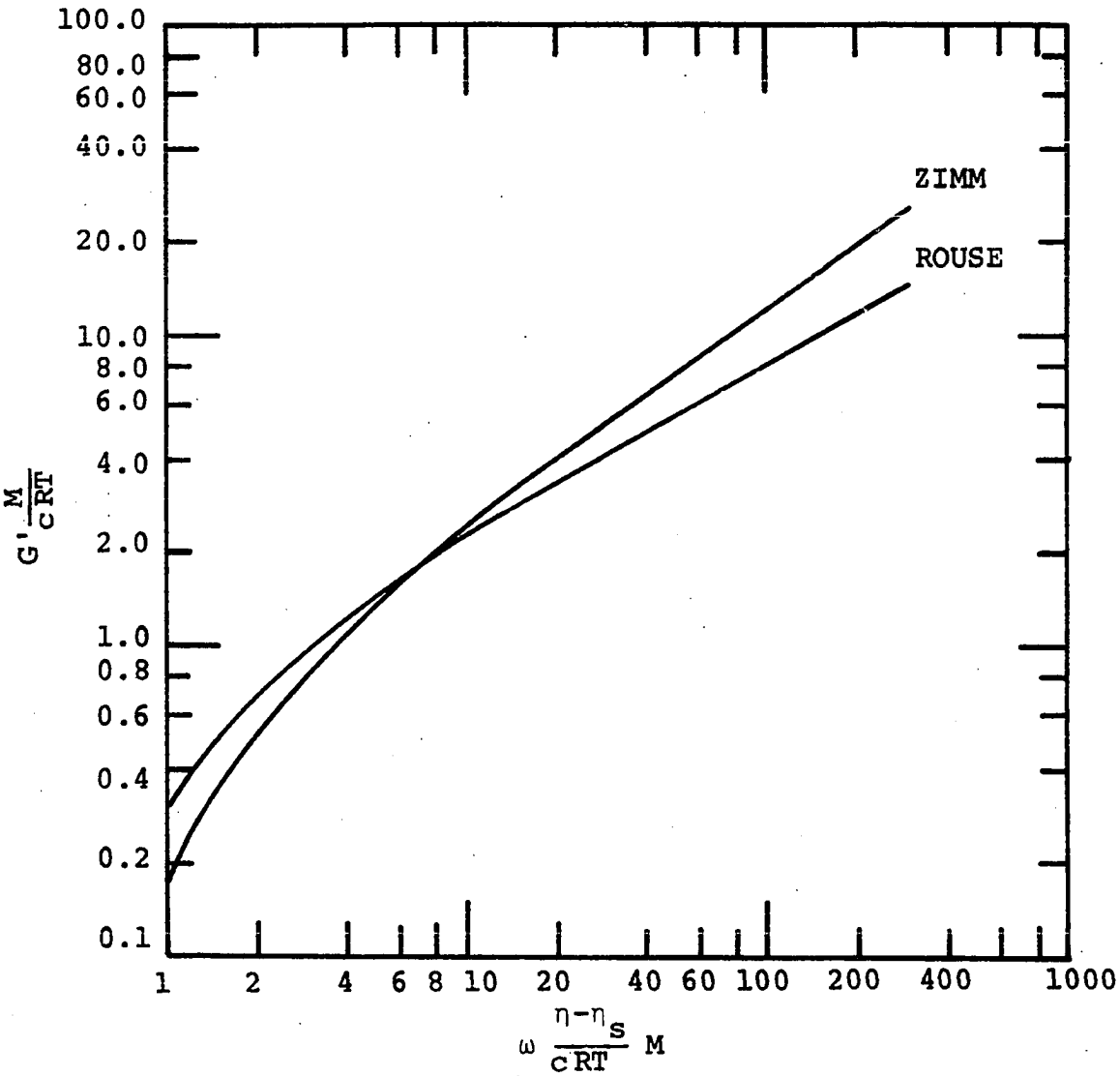

Figure 14. Dimensionless Elastic Modulus versus Dimensionless Angular Frequency for Rouse and Zimm Theories.

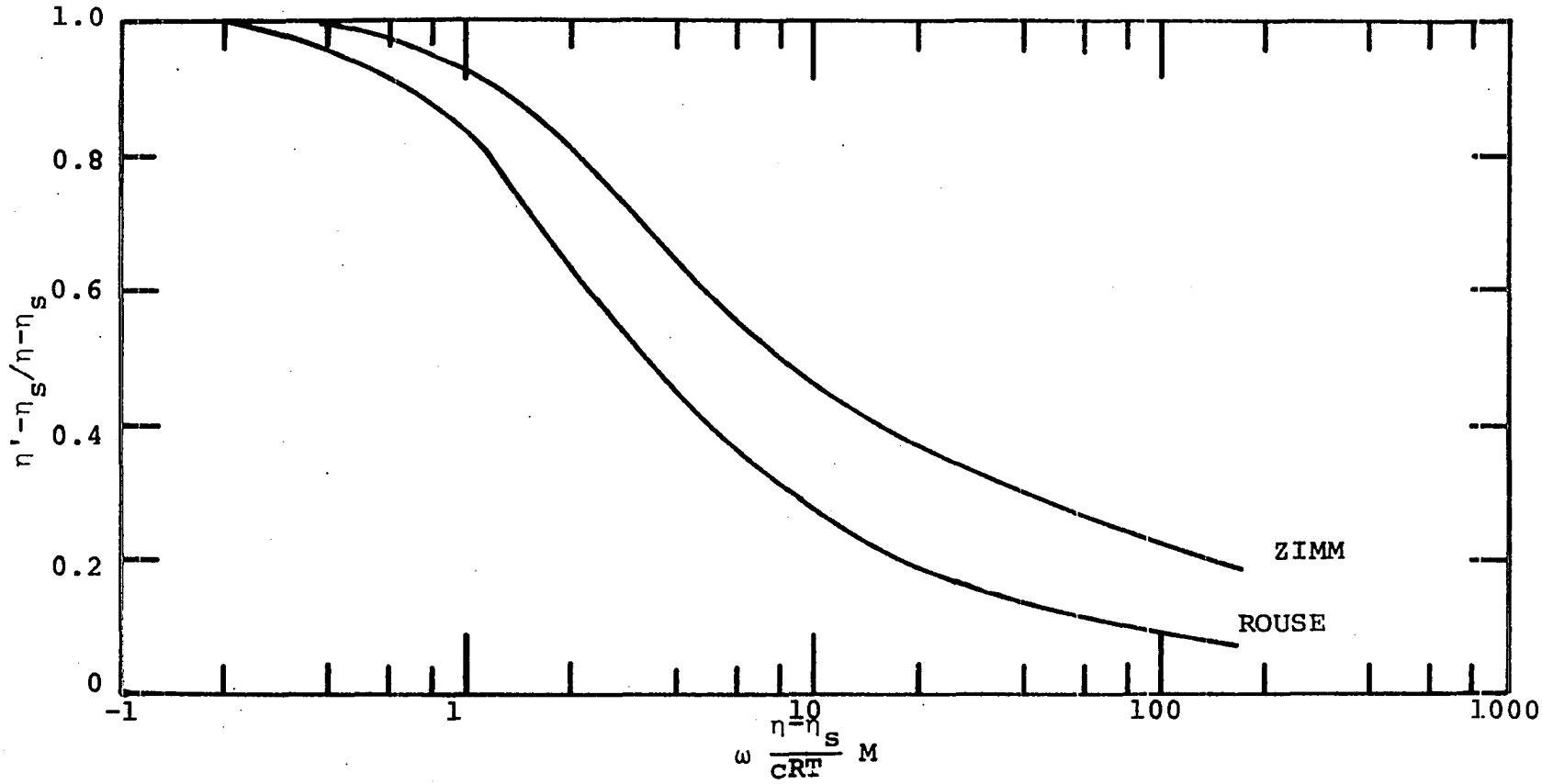

Figure 15. Dimensionless Dynamic Viscosity versus Dimensionless Angular Frequency for Rouse and Zimm Theories.

"theta solvent" (17, 34) in which the interactions between polymer-solvent and polymer-polymer molecules are equal and the solution behaves ideally. In a good solvent the attractive forces between the chain segments of the molecules and the solvent are greater than the attractive forces between the chain segments, and therefore the molecules assume a more spread-out configuration. The extent of this expansion can be approximated (33) by a parameter ε. This parameter is defined in such a way that the mean-square-distance between any two points on the chain separated by n bonds is proportional to $n^{1+\varepsilon}$ instead of n as it would be in a theta solvent. The limits of ε are found to be (16) zero and 1/3. The theory of Zimm has also been modified by Ptitsyn and Eisner (37, 38) and it has been shown (52) that the increase in the value of ε, corresponding to the application of better solvent, causes a shift from the Rouse-like to the Zimm-like behavior.

Subsequently, Tschoegl (51, 52) generalized the Rouse and Zimm theories such that they could be applied in the intermediate cases between free draining and non-free draining conditions and for non-theta solvents. For this purpose, Tschoegl introduced a parameter h to indicate the various degrees of hydrodynamic interaction (h is zero for Rouse theory and infinity for Zimm theory) and combined this parameter with ε. Thus the theory of Tschoegl contains the Rouse, Zimm, and Ptitsyn and Eisner theories as its special cases. In comparing the results of experiments with the Tschoegl theory, it is

customary to calculate the value of ϵ for the particular polymer-solvent system (51) and then use h as an adjustable parameter to obtain a good fit. The parameter ϵ is given by

$$\epsilon = \left(\frac{b}{a} M^{1/2}\right) / \left[\left(3 \frac{b}{a} M^{1/2} + 0.497\right) + 2.308\left(3 \frac{b}{a} M^{1/2} + 0.497\right)^{1/3}\right] \qquad (57)$$

where M is the molecular weight of the polymer, and a and b are the constants for a given polymer. The values of a and b can be found by following the method described by Stockmayer and Fixman (48): Plotting $[\eta]/M^{1/2}$ against $M^{1/2}$ and passing the best straight line through the points, a and b are determined as the intercept and slope of the line, respectively.

All of the theories described above assume that the polymer molecule is completely flexible, and any possibility of the internal resistance of the polymer is ignored. More recently Peterlin (34) used the concept of internal viscosity to represent the inability of the polymer coil to undergo an instantaneous deformation in response to an applied stress at high frequencies. In contrast with the predictions of the previous theories, this consideration leads to a limiting viscosity for the solution at high frequencies which is greater than that of the solvent. Finally it should be mentioned that all of the above theories apply to a very dilute solution of a monodisperse polymer because they deal only with the behavior of an isolated molecule and therefore they apply to

infinite dilution. To evaluate these theories, the experimental results should actually be extrapolated to infinite dilution (zero concentration) in the same manner as in the determination of intrinsic viscosity. This technique was first used by Baker (5) in 1952, but since at that time the above theories had not been developed, his data were not presented in a form which would enable one to evaluate these theories. Later, Tanaka, Sakanishi, Kaneko and Furuichi (46, 47, 49), by extrapolating their viscoelastic functions to zero concentration, indicated that the Tschoegl theory in fact describes the viscoelastic behavior of polymer solutions in theta solvents ($\varepsilon = 0$, $h = \infty$) and non-theta solvents ($\varepsilon > 0$, $h < \infty$). The behavior of the solution at higher concentrations and the effect of polydispersity of the polymer have also been investigated and are described in the literature (16).

CHAPTER III

ULTRASONIC TECHNIQUE FOR MEASURING MECHANICAL PROPERTIES OF VISCOELASTIC LIQUIDS

In this chapter the experimental technique used to obtain the data is discussed, and for the purpose of later analysis of the data, the necessary relations among the measured quantities and the viscoelastic properties of the liquids investigated are developed.

Torsional Quartz Crystal

The application of ultrasonic vibrations in the investigation of viscoelastic properties of liquids was first introduced by Mason (29). He used a quartz crystal which was excited in a torsional mode by application of an alternating current. The quartz crystal can be made to vibrate torsionally according to the following method (28): A cylinder is cut out of a quartz crystal such that the "X" crystal axis lies parallel to the length of the cylinder. The cylindrical crystal is then divided into four electrodes by evaporative application of a highly conductive material such as gold or silver running the length of the crystal. A wire is then connected to each electrode at the middle of the crystal, and

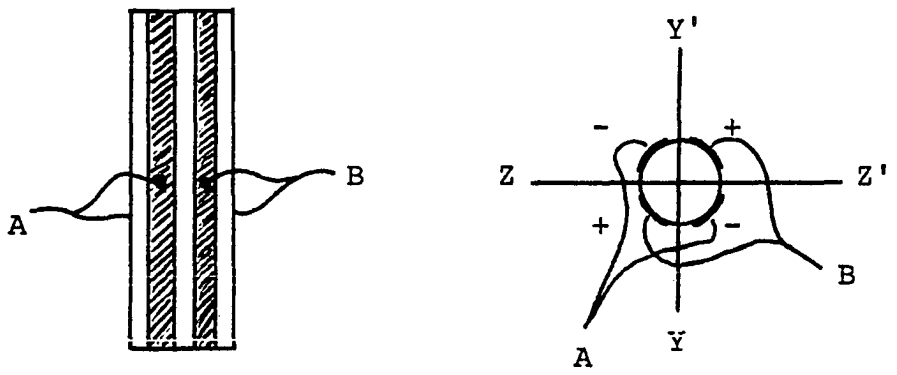

Figure 16. Electrode Arrangement for Torsionally Vibrating Quartz Crystal.

the wires on the opposite sides of the cylinder are connected together as shown in Figure 16.

When the leads A and B are connected to an a-c source, the electric fields on the two sides of the axis YY' will be of opposite sign and produce two opposing shear stresses which make the cylinder react with a torsional motion. A lengthwise motion may also be present, especially if the wires are not connected to the precise middle of the crystal. Usually, for a large length to diameter ratio of the crystal, this longitudinal motion can be ignored as compared to the torsional motion. In the liquid surrounding the crystal, a series of highly damped plane shear waves can thus be generated which introduce a resistance and capacitance loading on the crystal. This loading changes the resonant frequency and resistance at resonant frequency of the crystal, as the crystal

environment is changed from vacuum to a liquid. Mason related these changes to the viscous and elastic properties of the liquid (29).

The frequency of oscillation of the crystal in ultrasonic ranges is so high that the wave length of the rapidly attenuated shear wave will necessarily be very small, so that the vibrations die off within a very short distance (less than one millimeter) from the surface of the crystal. Therefore the shear waves produced by the crystal can be readily approximated by the true plane waves. The error introduced by this approximation has been determined by McSkimin (30) and a correction factor has been suggested. However, in almost all of the investigations in which ultrasonic technique has been used, the error has proved to be negligible compared to the other errors involved in measurements.

Assuming a sinusoidal motion with an angular frequency of $\omega = 2\pi f$ and a maximum velocity of v_o, the velocity of the surface of the crystal can be represented by

$$v_s = v_o \, e^{i\omega t} \tag{58}$$

From hydrodynamics (24), the transverse velocity of the liquid at a distance x from the surface of the oscillating crystal is

$$v_\ell = v_o \, e^{-\Pi x} \, e^{i\omega t} \tag{59}$$

where Π is the propagation constant and is defined by

$$\Pi = (i\omega\rho/\eta^*)^{1/2} \tag{60}$$

with the liquid density equal to ρ and η^*, the complex viscosity. The force exerted upon the liquid from a unit area of the crystal surface is

$$\sigma = -\eta^* \left(\frac{\partial v_\ell}{\partial x}\right)_{x=0} \tag{61}$$

From Equations 58 and 59,

$$\begin{aligned}\left(\frac{\partial v_\ell}{\partial x}\right)_{x=0} &= \left(-v_o \Pi\, e^{-\Pi x}\, e^{i\omega t}\right)_{x=0} \\ &= -\Pi\,(v_o e^{i\omega t}) \\ &= -\Pi v_s \end{aligned} \tag{62}$$

Combining Equations 61 and 62

$$\sigma = \eta^* \Pi\, v_s \tag{63}$$

Now a complex mechanical impedance can be defined as the ratio of the shear stress σ to the velocity of the liquid at the surface (the same as the surface velocity of the crystal) by

$$Z_M = R_M + iX_M = (i\omega\rho\,\eta^*)^{1/2} \tag{64}$$

where R_M and X_M are known as mechanical resistance and mechanical reactance, respectively. From Equation 64 the components of the complex viscosity, η^*, and the components of the mechanical impedance, R_M and X_M, can be related by

$$\eta' = \frac{G''}{\omega} = \frac{2R_M X_M}{\omega\rho} \tag{65}$$

$$\eta'' = \frac{G'}{\omega} = \frac{R_M^2 - X_M^2}{\omega\rho} \tag{66}$$

For a purely viscous liquid η'' is equal to zero and therefore

$$R_M = X_M = (\pi f \rho \eta)^{1/2} \tag{67}$$

Mason (29) observed that the changes in the resonant frequency, Δf, and the resistance at resonant frequency, ΔR, of the crystal are related to the mechanical resistance and reactance,

$$\Delta f = f - f_o = K_f X_M \tag{68}$$

$$\Delta R = R_E - R_{E_o} = K_R R_M \tag{69}$$

where f and R_E are the resonant frequency and resistance at resonant frequency of the crystal, respectively. The subscript o represents measurement in vacuum. The constants K_f and K_R can either be determined experimentally or calculated theoretically from the physical and electrical properties of the crystal. From Equations 67, 68, and 69 for purely viscous liquids

$$f - f_o = K_f(\pi f \rho \eta)^{1/2} \tag{70}$$

$$R_E - R_{E_o} = K_R(\pi f \rho \eta)^{1/2} \tag{71}$$

Therefore, plotting the measured values of f and R_E for different normal liquids (at one particular pressure and

temperature) versus their corresponding values of $(\pi f \rho \eta)^{1/2}$, gives straight lines from which K_f and f_o, as well as K_R and R_{E_o}, can be determined by measuring the slope and intercept of each line.

The crystal constants may also be determined theoretically (2, 45) from the following relations:

$$K_f = \frac{1}{\pi \rho_c} \left(\frac{1}{r} + \frac{1}{\ell}\right) \tag{72}$$

$$K_R = 4\pi L_c K_f \tag{73}$$

where r is the crystal radius, ℓ is the crystal length, ρ_c the crystal density and L_c the effective electrical inductance of the crystal. The value of L_c can be calculated from the conductance at the resonance, G_c, and the difference between the two frequencies (called the half power points) at which the conductance of the crystal is one half of G_c, as measured in any liquid:

$$L_c = \frac{1}{2\pi \Delta f G_c} \tag{74}$$

Before introduction of the ultrasonic technique described above the dynamic measurements of viscoelastic properties of liquids were carried out by either purely mechanical methods or electromagnetic devices. With purely mechanical methods, the frequencies obtained were usually in the order of a few hundred Hz. With electromagnetic devices the frequency range was increased to below 20 kHz. Up to

20 kHz, the liquids having viscosities of a few poise or less usually did not show any reduction in the dynamic viscosity with frequency and no measurable elastic effect could be observed. Application of torsionally oscillating piezoelectric crystals has extended the frequency range by about 10 times. Since each crystal has only one fundamental resonant frequency, a separate crystal has to be employed for each desired frequency. However, the increase in the frequency range together with the utilization of the method of reduced variables to be described shortly has provided an abundance of data from which the viscoelastic properties of many liquids as well as molecular behavior of many polymer systems can be predicted. The use of ultrasonic technique is especially advantageous because, as was shown by Mason (29), no heating complications are observed.

The Effect of Temperature and Pressure and the Method of Reduced Variables

As mentioned previously, since the variety of the molecular motions of the polymers in a polymer system can only be observed over a very wide range of time or frequency, an experiment is required that can cover a broad frequency range. However, none of the available experimental techniques can provide such a wide range of information, and therefore the information must be obtained from different experiments, the results of which are then combined. Consequently,

obtaining the data is time consuming and expensive. Specifically, in the oscillating quartz crystal technique used in this investigation, measurement at various shear rates requires many different quartz crystals with different fundamental frequencies because each crystal provides only one frequency (or shear rate) measurement.

The introduction of the method of reduced variables (2, 16, 35, 36) has alleviated the experimental burden. With only one experimental method which covers a very short range of the frequency scale, the viscoelastic functions, such as the components of complex viscosity and elasticity, can be extended over a much wider effective range of frequencies. By taking the data at different temperatures and pressures, it is possible, by using the method of reduced variables, to convert the information obtained at one frequency and various conditions of temperature and pressure to one reference condition (T_o and P_o) and various equivalent shear rates. In this manner the range of the available frequencies can be enlarged much beyond the range of isothermal and isobaric measurements.

According to Equations 52 and 53, the contributions of the polymer to the shear elastic modulus, G', and loss modulus, G" - $\omega\eta_s$ are proportional to cRT/M. Thus, the temperature dependence of G' and G" - $\omega\eta_s$ is partly due to the change of the temperature itself and partly due to the change in concentration, which decreases slightly with increasing

temperature because of thermal expansion. Since the influence of the temperature on the concentration is the same as its effect on the density of the solution, the moduli, G' and G" - $\omega\eta_s$, can be converted to "reduced moduli" G'_r and G''_r which are dependent only on the value of $\omega\tau$ and are independent of temperature. Therefore, at two temperatures, T and T_o, where T is the temperature of the measurement and T_o is the reference temperature,

$$G'_r = G_T' \frac{T_o\rho_o}{T\rho} \tag{75}$$

$$G''_r = G_T'' \frac{T_o\rho_o}{T\rho} \tag{76}$$

From Equations 55 and 56 it is also apparent that all the relaxation times are proportional to $(\eta - \eta_s)M/cRT$. Therefore, the temperature dependence of the relaxation times is influenced by the changes in $(\eta - \eta_s)$ as well as c and T. As a result, the above dependence can be represented by

$$[\tau_p]_{T_o} = [\tau_p]_T/a_T = [\tau_p]_T[(\eta-\eta_s)_{T_o}/\rho_o T_o] \div [(\eta-\eta_s)_T/\rho T] \tag{77}$$

or

$$a_T = \frac{[\tau_p]_T}{[\tau_p]_{T_o}} = (\eta - \eta_s)_T\rho_o T_o/(\eta - \eta_s)_{T_o}\rho T \tag{78}$$

In Equation 78 the value of a_T is primarily determined from the ratio of the viscosities because ρ and T change more slowly. In many cases, especially in dilute solutions, the

ratio composed of values of $(\eta - \eta_s)$ at the two temperatures is equal to the ratio of the solvent viscosities so that a_T can also be determined from

$$a_T = \frac{(\eta_s)_T}{(\eta_s)_{T_o}} \frac{\rho_o T_o}{\rho T} \tag{79}$$

Recalling that $\tau = \eta/G$,

$$\eta_r' = (G_r')(\tau_p)_{T_o} = (G_T' \frac{T_o\rho_o}{T\rho})(\tau_p)_T (\frac{(\eta_s)_{T_o}\rho T}{(\eta_s)_T \rho_o T_o})$$

$$= \eta_T' \frac{(\eta_s)_{T_o}}{(\eta_s)_T} \tag{80}$$

Therefore, the effect of a temperature change from T to T_o is to multiply G' and $(G'' - \omega\eta_s)$ by $\rho_o T_o/\rho T$, to multiply η' by $(\eta_s)_{T_o}/(\eta_s)_T$ and to multiply each relaxation time τ_p by a_T. Because of the form of Equations 52 and 53, the latter result is the same as though ω were multiplied by a_T. As a result, it follows that measurements of G', $G'' - \omega\eta_s$ and η' at various temperatures can be plotted as $G'[\rho_o T_o/\rho T]$, $(G'' - \omega\eta_s)\rho_o T_o/\rho T$ and $\eta T'(\eta_s)_{T_o}/(\eta_s)_T$ against the reduced angular frequency, ωa_T, to give single composite curves (or master curves) which are equivalent to measurements carried out at T_o over a wide range of frequencies. From the value of a_T in Equation 79, it is apparent that an increase in the temperature is equivalent to a decrease in a_T, and, consequently, the reduced frequency (noting that η is the controlling factor).

Philippoff (36) later showed that the same reasoning can be applied to the effect of pressure on the viscoelastic properties of dilute polymer solutions. He combined the pressure and temperature effects in a new factor $a_{T,P}$ represented by

$$a_{T,P} = \frac{(\eta)_{T,P}}{(\eta)_o} \frac{\rho_o T_o}{\rho T} \tag{81}$$

where η is now the zero shear rate viscosity of the solution and ρ is the density at pressure P and temperature T. The subscript zero in Equation 81 indicates the values at the reference pressure and temperature.

The difficulty encountered in applying Equation 81 to describe the effect of pressure was mainly the need to know the low shear rate viscosity of the solution at each pressure and temperature, which required independent pressure-viscosity equipment. Philippoff solved this problem by observing that the relative viscosity of polymer solutions, η/η_s, is generally independent from changes in pressure. Thus, it is sufficient to know the viscosity of the solvent as a function of pressure. As a result, Philippoff divided the factor $[(\eta)_{T,P}/(\eta)_o]_{solution}$ into two factors: one describing the effect of pressure and the other describing the effect of temperature, i.e.,

$$\left(\frac{(\eta)_{T,P}}{(\eta)_o}\right)_{solution} = \alpha = \left(\frac{\eta_T}{\eta_o}\right)_{solution} \left(\frac{\eta_p}{\eta_o}\right)_{solvent} \tag{82}$$

where $(\eta_T)_{solution}$ = viscosity of solution at temperature T and pressure P_o

$(\eta_o)_{solution}$ = viscosity of solution at temperature T_o and pressure P_o

$(\eta_p)_{solvent}$ = viscosity of solvent at temperature T and pressure P

$(\eta_o)_{solvent}$ = viscosity of solvent at temperature T and pressure P_o

The first factor on the right side of Equation 82 represents the temperature dependence of the solution, and the second factor indicates the pressure dependence of the solvent (which is assumed to be the same as that of the solution). In this representation Equations 75 and 76 remain unchanged and Equation 80 becomes

$$\eta_r' = \eta'_{T,P} \left(\frac{(\eta)_{T,P}}{(\eta)_o}\right)_{solution}$$

$$= \eta'_{T,P} \left(\frac{\eta_T}{\eta_o}\right)_{solution} \left(\frac{\eta_p}{\eta_o}\right)_{solvent} = \eta'_{T,P}{}^{\alpha} \tag{83}$$

with

$$a_{T,P} = \alpha \frac{T_o \rho_o}{T \rho} \tag{84}$$

CHAPTER IV

DESCRIPTION OF EQUIPMENT AND MATERIAL

In the following sections the equipment and materials used in this investigation are described. The equipment can be divided into the following categories: pressure cell, pressure generating system, pressure measuring devices, quartz crystal, electronic components used for oscillating the crystal and measuring the frequency of oscillation and resistance of the crystal, and finally, temperature controller and recorder.

Pressure Cell

The pressure cell as shown in Figure 17 was a duplex vessel with 1-1/2 inches internal by 9-1/2 inches external diameters and 12-7/16 inches internal depth. It was designed and fabricated by Autoclave Engineers, Incorporated, for a working pressure and temperature of 150,000 psig and 250°F, respectively. The outer body of this shrink-fit vessel was built with HY-140 and the inner with 4340 stainless steel. Bridgman type self-sealing rings (7, 20) were employed to seal the pressure at the two end-covers. These rings were made of beryllium-copper alloy (Berilco-25).

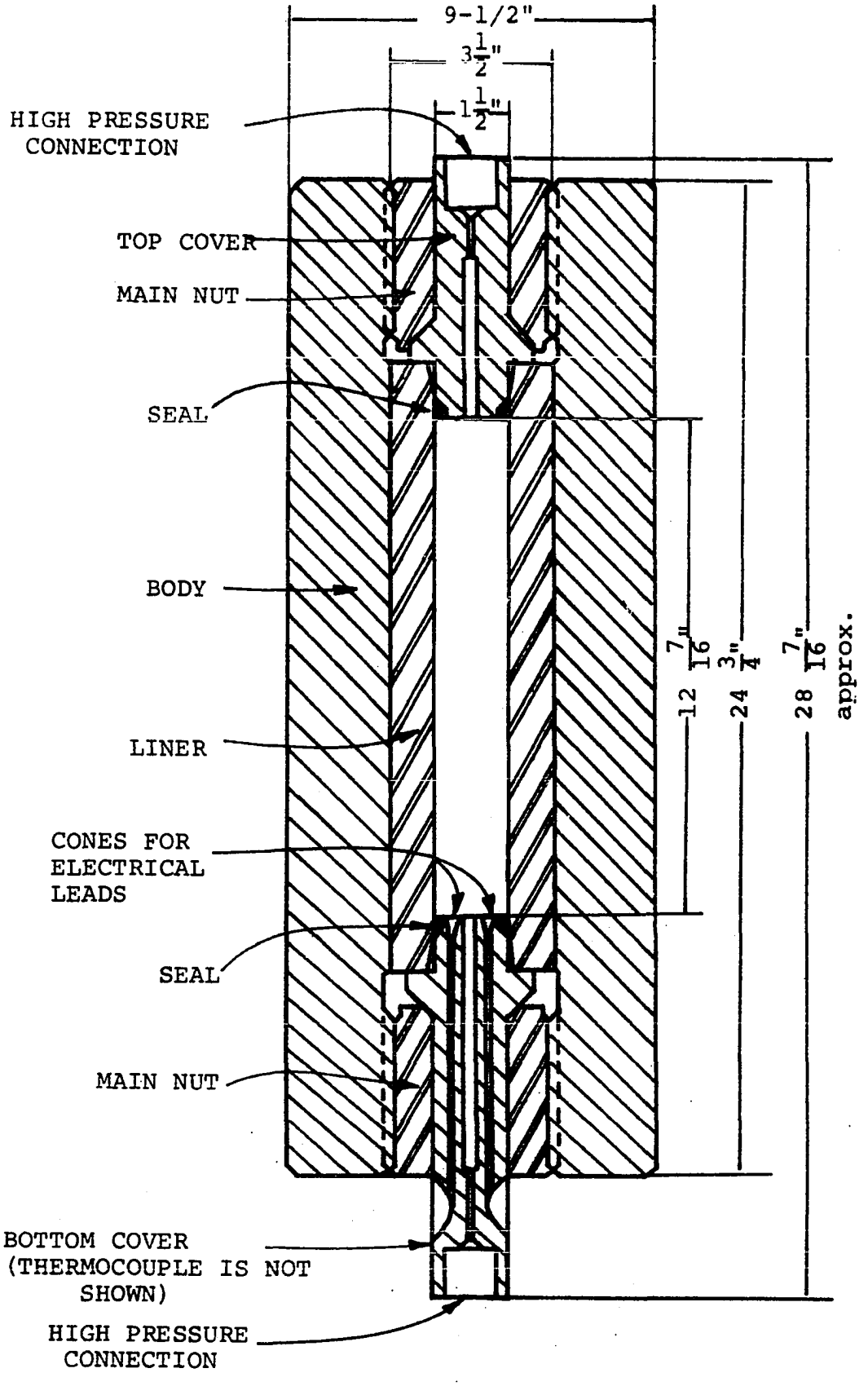

Figure 17. The Assembly Diagram of the 150,000 psig High Pressure Vessel.

The top and bottom covers (Figure 18) were drilled through so that the pressure cell could be filled or drained from either end. Four holes 90° apart (3/8 inch deep and tapped in 10-24) on the inside end of the bottom cover were provided for the crystal holder. The electrical leads for connecting to the quartz crystal passed through two additional holes in the bottom cover and were sealed with steel-pipestone, conical-shape plugs. A thermocouple well, 1/8 inch diameter and 5-7/8 inches deep, was also drilled from the bottom face of the bottom cover and was used for measuring the temperature of the pressure cell and the liquid inside. Except for the holes for the crystal holder, electrical leads and the thermocouple well, the top cover was identical to the bottom cover.

Pressure Generating System

The liquid in the system was pressurized by an air driven hydraulic pump, model SC40-500-16, purchased from Hydraulic Engineering Corporation. For an air supply of 100 psig, the pump was designed to deliver a maximum hydraulic fluid pressure of 27,500 psig. When necessary, a pressure regulator was used on the inlet air supply line to control the pressure of the hydraulic fluid at the outlet.

The hydraulic fluid used in the pump was di(2-ethylhexyl) sebacate which is a synthetic lubricant. This liquid was stored in a reservoir and was filtered before entering

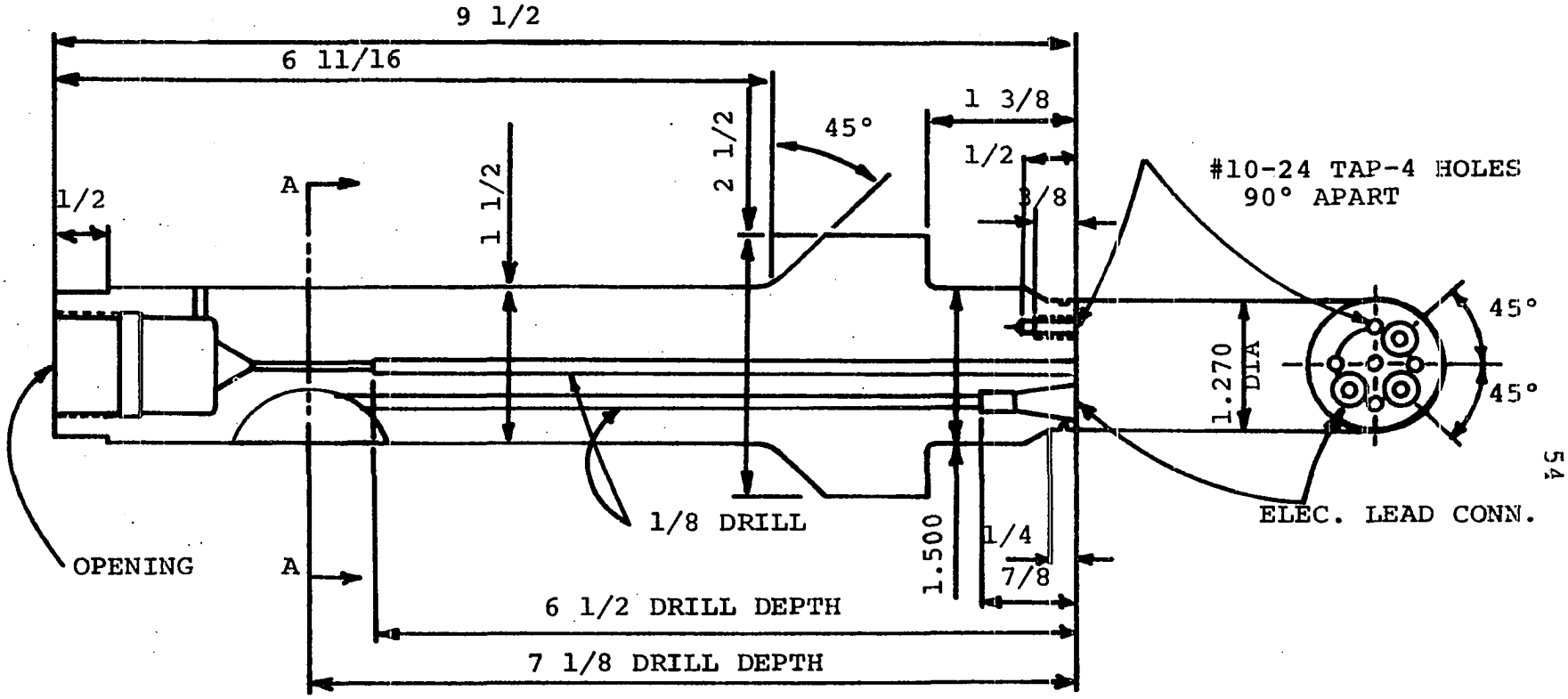

Figure 18. Bottom Cover of the Pressure Cell.

the pump. The pressure of the hydraulic oil from the pump outlet was transferred to the liquid under investigation through either of the two liquid separators as shown in Figure 19. Each of these separators was simply a cylinder containing a moving piston. The separation of the two liquids at each side of the piston was achieved by using one O-ring, supported by teflon back-up rings, at each end of the piston. The two separators provided for introducing the testing liquid into the pressure cell from either its top or bottom. The advantage of having this flexibility will be described later.

The liquid separator number 1, rated at 20,000 psig, was designed by Charng (14). This separator had 1-1/2 inch I.D., 4 inch O.D. and 17 inch internal length. The original piston used in this separator was made of aluminum, and the liquids at the two sides of the piston were separated by a single O-ring fitted in the groove cut at the middle of the piston. The relatively high compressibility of aluminum and presence of only one O-ring later proved to be inefficient in separating the two liquids. To improve separator performance, the aluminum piston was replaced with a brass piston with two-O-rings. The specifications for the brass piston are shown in Figure 20. Also, the O-rings used earlier by Charng for sealing the two end covers of separator number 1 were too thin and broke frequently during the compression of the liquid. These O-rings and their sealing grooves were subsequently modified and the problem was solved. The design of the new grooves

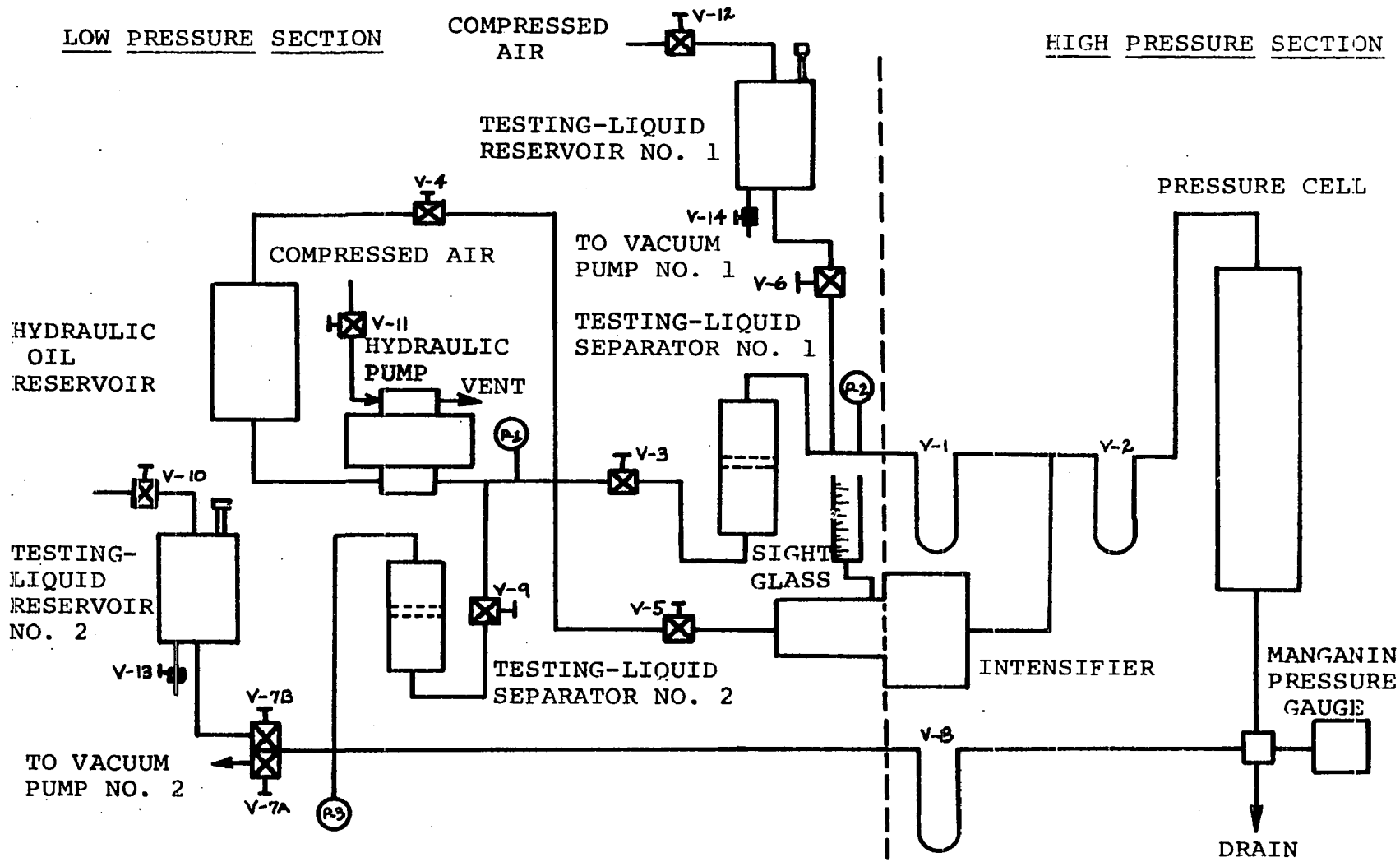

Figure 19. Schematic Diagram of the Pressure System.

CYLINDER

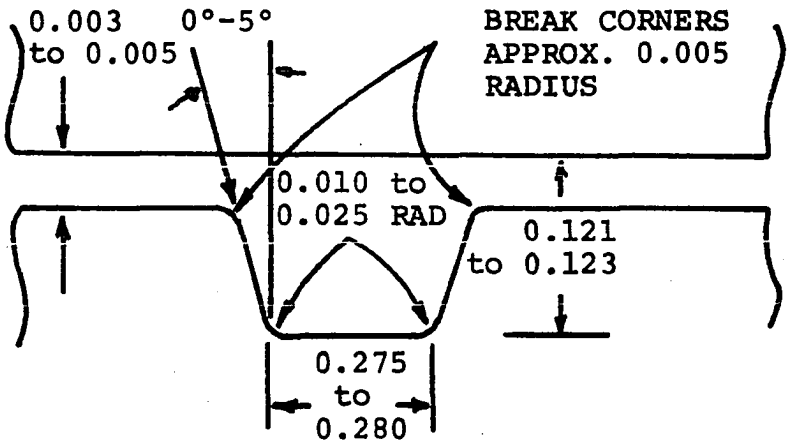

PISTON

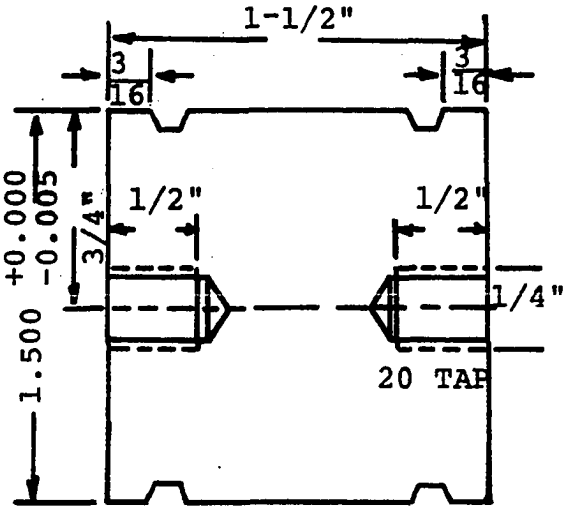

Figure 20. Design and Specifications of the Free Piston in Separator Number 1.

for the two end covers of separator number 1 are shown in Figure 20.

Liquid separator number 2 was a cylinder fabricated by Autoclave Engineers, Inc., It has an 1 inch I.D., 2 inch O.D., and 8-1/8 inch internal length. This separator was rated for a maximum pressure of 6,900 psig. A piston with 1 inch diameter and 1 inch length with the same groove specifications shown in Figure 20 was fabricated and used in this cylinder to provide separation of the testing liquid from the hydraulic oil.

To obtain pressures higher than about 20,000 psig, an intensifier was used. The intensifier had a working pressure of 200,000 psig and was designed and constructed by Harwood Engineering, Inc. The high pressure side of the intensifier was a shrink-fit duplex with 5/8 inch I.D., 6 inch O.D. and 4 inch internal length. The ratio of the areas of the pistons in the low and high pressure sections of the intensifier was 16:1; therefore, the intensifier was capable of multiplying the pressure at its low pressure end by 16 and delivering it at its high pressure end. In addition to the inlet and outlet openings at the low and high pressure ends of the intensifier, there was a third opening which was located on the low pressure side of the intensifier, adjacent to the high pressure side. This opening was used as a vent for the liquid in the cavity between the high and low pressure pistons of the intensifier during each pressure stroke. The

cavity was connected through the vent to a polyglass indicator which was graduated in 1/8 inch divisions. The change in the level of oil in this indicator was used as an indication of the location of the high pressure piston of the intensifier. Figure 21 shows the assembly diagram of the intensifier.

Pressure Measurement

Several conventional pressure gauges were used in the system (Figure 19) for measurements below 20,000 psig. These pressure gauges served as an approximate indication of the values of pressure in different parts of the system and showed if the pressurization was being carried out properly. Most importantly, they were used to ensure that pressure in each section was always kept below its design rating for safe operation.

For precise measurement of the pressure in the pressure cell, a manganin cell connected to a Carey-Foster type pressure measuring bridge was used. The manganin cell works on the principle that the resistance of a manganin wire increases with the pressure. Bridgman (8) observed that the resistance of a manganin wire increases linearly up to 13,000 atmospheres. This effect was then used as the basis of a pressure gauge which is widely used in scientific and laboratory work because of its rapid response and adaptability for automatic recording.

The manganin gauge used in this investigation had an active and a reference coil. The active coil was subjected

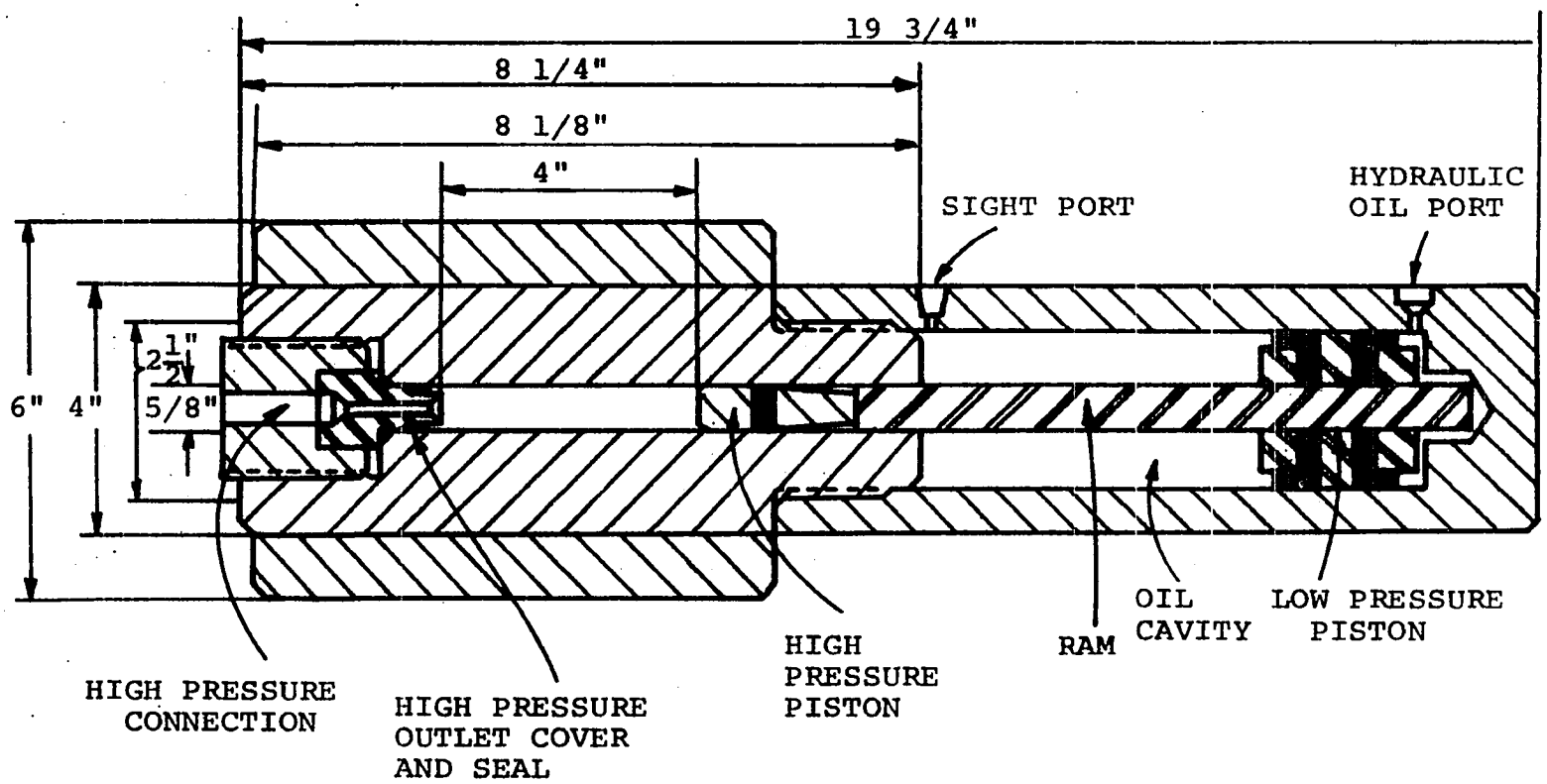

Figure 21. The Assembly Diagram of High Pressure Intensifier.

to the hydrostatic pressure to be measured. The reference coil was mounted very close to the active coil, where it would be at the same temperature but at atmospheric pressure. The two coils had the same resistance, and each formed one arm of the accompanying direct current bridge as shown in Figure 22. The other two arms of the bridge consisted of two

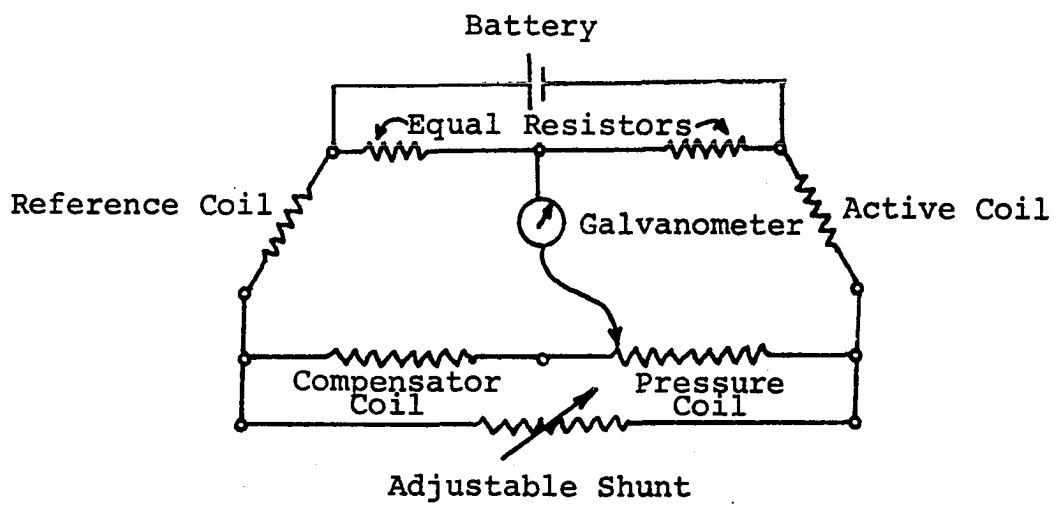

Figure 22. Schematic Diagram of the Pressure Measuring Equipment.

other equal resistance coils which were called the compensator and pressure coils. When the active coil was at atmospheric pressure, the bridge was balanced and the galvanometer did not show any deflection when the pressure dial was set on zero psig. If the active coil was subjected to a hydrostatic pressure, its resistance increased by an amount such as ΔR. This change in the resistance of the active coil threw the bridge out of balance. Since the bridge ratio was one-to-one, the balance could be restored by deducting $\Delta R/2$ from the arm

containing the active coil and by adding the same amount to the arm containing the reference coil. This operation was executed by shifting the pressure contact through the pressure dial on the bridge until the bridge was again balanced, as indicated by the zero deflection of the galvanometer. Thus the pressure could be directly read on the pressure dial of the bridge. Because the sensitivity of the galvanometer was essential in this measurement, a model 419A DC Null voltmeter by Hewlett-Packard Company was used. This voltmeter had a range of ± 3 μv to ±1,000 v DC, and an accuracy of ± (2 percent of end scale plus 0.1 μv).

The pressurization of the liquid in the system always generated some heat of compression which affected the pressure reading. In order to obtain the desired reading at steady state conditions, a fifteen to twenty minute period was required after each stage of compression. To have a clear indication that steady state conditions were achieved, the voltmeter was connected to a Leeds and Northrup Speedomax recorder. The decrease in the pressure of the system during the time when the adiabatic heat of compression was released was shown by the position change of the recorder pen. The pressure was read after there was no change in the position of the pen for at least ten minutes. If the position of the pen continuously changed after fifteen to twenty minutes following the compression, it indicated that a leak had developed somewhere in the system, which then had to be located and corrected.

Quartz Crystal

The quartz rod for this investigation was prepared by the Valpey-Fisher Corporation. It was a cylindrical rod cut out of a twin free single quartz crystal with the axis of the rod parallel to the "X" crystal axis of the original quartz crystal. The final dimensions of the quartz rod, after being polished with a 600 diamond abrasive on all surfaces, were 0.3753 inch diameter by 1.3010 inches long. The "Z" crystal axis of the quartz rod was determined by Professor van der Helm of the University of Oklahoma Chemistry Department; it was marked on the two flat ends of the crystal.

In order to provide a good support for the crystal inside the pressure cell and to keep it centered during the course of taking data, a 90° cone was machined on each end of the quartz rod as seats for the sapphire bearings of the crystal holder. Then, following the method first described by Mason (28) and later used by Rein (39, 40) and Charng (14), the crystal was coated:

1. The crystal was etched for about fifteen minutes in hydrofluoric acid and then rinsed in distilled water and dried. By this means a more uniform surface was obtained and the loose quartz dust possibly remaining from the machining of the rod was removed.
2. The crystal was then cleaned for about thirty minutes in aqua-regia to remove grease, finger prints and other foreign particles.

3. The cylindrical surface of the quartz rod was separated into four parts by attaching four tape strips, 1/16 inch wide, longitudinally on the surface of the crystal.
4. The crystal was then placed in a vacuum evaporation unit and mounted in a motor driven crystal holder which held the crystal by its two ends and rotated it at a speed of about 1/2 rpm.
5. A conductive gold film was evaporated on the surface of the crystal. The thickness of this coating was carefully controlled so that the surface was completely coated without getting a too thick coating (a thick coating usually flaked off).
6. The coated crystal was then taken out of the vacuum evaporation chamber, and the tape strips were removed from its surface which resulted in four separate electrodes. The electrical isolation of these electrodes was then tested by an ohmmeter and the resistance between each two electrodes was measured. A resistance of at least 100 megaohms was obtained for a good separation.

After the crystal was thus prepared, it had to be mounted inside the pressure cell. The mounting of the crystal was especially important because any slight slippage of the crystal during the period when the data was taken could cause a significant change in its resonant frequency, and therefore in the calculated viscosities. As a result, the mounting system reported by Rein, et al. (40) which had proved to be

successful in earlier experiments was adapted and used with some minor modifications. Figure 23 shows the details of the crystal mounting. The advantage of this mounting was that the weight of the crystal was supported by the sapphire bearings at the two ends of the crystal rather than by the electrical leads attached to the crystal. The latter mounting was found to be unreliable because the leads often broke off the crystal due to the crystal weight and vibrations (45). In this experiment the leads were attached to the quartz crystal with a small amount of E-Solder #3021 silver epoxy, made by Epoxy Products Company. This material was highly conductive and could be safely used up to 300°F without any loss in either conductivity or strength of the contact.

As mentioned earlier, the quartz crystal acted as the sensor of the viscometer; the changes in the resonant frequency of the crystal and its resistance at resonant frequency with various liquids, and various pressures and temperatures were used as the basis of determining the viscoelastic behavior of the liquids under investigation. The electronic components used to determine the resonant frequency and resistance at resonant frequency of the quartz crystal included an oscillator, impedance bridge, detector and frequency counter. Figure 24 shows a schematic diagram of these components which will now be described.

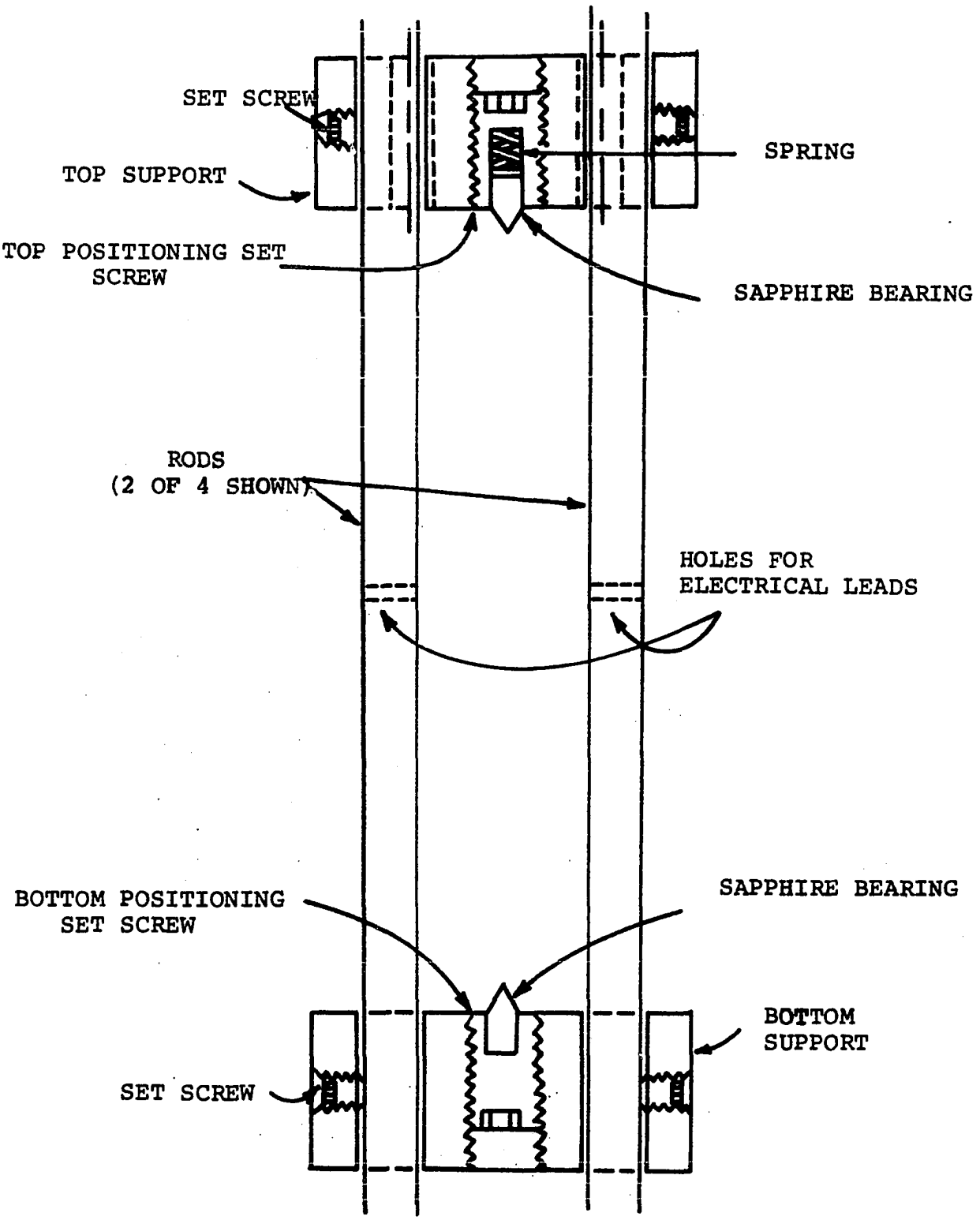

Figure 23. Details of an Improved Crystal Mounting.

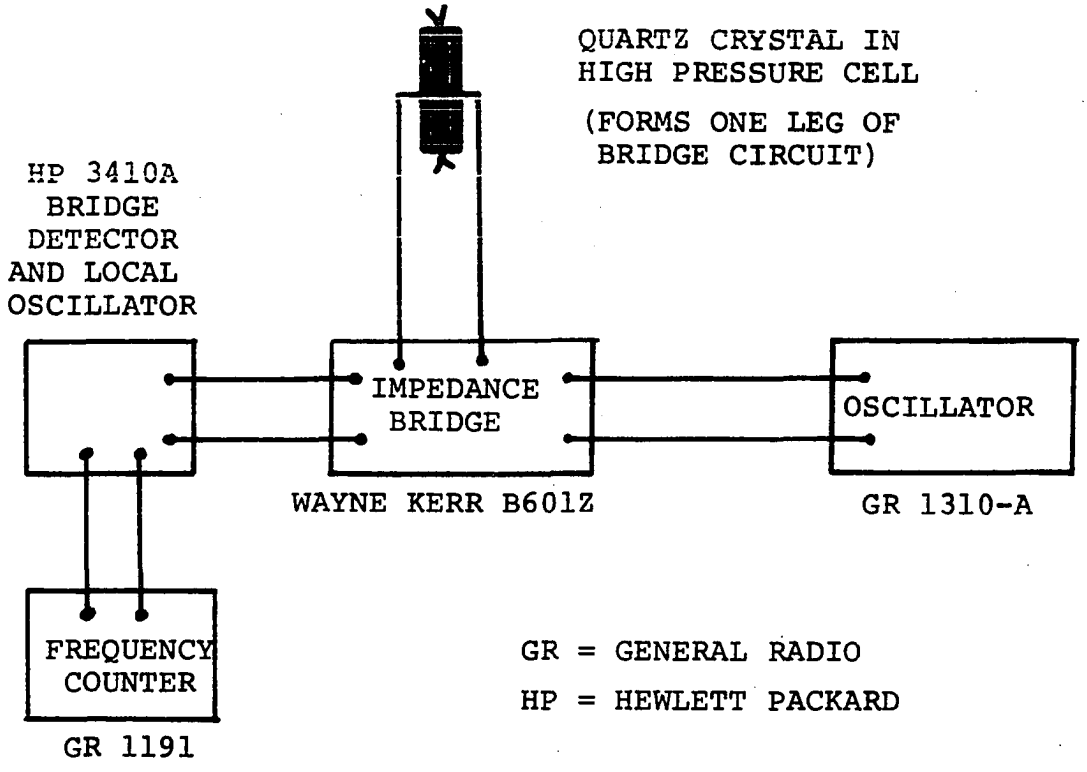

NOTE: ALL LEADS ARE SHIELDED.

Figure 24. Electronic Equipment Required for Measurements.

Oscillator

The oscillator was a type 1310-A manufactured by the General Radio Company. It had a frequency range of 3 Hz to 2 mHz in six decade ranges with 5 percent overlap between ranges (since in this investigation only one quartz crystal was used, only one of the frequency ranges could be utilized). The output amplitude of this oscillator could be varied from zero to twenty volts with a level-control knob. This relatively wide range of output level was very helpful to get the desired response in the liquids with various viscosities; a higher output level was necessary for a more viscous liquid.

High stability was another feature of this oscillator. According to the company's specification manual, the drift in the frequency after the warm-up period was less than 0.003 percent. This particular specification was quite essential in the accuracy of the measurements, because the viscosity and elasticity calculations both depended on the difference between the resonant frequency of the crystal in the testing liquid and inviscid fluid. These frequencies were usually very close to each other, especially for low viscosity liquids, and therefore a highly stable oscillator was required.

Impedance Bridge

The impedance bridge was a model B-601 manufactured by the Wayne-Kerr Company. The resistance and capacitance ranges of this bridge were 10 ohms to 10 megohms and 0.01 pF

to 20,000 pF, respectively. It could operate in a frequency range of 15 kHz to 5 mHz.

The quartz crystal formed one arm of the bridge. The other arm consisted of the resistance and reactance standards which could be adjusted by two dials on the bridge panel. The voltage was distributed between these arms in equal magnitude but in opposite directions. The difference between the impedances of the two arms caused a deflection in the indicating arm of a detector which was connected to the bridge. Through adjustment of the resistance and reactance dials on the bridge to provide a null indication on the detector, the resistance and reactance of the quartz crystal under any conditions of measurement could be determined.

The bridge was also provided with separate range factors and multiplier switches for the standards arm and the unknown impedance arm, respectively. The values of resistance and reactance of the unknown impedance could be obtained by multiplying the associated dial reading at balance by the above two factors. The resistance measuring accuracy on the lower portion of the dial was about ± 2 percent, but due to the arrangement of the readings on the dial this accuracy decreased to about ± 5 percent on the high end of the dial.

Detector

The detector was an a-c microvoltmeter model 3410-A manufactured by Hewlett-Packard Company. This detector was

a tunable phase locking voltmeter which could measure a-c voltages from 3 microvolts to 3 volts full scale. The detector had a narrow band filter which eliminated the effects of stray or undesirable signals. It was also equipped with a 4-volt square wave at the same frequency as the phase locked input signal which was used to drive the electronic counter for making precise frequency measurements. Also, when tuned to any discrete frequency between 5 and 600 kHz, the detector could indicate the amplitude of the signal present at the tuned frequency, rejecting all noise and non-harmonically related signals.

Frequency Counter

A General Radio model 1191 counter was used. It had the capability of measuring the frequency from zero to 20 mHz with a resolution up to 0.1 Hz and with gate times from 1 μs to 10 seconds. The gate times could be set by a range switch on the counter panel. With increased gate time, the number of oscillations was averaged over a longer period of time and therefore a more accurate measurement resulted. The measured frequency was displayed by an eight digit, high intensity neon read-out tube with automatically positioned decimal point and measurement dimensions.

It was previously mentioned that calculation of viscosity and elasticity of liquids depends on the difference between the frequency measurements. Therefore, in

measuring the frequency of the quartz crystal oscillation, precision was a very important requirement for the counter used. For the liquids with very low viscosity, the difference between the resonant frequency of the crystal immersed in the liquid and f_o, the resonant frequency of the crystal in an inviscid fluid, was very small (for example, 10-20 Hz). In these cases a more precise measurement could be achieved by using a 10-second gate time. The resulting frequency measurement was then precise to ± 0.1 Hz. For more viscous liquids, the difference between the two frequencies was larger, and therefore a gate time of one second was used. In these cases the resulting frequency measurements were precise to within ± 1 Hz.

Temperature Controller

Due to the significant effect of temperature on the viscosity of liquids, it was essential to control the temperature of the liquids very closely during each measurement. For this purpose a model 400 temperature controller, manufactured by Thermo-Electric Company, was used.

The heating of the pressure cell and the liquid inside was accomplished by four 750-watt strip-heater elements. These elements were bent in a circular shape and clamped on the outer surface of the pressure cell at equal distances. The power for these elements was supplied by the temperature controller. Since the working temperature of the pressure cell was 250°F, it was imperative that the heating of the

pressure cell be carried out in such a way that over-heating of the cell or hot spots would be prevented. This job was accomplished by using the controller to control the surface temperature of one of the strip heaters by installing a chromel-alumel thermocouple on the surface of the pressure cell in direct contact with the heating element. Since the power was distributed equally to all four elements, it did not matter under which element the thermocouple was installed. The temperature of the pressure cell could always be kept within its design range by controlling the temperature at the hottest point on the pressure cell, i.e., the surface of the heater in immediate contact with the cell.

The thermocouple mentioned above served as the sensor of the controller. The output of this thermocouple was measured by the controller and was compared against the desired value of temperature adjusted on the set point thumb wheel on the controller front panel. The power to the strip heaters was continuously supplied by the controller until the desired temperature was achieved.

By keeping the surface temperature of the pressure cell at the desired value, the whole pressure cell reached a steady state condition after a sufficient length of time. But due to the heat losses and the temperature gradient from the outer surface towards the inside of the pressure cell, the temperature of the liquid inside was obviously lower than the desired value. This problem was taken care of by

inserting another chromel-alumel thermocouple in the thermocouple well provided on the bottom cover of the pressure cell. The depth of this thermowell was sufficiently long to ensure a reading very close to the actual temperature of the liquid inside the pressure cell. This thermocouple was brought into a reference junction and connected to a Leeds and Northrup Speedomax recorder. The recorder had already been calibrated, and the expected position of the pen for each temperature was known. The recorder pen also served as a good indication of when the steady state condition was reached. If the recorder pen was below the expected value after the steady state condition was reached, the set point of the controller was adjusted manually until the recorder finally indicated the proper value.

Two of the heating elements (the ones installed at the upper and lower surface of the pressure cell) could be put out of service by a switch after the pressure cell reached the desired temperature. For this investigation, the temperature of the pressure cell was maintained with only two heaters. This precaution was originally intended to prevent overshoot or cycling at the set point which could have been caused by an on-off controller. However, the controller used in this investigation was equipped with a proportional power output over a span which extended above and below the set point, and therefore the problem of cycling and overshoot was automatically solved. The width of the proportional band could

be adjusted by a screw mounted on the front panel of the controller. The controller was also equipped with a deviation-indicating meter which continuously displayed the deviation of the actual temperature from the set value within 50°F above and below the set point.

Auxiliaries

The pressure system can be separated into a low pressure (under 20,000 psig) and a high pressure (up to 150,000 psig) section as indicated by the dashed line in Figure 19. Thus, the high pressure section is composed only of valves V-1, V-2 and V-8, the high pressure side of the intensifier, and the pressure cell or viscometer.

All the tubing (0.083 inch I.D. by 1/4 inch O.D., made of 304 stainless steel), fittings and valves used in the low pressure section had a minimum pressure rating of 30,000 psig. In the high pressure section, the tubing (1/32 inch I.D. by 3/16 inch O.D., made of 304 stainless steel) and fittings used were rated for 200,000 psig. Valves number 1, 2 and 8 were simply a U section of the tube which could be immersed in thermobottles containing liquid nitrogen. The liquid inside the tube solidified and formed an essentially leak-proof valve. These frozen valves, as they are called, were first introduced by Babb (4) and later used by Rein (39, 40, 41) and Charng (14).

Materials

The liquids used in this investigation can be divided into two groups. The first group consisted of normal pentane, normal octane, methyl-cyclohexane, toluene and sebacate. These liquids were used for calibration of the viscometer as will be described later. The second group of liquids consisted of those which were suspected of being viscoelastic. Determination of viscoelastic properties of the liquids in the second group was the main objective of this investigation. These liquids were prepared by dissolving crystals of polystyrene in toluene. Two polystyrenes with different molecular weights were used: S-109 with a weight average molecular weight of 193,000 and S-108 with a weight average molecular weight of 267,000. Both S-108 and S-109 polystyrenes had a ratio of weight average to number average molecular weight of 1.08. The solutions were prepared in 1, 2 and 3 weight percent concentrations.

In the calibration of the viscometer it was necessary to know the density and viscosity of the liquids used for calibration over the entire range of pressure and temperature of this investigation. In the following, the sources of density and viscosity data will be presented.

Density

The density data for normal pentane and normal octane were taken from Bridgman (9). Bridgman reported his data in terms of relative volumes based on the unit volume of the

liquid at 32°F and atmospheric pressure. These data for normal pentane and normal octane cover a pressure range from atmospheric to 10,000 kg/cm^2 at three different temperatures: 32°, 122° and 203°F. The density of either of the two liquids at each temperature and pressure could be easily obtained by dividing the density of that liquid at 32°F and atmospheric pressure by its relative volume at the desired condition. The density data thus obtained for each liquid were then linearly interpolated to get the necessary values at 77° and 100°F.

The relative volumes of methyl-cyclohexane at 77°F and from atmospheric pressure up to 10,000 kg/cm^2, again reported by Bridgman (10), were used to obtain the density versus pressure data of this liquid at 77°F.

During each pressure stroke of the intensifier, the liquid in the cavity between the low and high pressure pistons was pushed into a graduated sight glass. The change in the level of the liquid inside the sight glass not only served to indicate the relative position of the intensifier high pressure piston, but also the amount of liquid pushed into the pressure cell by forward movement of the piston. Therefore $(\Delta L)_o^P$, the accumulated change of the level in the sight glass from atmospheric pressure to any other pressure P, could be related to the compressibility of the liquid under investigation. During the pressurization of methyl-cyclohexane and normal octane in the pressure cell at 100°F, it was

observed that by subtracting 4 percent from $(\Delta L)_o^P$ of normal octane at each pressure P, the value of $(\Delta L)_o^P$ of the methyl-cyclohexane at that same pressure was obtained. Therefore the compressibility data of Bridgman (9) for normal octane at 100°F were corrected by 4 percent and were then used for calculating the density for methyl-cyclohexane at 100°F.

Similarly, considering the errors in the measurement and the possible leak around the packing of the high pressure piston of the intensifier, the corresponding values of $(\Delta L)_o^P$ for toluene and 1, 2 and 3 weight percent solutions of polystyrene in toluene proved to be equal at each temperature level as shown in Tables 1 and 2. These values were generally larger by about 2 to 3 percent at 100°F compared to the corresponding values at 77°F. Chang (13) has reported the density of toluene at 86°F and over a pressure range of 1 to 9,500 kg/cm^2. From his data the compressibility of toluene at 86°F over the above range of pressure was determined. According to the above discussion, these values could not be different from their corresponding values at 77° and 100°F by more than 1 to 1-1/2 percent, and therefore this error was ignored. Furthermore, the densities of toluene and 1, 2 and 3 weight percent S-108 and S-109 in toluene were also measured at 77° and 100°F and at atmospheric pressure by using a hydrometer. These measurements indicated that there were no measurable differences among the densities of the above liquids at these conditions. As a result, by combining the compressibility

TABLE 1

COMPARISON OF $(\Delta L)_o^P$ OF TOLUENE AND 1, 2 AND 3 WEIGHT PERCENT SOLUTIONS OF S-108 IN TOLUENE AT 77° AND 100°F

Pressure 10^3 psig	$(\Delta L)_o^P$ at 77°F, cm				$(\Delta L)_o^P$ at 100°F, cm			
	Toluene	1% S-108	2% S-108	3% S-108	Toluene	1% S-108	2% S-108	3% S-108
0	0	0	0	0	0	0	0	0
10	23.6	23.8	23.7	23.9	24.2	24.5	24.6	24.3
20	40.9	41.2	41.0	41.1	42.0	42.6	42.5	42.5
30	54.2	54.6	54.2	54.3	55.3	56.4	56.2	55.8
40	65.5	--	--	--	66.7	--	--	--
50	75.1	75.4	75.2	74.9	76.7	77.5	76.7	76.5
60	--	--	--	--	85.4	--	--	--
70	91.3	91.4	92.2	90.8	93.2	93.8	93.1	92.7
80	--	--	--	--	100.2	--	--	--
90	104.8	104.9	105.6	104.3	--	107.4	106.7	106.3
100	--	--	--	--	112.9	--	--	--
110	116.6	116.7	117.4	116.0	--	119.3	118.8	118.4
120	121.9	122.1	122.8	121.4	124.2	124.8	124.2	123.9

TABLE 2

COMPARISON OF $(\Delta L)_o^P$ OF TOLUENE AND 1, 2 AND 3 WEIGHT PERCENT SOLUTIONS OF S-109 IN TOLUENE AT 77° AND 100°F

Pressure 10^3 psig	$(\Delta L)_o^P$ at 77°F, cm				$(\Delta L)_o^P$ at 100°F, cm			
	Toluene	1% S-109	2% S-109	3% S-109	Toluene	1% S-109	2% S-109	3% S-109
0	0	0	0	0	0	0	0	0
10	23.6	23.9	26.3	22.9	24.2	25.2	24.2	25.7
20	40.9	41.0	43.4	40.0	42.0	42.8	42.0	43.5
30	54.2	54.5	56.8	53.5	55.3	56.2	56.7	57.3
40	65.5	--	--	--	66.7	--	--	--
50	75.1	75.2	77.4	74.1	76.7	77.3	77.7	78.4
60	--	--	--	--	85.4	--	--	--
70	91.3	91.4	93.4	90.3	93.2	93.8	94.2	94.7
80	--	--	--	--	100.2	--	--	--
90	104.8	105.1	107.0	104.0	--	107.5	108.1	108.4
100	--	--	--	--	112.9	--	--	--
110	116.6	117.1	118.9	115.9	--	119.6	120.0	120.4
120	121.9	122.5	124.4	121.2	124.2	125.0	125.6	125.8

data determined by Chang (13) with the reported values of density of toluene at 77° and 100°F and at atmospheric pressure, the densities of toluene and the polymer solutions at 77° and 100°F, over the entire pressure range, were obtained.

The values of density for sebacate at 77° and 100°F were directly taken from the ASME Pressure Viscosity Report (3). Appendix A gives the density values for calibration liquids.

Viscosity

Except sebacate, the source of viscosity data for all calibration liquids was Bridgman (11). The viscosity data of Bridgman has been reported at 86° and 167°F. To obtain the necessary data at 77° and 100°F, the Andrade Equation (1) was used.

$$\eta = A\, e^{B/T} \qquad (85)$$

The constants A and B were easily obtained from the knowledge of the viscosity at 86° and 167°F at each pressure level. Equation 85 together with the constants obtained for each pressure level were then used to calculate the viscosities at 77° and 100°F.

The source of viscosity data for di(2-ethylhexyl) sebacate was the ASME Pressure Viscosity Report (3). The values of viscosity of sebacate were directly reported at 77° and 100°F for a pressure range of atmospheric to 150,000 psig. The values of viscosities of calibration liquids are given in Appendix B.

TABLE 3

LOW SHEAR RATE VISCOSITIES OF 1, 2 AND 3 WEIGHT PERCENT S-108 AND S-109 POLYSTYRENES IN TOLUENE AT 77° AND 100°F

Temperature °F	Viscosity, centipoise					
	S-109			S-108		
	1%	2%	3%	1%	2%	3%
77	0.955	1.496	2.231	1.028	1.810	2.827
100	0.815	1.276	1.850	0.915	1.587	2.392

As mentioned in the discussion of the method of reduced variables, there was no need for viscosity versus pressure data of polymer solutions. The only viscosity values necessary in determination of viscoelastic properties of these liquids were their low shear rate viscosities at atmospheric pressure and at temperatures of measurements. For these determinations, two different size capillary viscometers were used, and the viscosity of each of the six polymer solutions (1, 2 and 3 weight percent solutions of S-108 and S-109 polystyrenes in toluene) were separately determined with each viscometer at 77° and 100°F. The average of the two viscosity values independently obtained with the two viscometers for each solution at each temperature was used to get a more accurate result. Table 3 shows the results of these measurements.

Normal pentane, normal octane, methyl-cyclohexane and toluene used in this investigation were of pure grade quality

(with minimum purity of 99 mol percent) and were purchased from Phillips Petroleum Company. The di(2-ethylhexyl) sebacate was purchased from Rohm and Haas Company under the commercial name of Plexol-201.

CHAPTER V

EXPERIMENTAL PROCEDURE

In this chapter the preliminary preparation and cleaning of the system, the pressure generation and calibration of the viscometer are discussed.

Preliminary Preparation and Cleaning of the System

Before introducing a new liquid into the system, the previous liquid had to be drained and the quartz crystal in the pressure cell had to be thoroughly cleaned. To evacuate the calibration or the unknown liquid already present in the system (not to be confused with the hydraulic oil), the drain near the manganin gauge (Figure 19, Chapter IV) was opened. The liquid remaining in separators number 1 and 2 and the high pressure side of the intensifier was pushed out by driving the pistons in each one of them all the way toward their testing liquid sides by closing valve number 4 and opening valves number 3, 5 and 9 and using the hydraulic pump to push the pistons. The completion of this process was shown by the first indication of pressure on the pressure gauge P-1. Then valves 3, 5 and 9 were closed, and by introducing compressed air into reservoirs 1 and 2, the testing

or the calibration liquid was forced out of the drain. By this procedure most of the liquid in the system was drained out, although usually some remained in the dead volumes. To get the remaining liquid out of the system, petroleum ether was introduced several times from reservoirs number 1 and 2 alternately, was kept in the system for about an hour, and then was drained. The petroleum ether thus diffused into the dead sections, diluted the liquid left in them, and carried the liquid out when it was drained. When the system was judged to be thoroughly clean, dry compressed air was blown into the system through reservoirs 1 and 2 for about two hours in order to evaporate any petroleum ether left in the dead sections. Finally, any remaining vapors were evacuated by using vacuum pumps number 1 and 2 for about 6 to 8 hours. The last check was to measure the resonant frequency and resistance of the quartz crystal at resonant frequency. These values were compared with the corresponding values obtained in the previous runs. A crystal resistance considerably higher than the previous values indicated that the crystal had not been thoroughly cleaned and some oil or other liquid was still left on its surface. In this case the system was washed with petroleum ether several more times and the above procedure was repeated.

To fill the system with a new liquid, the liquid was introduced into reservoir number 2 and was then pushed into the pressure cell through the bottom cover by means of

compressed air. The appearance of the liquid in the sight glass of reservoir number 1 indicated that the system was filled with the liquid. At this time valve number 7 was closed and additional liquid was added from the top of reservoir number 1 until the liquid filled about half of this reservoir. The additional liquid was necessary for subsequent pressurization of the liquid inside the pressure cell.

Introducing the liquid into the pressure cell through its bottom cover was done to sweep out the air present in the pressure cell. Filling the pressure cell from the top always left the possibility of having some air bubbles trapped around the quartz crystal. These air bubbles produced erroneous results in measurement of frequency and resistance of the crystal.

Pressurization of the System

At the beginning of this stage the pistons in the intensifier and in liquid separators number 1 and 2 were still at the end of their testing liquid sides. To pressurize the liquid in the pressure cell, liquid separator number 1 and the intensifier had to be filled with the testing liquid. For this purpose valve number 8 was closed by lowering the U-section of the tube into a thermobottle containing liquid nitrogen. Then valves number 5 and 9 were closed and valves 3, 4 and 6 were opened, and the liquid was introduced into liquid separator number 1 by means of compressed air. The

hydraulic oil originally present in liquid separator number 1 was thus drained into the oil reservoir and was replaced by the testing liquid. The pressure of the compressed air was not sufficient to overcome the friction of the high pressure piston of the intensifier; therefore, to fill the intensifier with testing liquid it was necessary to close valves number 2, 4, 5, 6 and 9 and then to use the hydraulic pump to generate a pressure of about 15,000 psig in liquid separator number 1 (as indicated on the pressure gauges P-1 and P-2). Then valve number 3 was closed and valves number 4 and 5 were opened. The pressure of the liquid in liquid separator number 1 pushed the intensifier piston all the way back towards the low pressure end and filled it with testing liquid. At this time the testing liquid side of the system was completely filled, and the pressurization could start.

It was mentioned previously that the hydraulic pump was capable of delivering a pressure of 27,500 psig and that liquid separator number 1 had a pressure rating of 20,000 psig. Pressurization of the system up to 20,000 psig could be achieved by utilizing only the hydraulic pump and liquid separator number 1. In fact when no density (or compressibility) measurements were required, the pressure to 20,000 psig was preferably generated without making use of the intensifier. This procedure was advantageous because it eliminated unnecessary wear of the packings of the high pressure piston of the intensifier. However, when the density

measurement was necessary, the generation of pressure from atmospheric to the highest pressure had to be achieved solely by the intensifier. To measure the density, the volume of the testing liquid pushed into the pressure cell (indicated by the changes in the level of the oil in the sight glass) had to be recorded. Further information on the method of density measurement can be found in References 14 and 40.

The pressurization of the liquid was carried out as follows (valve number 8 had to be kept closed all the time because the pressure rating of liquid separator number 2 was only 6,000 psig): Valves number 3, 4 and 1 were closed. Valves number 6 and 9 remained closed during the pressurization process. The testing liquid in the intensifier was pushed into the pressure cell by running the hydraulic pump. At this time the intensifier had to be filled again with the testing liquid. For this purpose valve number 2 was closed and the intensifier was refilled by driving the high pressure piston back according to the procedure earlier described. The recycling of the intensifier was carried out as many times as necessary to attain the required pressure.

To release the pressure of the system, the reverse procedure was employed; the testing liquid in the pressure cell was allowed to expand and drive the high pressure piston of the intensifier towards its low pressure end. Then valve number 2 was closed and the testing liquid, thus introduced into the high pressure side of the intensifier, was pushed

into testing liquid reservoir number 1 through valves number 1 and 6 by using the hydraulic pump to introduce hydraulic oil into the low pressure side of the intensifier. Valve number 1 was closed and valve number 2 was opened and the above procedure was repeated until the pressure dropped below 20,000 psig. At this time the pressure could be safely released through liquid separator number 1 by opening valves number 3 and 4.

The addition of liquid separator number 2 was originally intended to serve the following purpose: It had been noticed earlier (40) that some of the testing liquids, especially the more viscous ones, froze in the transfer line connecting the intensifier to the pressure cell, at a pressure well below the design pressure of the pressure cell. To utilize the whole range of pressure of the pressure cell it was suggested (40) that pentane, which could be compressed to 150,000 psig at room temperature without freezing in the transfer line, be used as a means of transmitting the pressure from the intensifier to the testing liquid in the pressure cell. A freely moving piston was then designed for the pressure cell which transferred the pressure from normal pentane to the testing liquid and at the same time isolated each liquid from the other. The testing liquid was pushed from liquid reservoir number 2 into the pressure cell either by means of the compressed air or the hydraulic pump and liquid separator number 2. The piston in the pressure cell was

forced all the way to the top of the pressure cell by introducing more liquid into the pressure cell from the bottom. Arrival of the piston at the top of the pressure cell was indicated by pressure gauges P-2 and P-3. At this condition, introduction of more liquid continuously increased the pressure in the bottom side of the pressure cell which was indicated by P-3 and the manganin gauge while P-2 indicated no pressure. Subsequently, valve number 8 was closed and the testing liquid in the pressure cell was pressurized from the top by the method described above. The calculations performed for this design indicated that if the pressurization started with the piston at the top of the pressure cell, a pressure of 150,000 psig could be achieved without the piston touching the crystal and its holder which were mounted on the bottom cover. This method was successfully used for several runs, but, unfortunately, sometimes during the depressurization process, the piston had cocked inside the pressure cell and had not moved to the top of the pressure cell. Subsequent pressurization had forced the piston downward and badly damaged the quartz crystal and its holder (Figure 25). For this reason, and since the position of the piston could not be predicted with complete certainty, this idea was abandoned and the piston was removed from the pressure cell to prevent other such accidents.

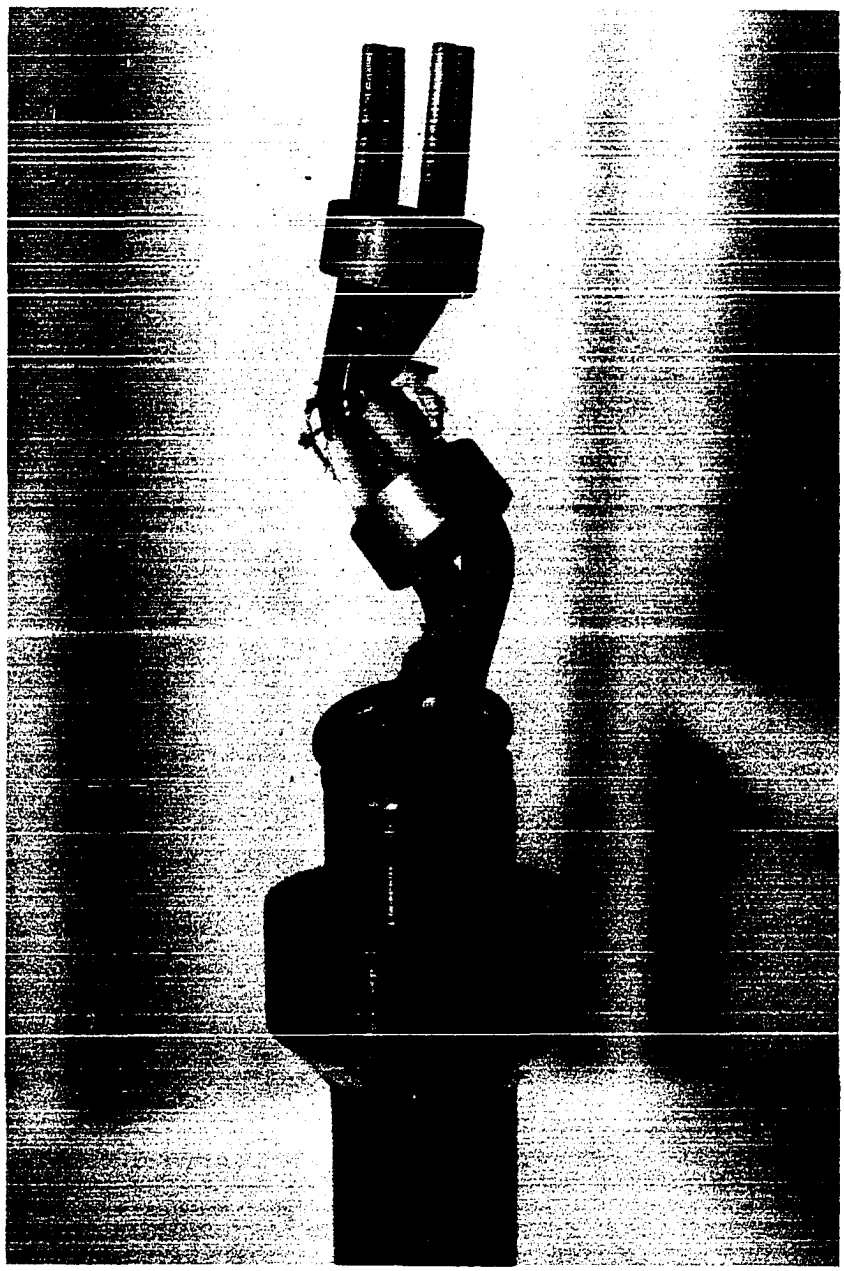

Figure 25. Damaged Crystal and Crystal Holder.

Calibration of the Viscometer

The quartz crystal viscometer could be used for determining the viscoelastic properties of the unknown liquids only after it was calibrated against the liquids having known viscosity and density (the need for density information on both calibration and unknown liquids is apparent from Equations 64 to 71 in Chapter III).

Calibration of the viscometer means determining the constants K_f, K_R, f_o and R_{E_o} of the quartz crystal at each particular pressure and temperature. Equations 70 and 71 indicate that the values of resonant frequency and resistance at resonant frequency of the crystal in Newtonian liquids can be linearly plotted as a function of $(\pi f \rho \eta)^{1/2}$ for those liquids. Each data point on such plots corresponds to the resonant frequency f, or the resistance at the resonant frequency R_E, and the corresponding value of $(\pi f \rho \eta)^{1/2}$ for one particular liquid. The data points of each plot are all at the same pressure and temperature.

Considering the quartz crystal as a series combination of resistance, capacitance and inductance, it is clear that at the resonant frequency the reactances of the capacitance and inductance will be equal in magnitude and opposite in direction and, therefore, cancel each other out. At this condition the crystal has its maximum conductance. This information was used to determine the resonant frequency of the crystal in each liquid at each condition; the frequency of

oscillation of the crystal was changed by changing the frequency of the oscillator, and for each frequency the resistance of the crystal was measured by the bridge. The frequency corresponding to the minimum resistance was taken as the resonant frequency. In practice this value was calculated by fitting a polynomial of the second degree to the data according to the least squares technique and then finding the minimum resistance by differentiation. Figure 26 shows a typical example of such data.

The shape of the curve shown in Figure 26 is highly dependent upon the viscosity of the medium in which the quartz crystal is submerged. If the medium is relatively inviscid, like air or liquids with low viscosities, the curve is very sharp and the resistance is low and very sensitive to the changes in frequency. At these conditions the minimum resistance is quite distinct and can be determined accurately. However, for viscous liquids the curve assumes a flat shape, and measurement over a very wide range of frequency is required to approximate the minimum value of resistance and the resonant frequency of the crystal. Also, for viscous liquids the values of resistance are very high and cannot be read accurately on the resistance dial of the bridge. To bring the values of the resistance of the crystal to a lower range and increase the readability on the bridge dial, a 1.5 megohm resistor was connected to the bridge terminals in parallel with the crystal and thus the effective resistance was lowered.

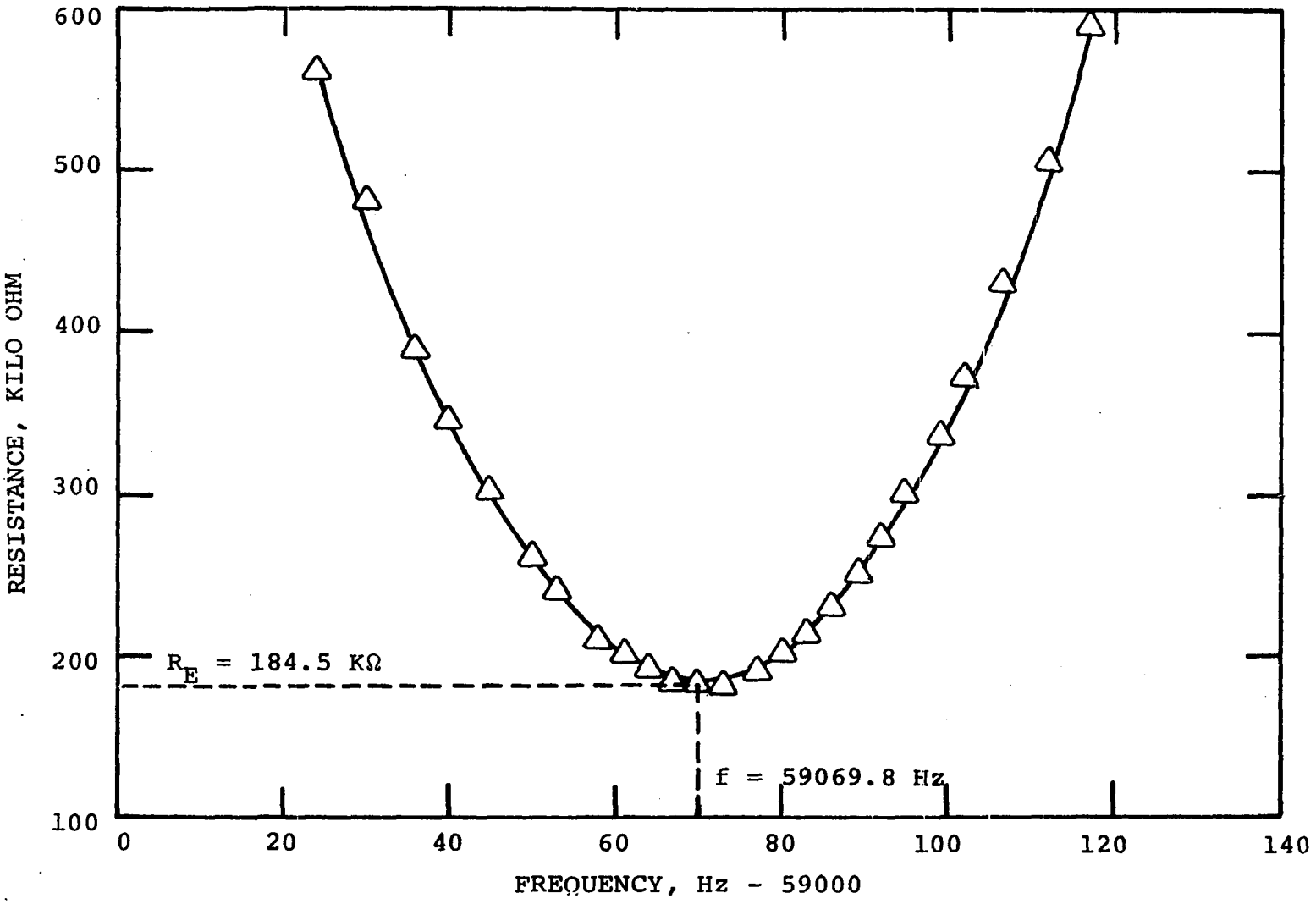

Figure 26. Typical Data for Determining Resonant Frequency (Data for Methyl Cyclohexane at 20,000 psig and 77°F).

The actual resistance of the crystal in these cases were calculated from the following relation for parallel resistors.

$$1/R_m = 1/1500 + 1/R_c \qquad (86)$$

In the above equation R_m is the measured resistance and R_c the actual resistance of the crystal, both in kilo ohms.

Sometimes during the experiment it was observed that the resistance was always very high and the slope of the resistance versus frequency curve remained unchanged no matter how high or low the viscosity of the liquid. Very large resistances indicated that the leads were broken off the crystal and therefore no response could be obtained. In these cases the crystal was removed from the pressure cell, the malfunction was corrected and the crystal was remounted in the pressure cell. Removal of the crystal from the pressure cell necessitated a new calibration of the viscometer.

After the values of resonant frequency and resistance at resonant frequency were obtained for different liquids at one particular temperature and pressure, they were plotted against $(\pi f \rho \eta)^{1/2}$ and their slopes and intercepts were determined. These slopes and intercepts were then used as K_f, K_R, f_o and R_{E_o} of the quartz crystal at the conditions of measurement. An example of such plot is shown in Figure 27. Equations 70, 71 and the plots of R_E and f versus $(\pi f \rho \eta)^{1/2}$ (similar to the one shown in Figure 27) confirm the linear relationship between these values. However, sometimes the

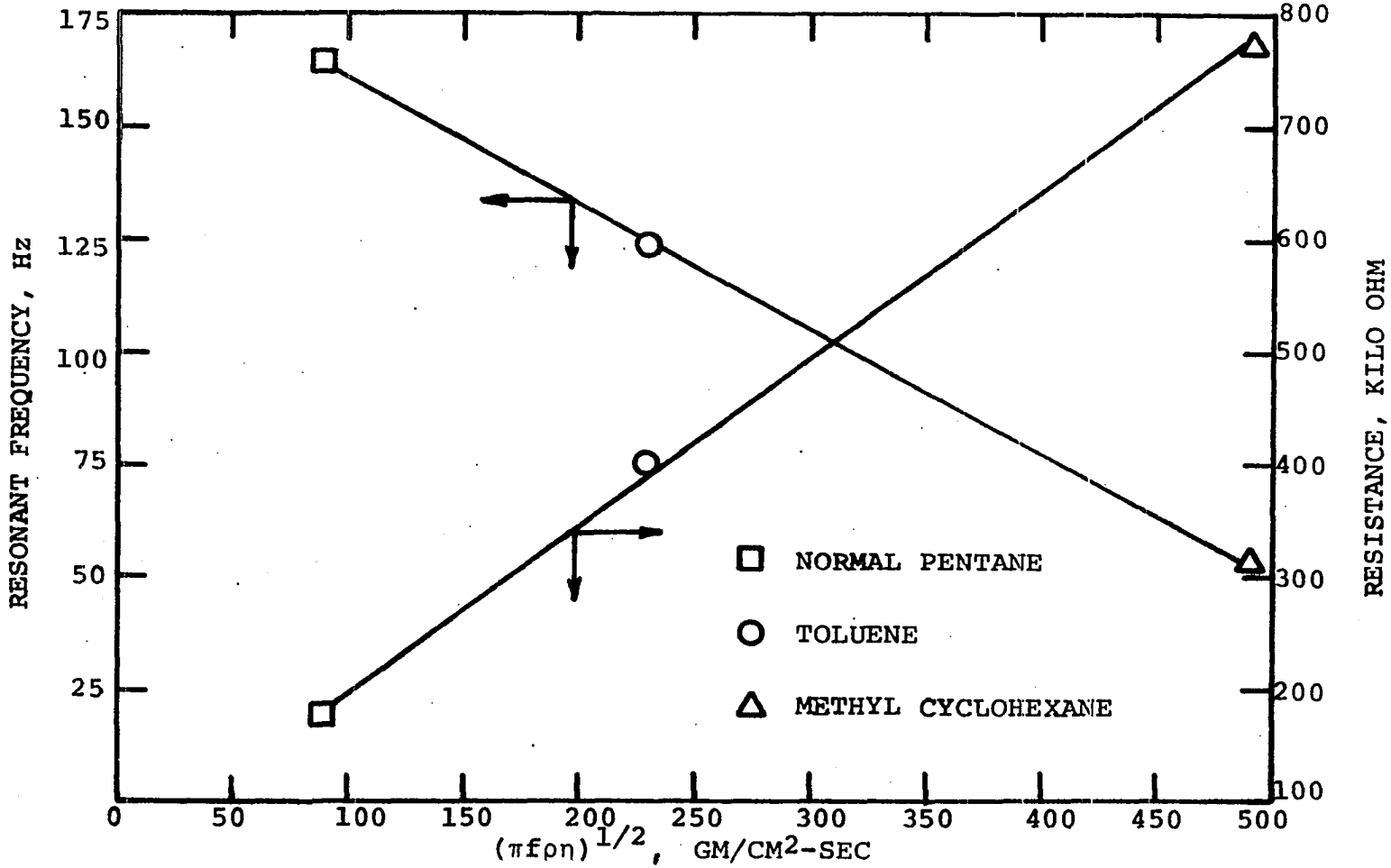

Figure 27. Typical Plot of R_E and f as a Function of $(\pi f \rho \eta)^{1/2}$. Measurements at 77°F and 110,000 psig.

values of resistance and frequency thus plotted did not result in a linear relationship. This nonlinearity was usually caused by leads not being connected exactly to the middle of the quartz crystal, so that the crystal oscillated in a longitudinal mode as well as in pure torsional shear. The longitudinal oscillation is especially significant when a shorter crystal is used because the middle point of the crystal cannot be marked accurately and the relative error is more pronounced. In the case of the 59 kHz crystal used in this investigation this relative error always existed and some scatter in the data around the linear relation was usually observed.

To eliminate extra time and effort necessary to clean the system, the liquid under investigation was not drained until all the data for different pressures at one particular temperature were taken. Therefore the plots of resonant frequency and resistance at resonant frequency versus $(\pi f \rho \eta)^{1/2}$ could not be prepared and the calibration constants could not be determined until the measurements on all calibration liquids at one temperature were completed. This procedure had its own shortcomings; that is, the crystal malfunction causing nonlinearity of the plots could not be predicted and corrected until measurements on all calibration liquids were completed.

CHAPTER VI

RESULTS AND DISCUSSION

In this chapter the calibration results are presented first, and the dependence of the calibration parameters on pressure is discussed. Next, the results of measurements of the viscoelastic properties of the polymer solutions are presented, and the effects of pressure, temperature, concentration and molecular weight of the polymers on the viscoelastic properties are discussed.

Calibration Parameters

The liquids used to calibrate the viscometer were normal pentane, normal octane, methyl-cyclohexane, toluene and di(2-ethylhexyl) sebacate. The use of normal octane for calibration was limited to pressures less than 70,000 and 80,000 psig at 77° and 100°F, respectively, because this fluid froze in the transfer line at higher pressures. Similarly, sebacate could only be used at pressures below 50,000 and 70,000 psig at 77° and 100°F, respectively. However, normal pentane, methyl-cyclohexane and toluene could be used for calibration over the entire pressure range of 0-120,000 psig.

As previously mentioned, the quartz crystal was calibrated by finding the linear relations, f versus $(\pi f\rho\eta)^{1/2}$ and R_E versus $(\pi f\rho\eta)^{1/2}$, for the calibration liquids. Therefore, for each calibration fluid, the resonant frequency, f, and the resistance at resonant frequency, R_E, of the quartz crystal were measured at 77° and 100°F over the entire range of pressures. The results for each calibration fluid are given in Tables 4 and 5.

In order to determine the calibration parameters the values of f and R_E obtained in different calibration liquids, at each particular pressure and temperature, were then fitted as straight lines by least squares according to Equations 70 and 71.

$$f - f_o = K_f (\pi f\rho\eta)^{1/2} \tag{70}$$

$$R_E - R_{E_o} = K_R (\pi f\rho\eta)^{1/2} \tag{71}$$

The slopes and intercepts of these straight lines were then taken as the calibration parameters, as described earlier. The resulting values of f_o, R_{E_o}, K_f and K_R are summarized in Tables 6 and 7 for 77° and 100°F, respectively.

In order to determine the viscoelastic properties of unknown solutions at pressures other than those at which the calibrations were actually performed, correlations of the effect of pressure on the calibration constants were developed. These correlations gave continuous functions rather than discrete values of calibration constants in terms of pressure and were more convenient for computer applications.

TABLE 4

RESONANT FREQUENCY AND RESISTANCE AT RESONANT FREQUENCY OF THE QUARTZ CRYSTAL IN VARIOUS CALIBRATION LIQUIDS AT 77°F

Liquid	P 10^3 psig	ρ g/cc	η poise	f Hz	R_E k ohms	$(\pi f \rho \eta)^{1/2}$ g/cm^2-sec
Normal pentane	0	0.622	0.002324	59074.7	63.886	16.379
	10	0.683	0.00399	59077.4	73.462	22.490
	20	0.720	0.0060	59081.8	86.294	28.317
	30	0.747	0.00823	59085.9	90.120	33.781
	40	0.768	0.0109	59096.2	104.447	39.423
	50	0.787	0.0140	59102.0	115.989	45.230
	70	0.816	0.0217	59118.2	138.047	57.347
	90	0.841	0.0338	59142.0	160.476	72.674
	110	0.862	0.050	59164.3	176.242	89.504
	120	0.871	0.062	59177.3	190.791	100.198
Normal octane	0	0.698	0.005112	59065.6	113.1	25.7
	10	0.747	0.0095	59069.0	111.3	36.3
	20	0.776	0.0154	59070.1	123.9	47.1
	30	0.797	0.0238	59073.6	151.5	59.3
	40	0.815	0.0353	59079.6	169.2	73.1
	50	0.832	0.0510	59083.3	191.6	88.7
	70	0.863	0.0990	59096.4	241.4	125.9
Toluene	0	0.863	0.005548	59069.5	90.6	29.8
	10	0.905	0.0089	59066.6	123.1	38.7
	20	0.934	0.01301	59071.7	129.2	47.5
	30	0.959	0.0183	59076.0	146.7	57.1
	40	0.977	0.0261	59081.5	166.9	68.8
	50	0.994	0.0367	59087.6	179.1	82.3
	70	1.025	0.0716	59100.2	234.4	116.7
	90	1.052	0.134	59112.7	308.4	161.8
	110	1.073	0.265	59122.7	400.4	229.8
	120	1.082	0.375	59126.1	466.7	274.5
Sebacate	0	0.912	0.1744	59029.2	355.7	171.7
	10	0.949	0.51	59000.2	567.0	299.5
	20	0.973	1.20	58958.4	796.1	465.0
	30	0.995	2.69	58904.3	1119.7	703.8
	40	1.013	5.50	58838.5	1479.2	1014.8
	50	1.029	11.0	58751.8	1943.9	1445.4

TABLE 4--Continued

Liquid	P 10^3 psig	ρ g/cc	η poise	f Hz	R_E k ohms	$(\pi f \rho \eta)^{1/2}$ g/cm^2-sec
Methyl-cyclo-hexane	0	0.767	0.006875	59070.1	120.8	31.3
	10	0.8065	0.0136	59076.7	164.5	45.1
	20	0.840	0.0240	59069.8	184.6	61.2
	30	0.859	0.0392	59070.4	231.0	79.0
	40	0.880	0.0624	59077.3	255.0	101.0
	50	0.897	0.099	59078.9	266.7	128.4
	70	0.9275	0.230	59081.3	366.6	199.0
	90	0.951	0.575	59073.3	542.1	318.6
	110	0.970	1.34	59053.4	772.6	491.1
	120	0.978	2.02	59033.5	940.7	605.3

TABLE 5

RESONANT FREQUENCY AND RESISTANCE AT RESONANT FREQUENCY OF THE QUARTZ CRYSTAL IN VARIOUS CALIBRATION LIQUIDS AT 100°F

Liquid	P 10^3 psig	ρ g/cc	η poise	f Hz	R_E K ohms	$(\pi f \rho \eta)^{1/2}$ g/cm^2-sec
Normal pentane	0	0.609	0.00203	59078.7	43.2	15.1
	10	0.674	0.00354	59081.3	53.1	21.0
	20	0.714	0.00538	59085.5	63.4	26.7
	30	0.742	0.00735	59091.2	73.0	31.8
	40	0.7645	0.0097	59098.5	83.3	37.1
	50	0.782	0.0121	59107.0	93.1	41.9
	60	0.797	0.0154	59116.0	103.0	47.7
	70	0.811	0.0189	59126.2	113.2	53.3
	80	0.825	0.0235	59137.5	123.4	60.0
	100	0.847	0.0348	59160.9	142.9	74.0
	120	0.8665	0.0514	59188.5	162.8	91.0
Normal octane	0	0.687	0.004438	59076.9	81.2	23.8
	10	0.739	0.0080	59082.3	100.3	33.1
	20	0.769	0.0129	59076.4	117.9	42.9
	30	0.792	0.020	59082.3	131.9	54.2
	40	0.811	0.0291	59089.0	148.6	66.2
	50	0.828	0.0412	59096.2	170.7	79.6
	60	0.843	0.0564	59103.0	192.4	94.0
	70	0.857	0.0779	59111.2	213.6	111.3
	80	0.871	0.105	59118.9	243.9	130.3
Toluene	0	0.8502	0.004789	59072.2	115.8	27.5
	10	0.8922	0.0076	59075.9	109.4	35.5
	20	0.9222	0.0111	59080.9	122.0	43.6
	30	0.9452	0.0154	59085.3	147.3	52.0
	40	0.9642	0.0214	59090.7	154.8	61.9
	50	0.9807	0.0293	59092.4	173.0	73.0
	60	0.997	0.0398	59099.2	194.9	85.8
	70	1.012	0.0542	59107.2	212.7	100.9
	80	1.027	0.074	59114.0	240.6	118.8
	100	1.049	0.137	59128.6	304.4	163.4
	120	1.069	0.248	59142.5	390.6	221.9

TABLE 5--Continued

Liquid	P 10^3 psig	ρ g/cc	η poise	f Hz	R_E K ohms	$(\pi f \rho \eta)^{1/2}$ g/cm^2-sec
Methyl-cyclo-hexane	0	0.756	0.005729	59072.2	96.8	28.4
	10	0.7954	0.0111	59075.7	103.2	40.5
	20	0.829	0.0195	59078.0	126.9	54.8
	30	0.848	0.0312	59083.2	164.1	70.1
	40	0.869	0.049	59083.0	189.6	88.9
	50	0.886	0.0765	59084.7	238.9	112.2
	60	0.902	0.116	59090.0	273.8	139.4
	70	0.9164	0.175	59091.6	323.7	172.5
	80	0.929	0.268	59091.3	385.4	215.0
	100	0.950	0.620	59092.8	513.0	330.7
	120	0.967	1.34	59079.8	742.5	490.4
Sebacate	0	0.903	0.1118	59036.6	274.1	136.8
	10	0.9405	0.290	59018.6	411.8	224.9
	20	0.967	0.67	58991.7	590.7	346.5
	30	0.989	1.41	58957.0	882.7	508.2
	40	1.008	2.75	58912.3	1138.0	716.3
	50	1.024	5.27	58850.3	1395.4	998.9
	60	1.039	9.6	58777.3	1752.6	1357.1
	70	1.052	17.3	58683.6	2274.8	1831.7

TABLE 6

VALUES OF CALIBRATION CONSTANT FOR THE QUARTZ CRYSTAL AT 77°F AND AT VARIOUS PRESSURES

P 10^3 psig	f_o Hz	$\Delta f_o(P)$ Hz	$-K_f$	R_{E_o} K ohms	K_R
0	59077.2	0	0.280	50.8	1.76
10	59082.1	4.9	0.273	56.6	1.71
20	59086.0	8.8	0.275	57.3	1.59
30	59091.8	14.6	0.267	68.4	1.50
40	59102.0	24.8	0.260	75.6	1.39
50	59109.3	32.1	0.278	32.0	1.29
70	59131.4	54.2	0.260	44.0	1.61
90	59160.2	83.0	0.276	52.2	1.54
110	59187.7	110.5	0.275	50.6	1.48
120	59205.1	127.9	0.284	49.9	1.48

TABLE 7

VALUES OF CALIBRATION CONSTANTS FOR THE QUARTZ CRYSTAL AT 100°F AND AT VARIOUS PRESSURES

P 10^3 psig	f_o Hz	$\Delta f_o(P)$ Hz	$-K_f$	R_{E_o} K ohms	K_R
0	59083.2	0	0.342	46.2	1.67
10	59087.1	3.9	0.305	56.5	1.58
20	59093.7	10.5	0.294	49.0	1.59
30	59099.2	16.0	0.280	46.9	1.64
40	59109.4	26.2	0.300	57.0	1.51
50	59120.6	37.4	0.317	68.0	1.33
60	59129.6	46.4	0.284	52.1	1.58
70	59140.1	56.9	0.284	40.2	1.64
80	59153.7	70.5	0.292	40.6	1.60
100	59176.4	93.2	0.259	51.8	1.42
120	59208.3	126.1	0.266	48.9	1.43

A random variation of K_f and R_{E_o} with respect to pressure is shown in Tables 6 and 7. Therefore, it was concluded that K_f and R_{E_o} are independent of pressure, in agreement with conclusions of other investigators (2, 14, 39, 40). The means and standard deviations of K_f and R_{E_o} at 77° and 100°F are shown in Table 8.

TABLE 8

MEANS AND STANDARD DEVIATIONS OF K_f AND R_{E_o}

Temperature °F	K_f		R_{E_o}	
	Mean	Standard Deviation	Mean	Standard Deviation
77	-0.273	8.1×10^{-3}	53.7	12.1
100	-0.293	2.3×10^{-2}	50.7	7.9

Defining Δf_o by

$$\Delta f_o(P) = f_o(P) - f_o(atm) \tag{87}$$

where $f_o(P)$ and $f_o(atm)$ are the intercepts of the straight lines for f versus $(\pi f \rho \eta)^{1/2}$ at pressure P and atmospheric pressure, respectively, Tables 6 and 7 indicate that Δf_o is a function of pressure and increases with increasing pressure. Figures 28 and 29 show plots of $\Delta f_o(P)$ at 77° and 100°F, respectively. The curve shown on each plot is a least-squares polynomial whose equation is indicated in each figure.

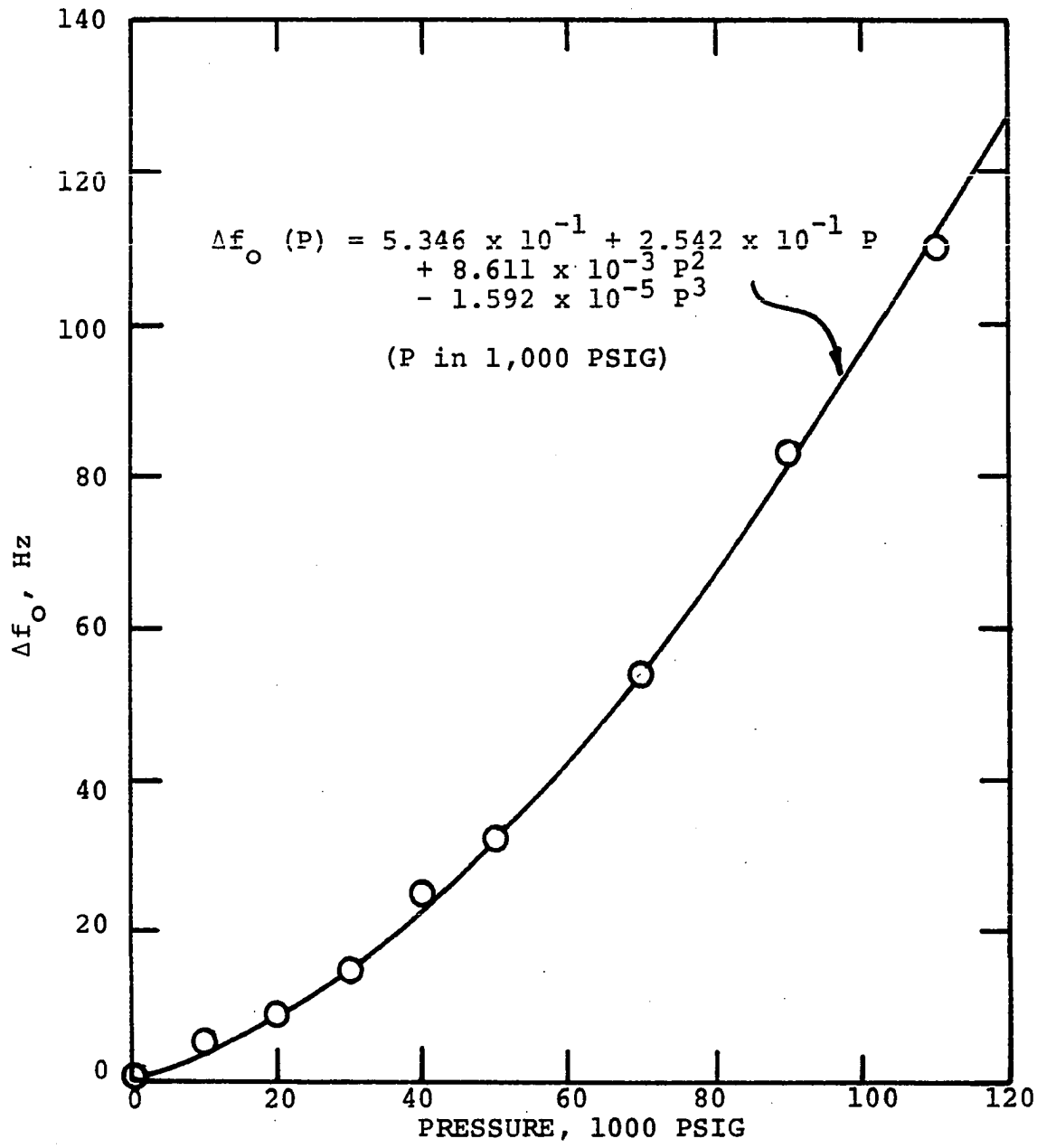

Figure 28. Effect of Pressure on Δf_o at 77°F.

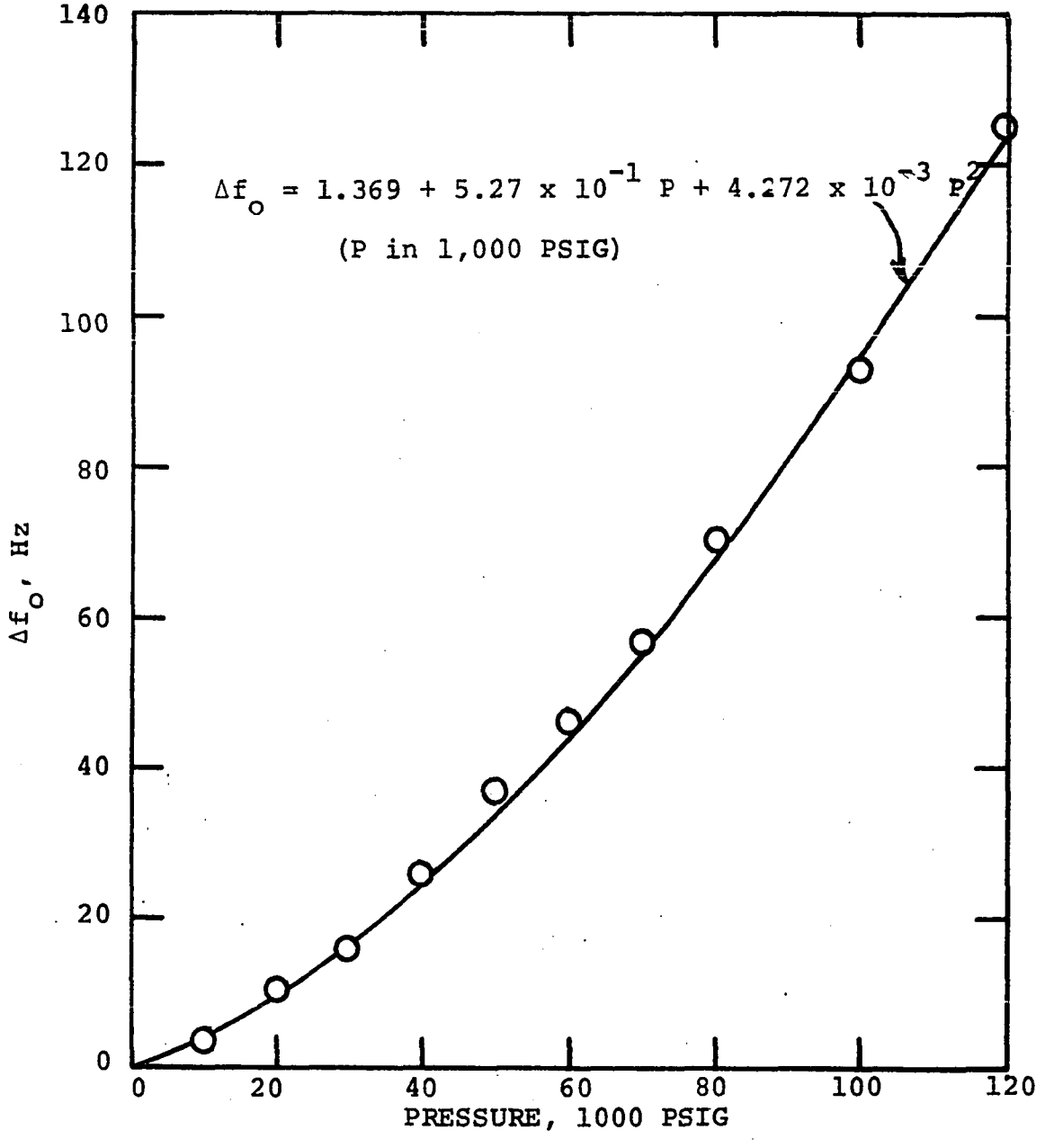

Figure 29. Effect of Pressure on Δf_o at 100°F.

To provide a common basis for comparing the dependence of Δf_o on pressure with the results of other investigators (14, 39, 40, 42), a least-squares parabola for $\Delta f_o/f_o$ as a function of pressure at 100°F was determined. In Figure 30, the least-squares parabola obtained in this investigation is compared with the corresponding curves obtained by Charng (14) and Rein (42). The units of pressure reported by Rein (42) are in kilo atmospheres; these data were converted to psig to provide a consistent set of units. Figure 30 indicates a close agreement among the $\Delta f_o/f_o$-pressure curves obtained in the three investigations. Table 9 gives the values of the parameters for each curve shown in Figure 30. With the exception of the first parameter, which rapidly loses its significance as the pressure increases, a close agreement among the parameters is also noticed.

TABLE 9

COMPARISON OF PARABOLIC CONSTANTS OF
$\Delta f_o/f_o = a_o \times 10^{-6} + a_1 \times 10^{-9} P + a_2 \times 10^{-14} P^2$*

Parameters	This Investigation	Charng (14)	Rein (42)
a_o	-0.222	-7.99	-0.690
a_1	8.84	7.57	7.63
a_2	7.47	8.76	9.47

*P is in psig.

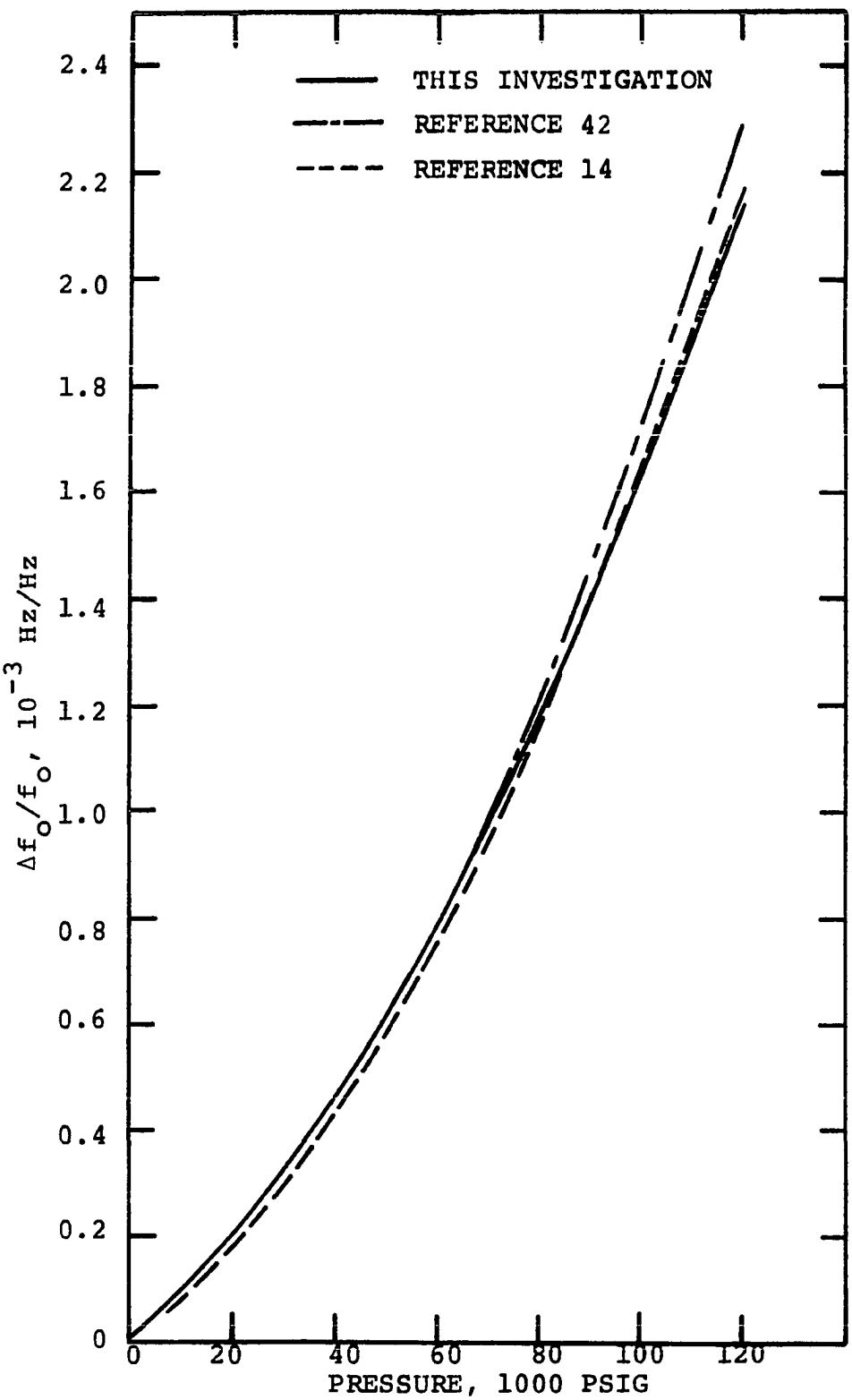

Figure 30. Comparison of the Pressure Effect on $\Delta f_o/f_o$ for Various Investigations.

The K_R values show more dispersion and it is difficult to arrive at a definite conclusion regarding the dependence of K_R on pressure. The values of K_R obtained at each temperature (Tables 6 and 7) were separately correlated with pressure by means of various function. To determine what function gives the best overall results the correlations obtained for $\Delta f_o(P)$ and the average values of R_{E_o} and K_f were used together with various correlations of K_R with pressure at each temperature to calculate the viscosity of the calibration liquids according to the method to be discussed shortly. The values of viscosity thus calculated were then compared with the reported values of the viscosity of the calibration liquids. It was observed that among various functions used to correlate K_R with pressure, the relations indicated in Figures 31 and 32 resulted in the least overall average deviation between reported and calculated viscosities at 77° and 100°F, respectively. These correlations were therefore used for later calculations of viscoelastic properties of polymer solutions.

The viscosity of the calibration liquids were calculated according to the following method: Using the values of K_R, K_f, R_{E_o} and f_o together with the measured values of f and R_E in each of the calibration liquids at a particular pressure and temperature, X_M and R_M were calculated by means of Equations 68 and 69.

$$X_M = \frac{f - f_o}{K_f} = \frac{\Delta f}{K_f} \qquad (68)$$

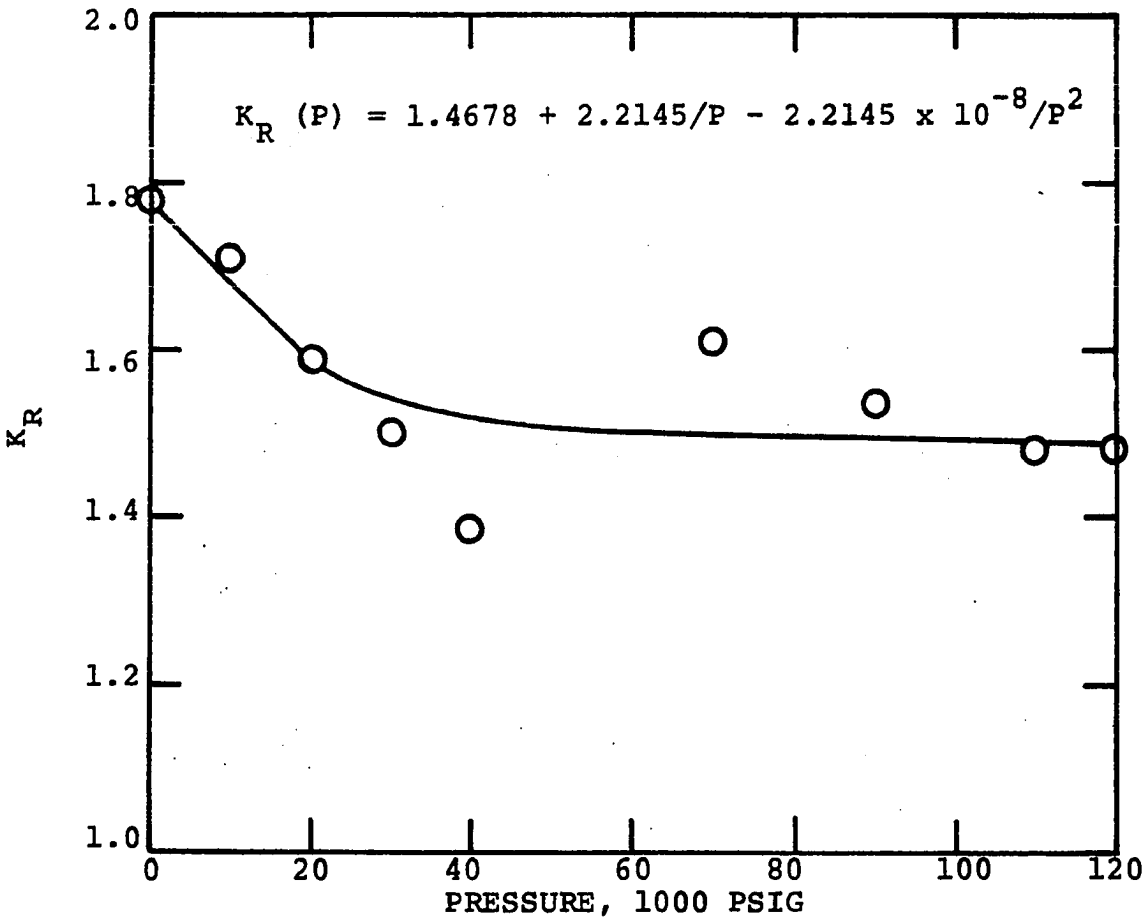

Figure 31. Effect of Pressure on K_R at 77°F.

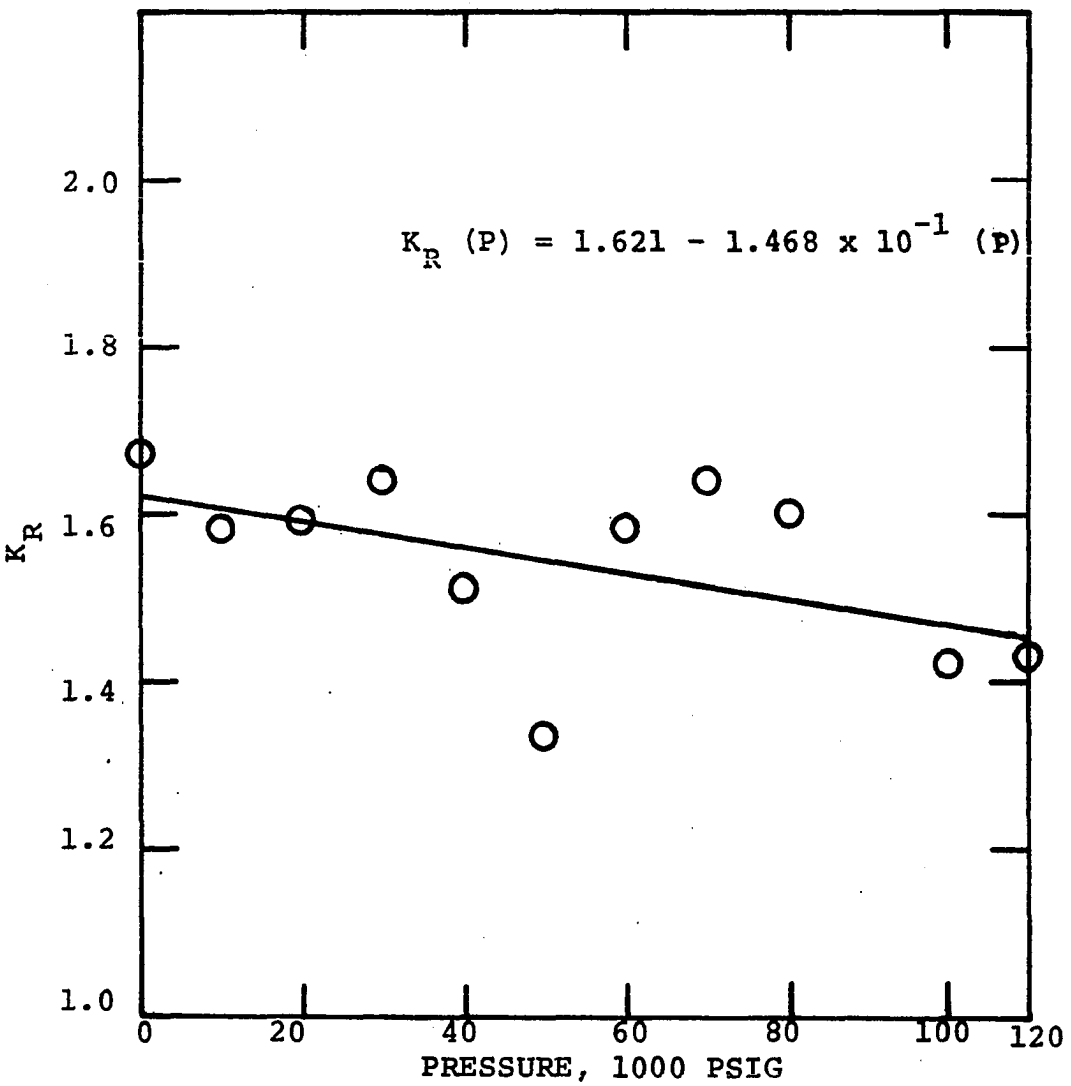

Figure 32. Effect of Pressure on K_R at 100°F.

Filmed as received

without page(s) 113 .

UNIVERSITY MICROFILMS.

be independent of pressure while Charng (14) combined the values of K_R obtained at 77° and 100°F and correlated them with pressure by a second degree polynomial.

The values of K_f and K_R were also calculated according to the theoretical predictions of Equations 72 and 73 in Chapter III. The value of K_f thus calculated was very close to the values obtained from calibration. However, the calculated values of K_R were higher than the corresponding values determined by calibration and resulted in higher deviations between the reported and calculated values of the viscosity of the calibration liquids. The reason for this deviation seems to be the inaccuracy involved in determining the half power points required for calculating L_c, the effective electrical inductance of the crystal (Equation 74 in Chapter III). As a result, the calibration constants obtained by experiment were used for later calculations.

Since the measurements in this investigation were only carried out at two temperatures, no definite conclusion could be reached about the temperature dependence of the calibration constants. For this reason, the calculations of viscoelastic properties of the polymer solutions at each temperature were carried out with the calibration constants and correlations obtained for that particular temperature.

The accuracy of the calibration constants is within ± 20 percent. This figure has been arrived at by back calculating the viscosity of calibration liquids with the calibration

parameters obtained as described above and, subsequently, finding the overall average percent deviation between the reported and calculated values. For a perfect calibration this deviation should, of course, be close to zero. The reason for this relatively high inaccuracy was mostly due to the choice of calibration liquids as well as their limited number. For instance, in the lower ranges of pressure, the values of resonant frequency and resistance at the resonant frequency of the crystal in all of the liquids except sebacate and, to some extent, methyl-cyclohexane were so close that they could effectively be obtained from only one liquid. On the other hand, at pressures above 70,000 to 80,000 psig sebacate and normal octane could not be used for calibration because they became so viscous that they effectively froze in the transfer line. Therefore, at pressures above 80,000 psig only three liquids remained for calibration. Unfortunately, lack of data on the viscosity and density of other Newtonian liquids suitable for calibration purposes over the range of this investigation leaves few liquids suitable for calibration.

Measurement of the Viscoelastic Properties of Polymer Solutions

As mentioned earlier, the values of R_M and X_M are equal for a Newtonian liquid. However, calculation of R_M and X_M in viscoelastic liquids always results in a larger value for R_M than X_M. The difference in the value of R_M and X_M makes

it possible to calculate a storage modulus, in addition to the loss modulus, for viscoelastic liquids according to Equations 65 and 66.

Since calculation of R_M and X_M for polymer solutions used in this investigation always resulted in a larger value for R_M than X_M, therefore it was concluded that these liquids behave in a viscoelastic manner at both 77° and 100°F and over the entire pressure range of this investigation.

The results for the viscoelastic properties obtained for 1, 2 and 3 weight percent solutions of S-109 and S-108 polystyrenes in toluene are presented and discussed in the following sections.

Pressure Effect

Figures 33 through 36 show the real part of the dynamic viscosity, η', of 1, 2 and 3 weight percent solutions of S-108 and S-109 polystyrenes in toluene as a function of pressure at 77° and 100°F. To facilitate comparison of the solution viscosities with the corresponding values of solvent viscosity, the viscosity pressure curve of toluene is also plotted in each figure. The following results are obtained from Figures 33 through 36:

1. The viscosity of both S-108 and S-109 polystyrene solutions increases exponentially with pressure. Comparison of the viscosity-pressure curve of each polymer solution with the viscosity-pressure curve of toluene at the same

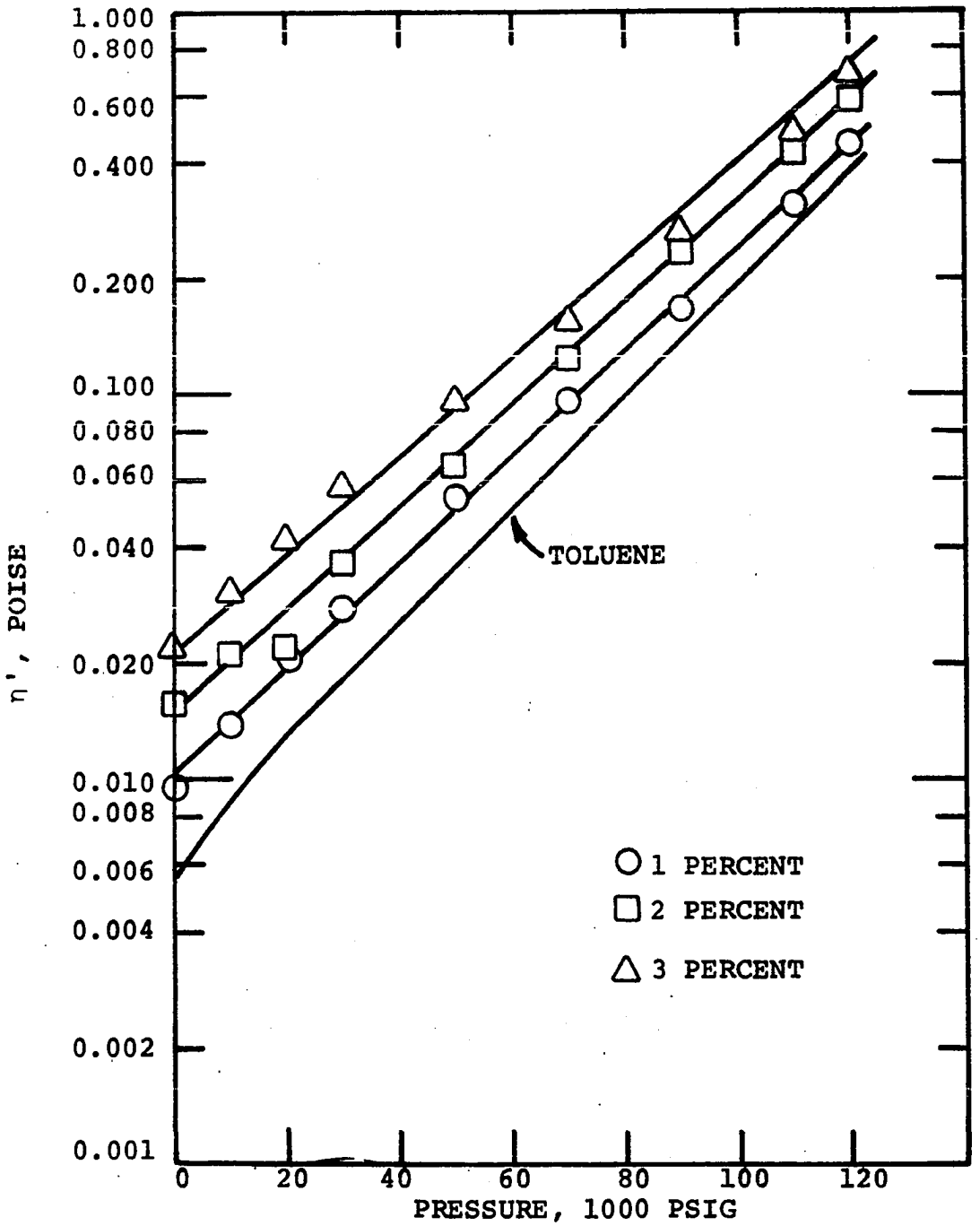

Figure 33. Effect of Pressure on Dynamic Viscosity of S-108 Polystyrene ($\overline{M}_w = 2.67 \times 10^5$) Solutions at 77°F.

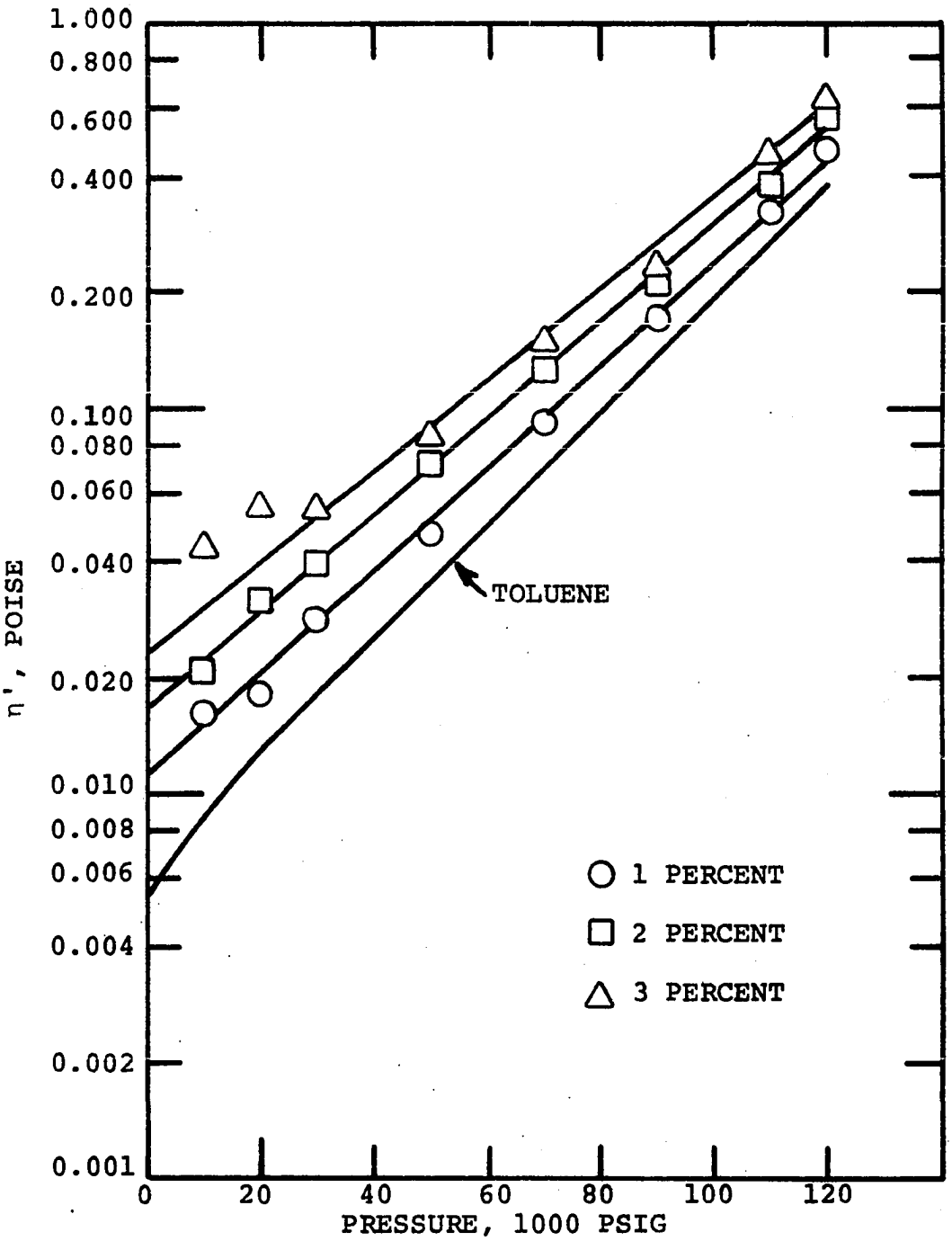

Figure 34. Effect of Pressure on Dynamic Viscosity of S-109 Polystyrene ($\bar{M}_w = 1.93 \times 10^5$) Solutions at 77°F.

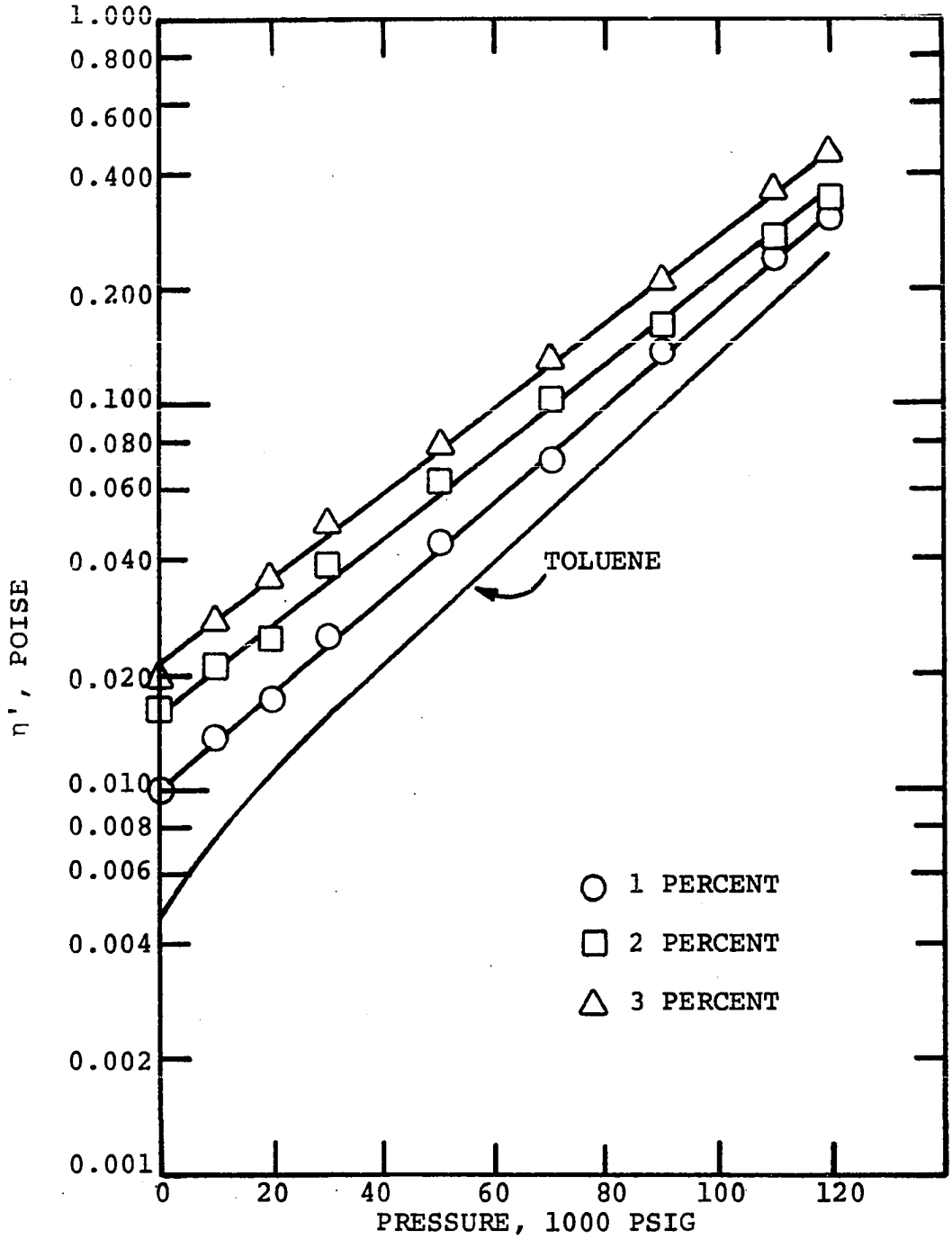

Figure 35. Effect of Pressure on Dynamic Visocisity of S-108 Polystyrene ($\bar{M}_w = 2.67 \times 10^5$) Solutions at 100°F.

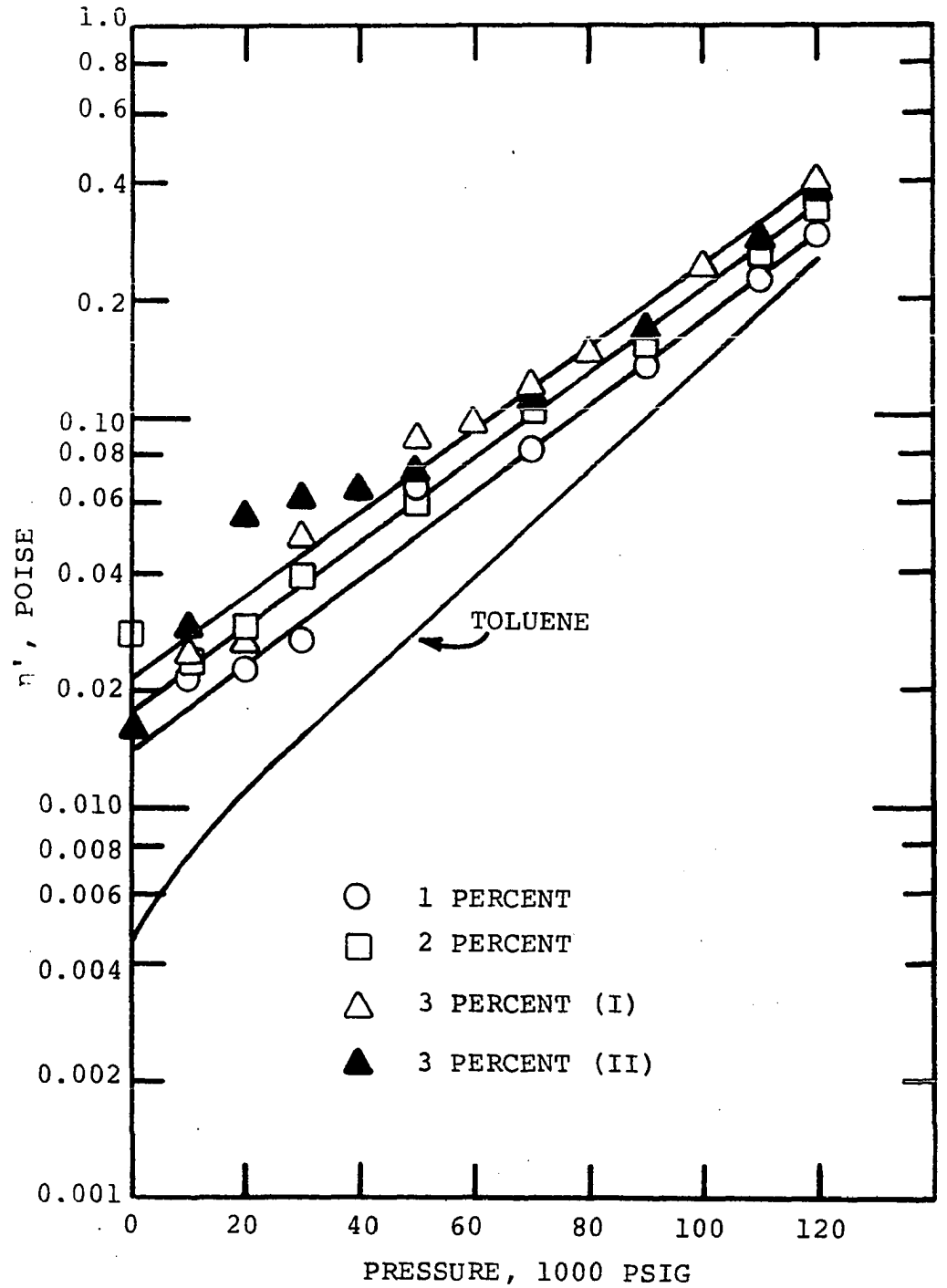

Figure 36. Effect of Pressure on Dynamic Viscosity of S-109 Polystyrene ($\bar{M}_W = 1.93 \times 10^5$) Solutions at 100°F.

temperature indicates that at lower pressures the viscosity of toluene increases slightly more rapidly with increasing pressure than the viscosity of any of the polymer solutions. However, as the pressure increases the slopes of the viscosity-pressure curves of polymer solutions approach the slope of the viscosity-pressure curve of toluene, and the rate of increase of the viscosity with pressure becomes almost equal for both solvent and solutions. These observations are in agreement with the results of Appeldoorn (2), Philippoff (36) and Charng (14).

2. Comparison of the viscosity-pressure curves of S-108 polystyrene solutions at 77°F with the corresponding curves at 100°F (Figure 37) indicates that the viscosity of each solution at any particular pressure is higher at 77° than at 100°F. Figure 37 also indicates that the viscosity of each solution increases more rapidly with pressure at 77°F than at 100°F. These conclusions also apply to the viscosity-pressure curves of S-109 polystyrene solutions as shown in Figure 38. At low pressures the viscosity of the 1 and 2 weight percent S-109 polystyrene solutions at 100°F are higher than the corresponding values at 77°F. However, the difference is small and may be due to the greater scatter of the data at lower pressures. The data points in Figures 37 and 38 are omitted for clarity.

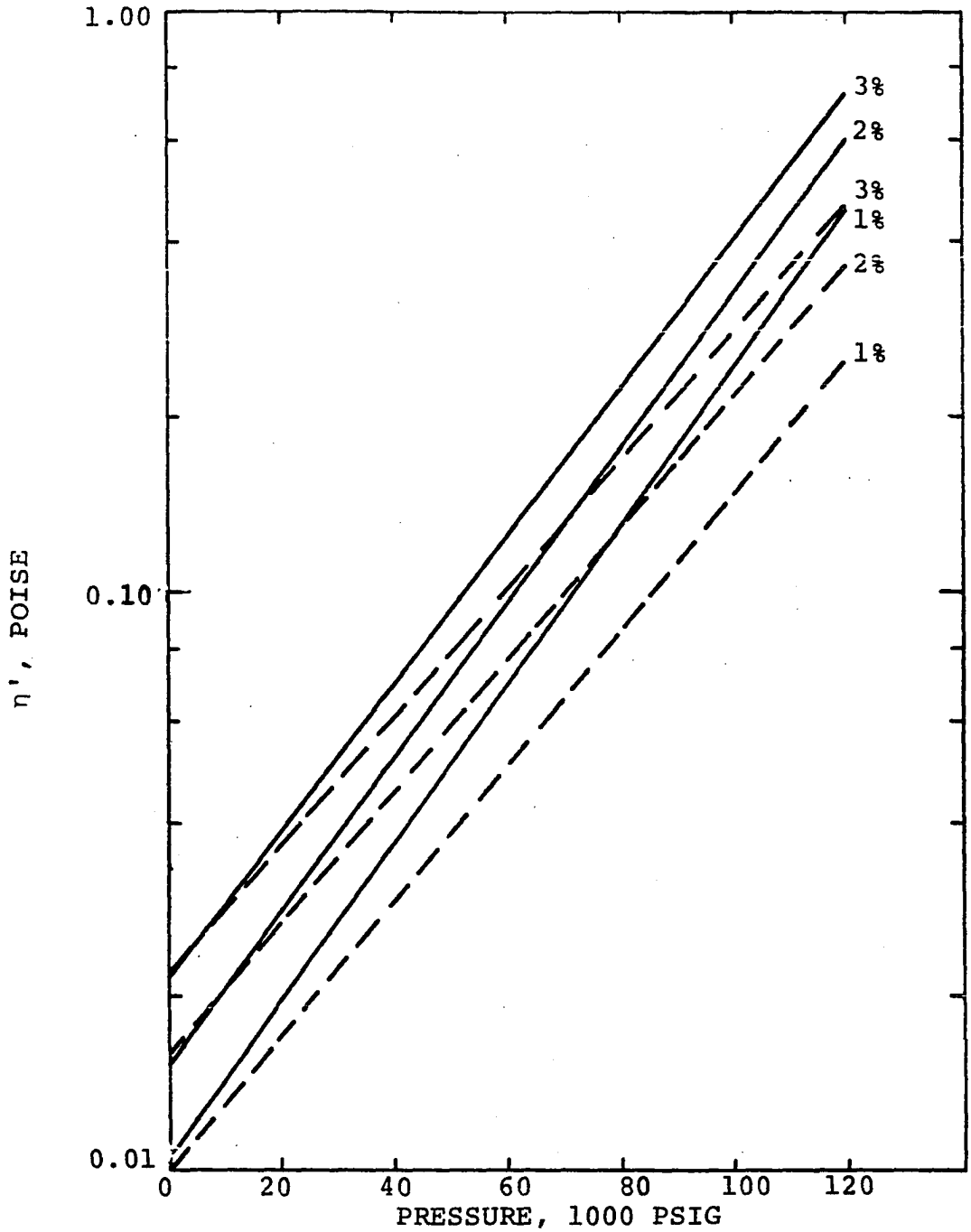

Figure 37. Effect of Pressure on Dynamic Viscosity of S-108 Polystyrene ($\bar{M}_w = 2.67 \times 10^5$) Solutions at 77° (solid lines) and 100°F (dashed lines).

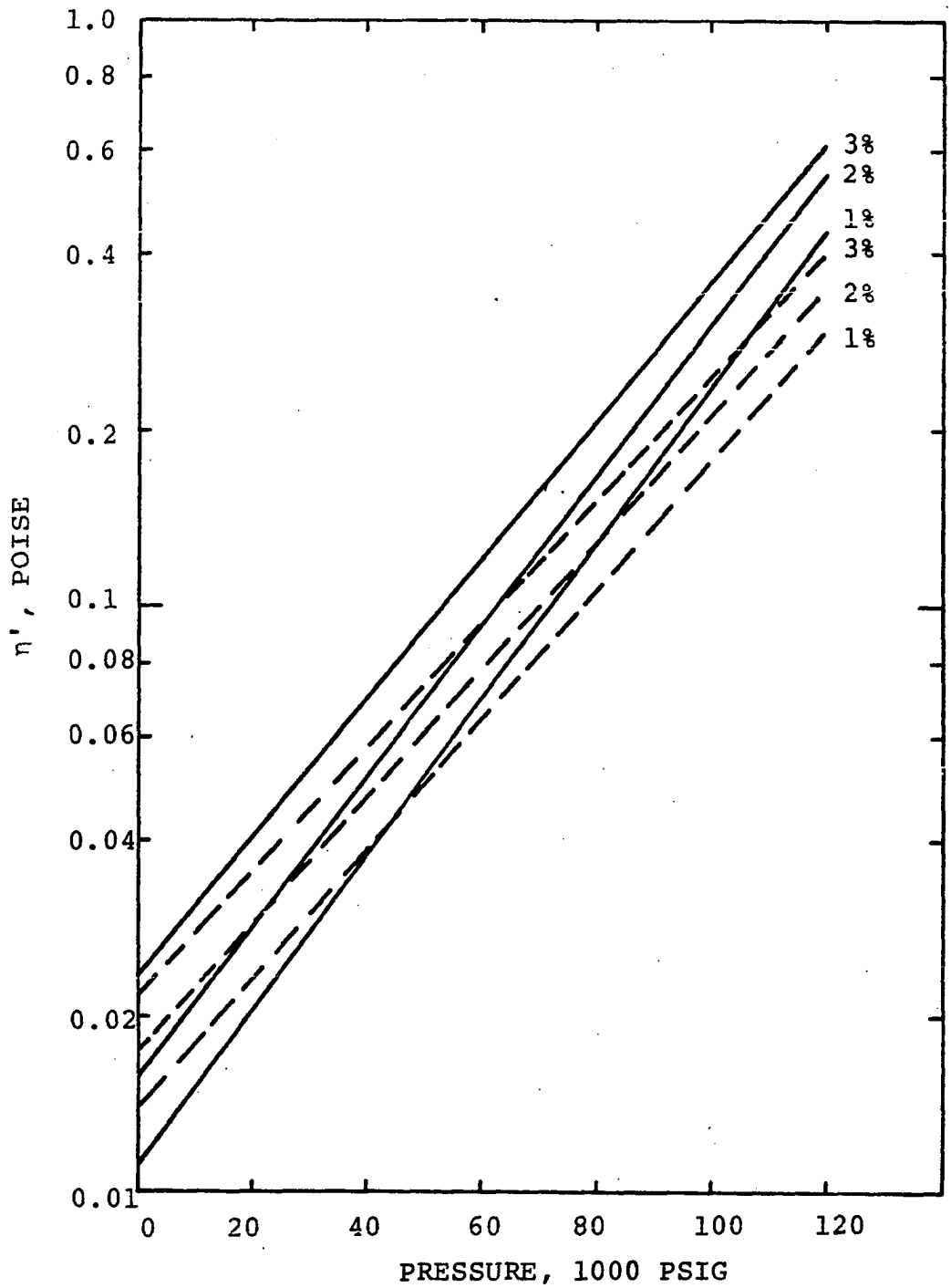

Figure 38. Effect of Pressure on Dynamic Viscosity of S-109 Polystyrene ($\bar{M}_w = 1.93 \times 10^5$) Solutions at 77° (Solid Lines) and 100°F (Dashed Lines).

3. Comparison of Figures 33 with 34 and Figures 35 with 36 indicates that for a given concentration the viscosity values of S-108 polystyrene solutions are generally higher, though not by a large amount, than the corresponding viscosity values of the lighter polymer solutions, S-109. This difference can be attributed to the higher molecular weight and, as a result, the longer polymer chain length of S-108 polystyrene.

The effect of pressure on the elastic shear modulus, G', for 1, 2 and 3 weight percent solutions of S-108 and S-109 polystyrenes in toluene at 77° and 100°F are shown in Figures 39 through 42. Figures 39 through 42 indicate an exponential relation between the elastic modulus, G', and pressure. This behavior is similar to the viscosity-pressure relationship of these solutions.

Comparison of the elasticity-pressure curves of S-108 solutions at 77°F with the corresponding curves at 100°F (Figure 43) indicates that, for each particular concentration, the G' values have about the same value at both temperatures and low pressures. However, G' increases more rapidly with pressure at 77° than at 100°F. This conclusion cannot be generalized to the elastic shear modulus of S-109 solutions; comparison of the 1 and 2 weight percent solutions of S-109 polystyrene at 77°F with the solutions of similar concentrations at 100°F (Figure 44) indicates that G' starts with a lower value at 100°F, as expected, but it increases more

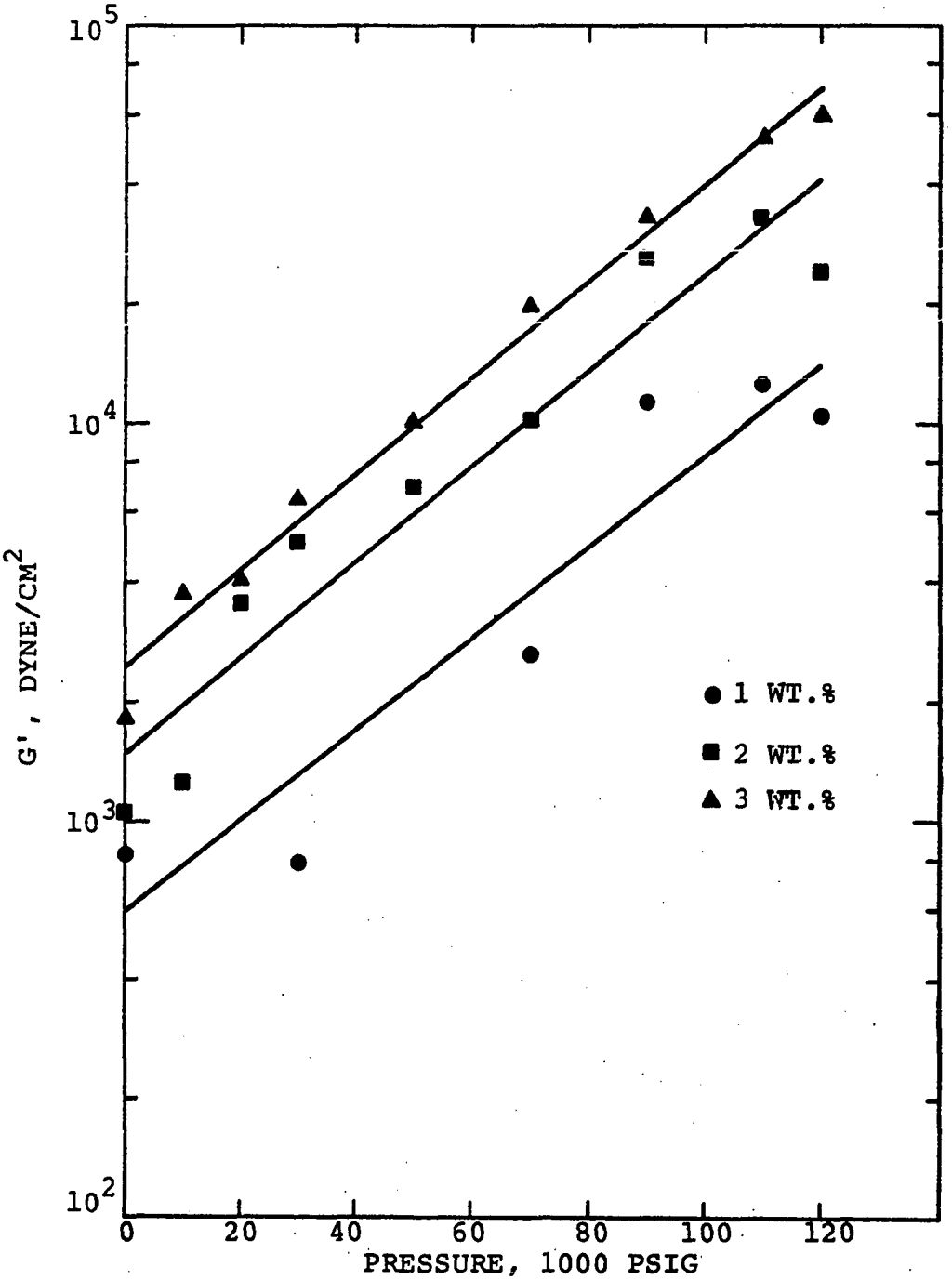

Figure 39. Effect of Pressure on Elastic Shear Modulus of S-108 Polystyrene ($\bar{M}_w$ = 2.67 x 10^5) Solution at 77°F.

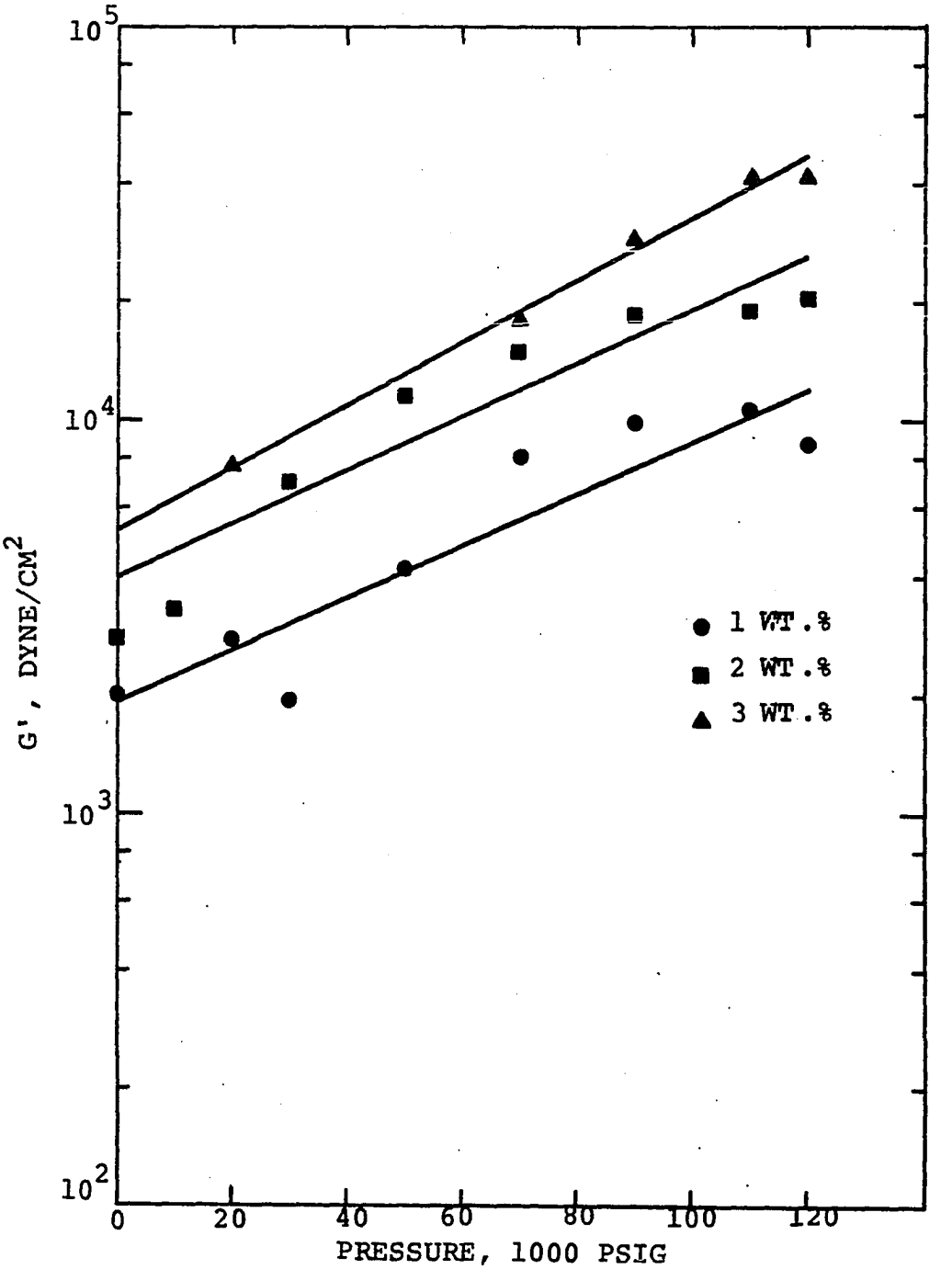

Figure 40. Effect of Pressure on Elastic Shear Modulus of S-109 Polystyrene ($\bar{M}_w$ = 1.93 x 10^5) Solutions at 77°F.

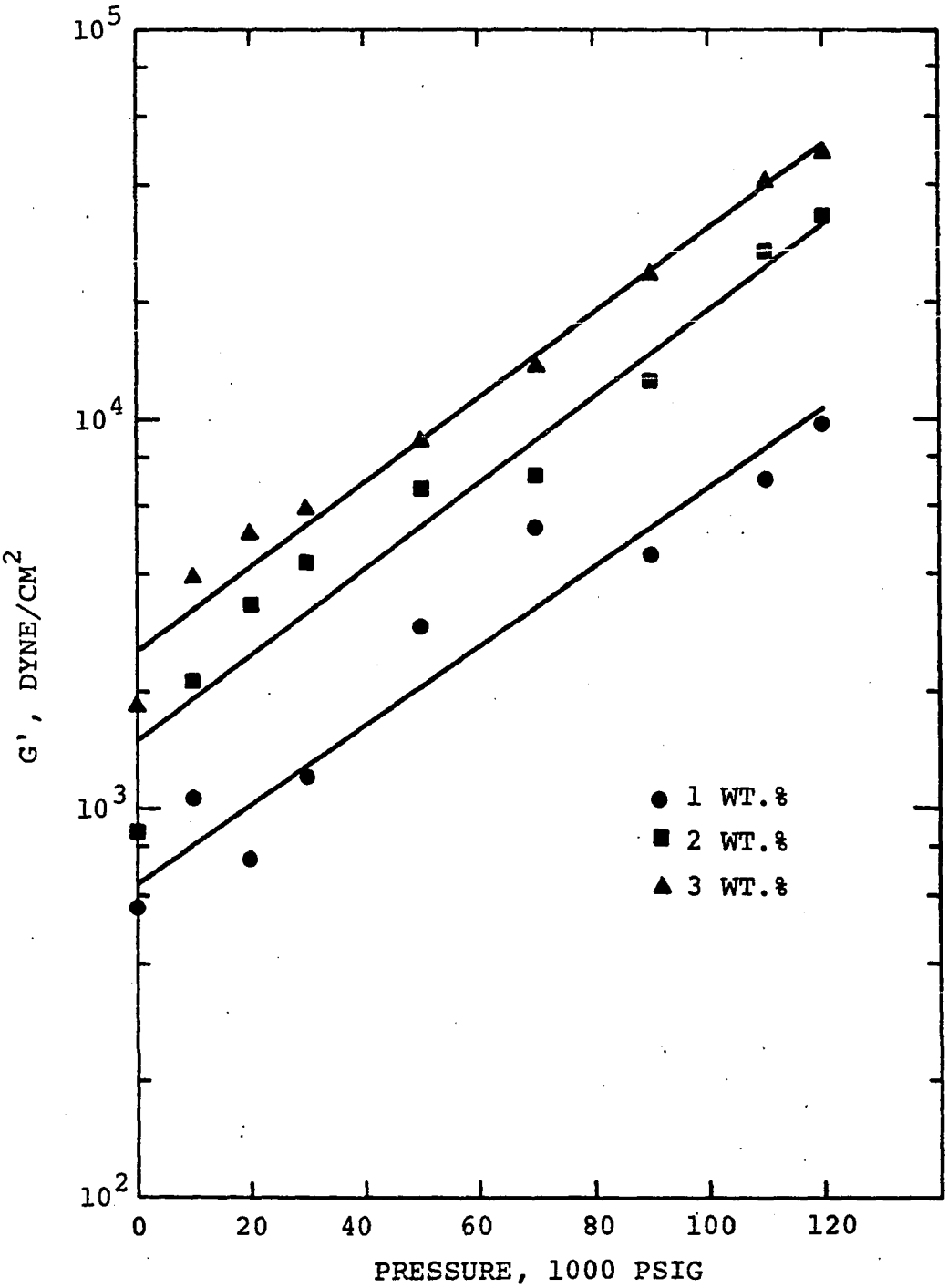

Figure 41. Effect of Pressure on Elastic Shear Modulus of S-108 Polystyrene ($\bar{M}_W$ = 2.67 x 10^5) Solutions at 100°F.

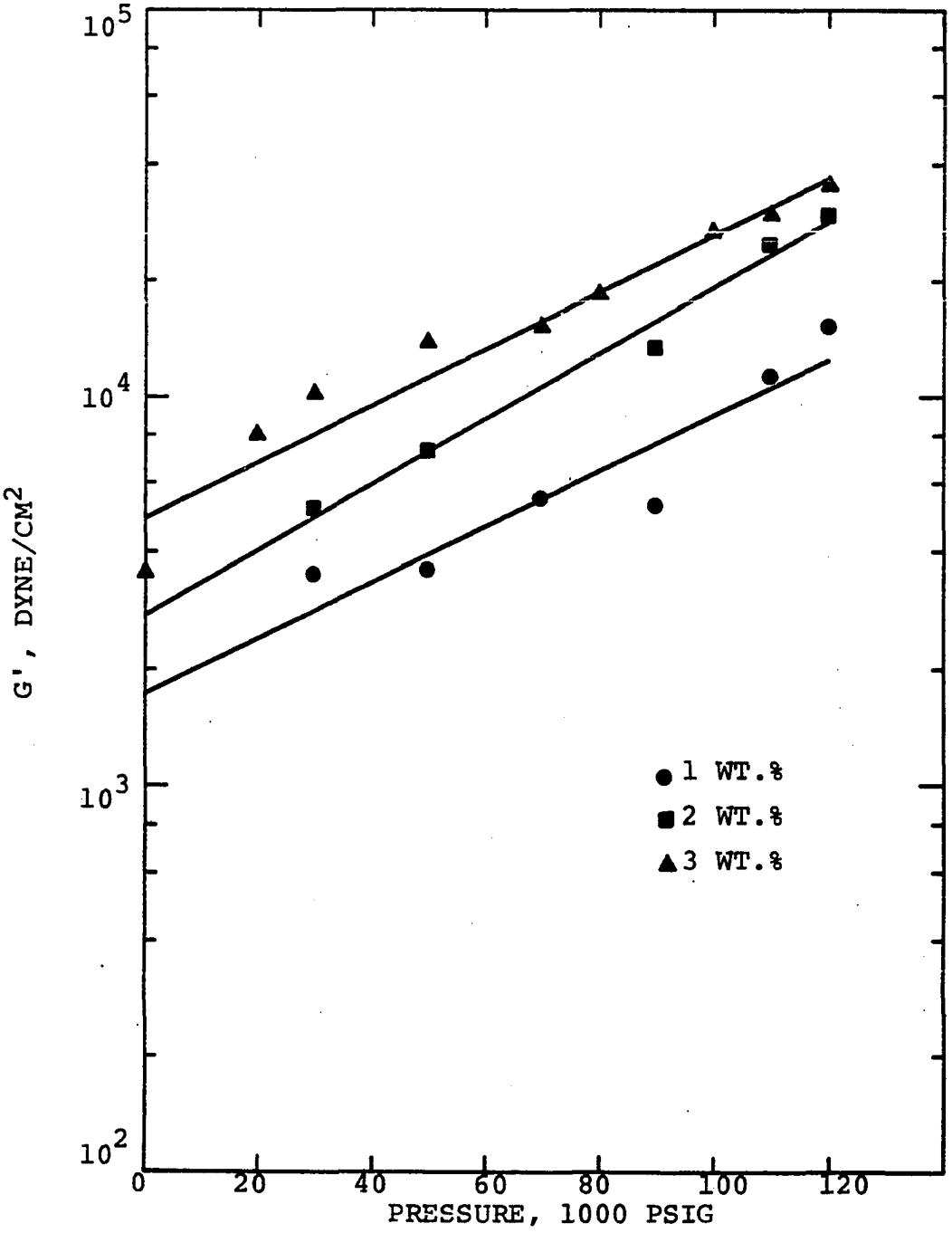

Figure 42. Effect of Pressure on Elastic Shear Modulus of S-109 Polystyrene ($\bar{M}_w$ = 1.93 x 10^5) Solutions at 100°F.

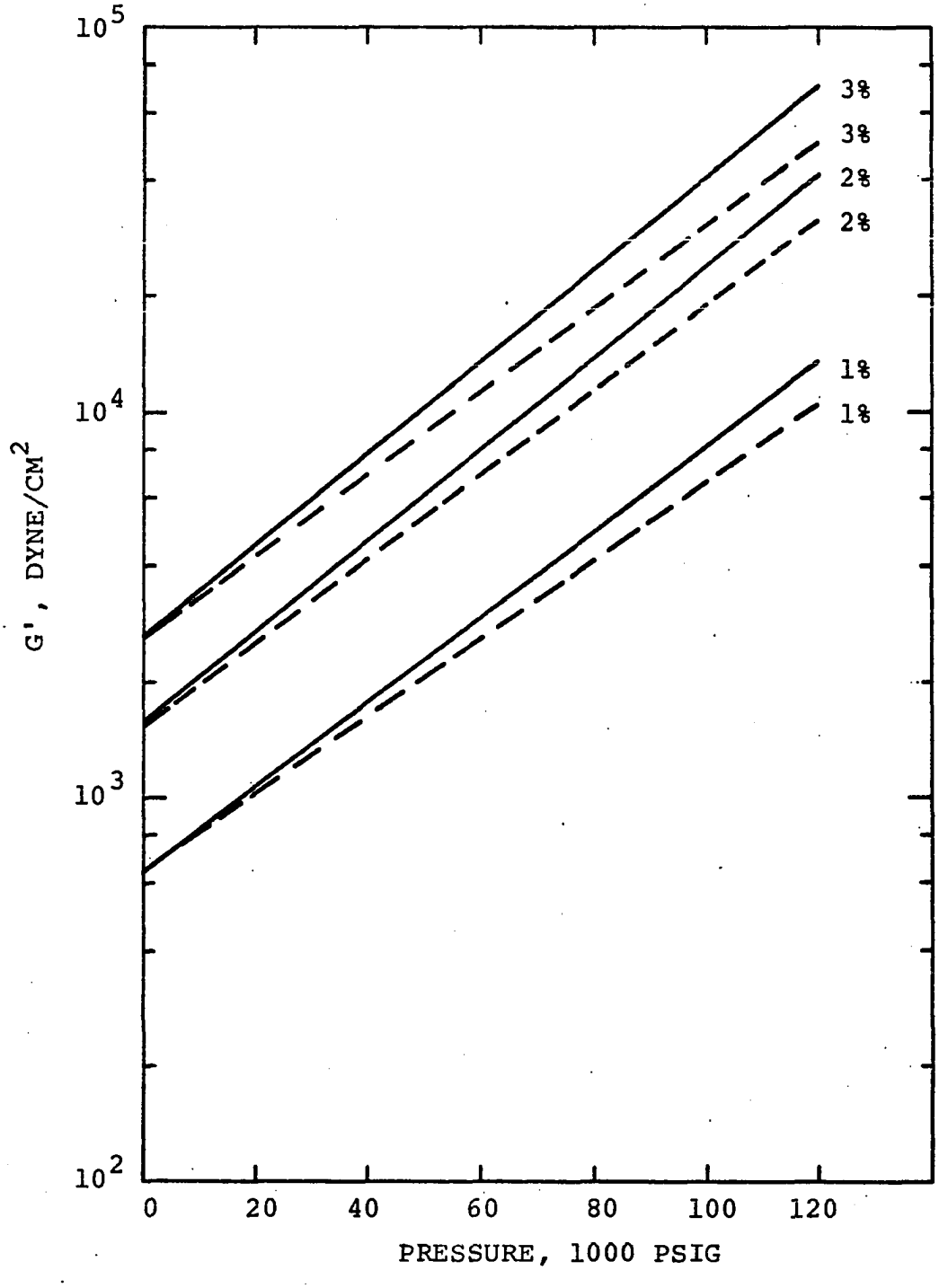

Figure 43. Effect of Pressure on Elastic Shear Modulus of S-108 Polystyrene ($\bar{M}_W = 2.67 \times 10^5$) Solutions at 77° (Solid Line) and 100°F (Dashed Line).

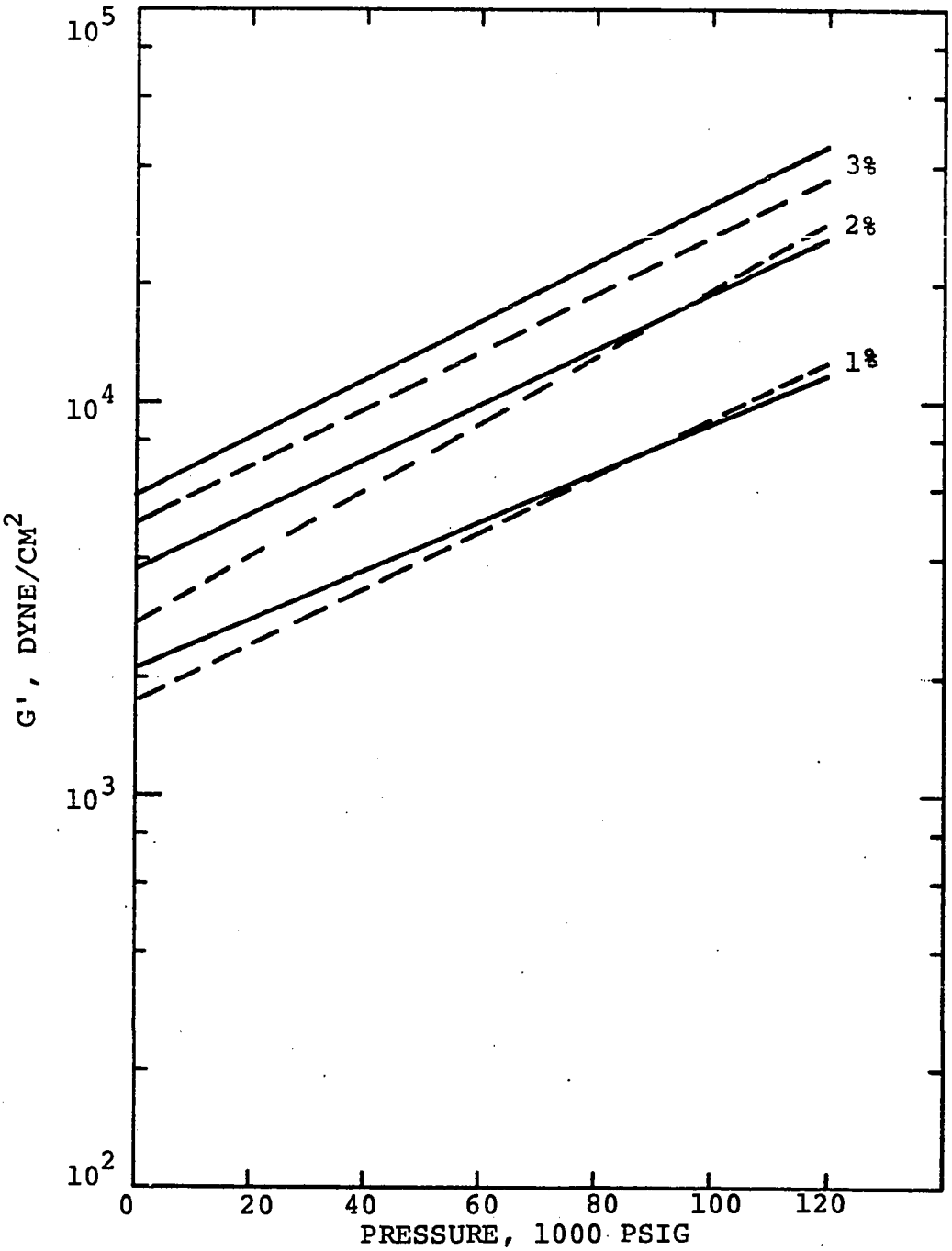

Figure 44. Effect of Pressure on Elastic Shear Modulus of S-109 Polystyrene ($\bar{M}_w$ = 1.93 x 10^5) Solutions at 77°F (solid lines) and 100°F (dashed lines).

rapidly with pressure than the curves for 77°F until the curves intersect at about 90,000 psig. However, the shear elasticity of the 3 weight percent solution of S-109 at 77°F is always larger than the corresponding value at 100°F and the two curves have almost the same slope at both temperatures.

The effect of the molecular weight on shear elasticity, G', is shown in Figures 45 and 46 for 77° and 100°F, respectively. These figures indicate that at low pressures the G' of each S-108 solution has a lower value than the S-109 solution but that G' for S-108 solutions increases more rapidly with pressure than the S-109 solutions. Eventually, at high pressures, the G' of the S-108 solutions is greater than the G' of S-109 solutions. The 1 percent solutions of S-108 and S-109 at 100°F are an exception to this observation and the G' curves of 1 percent solution may cross at a pressure above 120,000 psig. The crossing of the elasticity-pressure curves of S-108 and S-109 solutions occurs at a lower pressure as the concentration increases.

The above result is unexpected and is in contrast with the data of Frederick, et al. (18) which show a higher G' value for a solution of a higher molecular weight polymer at one particular concentration and temperature.

Concentration Effect

Figures 47, 48, 49 and 50 show the real part of the dynamic viscosity, η', of the S-108 and S-109 solutions as a function of concentration. A linear relationship between η'

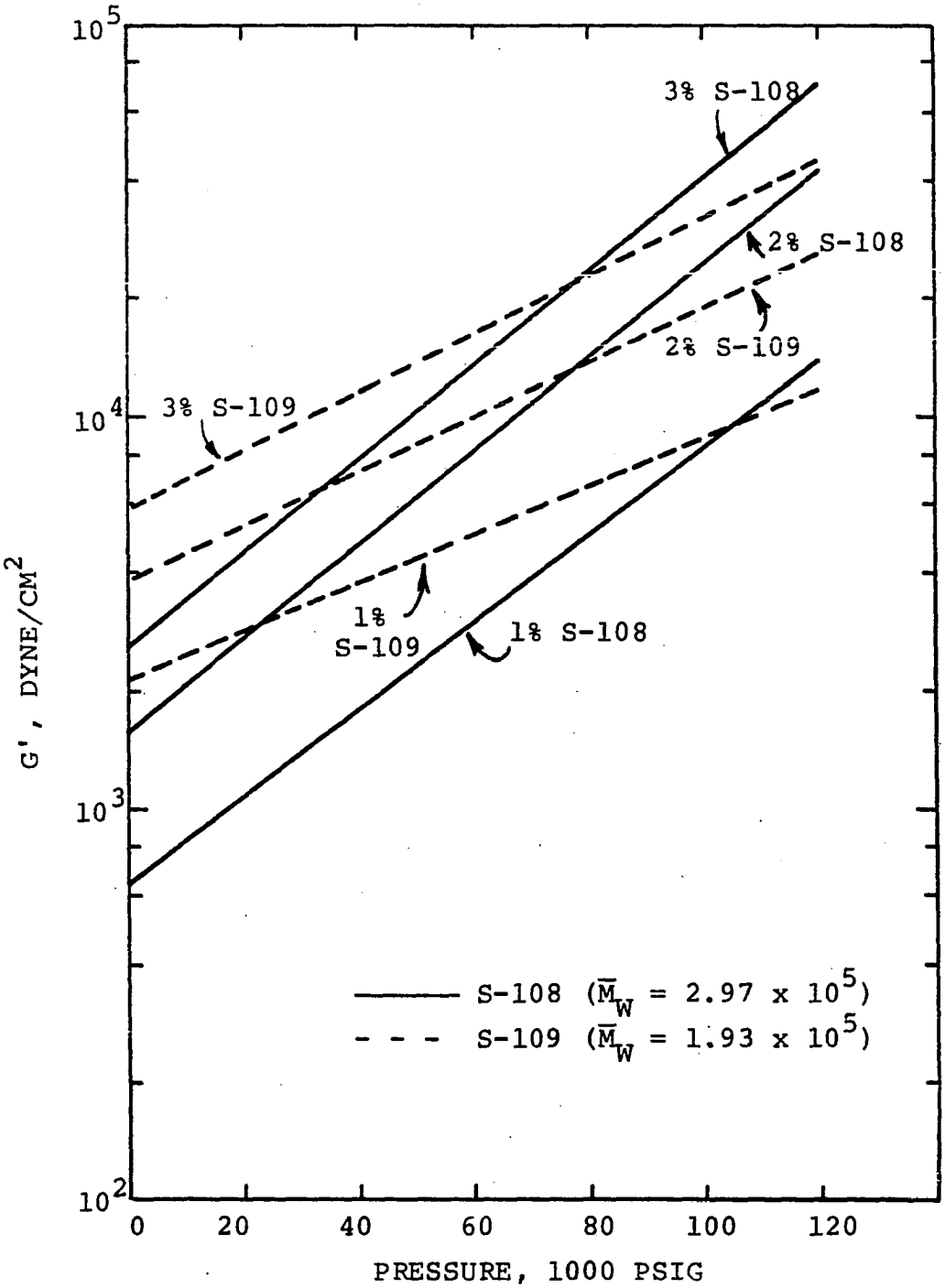

Figure 45. Effect of Polymer Molecular Weight on Elastic Shear Modulus at 77°F.

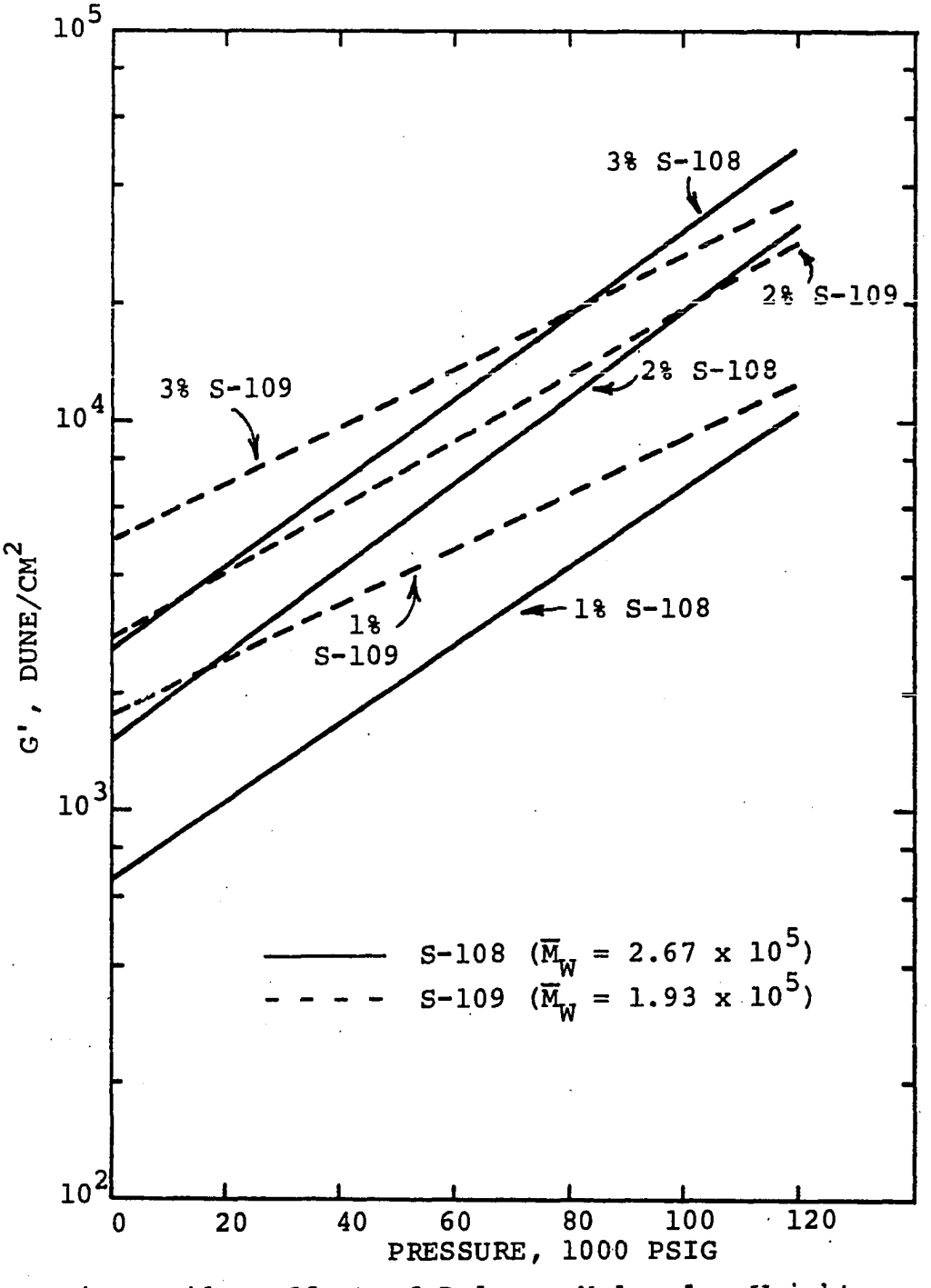

Figure 46. Effect of Polymer Molecular Weight on Elastic Shear Modulus at 100°F.

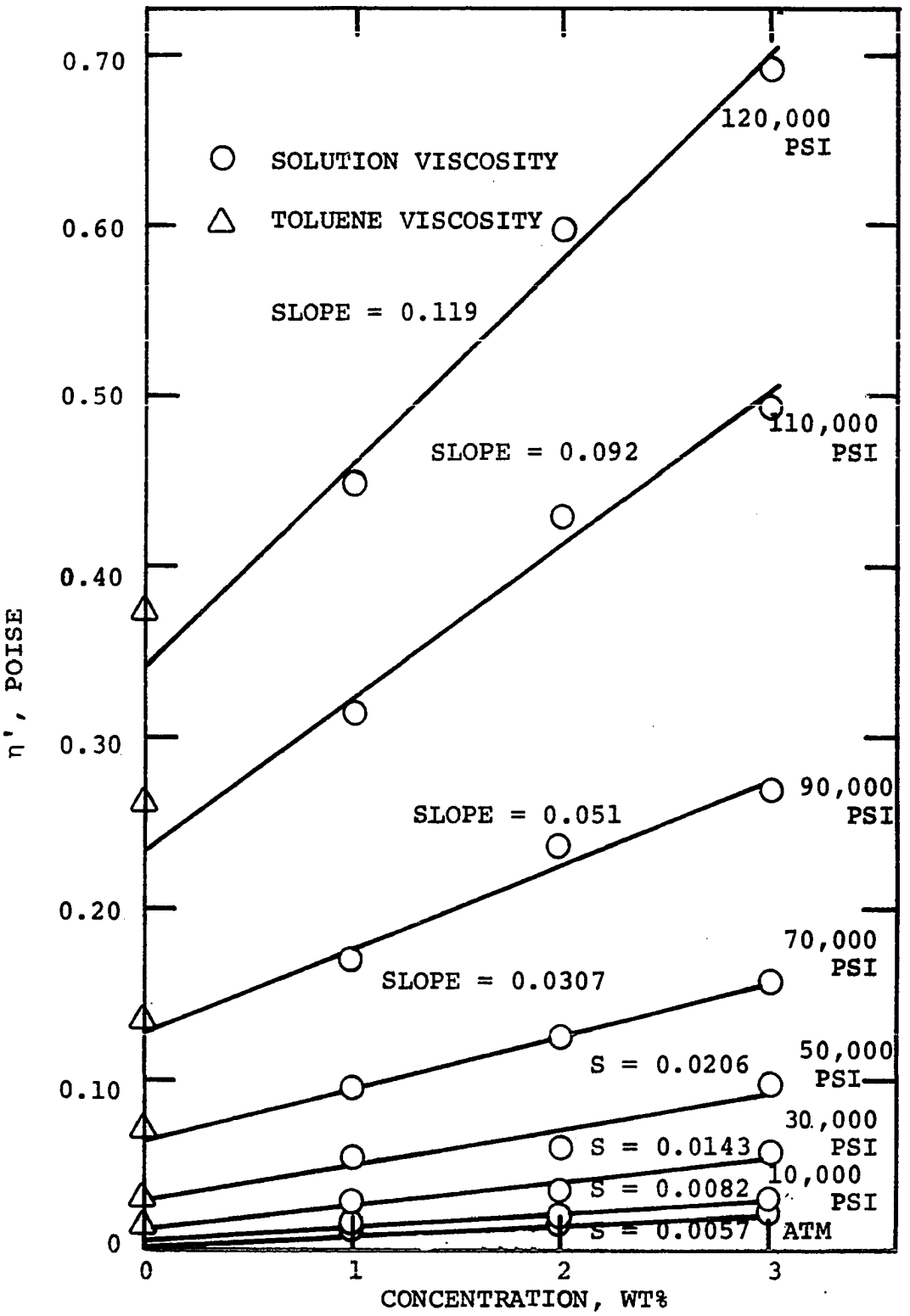

Figure 47. Effect of Concentration on Viscosity of S-108 Polystyrene ($\bar{M}_w = 2.67 \times 10^5$) Solutions at 77°F and Various Pressures.

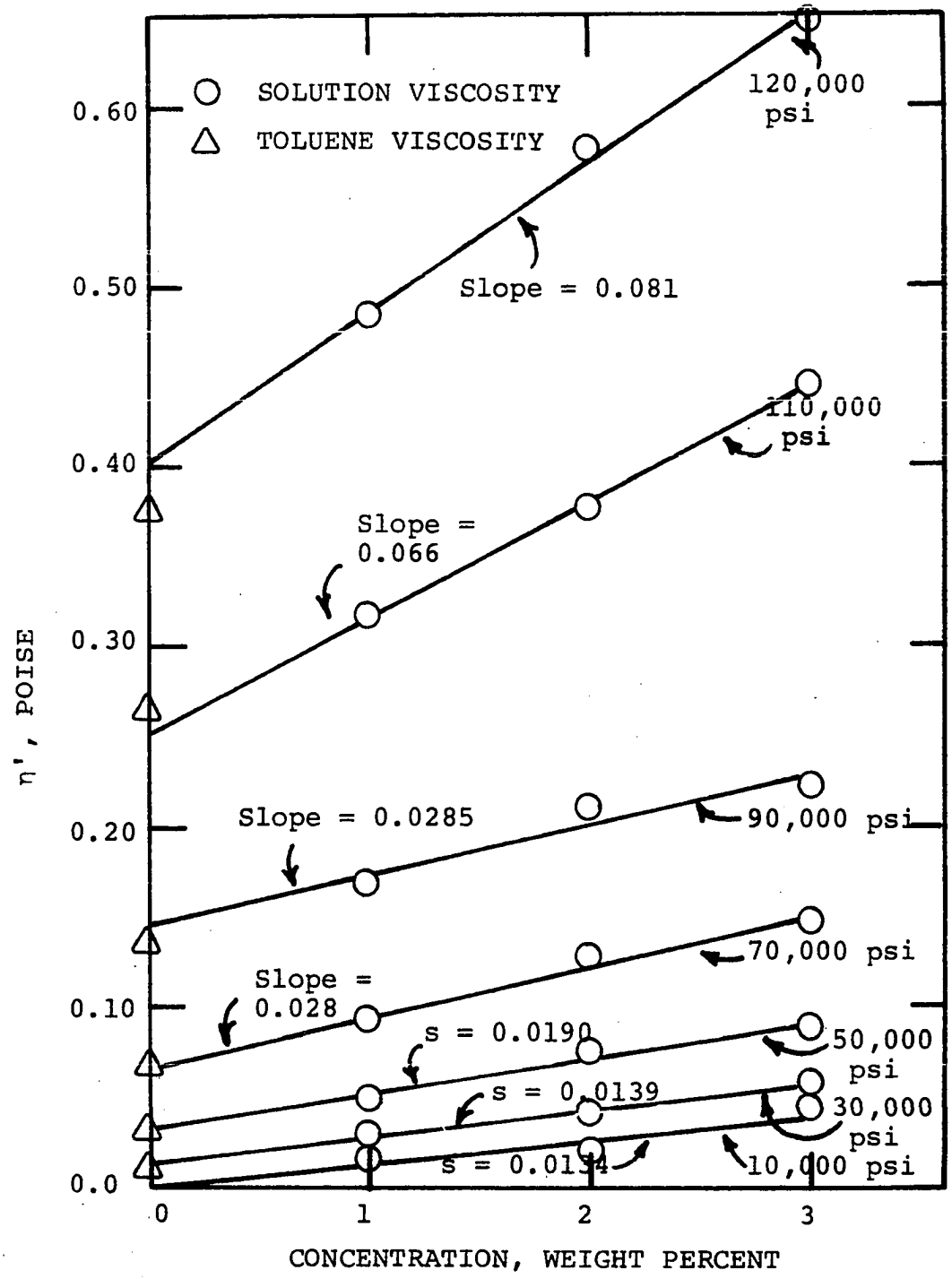

Figure 48. Effect of Concentration on Viscosity of S-109 Polystyrene ($\bar{M}_W$ = 1.93 x 10^5) Solutions at 77°F and Various Pressures.

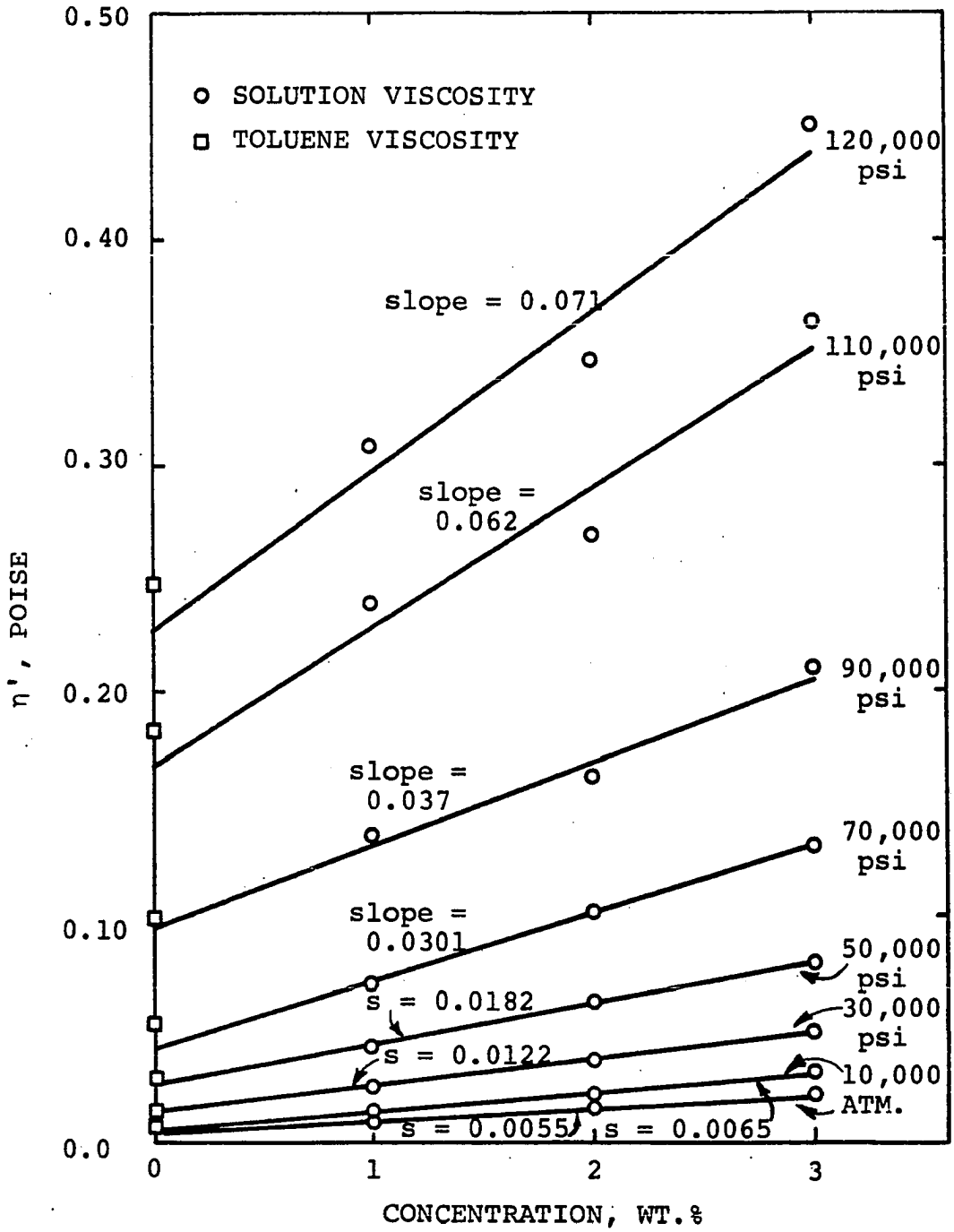

Figure 49. Effect of Concentration on Viscosity of S-108 Polystyrene ($\bar{M}_W = 2.67 \times 10^5$) Solutions at 100°F and Various Pressures.

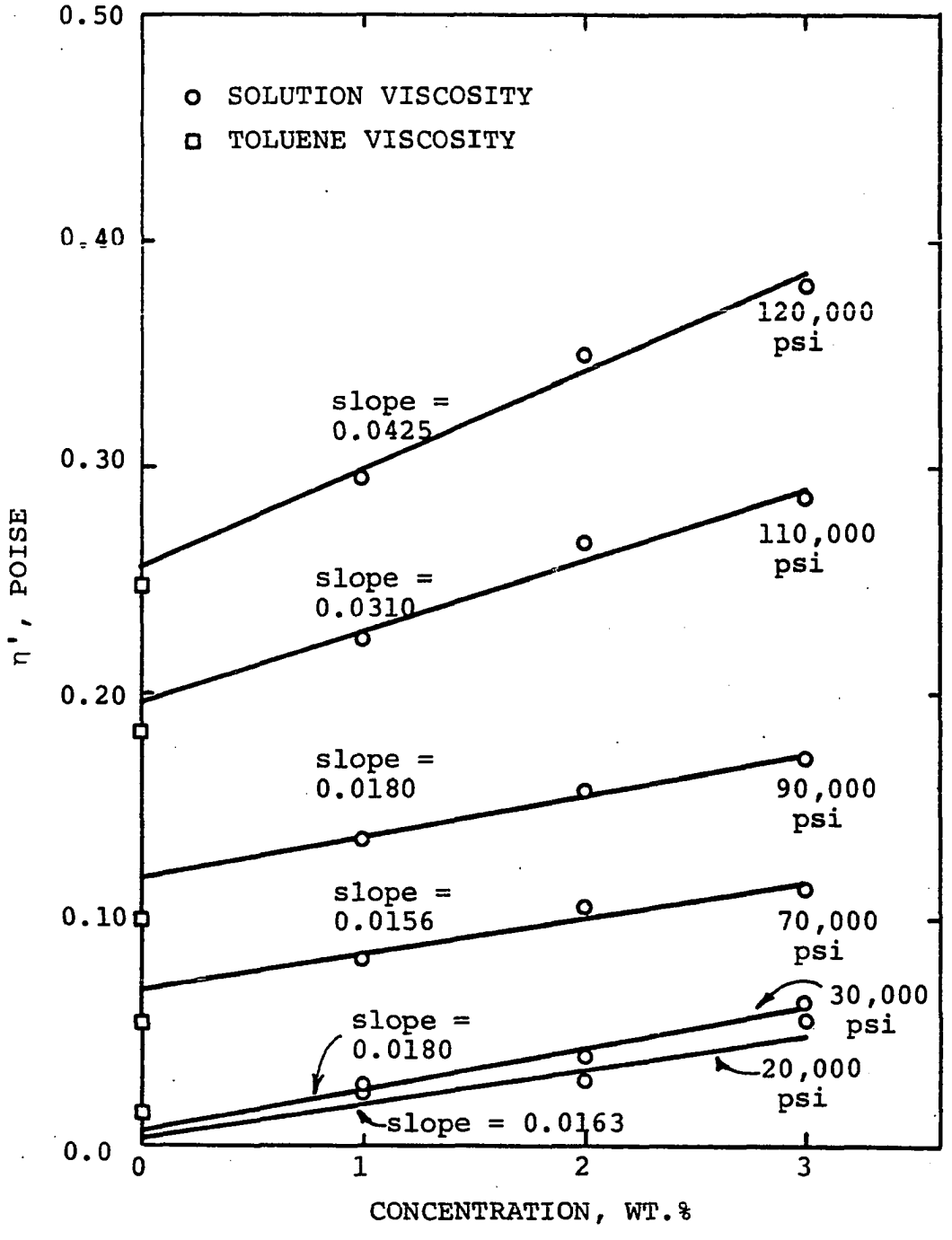

Figure 50. Effect of Concentration on Viscosity of S-109 Polystyrene ($\bar{M}_W = 1.93 \times 10^5$) Solutions at 100°F and Various Pressures.

and concentration at each pressure level is observed. It is also evident that the slope of the viscosity-concentration curves, at each temperature, increases with pressure (the slope of each line is indicated on all figures).

To compare the solvent viscosity with the viscosity of the polymer solutions at zero concentration (obtained by extrapolation of the viscosity-concentration lines), the viscosity of toluene at corresponding pressures is indicated on the viscosity axis of each plot. The difference between these values and the intercepts obtained by extrapolation are in most cases small and within the experimental accuracy of the experiment. Therefore it can be assumed that the viscosity of S-108 and S-109 polystyrene solutions under the experimental conditions of this investigation can be linearly related to the polymer concentration from infinite dilution to 3 weight percent.

Comparison of the slopes of viscosity-concentration curves of S-108 and S-109 polystyrene solutions at the same temperature and pressure (Figure 51) indicates that the viscosity of S-108 solutions increases more rapidly with concentration, especially at higher pressures, than the viscosity of S-109 solutions does. This behavior can be attributed to the higher molecular weight and, as a result, the larger chain length of S-108 polystyrene molecules. Furthermore, Figure 51 indicates that at each particular pressure the viscosity of both S-108 and S-109 solutions changes more rapidly with concentration at 77° rather than at 100°F.

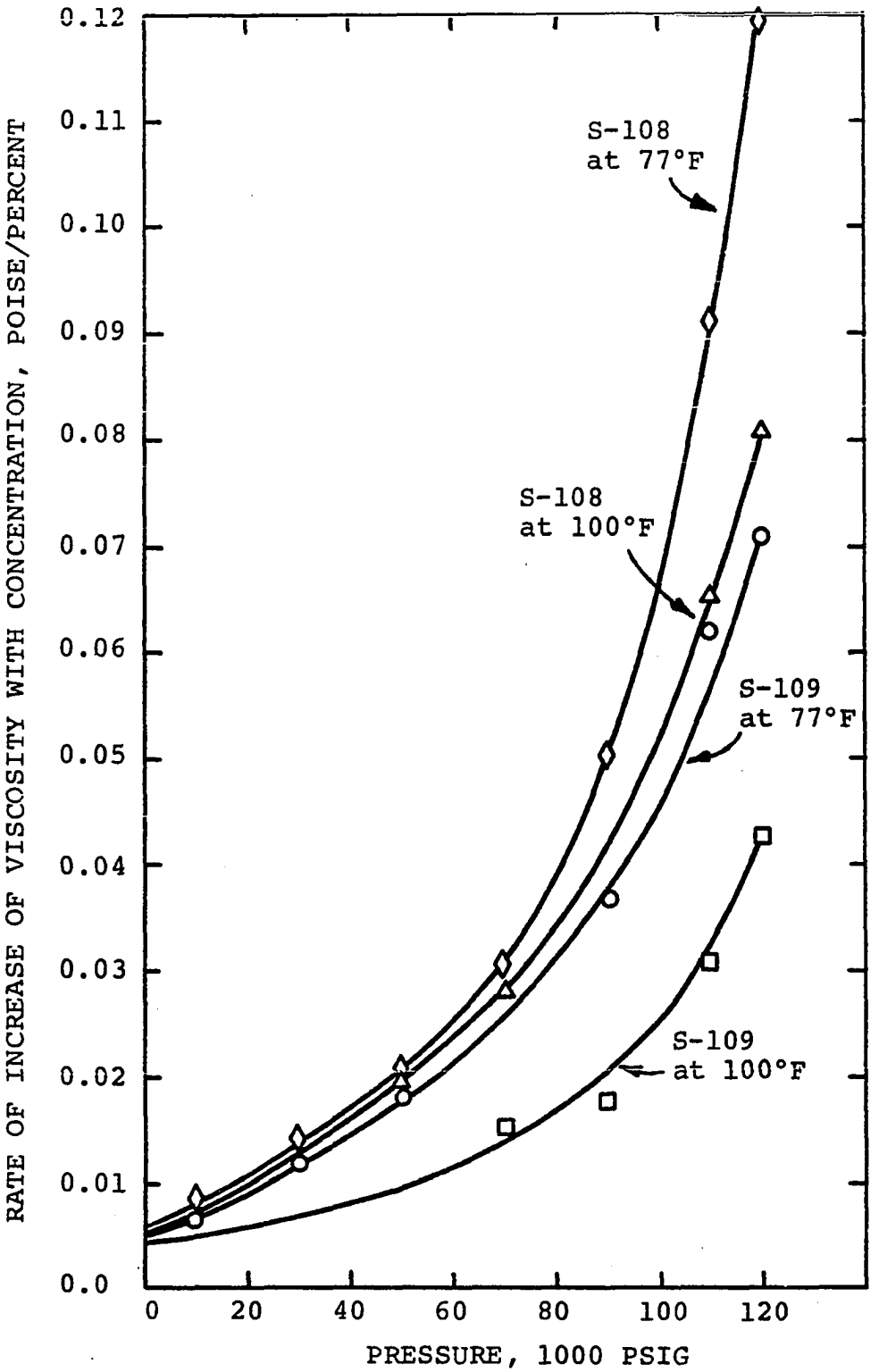

Figure 51. Effect of Pressure and Temperature on the Rate of Increase of Viscosity with Concentration for S-108 ($\overline{M}_W = 2.67 \times 10^5$) and S-109 ($\overline{M}_W = 1.93 \times 10^5$) Polystyrene.

Frequency Effect

As mentioned earlier, the various motions of polymers in solutions can be observed over a very wide range of frequency. Usually with any particular experimental technique, only a small frequency range can be covered. However, by using the method of reduced variables one can extend the effective range of frequency of the experiment. Reduced variables give a method of converting measurements at various pressures and temperatures for a single frequency to equivalent information that covers a wide range of frequencies at a single temperature and pressure.

Since the data of this investigation were obtained with only one quartz crystal with a single fundamental frequency, reduced variables were used to determine the viscoelastic properties, such as η' and G', of the solutions over a wide range of frequency. The method of reduced variables is based on calculation of a shift factor, $a_{T,P}$, which is defined by

$$a_{T,P} = \frac{\rho_o T_o}{\rho T} \left(\frac{\eta_T}{\eta_o}\right)_{\text{solution}} \left(\frac{\eta_P}{\eta_o}\right)_{\text{solvent}} = \frac{\rho_o T_o}{\rho T} \alpha \tag{84}$$

In the above equation $(\eta_T/\eta_o)_{\text{solution}}$ is the ratio of the solution viscosity at the temperature of measurement T, to the solution viscosity at reference temperature T_o, both measured at reference pressure P_o. $(\eta_P/\eta_o)_{\text{solvent}}$ is the ratio of the solvent viscosity at pressure of measurement P

to the solvent viscosity at reference pressure P_o, both measured at reference temperature T_o. Thus to calculate $a_{T,P}$ it is sufficient to have the solution density and viscosity at the temperatures T and T_o, and solvent densities and viscosities at pressures and temperatures P and T, and P_o and T_o, respectively; the viscosity of the solution at various pressures is not needed.

The calculation of the reduced quanties can be carried out according to the following equations:

$$f_r = f(a_{T,P}) \tag{89}$$

$$\omega_r = (2\pi f)\, a_{T,P} \tag{90}$$

$$G'_r = G' \frac{T_o \rho_o}{T \rho} \tag{75}$$

$$\eta'_r = \eta' \alpha \tag{83}$$

Atmospheric pressure and room temperature (77°F) were considered as the reference conditions in this investigation. The values of G' and η' obtained at each pressure and temperature were then converted to the equivalent values at the reference conditions according to the above equations.

Figure 52 shows a typical plot of $a_{T,P}$ as a function of pressure. In this figure the values of $a_{T,P}$ for all three different solutions of S-109 at 77°F, as well as the 1 percent S-109 solution at 100°F are plotted. Different $a_{T,P}$ values for solutions having different concentrations result at temperatures other than the reference temperature because

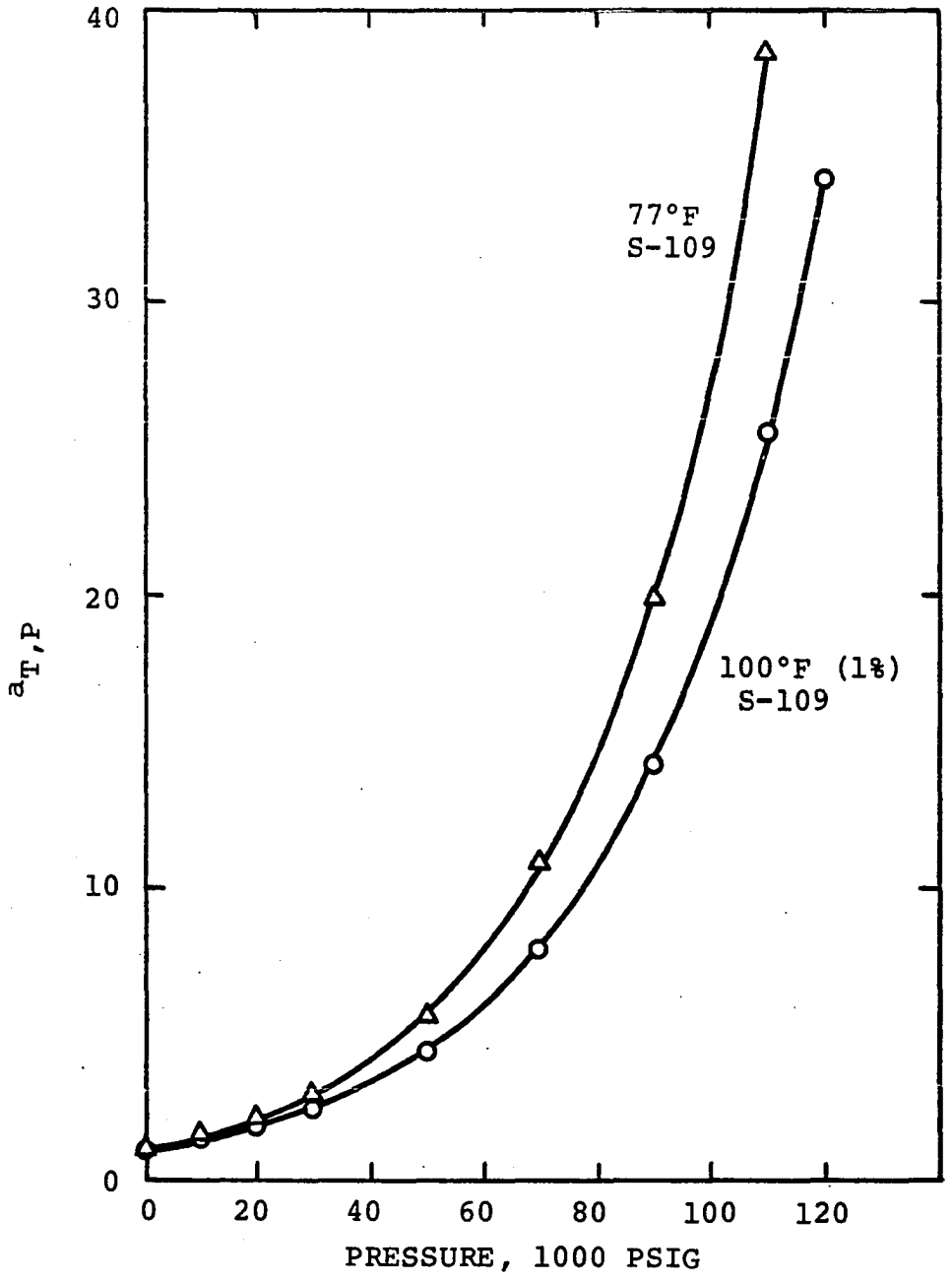

Figure 52. Effect of Pressure on $a_{T,P}$ of S-109 Solutions at 77°F and 1 percent S-109 Solution at 100°F.

the ratio $(\eta_T/\eta_o)_{solution}$ is different for different solutions. However, when the measurements are carried out at the reference temperature, the above ratio will always be equal to one for all solutions.

Examination of Figure 52 indicates that $a_{T,P}$ is much more sensitive to pressure at 77° rather than at 100°F. The increase in $a_{T,P}$ with pressure is due to the increase in the solution viscosity with pressure. This effect completely masks the contribution of changes in temperature and density as is evident from Figure 53. In this figure the contributions of viscosity and $(\rho_o T_o/\rho T)$ to $a_{T,P}$ for each of the curves shown in Figure 52 are plotted separately. The increase in the value of α for the curves at 77° and 100°F (for the entire pressure range) is about 70 and 50 times, respectively, while the corresponding decrease in the value of $(\rho_o T_o/\rho T)$ is only about 1.3 and 1.2 times, respectively. The values of $a_{T,P}$ are calculated for all polymer solutions and are given in Appendix C.

Using the $a_{T,P}$ values in Equations 89 and 90, the resonant frequency of the crystal in each solution, measured at each pressure and temperature, was reduced to the equivalent frequency at the reference conditions. Similarly the elastic modulus G' and the real part of the dynamic viscosity η' were reduced according to Equations 75 and 83. The results of these calculations are shown in Figures 54 through 59 for η' and Figures 60 through 65 for G', as a function of reduced

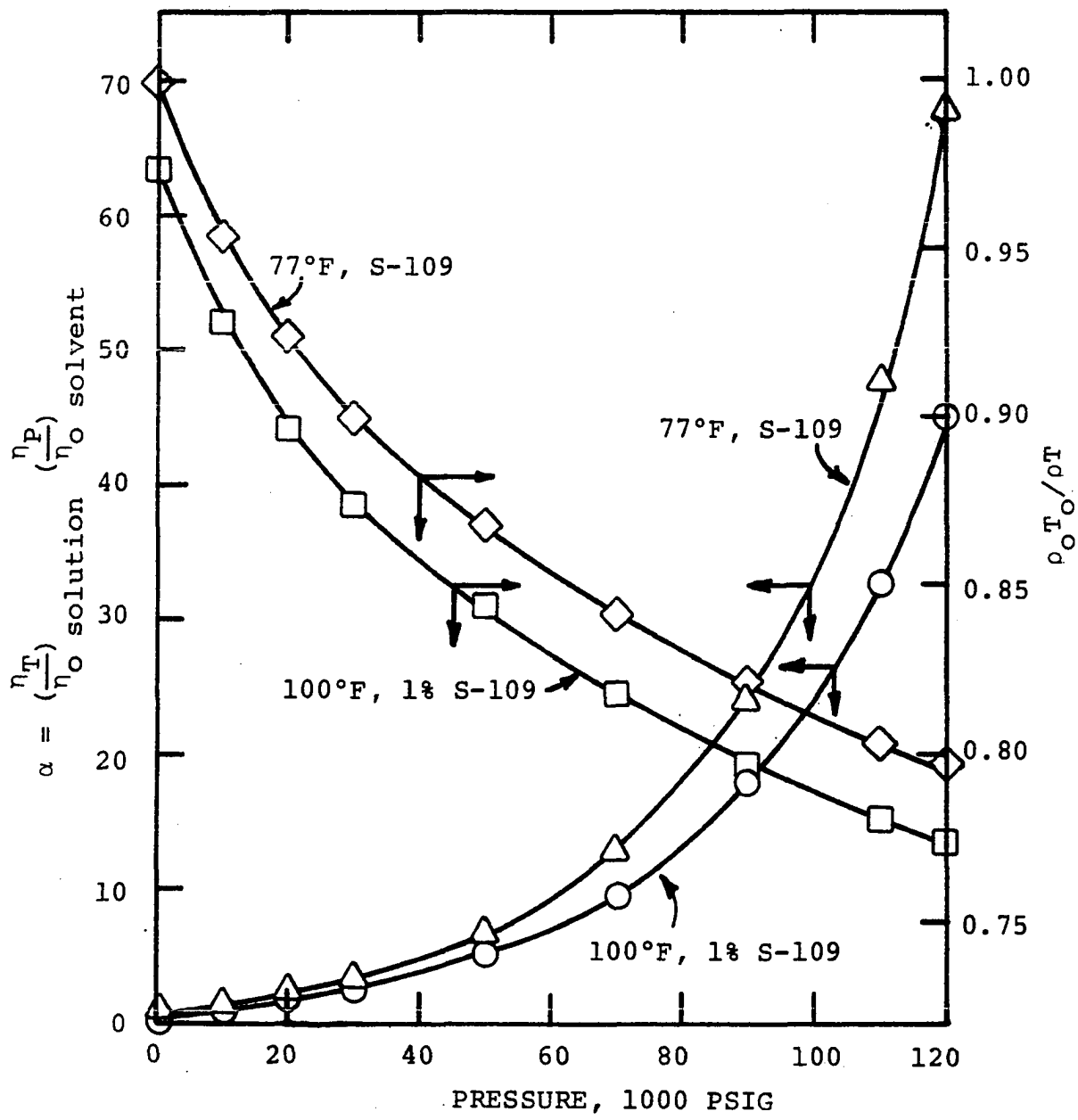

Figure 53. Effect of Pressure on α and $\rho_o T_o/\rho T$ of S-109 Solutions at 77°F and 1% S-109 Solution at 100°F.

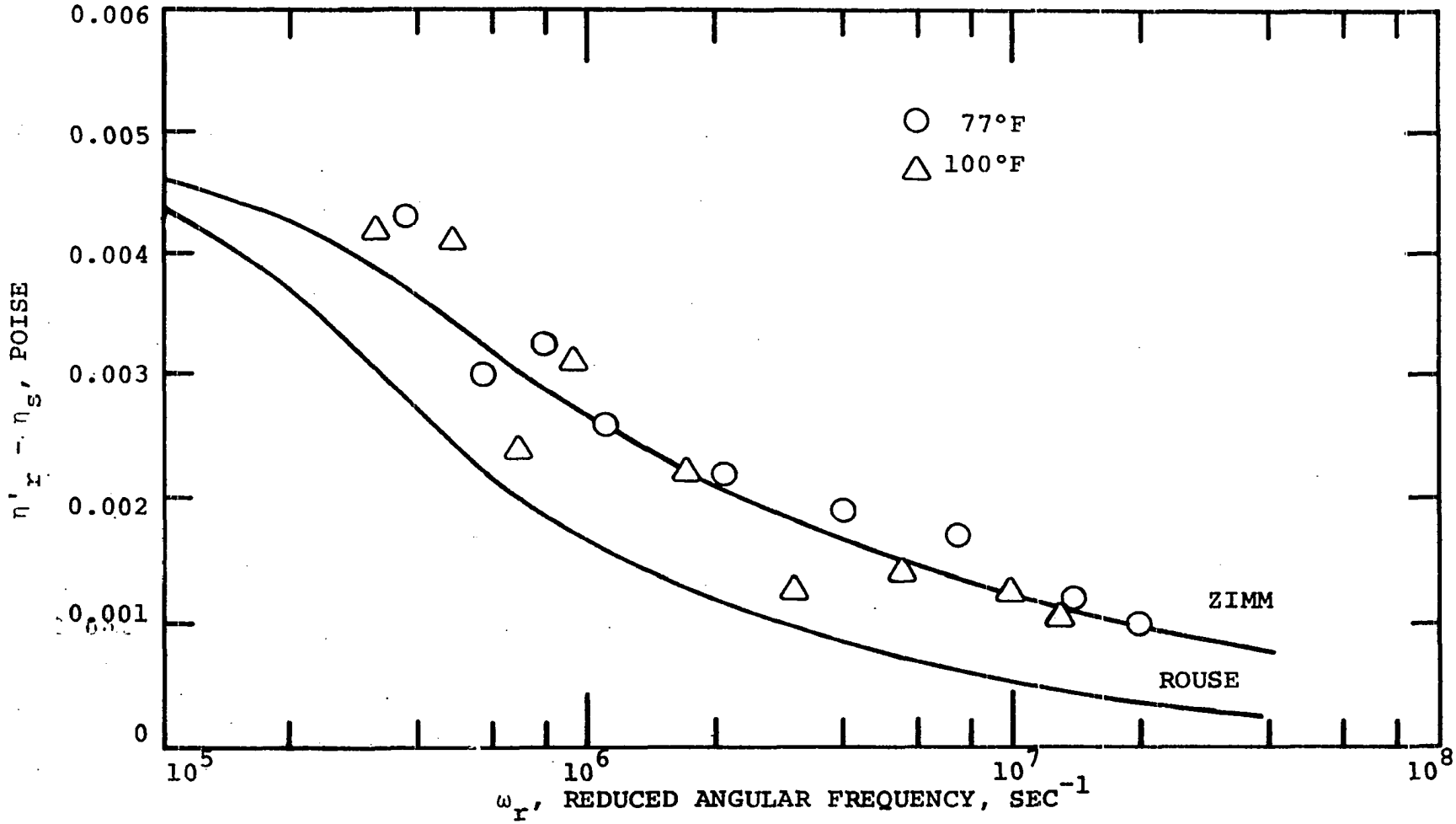

Figure 54. Effect of Reduced Angular Frequency on Reduced Dynamic Viscosity of 1 Percent S-108 Solution at 77° and 100°F.

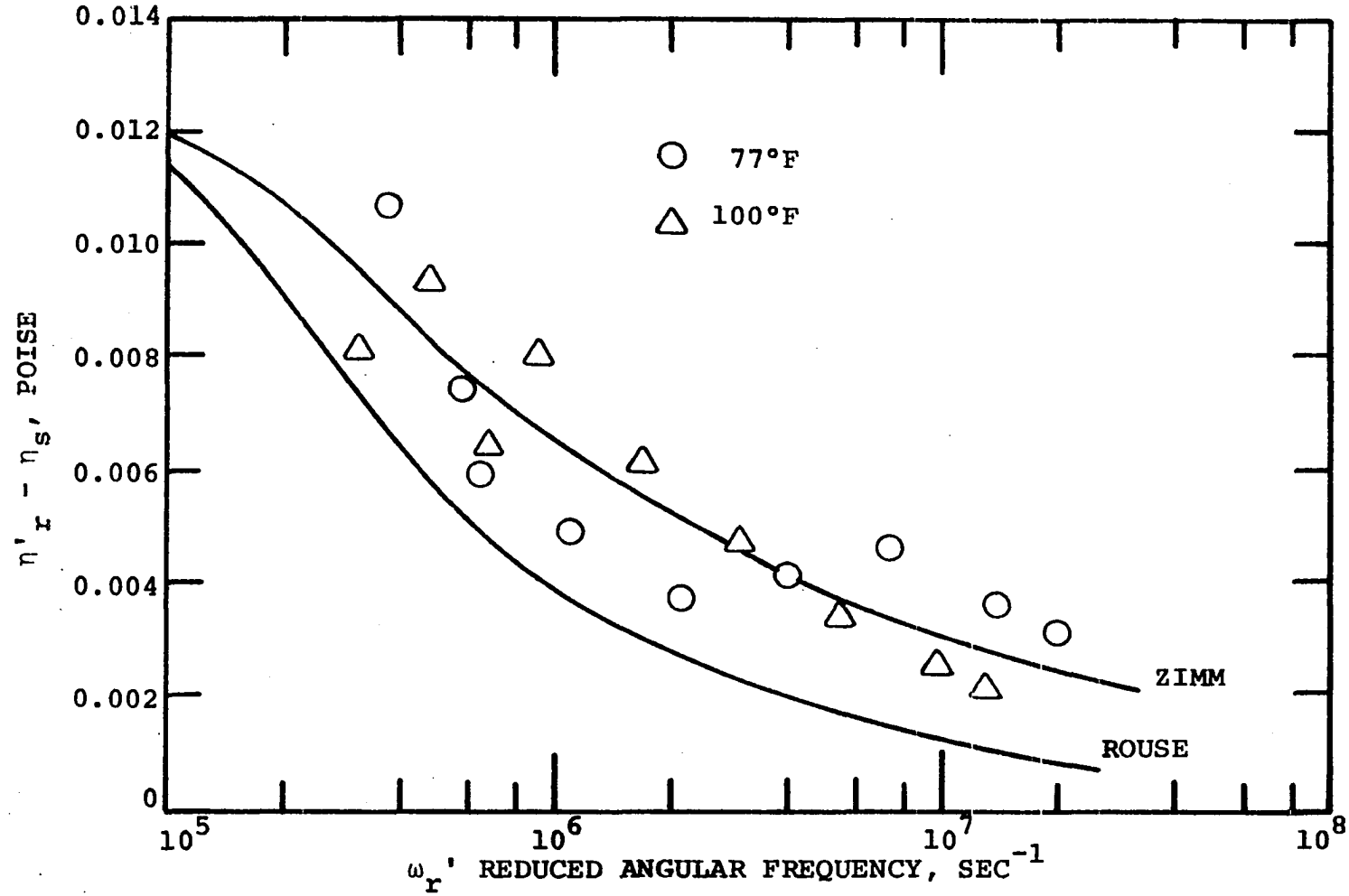

Figure 55. Effect of Reduced Angular Frequency on Reduced Dynamic Viscosity of 2 Percent S-108 Solution at 77° and 100°F.

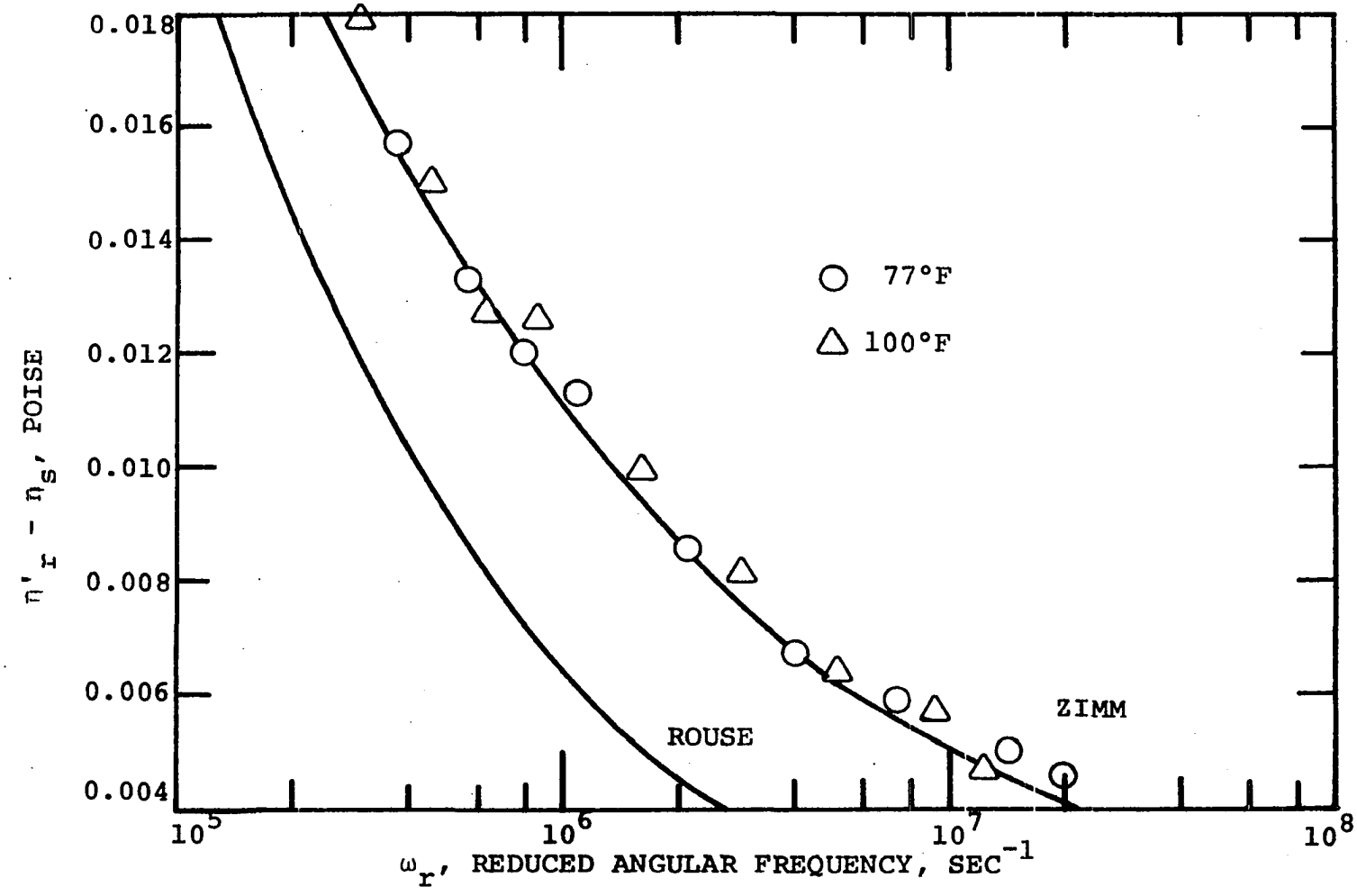

Figure 56. Effect of Reduced Angular Frequency on Reduced Dynamic Viscosity of 3 Percent S-108 Solution at 77° and 100°F.

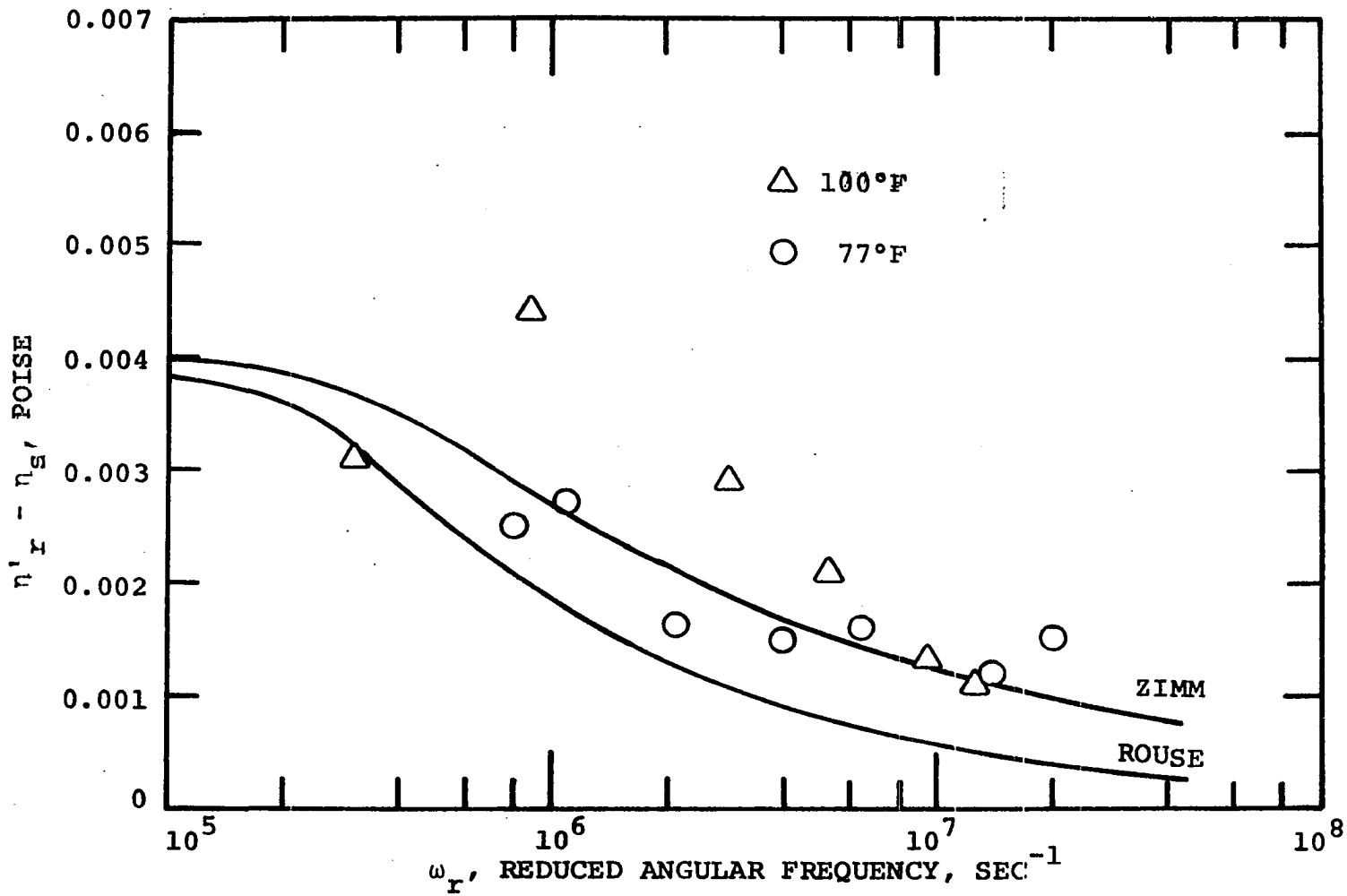

Figure 57. Effect of Reduced Angular Frequency on Reduced Dynamic Viscosity of 1 Percent S-109 Solution at 77° and 100°F.

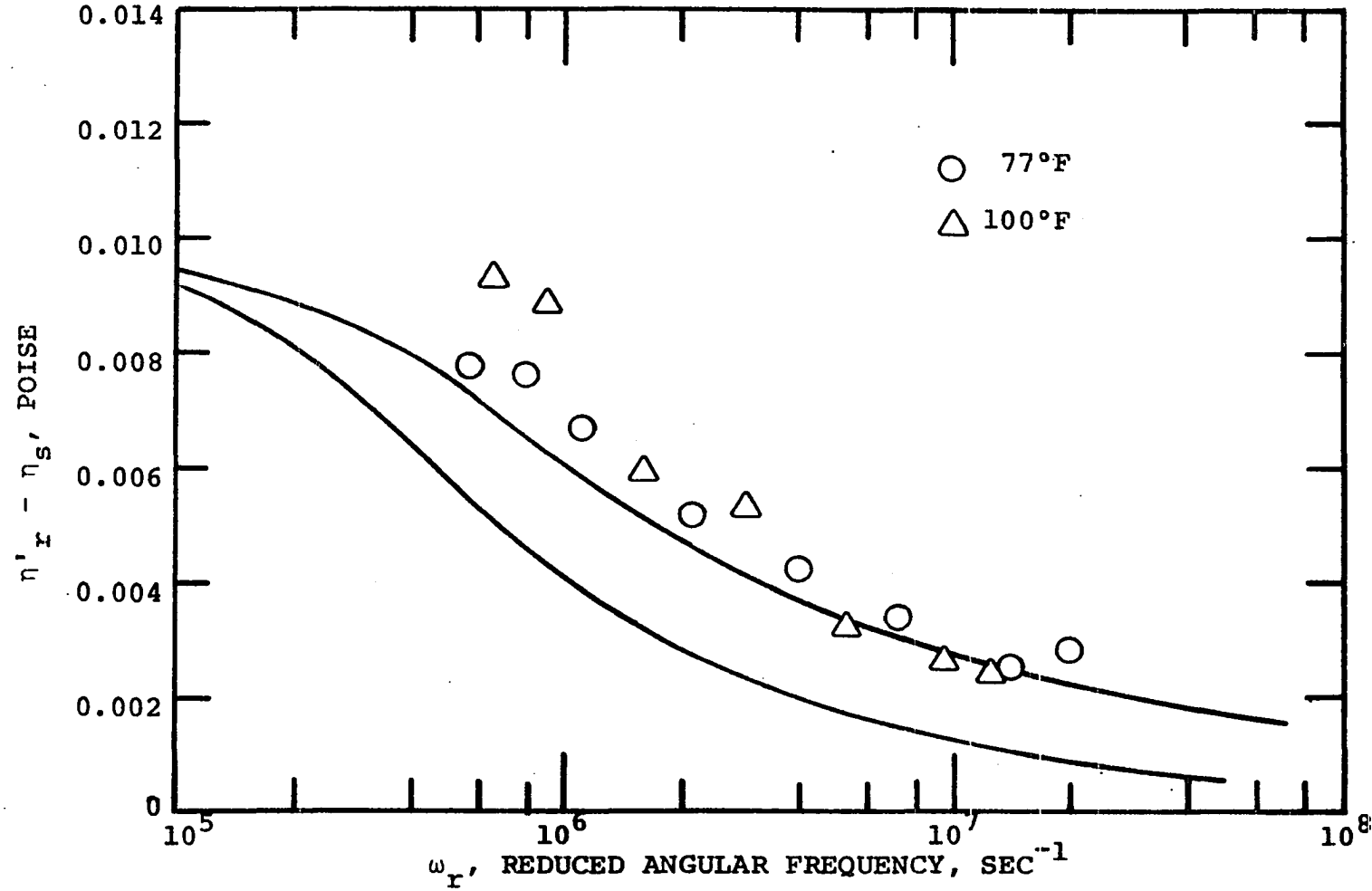

Figure 58. Effect of Reduced Angular Frequency on Reduced Dynamic Viscosity of 2 Percent S-109 Solution at 77° and 100°F.

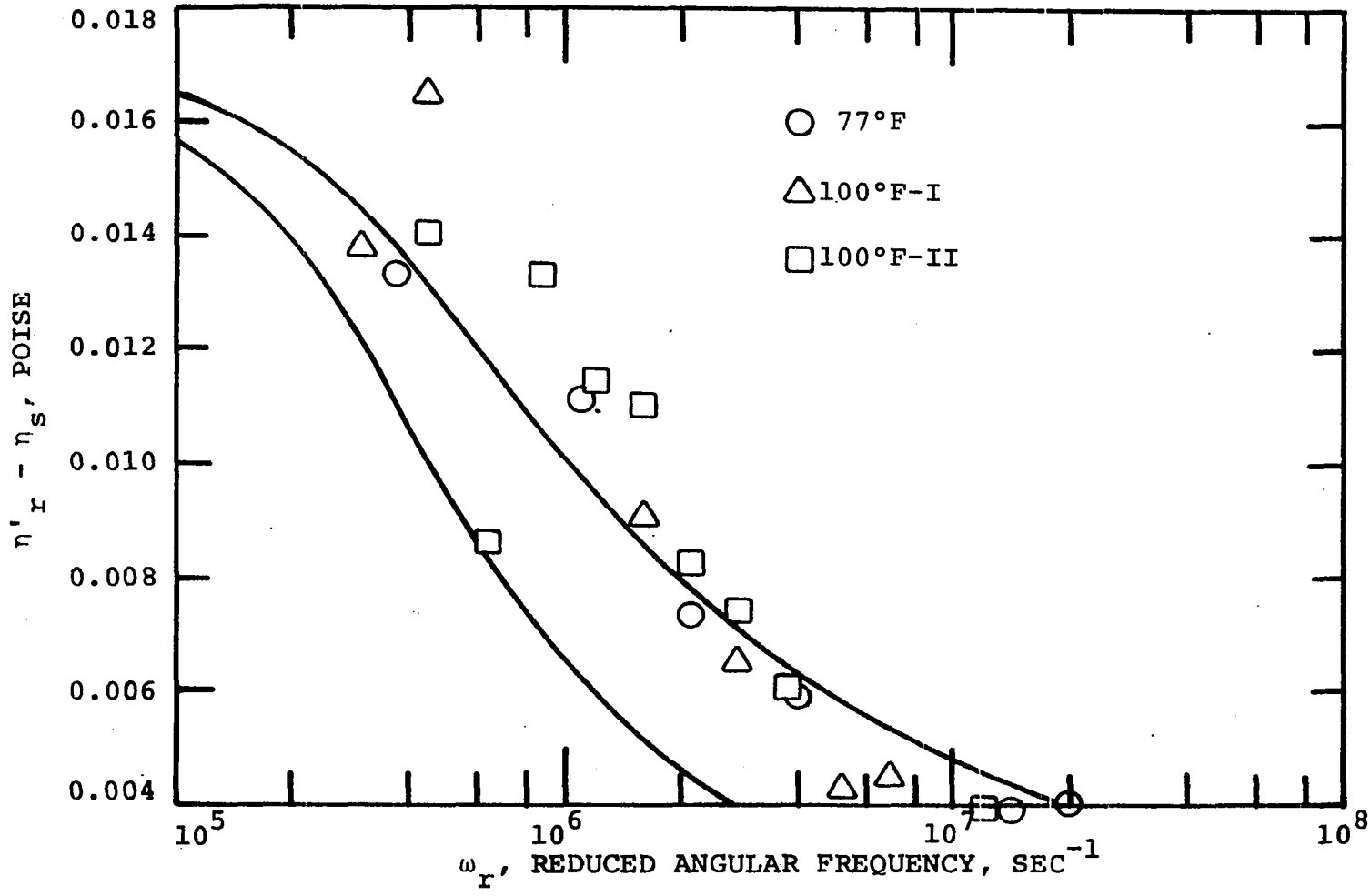

Figure 59. Effect of Reduced Angular Frequency on Reduced Dynamic Viscosity of 3 Percent S-109 Solution at 77° and 100°F.

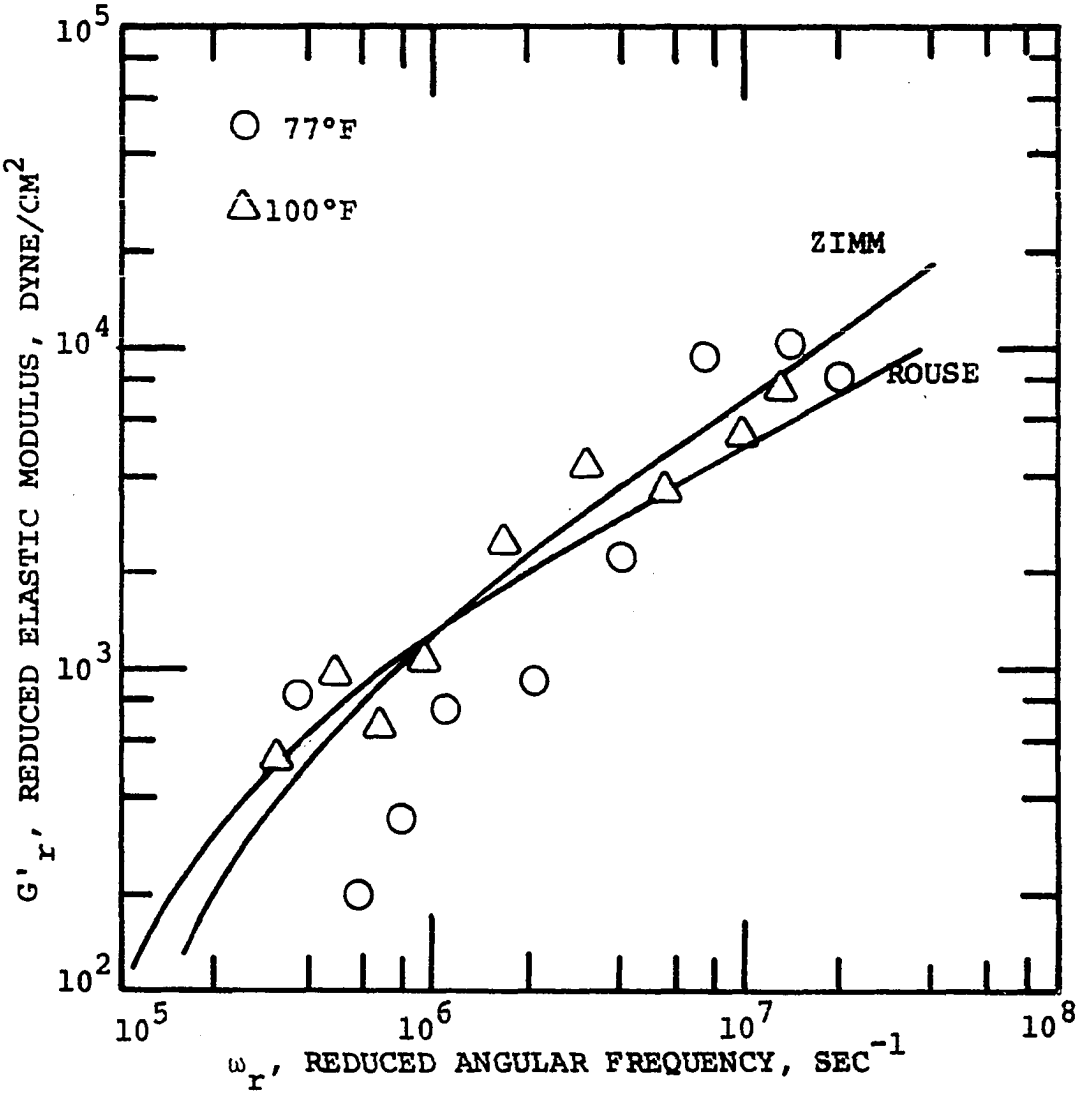

Figure 60. Reduced Elastic Modulus versus Reduced Angular Frequency of 1 Percent S-108 Solution.

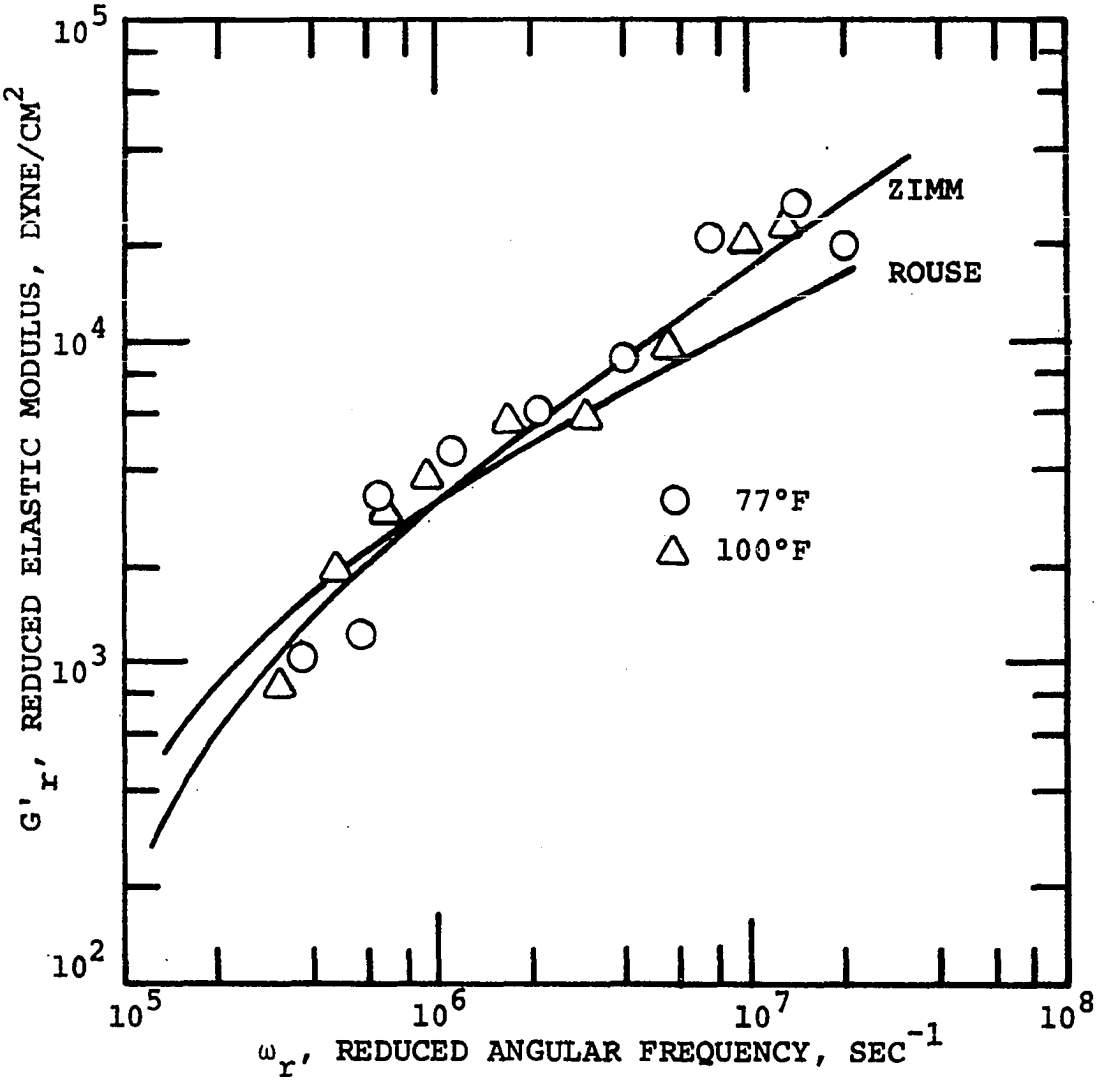

Figure 61. Reduced Elastic Modulus versus Reduced Angular Frequency of 2 Percent S-108 Solution.

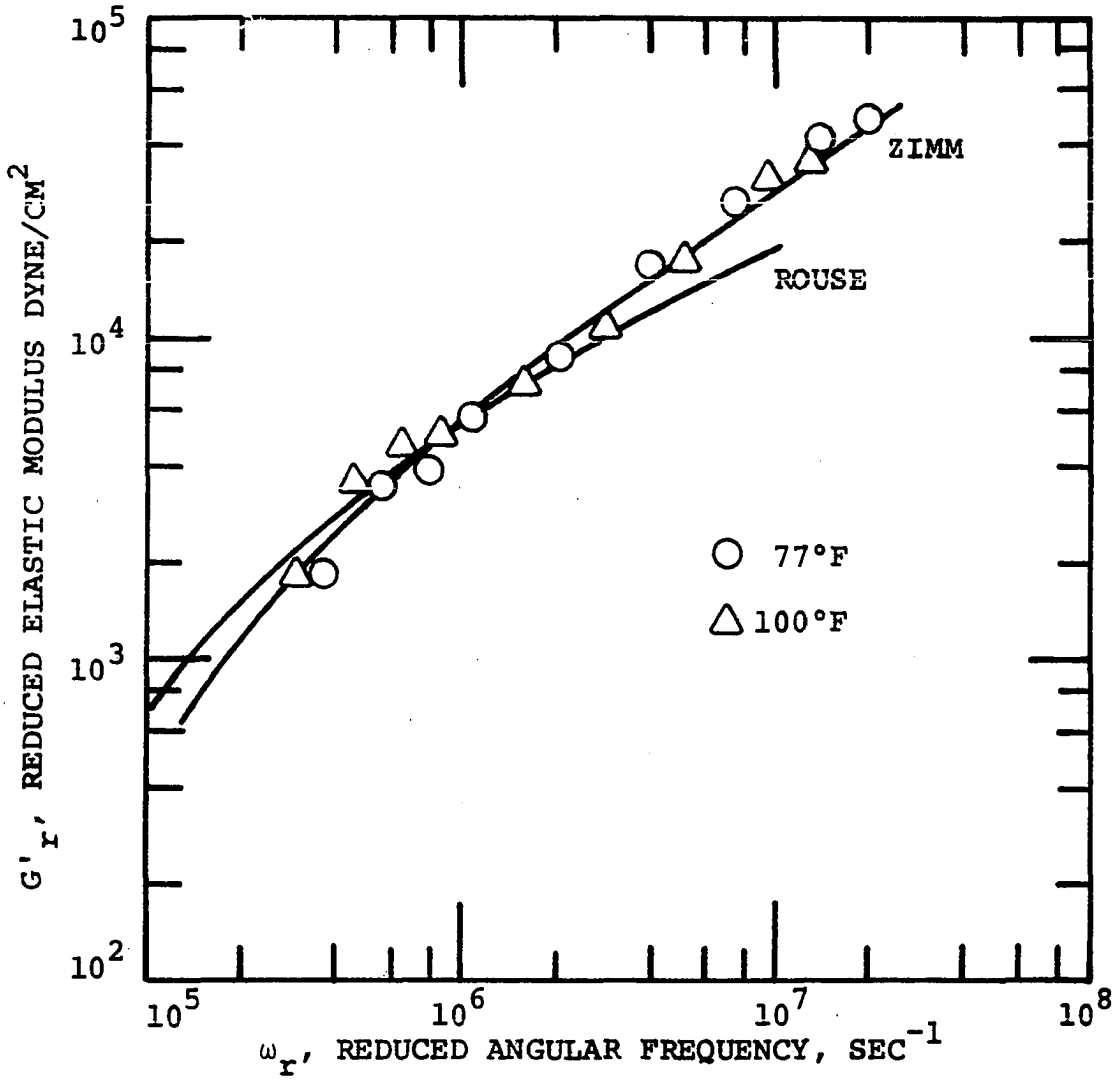

Figure 62. Reduced Elastic Modulus Versus Reduced Angular Frequency of 3 Percent S-108 Solution.

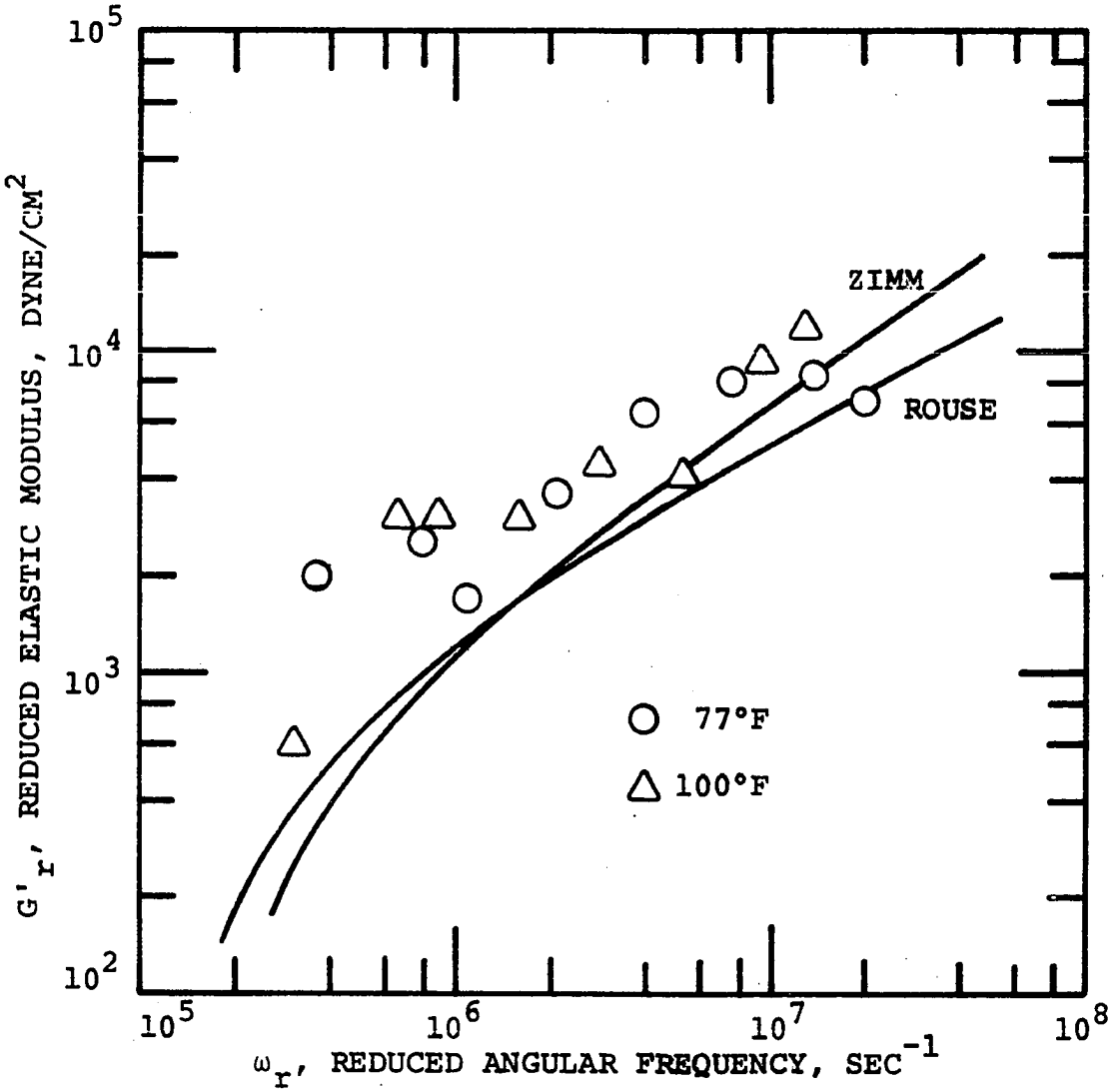

Figure 63. Reduced Elastic Modulus Versus Reduced Angular Frequency of 1 Percent S-109 Solution.

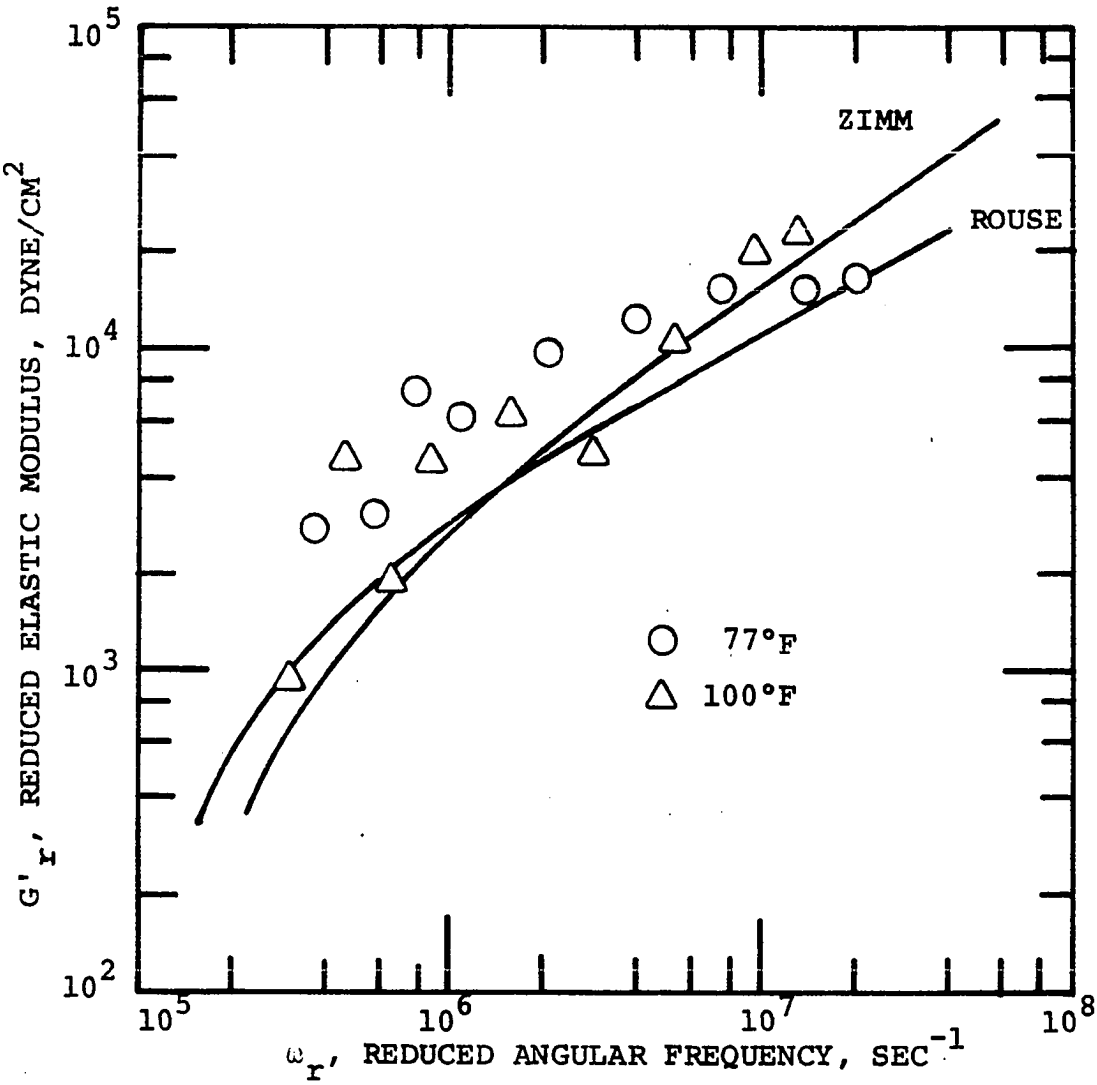

Figure 64. Reduced Elastic Modulus versus Reduced Angular Frequency of 2 Percent S-109 Solution.

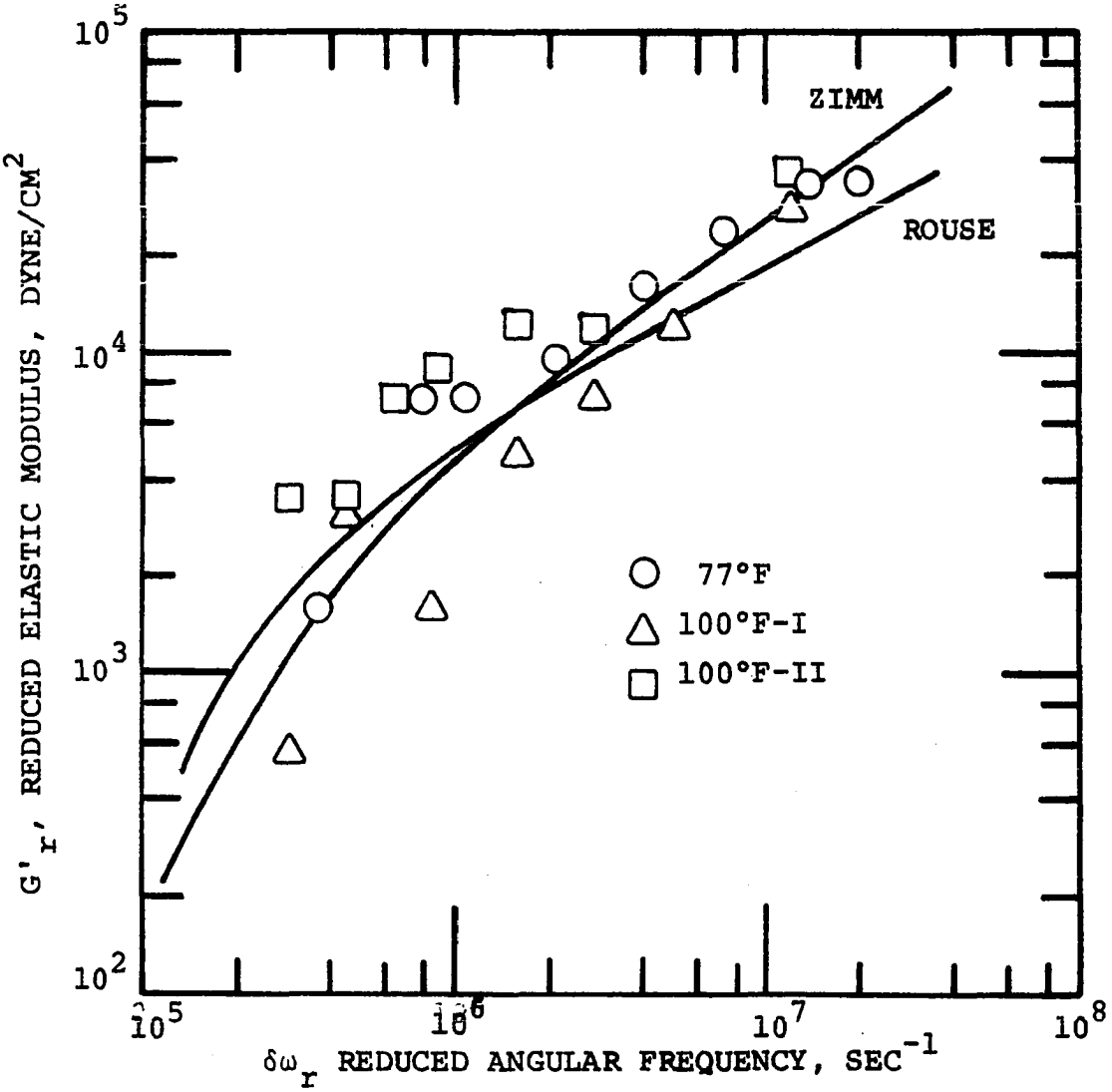

Figure 65. Reduced Elastic Modulus Versus Reduced Angular Frequency of 3 Percent S-109 Solution.

angular frequency ω_r. Data in these figures indicate that an equivalent angular frequency range of about 3×10^5 to 2×10^7 sec^{-1} was covered during these experiments.

To compare the results of this investigation with the predictions of the Zimm and Rouse theories, the values predicted by each theory for each solution were also calculated and are shown by the solid lines in each figure. The curves predicted by these theories were obtained as follows (see Chapter II):

$$G' = \frac{cRT}{M} \sum_{p=1}^{N} \frac{\omega^2 \tau_p^2}{1 + \omega^2 \tau_p^2} \qquad (52)$$

$$\eta' = \eta_s + \frac{cRT}{M} \sum_{p=1}^{N} \frac{\tau_p}{1 + \omega^2 \tau_p^2} \qquad (54)$$

$$\tau_p = \frac{6(\eta - \eta_s)}{\pi^2 p^2} \frac{M}{cRT} \qquad \text{Rouse} \quad (55)$$

$$\tau_p = \frac{1.71(\eta - \eta_s)}{\lambda' p} \frac{M}{cRT} \qquad \text{Zimm} \quad (56)$$

Substituting Equations 55 and 56 into Equation 54, the following equations result

$$\frac{\eta' - \eta_s}{\eta - \eta_s} = \frac{6}{\pi^2} \sum_{p=1}^{N} \frac{1}{p^2 \left[1 + \left(\frac{6}{\pi^2 p^2} \omega \frac{\eta - \eta_s}{cRT} M\right)^2\right]} \qquad \text{Rouse (91)}$$

$$\frac{\eta' - \eta_s}{\eta - \eta_s} = 1.71 \sum_{p=1}^{N} \frac{1}{\lambda_p' \left[1 + \left(\frac{1.71}{\lambda_p'} \omega \frac{\eta - \eta_s}{cRT} M\right)^2\right]} \qquad \text{Zimm (92)}$$

It is apparent that a plot of $(\eta' - \eta_s)/(\eta - \eta_s)$ versus dimensionless angular frequency, $\omega[(\eta-\eta_s)/cRT]M$, results in a single curve which is applicable to any polymer solution regardless of the molecular weight M, concentration, c, and temperature T (within the restrictions of each theory). The different values of τ_p associated with each theory result in a different curve for each theory.

Similarly, the elastic modulus G' can be reduced by multiplying both sides of Equation 52 by M/cRT.

$$G' \frac{M}{cRT} = \sum_{p=1}^{N} \frac{\omega^2 \tau_p^2}{1 + \omega^2 \tau_p^2} \tag{93}$$

Then, substituting for the value of τ_p from Equation 55 and 56 in the above equation one obtains

$$G' \frac{M}{cRT} = \frac{36}{\pi^4} \sum_{p=1}^{N} \frac{\frac{1}{p^4} \left(\omega \frac{\eta-\eta_s}{cRT} M\right)^2}{1 + \left[\frac{6}{\pi^2 p^2} \omega \frac{\eta-\eta_s}{cRT} M\right]^2} \quad \text{Rouse} \tag{94}$$

$$G' \frac{M}{cRT} = 2.92 \sum_{p=1}^{N} \frac{\frac{1}{\lambda'^2_p} \left(\omega \frac{\eta-\eta_s}{cRT} M\right)^2}{1 + \left[\frac{1.71}{\lambda'_p} \omega \frac{\eta-\eta_s}{cRT} M\right]^2} \quad \text{Zimm} \tag{95}$$

Therefore plotting G' M/cRT against $\omega[(\eta-\eta_s)/cRT]M$ results in a single curve for Rouse and a single curve for Zimm theories according to the above equations. Using Equations 91, 92, 94 and 95 the values of $(\eta'-\eta_s)/(\eta-\eta_s)$ and G' M/cRT for each theory were calculated by Lovell and Ferry (27) as a function of dimensionless frequency, $\omega[(\eta-\eta_s)/cRT]M$; their

results are reported in the literature (Reference 16). These values were used for plotting the curves shown in Figures 14 and 15 of Chapter II.

To obtain predictions of Rouse and Zimm theories for G' and $\eta' - \eta_s$ of any particular solution it is sufficient to multiply the ordinates of Figure 14 and 15 of Chapter II by cRT/M and $\eta - \eta_s$, respectively, and to multiply the abscissas of each curve by $cRT/M(\eta-\eta_s)$. This method was used to obtain the curve for each individual solution drawn in Figures 54 through 65. The above curves are drawn for 77°F (the reference temperature) and, therefore, the data obtained at other temperatures were first reduced to 77°F before being plotted. Appendix D gives the values of G' and $\eta' - \eta_s$ as a function of reduced angular frequency for S-108 and S-109 polystyrene solutions as predicted by the theories of Zimm and Rouse.

In polymer solutions, both polymer and solvent contribute to the dynamic viscosity of the solution, η'. Thus, by subtracting η_s from η' the contribution of the polymer molecules to the dynamic viscosity of the solution is obtained. It is this contribution which is plotted in Figures 54 through 59. However, the shear elasticity, G', of the solution is caused only by the polymer molecules.

The values of $\eta' - \eta_s$ plotted in Figures 54 through 59 generally indicate a good agreement with the Zimm theory. This agreement is especially apparent in case of the S-108

polystyrene solutions as shown in Figures 54, 55 and 56. The data of the S-109 polystyrene solutions plotted in Figures 57, 58 and 59 show some scatter especially at lower ranges of pressure. Nevertheless, these data also show a better agreement with the Zimm rather than with the Rouse theory.

In case of G', the predictions of Rouse and Zimm theories are so similar in the range of reduced frequencies of this experiment that a distinction between the theories is more difficult. Considering the general trend of the data, rather than the absolute magnitudes of G', it can be concluded that the behavior is more Zimm-like in the frequency and concentration ranges of this experiment.

Because of errors inherent in the data and calibration of the viscometer, no justification could be found to compare the data with other theories such as Tschoegl's theory (51, 52). The predictions of these other theories are intermediate between the predictions of the Rouse and Zimm theories. Therefore, to distinguish which one of these theories best represents the data obtained in this study would require a higher level of experimental accuracy. As a result, only the extreme cases (Rouse and Zimm theories) were considered.

To obtain a better overall picture of viscoelastic behavior of the solutions used in this investigation, values of $\eta_r' - \eta_s$ and G_r' were converted into dimensionless forms (by dividing them by $\eta - \eta_s$ and cRT/M, respectively) and were plotted as a function of reduced dimensionless angular

frequency $a_{T,p}\ \omega[(\eta-\eta_s)/cRT]M$. Thus, the data obtained from all solutions could be plotted on the same graph (similar to Figures 14 and 15 in Chapter II) regardless of the concentration, temperature and molecular weight of the polymer system.

Figure 66 shows the plot of reduced dimensionless dynamic viscosity $(\eta_r' - \eta_s)/(\eta - \eta_s)$, of 1, 2 and 3 weight percent solutions of S-108 polystyrene as a function of reduced dimensionless angular frequency, $a_{T,p}\omega[(\eta - \eta_s)/cRT]M$. This figure clearly indicates how the method of reduced variables, together with the conversion of data into dimensionless form, can be used to superimpose the data obtained with various solutions and at various conditions on one graph. Figure 67 shows a similar plot for the 1, 2 and 3 weight percent solutions of S-109 polystyrene in toluene. Similarly, the reduced dimensionless elastic modulus, $G_r'\ M/cRT$, of 1, 2 and 3 weight percent solutions of S-108 and S-109 polystyrenes are plotted against the reduced dimensionless angular frequency as shown in Figures 68 and 69. Figures 66 and 67 could be further combined into one plot for reduced dimensionless dynamic viscosity as a function of reduced dimensionless angular frequency. Similarly, Figures 68 and 69 could also be combined. However, to facilitate comparison of the results of this investigation with the results of other investigators, separate plots were prepared for S-108 and S-109 polymer systems.

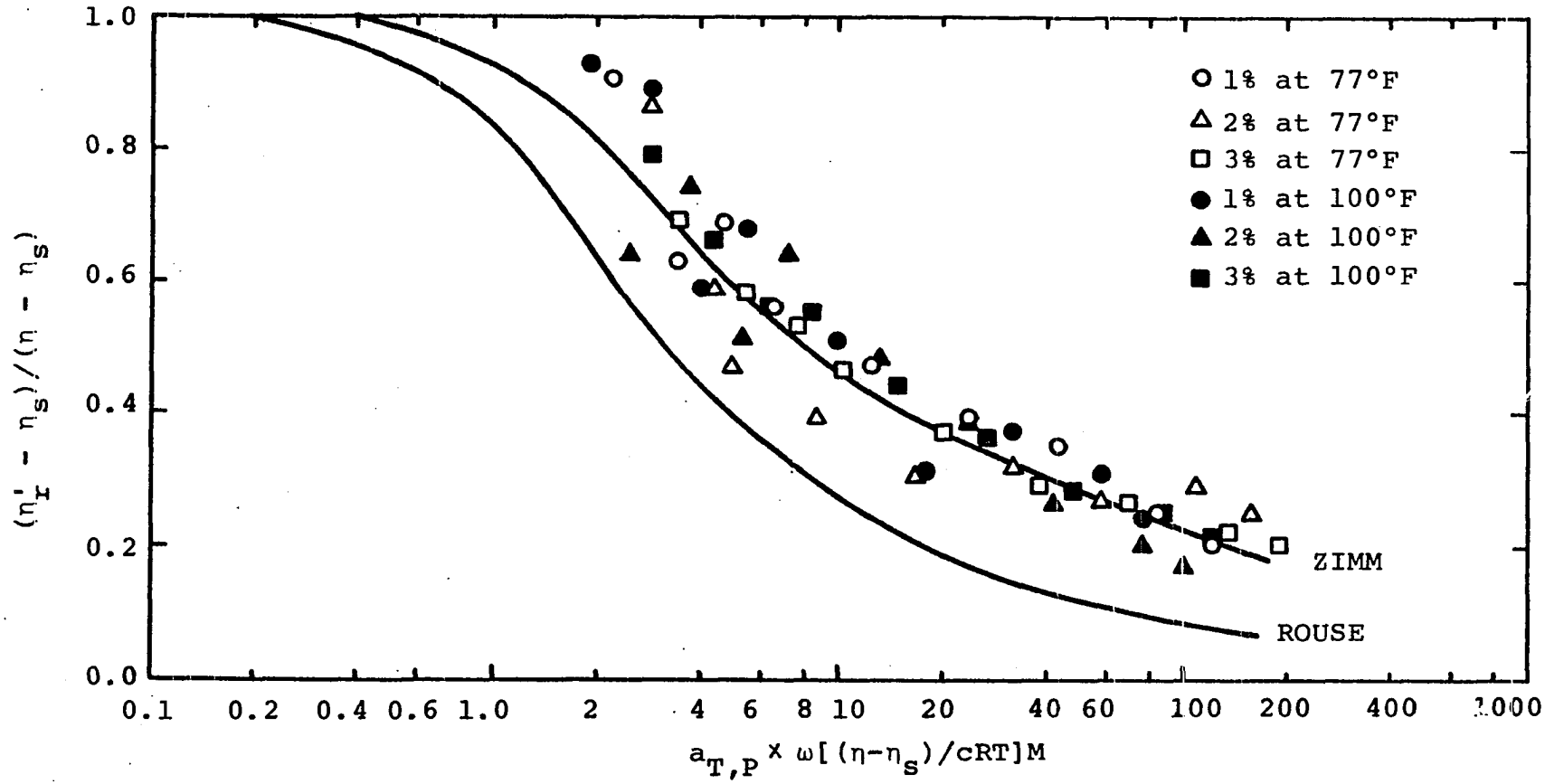

Figure 66. Reduced Dimensionless Dynamic Viscosity of 1, 2 and 3 Weight Percent S-108 Solutions as a Function of Reduced Dimensionless Angular Frequency at 77° and 100°F.

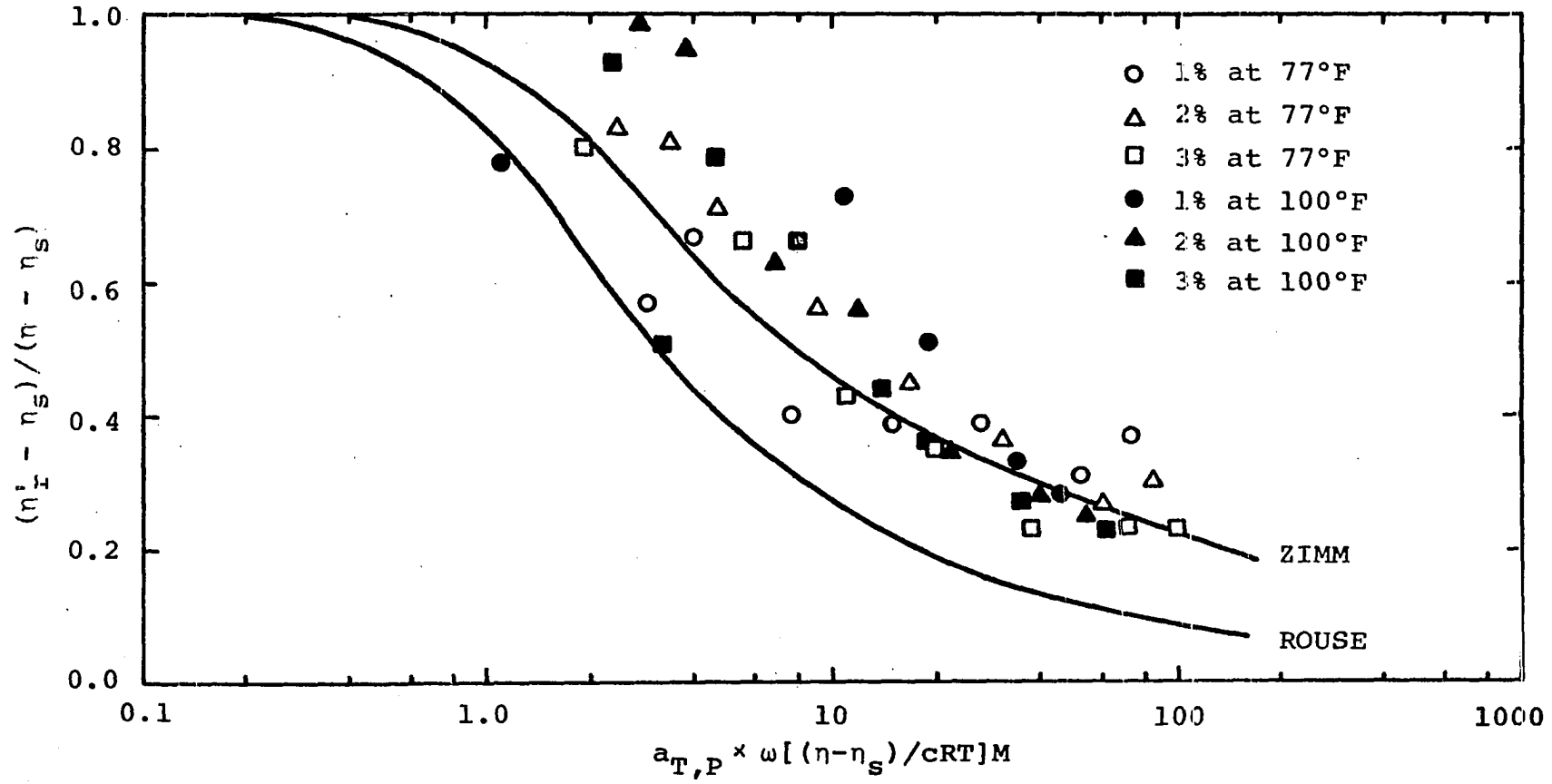

Figure 67. Reduced Dimensionless Dynamic Viscosity of 1, 2 and 3 Weight Percent S-109 Solutions as a Function of Reduced Dimensionless Angular Frequency at 77° and 100°F.

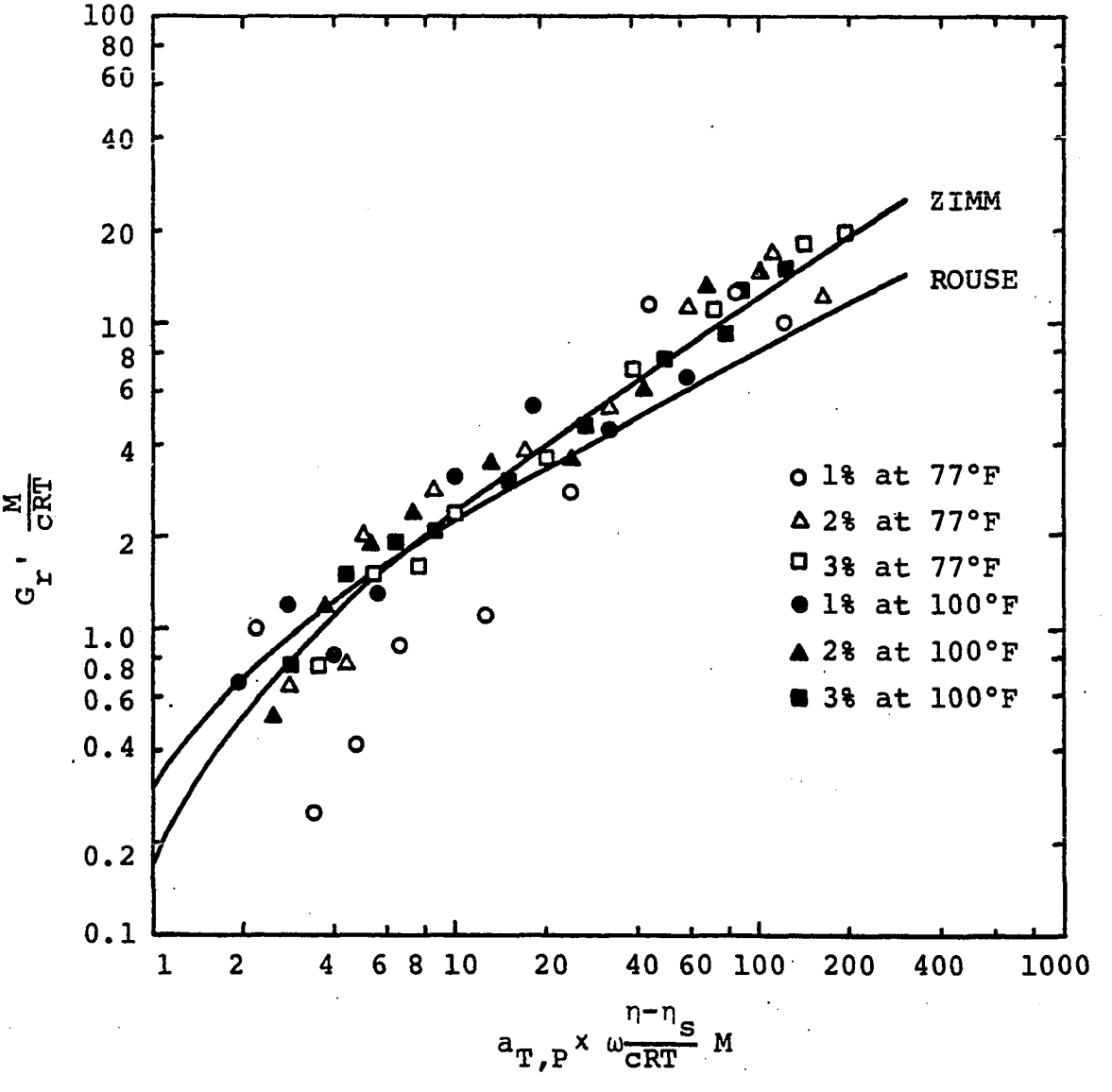

Figure 68. Reduced Dimensionless Elastic Modulus of 1, 2 and 3 Weight Percent S-108 Solutions as a Function of Reduced Dimensionless Angular Frequency at 77° and 100°F.

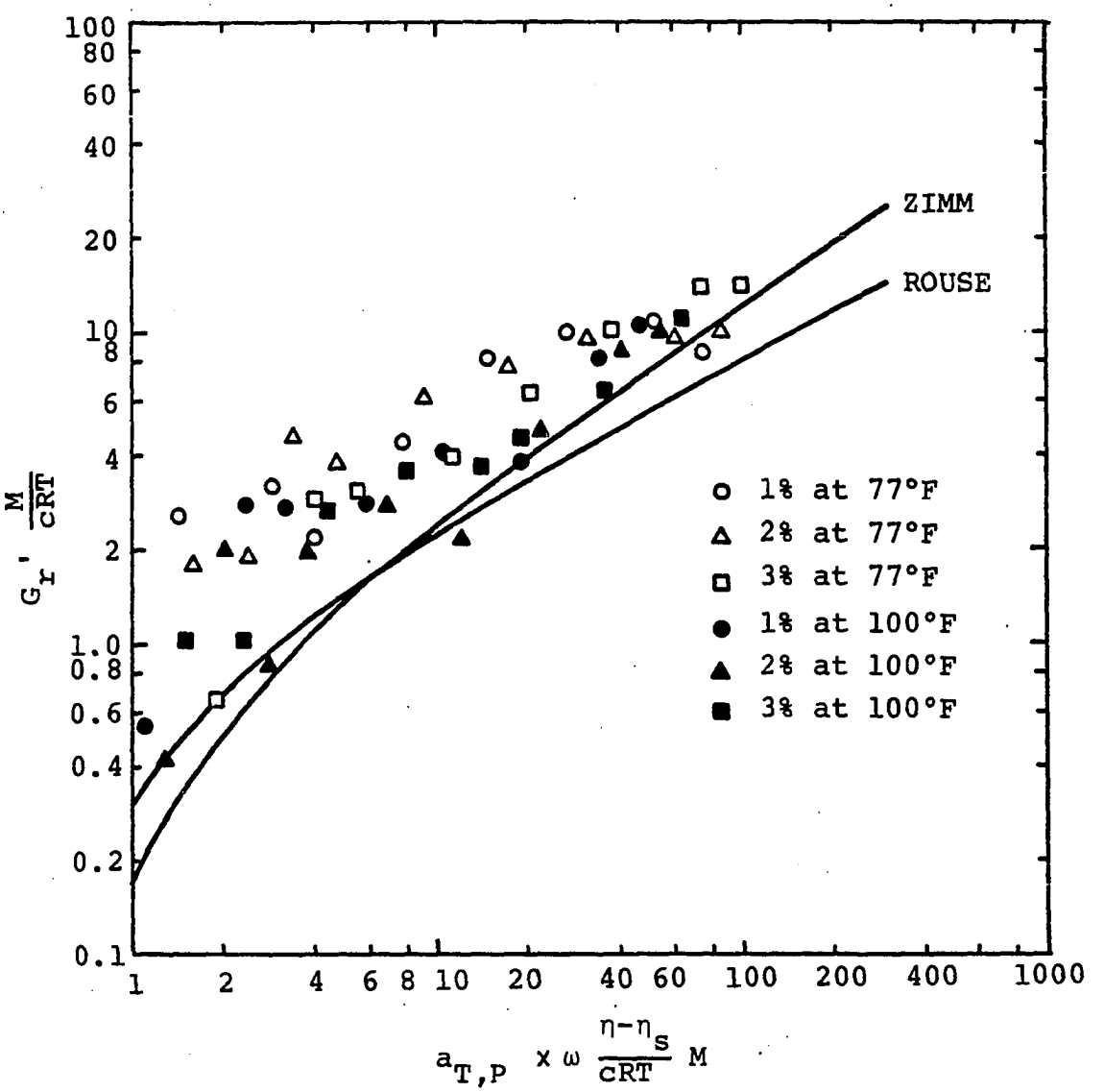

Figure 69. Reduced Dimensionless Elastic Modulus of 1, 2 and 3 Weight Percent S-109 Solutions as a Function of Reduced Dimensionless Angular Frequency at 77° and 100°F.

Figures 66 through 69 again indicate good agreement with the Zimm theory. This result also agrees with the results of other investigators for S-108 and S-109 polystyrene systems. DeMallie, et al. (15) measured the storage, G', and loss, G", shear moduli of dilute solutions of S-108 polystyrene in a highly viscous solvent (aroclor 1248, a chlorinated diphenyl) at atmospheric pressure and various temperatures from 0 to 40°C. The range of concentration was from 0.5 to 4.0 weight percent and the frequency range from 0.01 to 400 Hz. This range of frequency is much lower than the fundamental frequency of the quartz crystal used in this investigation. However, application of a much more viscous solvent than toluene resulted a similar range of reduced frequencies in both investigations. Up to 3 weight percent concentration, the data reported by DeMallie (15) closely agree with the Zimm theory in the same way as does the data of this investigation. However, a deviation from Zimm toward Rouse theory for the 4 percent solution at the highest reduced frequencies was observed.

Harrison, Lamb and Matheson (21) have also measured the viscoelastic properties of dilute solutions of polystyrene in toluene at atmospheric pressure with quartz crystals having resonant frequencies of 38 and 73 kHz. By using the temperature as a variable, and taking data at temperatures from +50° to -70°C, they covered essentially the same range of reduced frequencies as was obtained in this investigation. Their

measurement of the viscoelastic properties of solutions of polystyrenes of different molecular weights in toluene (with concentrations below 3 gm per 100 ml) indicated a good agreement with the Zimm theory up to a molecular weight of 3.64×10^5. Above this molecular weight a tendency toward Rouse-like behavior was observed. Deviation from the Zimm theory at higher molecular weights and concentrations has also been reported in later investigations (18, 25).

Figures 66 through 69 indicate an overall agreement of the data taken in this investigation with the Zimm theory, and no apparent trend toward the Rouse theory at higher reduced frequencies is observed. This result confirms the observations by other investigators regarding the agreement of dynamic data of dilute solutions of polystyrenes, depending on the molecular weight, with the Zimm theory over similar range of reduced dimensionless frequency obtained in this investigation.

As mentioned earlier, the range of reduced frequencies obtained in this investigation, by using pressure as a variable, is basically the same as the range of reduced frequencies obtained by DeMallie, et al. (15) and Harrison, et al. (21) by using temperature and frequency as variables. This observation indicates that pressure, temperature or frequency each can be used effectively to evaluate molecular theories of dilute polymer solutions and to provide information on viscoelastic behavior of polymer systems over a wide range of

shear rates. The above conclusion also indicates the importance of the concept of reduced variables in dynamic experiments. Thus, the choice of either temperature or pressure as the variable in dynamic experiments should be dictated by the ease and efficiency of its utilization in any particular investigation.

Finally, as it was mentioned in Chapter II, the theories of Zimm and Rouse deal with the behavior of an isolated polymer molecule and therefore apply to infinite dilution. For this reason, the evaluation of these theories should actually be carried out by plotting $[G']$ and $[\eta' - \eta_s]$ against $\omega[\eta]\eta_s M/RT$. The values of $[G']$ and $[\eta' - \eta_s]$ can be obtained in the same manner as in determination of the intrinsic viscosity $[\eta]$; in other words, G'/c and $(\eta' - \eta_s)/c$ are plotted against concentration c and extrapolated to zero concentration.

Due to some scatter in the viscosity and elasticity data as a function of concentration, the above procedure could not be employed in this investigation. However, according to Ferry (Reference 16, p. 223), in the concentration range such that $c[\eta] \lesssim 2$, the interpenetration of the random coils into the domains of each other is negligible and no significant deviation from the condition of Rouse and Zimm theories would result. To find out whether the solutions used in this investigation satisfy the above criteria, the values of $c[\eta]$ for each solution were calculated at both 77°

and 100°F and are reported in Table 10. Except for the 3 weight percent solution of S-108 at 100°F whose c[η] value is slightly above 2, the other c[η] values are all less than 2. Therefore, the deviation from the condition of Rouse and Zimm theories should be negligible.

TABLE 10

VALUES OF c[η] OF S-108 AND S-109 POLYMER SOLUTIONS AT 77° AND 100°F

Concentration	S-108		S-109	
	77°F	100°F	77°F	100°F
1 percent	0.603	0.712	0.578	0.578
2 percent	1.206	1.425	1.157	1.155
3 percent	1.809	2.137	1.735	1.733

The values of c used in calculation of the above figures are in grams of polymer per cubic centimeter of solution.

CHAPTER VII

CONCLUSIONS

The results of this investigation demonstrate that:

1. Viscoelastic behavior was observed in solutions of 1, 2 and 3 weight percent S-108 and S-109 polystyrenes in toluene at both 77° and 100°F, over the entire pressure range of this investigation, 0 to 120,000 psig.
2. The dynamic viscosity, η', and elasticity, G', of these solutions increased exponentially with pressure at both temperatures.
3. Variation of the dynamic viscosity of each solution with concentration followed a linear relationship at each particular pressure and temperature. Extrapolation of viscosity-concentration lines to zero concentration resulted in values which, within the experimental error, were equal to the toluene viscosity at those conditions. It was therefore concluded that the linear relationship between the viscosity and concentration could be extended to infinite dilution.
4. The method of reduced variables was used to convert the information obtained at various pressures and temperatures

to a wide range of reduced frequencies at a reference condition. Utilizing this method, in combination with data at 77° and 100°F and from zero to 120,000 psig, resulted in a reduced frequency range of 3×10^5 to 2×10^7 sec^{-1}.

5. Pressure can be used as effectively as temperature to simulate a wide range of reduced frequencies. Therefore, in future investigations the choice of either pressure or temperature as the variable should be dictated by the ease, efficiency and accuracy of its utilization in that particular investigation.
6. Plots of contributions of polymers to the viscosity and elasticity of each solution showed a much closer agreement with the Zimm than with the Rouse theory.

NOMENCLATURE

A	area, or constant in Andrade equation
a_T	ratio of relaxation times at two different temperatures
$a_{T,P}$	ratio of relaxation times at two different temperatures and pressures
B	constant in Andrade equation
c	concentration
e	base of natural logarithms
F	force
f	frequency, or resonant frequency
f_r	reduced frequency
f_o	resonant frequency measured in vacuum
G	shear modulus
G*	complex dynamic shear modulus
G'	dynamic shear storage modulus
G"	dynamic shear loss modulus
G_r'	reduced shear storage modulus
$G_r"$	reduced shear loss modulus
G_c	conductance at resonant frequency
H	shear relaxation spectrum
h	parameter indicating the degree of hydrodynamic interaction in the Tschoegl theory

i	$(-1)^{1/2}$
$J(t)$	shear creep compliance
K_f	crystal constant related to frequency measurement
K_R	crystal constant related to resistance measurement
k	Boltzmann's constant
k'	constant
L	level change in the sight glass
L_c	effective electrical inductance
ℓ	length
M	molecular weight
N	number of submolecules in a polymer molecule
n	number of polymer molecules per cc
P	pressure, or probability of the polymer molecules being in a deformed state of distribution
P_o	reference pressure, or probability of finding the polymer molecules in their most probable distribution
p	summation index in Zimm and Rouse theories
R	gas constant
R_E	resistance at resonant frequency
R_{E_o}	resistance at resonant frequency in vacuum
R_M	mechanical resistance
r	radius
S	entropy
T	absolute temperature

T_o reference temperature

t time

v velocity

v_o peak velocity

X_M mechanical reactance

x linear displacement in x direction

y linear displacement in y direction

Z_M complex mechanical impedance

Greek Letters

Γ Propagation constant

γ shear strain

$\dot{\gamma}$ rate of strain

γ^* complex shear strain

γ' real part of complex strain

γ'' imaginary part of complex strain

γ_o peak strain

δ phase angle between stress and strain

ε parameter describing extent of expansion of a macromolecule in a solvent

η Newtonian shear viscosity

η^* complex dynamic shear viscosity

η' real part of dynamic viscosity

η_r' reduced real part of dynamic viscosity

η'' imaginary part of dynamic viscosity

η_{rel} relative viscosity

η_s	solvent viscosity
η_{sp}	specific viscosity
θ	integration variable
λ	numerical coefficients in Zimm theory
ρ	density
ρ_o	density at reference conditions
σ	shear stress
σ^*	complex shear stress
σ'	real part of complex stress
σ''	imaginary part of complex stress
$\dot{\sigma}$	rate of stress
σ_o	peak stress, or applied stress at time zero
σ_1	applied stress at time t_1
τ	relaxation time
τ_i	relaxation time of the element of mechanical model
ϕ	volume fraction
ω	angular frequency
ω_r	reduced angular frequency

REFERENCES

1. Andrade, E. N. C. "The Viscosity of Liquids." Nature, 125, 309 (1930).

2. Appeldoorn, J. K.; Okrent, E.; and Philippoff, W. "Viscosity and Elasticity at High Pressures and High Shear Rates." Proc. Am. Pet. Inst., 42 (3), 163 (1962).

3. ASME Pressure Viscosity Report, Vol. II. The American Society of Mechanical Engineers, New York, 1953.

4. Babb, S. E., Jr. "Simple High Pressure Valves." Rev. Sci. Instrum., 35, 917 (1964).

5. Baker, W.; Mason, W. P.; and Heiss, J. "Mechanical Properties of Discrete Polymer Molecules." J. Poly. Sci., 8, 129 (1952).

6. Barlow, A. J.; Harrison, G.; Richter, J.; Seguin, H.; and Lamb, J. "Electrical Methods for the Viscoelastic Behavior of Liquids Under Cyclic Shearing Stress." Lab. Pract., 10, 786 (1961).

7. Bridgman, P. W. The Physics of High Pressure. London: G. Bell and Sons, 1952.

8. Bridgman, P. W. "The Measurement of Hydrostatic Pressures up to 20,000 Kilograms per Square Centimeter." Proc. Am. Acad. Arts Sci., 47, 321 (1911).

9. Bridgman, P. W. "The Volume of Eighteen Liquids as a Function of Pressure and Temperature." Proc. Am. Acad. Arts Sci., 66, 185 (1931).

10. Bridgman, P. W. "Further Rough Compression to 40,000 Kg/cm^2, Specially Certain Liquids." Proc. Am. Acad. Arts Sci., 77, 129 (1949).

11. Bridgman, P. W. "The Effect of Pressure on the Viscosity of Forty-Three Pure Liquids." Proc. Am. Acad. Arts Sci., 61, 57 (1926).

12. Bueche, F. Physical Properties of Polymers. New York: Interscience Publishers, 1962.

13. Chang, Z. T. "The Dielectric Constants of Liquids Under High Pressure." Chinese J. of Phys., 1, 1 (1934).

14. Charng, T. T. "Viscoelastic Properties of Dilute Polymer Solution and Lubricants at High Pressure." Ph.D. dissertation, University of Oklahoma, Norman, Oklahoma, 1974.

15. DeMallie, R. B., Jr.; Birnboim, M. H.; Frederick, J. E.; Tschoegl, N. W.; and Ferry, J. D. "Viscoelastic Properties of Dilute Polystyrene Solutions and Verification of the Zimm Theory." J. Phys. Chem., 66, 536 (1962).

16. Ferry, J. D. Viscoelastic Properties of Polymers, 2nd ed. New York: Wiley, 1970.

17. Flory, P. J. Principles of Polymer Chemistry. Ithaca, New York: Cornell University, 1953.

18. Frederick, J. E.; Tschoegl, N. W.; and Ferry, J. D. "Dynamic Mechanical Properties of Dilute Polystyrene Solutions: Dependence on Molecular Weight, Concentration and Solvent." J. Phys. Chem., 68, 1974 (1964).

19. Gross, B. Mathematical Structure of the Theories of Viscoelasticity. Paris: Hermann, 1968.

20. Hamann, S. D. Physico-Chemical Effect of Pressure. New York: Academic Press, 1957.

21. Harrison, G.; Lamb, J.; and Matheson, A. J. "The Viscoelastic Properties of Dilute Solutions of Polystyrene in Toluene." J. Phys. Chem., 68, 1072 (1964).

22. Huggins, M. L. "The Viscosity of Dilute Solutions of Long-Chain Molecules. I. Dependence on Concentration." J. Am. Chem. Soc., 64, 2716 (1942).

23. Kirkwood, J. G., and Riseman, J. "The Intrinsic Viscosities and Diffusion Constants of Flexible Macromolecules in Solution." J. Chem. Phys., 16, 565 (1948).

24. Lamb, H. Hydrodynamics. New York: Dover Publications, 1945.

25. Lamb, J., and Matheson, A. J. "The Viscoelastic Properties of Polystyrene Solutions." Proc. Roy. Soc. (London), A281, 207 (1964).

26. Leaderman, H. Elastic and Creep Properties of Filamentous Materials and Other High Polymers. Washington: The Textile Foundation, 1943.

27. Lovell, S. E., and Ferry, J. D. "Numerical Evaluation of Normal Coordinate Theories for Viscoelastic Properties of Polymers." Department of Chemistry, University of Wisconsin, Madison, Wisconsin, 1961.

28. Mason, W. P. Piezoelectric Crystals and Their Application to Ultrasonics. New York: Van Nostrand Co., 1950.

29. Mason, W. P. "Measurement of the Viscosity and Shear Elasticity of Liquids by Means of a Torsionally Vibrating Crystal." Trans. Am. Soc. Mech. Engrs., 69, 359 (1947).

30. McSkimin, H. J. "Measurement of Dynamic Shear Viscosity and Stiffness of Viscous Liquids by Means of Travelling Torsional Wave." J. Acoust. Soc. Am., 24, 355 (1952).

31. McSkimin, H. J. "Ultrasonic Methods for Measuring the Mechanical Properties of Liquids and Solids." Physical Acoustics, W. P. Mason, ed., Vol. IA, Chapter 4. New York: Academic Press, 1964.

32. Nielsen, L. E. Mechanical Properties of Polymers. London: Reinhold Publishing Corp., 1962.

33. Peterlin, A. "Excluded Volume Effect on Light Scattering of the Coiled Linear Macromolecule." J. Chem. Phys., 23, 2464 (1955).

34. Peterlin, A. "Frequency Dependence of Intrinsic Viscosity of Macromolecules with Finite Internal Viscosity." J. Polymer Sci., Pat. A-2, 5, 179 (1967).

35. Philippoff, W. "Relaxation in Polymer Solutions, Liquids and Gels." Physical Acoustincs, W. P. Mason, ed., Vol. IIB, Chapter 7. New York: Academic Press, 1965.

36. Philippoff, W. "Viscoelasticity of Polymer Solution at High Pressures and Ultrasonic Frequencies." J. Appl. Phys., 34, 1507 (1963).

37. Ptitsyn, O. B., and Eisner, Y. E. Zh. Fix. Khim., 32, 2464 (1958); as cited in Reference 16, page 217.

38. Ptitsyn, O. B., and Eisner, Y. E. Zh. Tekhn. Fix., 29, 117 (1959); as cited in Reference 16, page 217.

39. Rein, R. G., Jr. "Viscoelastic Behavior of Simple Hydrocarbons at High Pressure." Ph.D. dissertation. University of Oklahoma, Norman, Oklahoma, 1967.

40. Rein, R. G., Jr.; Charng, T. T.; Sliepcevich, C. M.; and Ewbank, W. J. "Measurement of Viscosity by Oscillating Crystal Method of Four Fluids as Function of Pressure, Shear Rate and Temperature." NASA, Contract NAS 3-13487 (1971).

41. Rein, R. G., Jr.; Sliepcevich, C. M.; and Babb, S. E. "Viscoelastic Behavior in Toluene at High Pressure." J. Chem. Eng. Data, 13, 511 (1968).

42. Rein, R. G., Jr.; Sliepcevich, C. M.; Babb, S. E., Jr.; and Tuma, G. "The Change in Resonant Frequency with Pressure to 8000 Atm of Quartz Crystal Viscometers." J. Appl. Phys., 40, 131 (1969).

43. Rosen, S. L. Fundamental Principles of Polymeric Materials. New York: Barnes and Noble, Inc., 1971.

44. Rouse, P. E., Jr. "A Theory of the Linear Viscoelastic Properties of Dilute Solutions of Coiling Polymers." J. Chem. Phys., 21, 1272 (1953).

45. Rouse, P. E., Jr.; Baily, E. D.; and Minkin, J. A. "Factors Affecting the Precision of the Viscosity Measurements with the Torsion Cyrstal." Proc. Am. Pet. Inst., 30 (3), 54 (1950).

46. Sakanishi, A. "Dynamic Viscoelastic Properties of Dilute Polyisobutylene Solutions." J. Chem. Phys., 48, 3850 (1968).

47. Sakanishi, A., and Tanaka, H. "Viscoelastic Properties of Styrene-Butadiene Copolymers in a Good Solvent." J. Phys. Soc. Japan, 24, 222 (1968).

48. Stockmayer, W. H., and Fixman, M. "On the Estimation of Unperturbed Dimensions from Intrinsic Viscosities." J. Polymer Sci., C1, 137 (1963).

49. Tanaka, H.; Sakanishi, A.; Kaneko, M.; and Furuichi, J. "Dynamic Viscoelastic Properties of Dilute Polymer Solutions." J. Polymer Sci., C15, 317 (1966).

50. Tobolsky, A. V. Properties and Structure of Polymers. New York: Wiley, 1960.

51. Tschoegl, N. W. "Influence of Hydrodynamic Interaction on the Viscoelastic Behavior of Dilute Polymer Solutions." J. Chem. Phys., 39, 149 (1963).

52. Tschoegl, N. W. "Influence of Hydrodynamic Interation on the Viscoelastic Behavior of Dilute Polymer Solutions in Good Solvents." J. Chem. Phys., 40, 473 (1964).

53. Wall, F. T. "Statistical Thermodynamics of Rubber. II." J. Chem. Phys., 10, 485 (1942).

54. Zimm, B. H. "Dynamics of Polymer Molecules in Dilute Solution: Viscoelasticity, Flow Birefringence and Dielectric Loss." J. Chem. Phys., 24, 269 (1956).

55. Zimm, B. H.; Roe, G. M.; and Epstein, L. F. "Solution of a Characteristic Value Problem from the Theory of Chain Molecules." J. Chem. Phys., 24, 279 (1956).

APPENDICES

APPENDIX A

DENSITY DATA OF CALIBRATION LIQUIDS

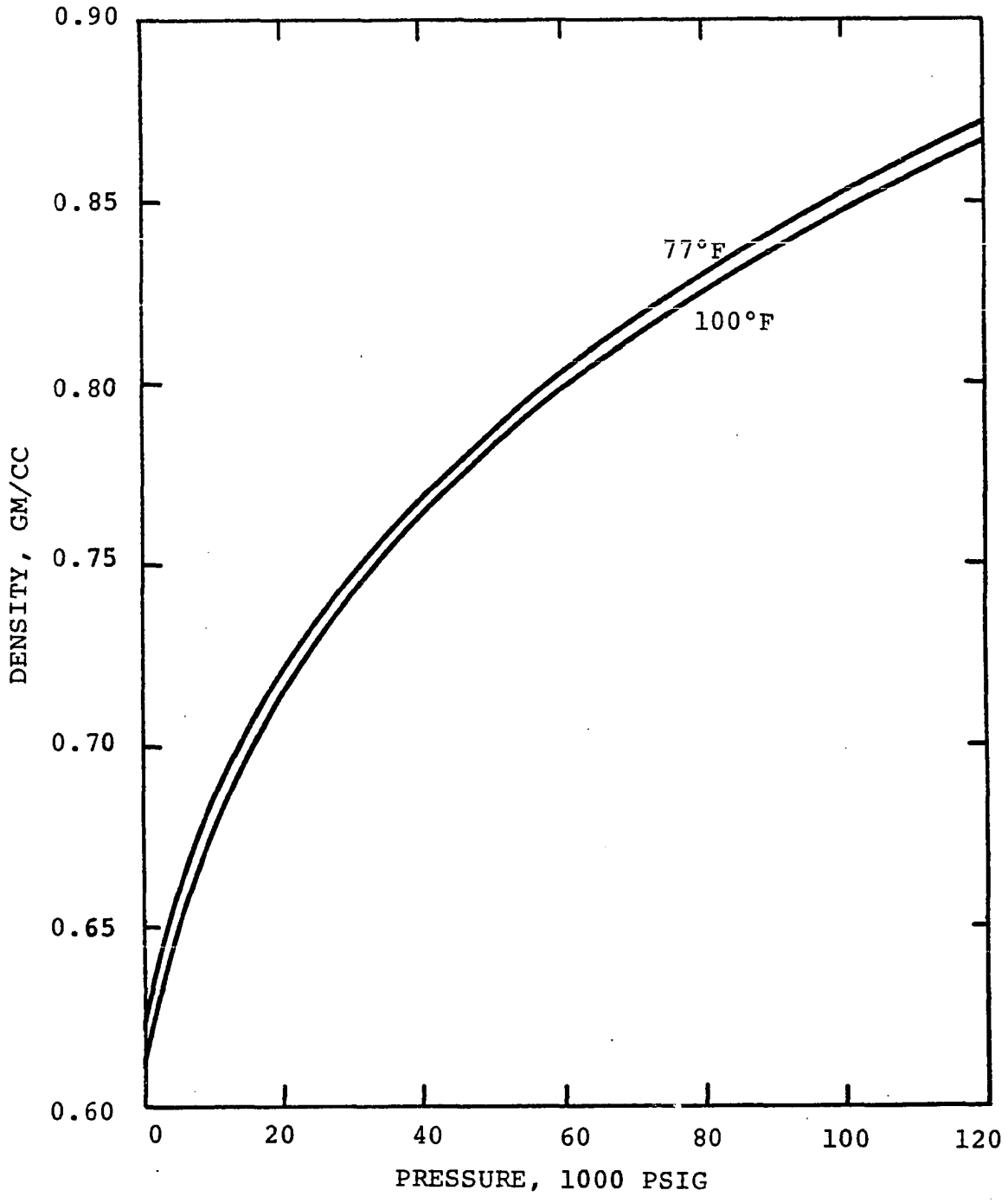

Figure 70. Effect of Pressure and Temperature on the Density of Normal Pentane.

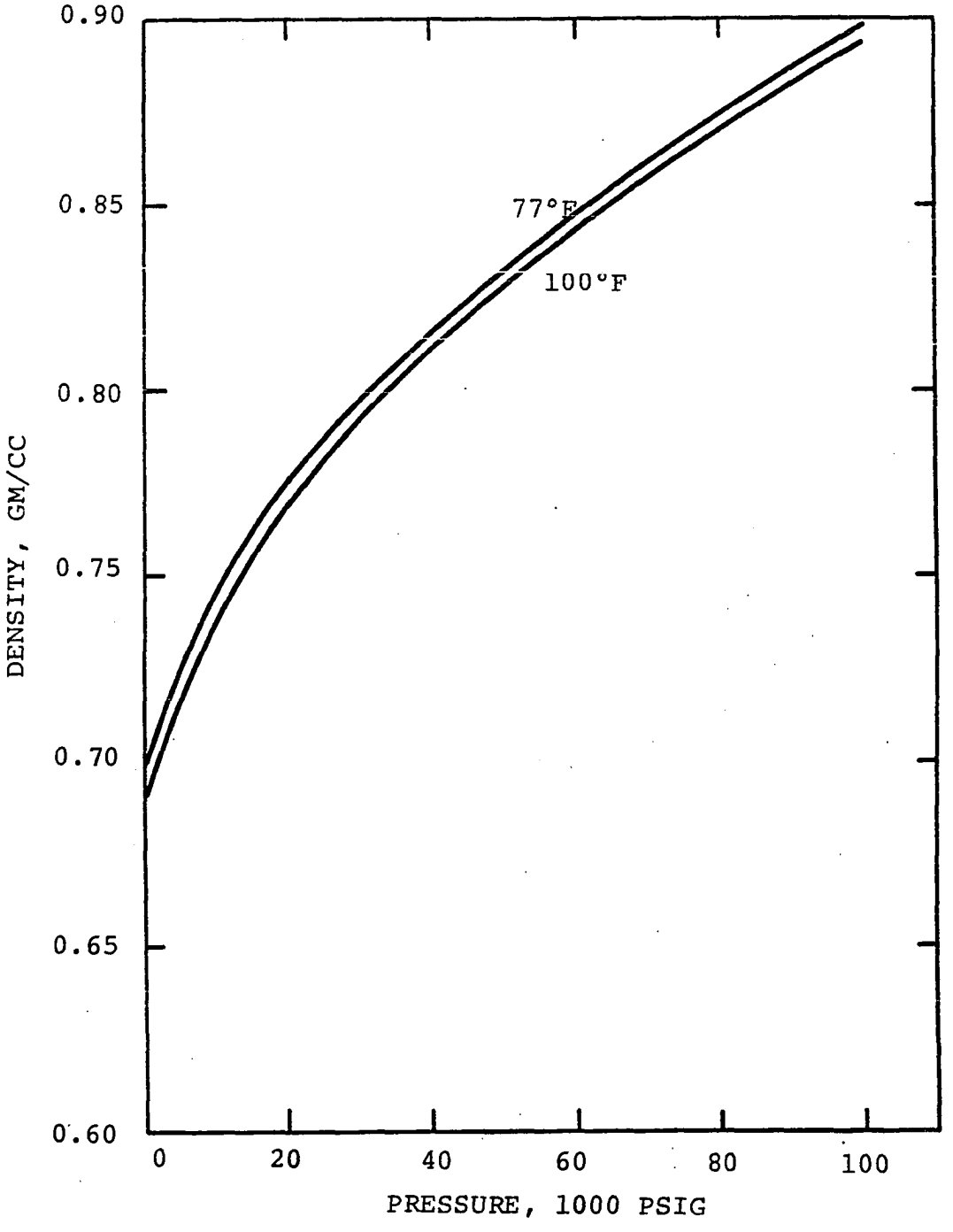

Figure 71. Effect of Pressure and Temperature on the Density of Normal Octane.

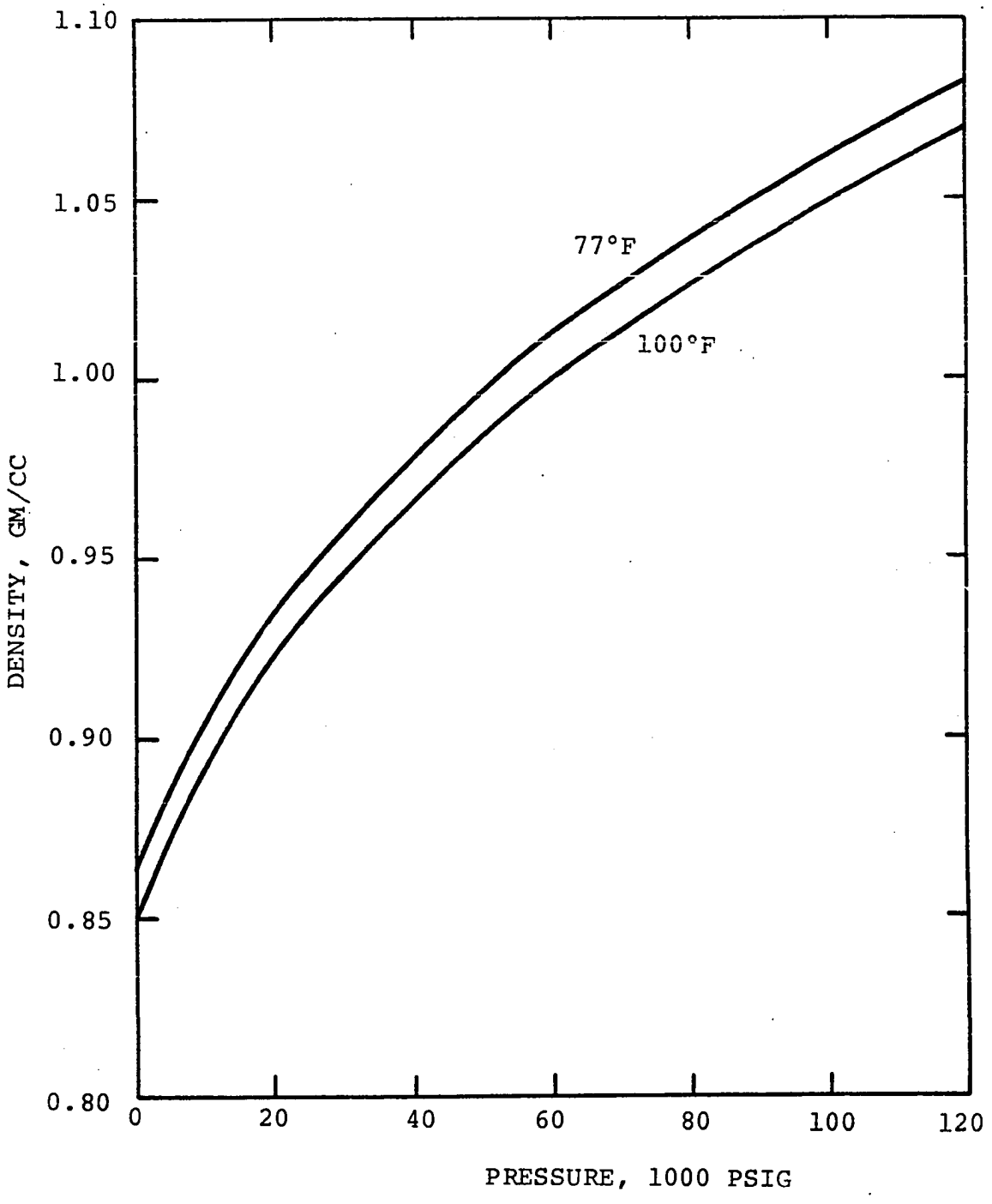

Figure 72. Effect of Pressure and Temperature on the Density of Toluene.

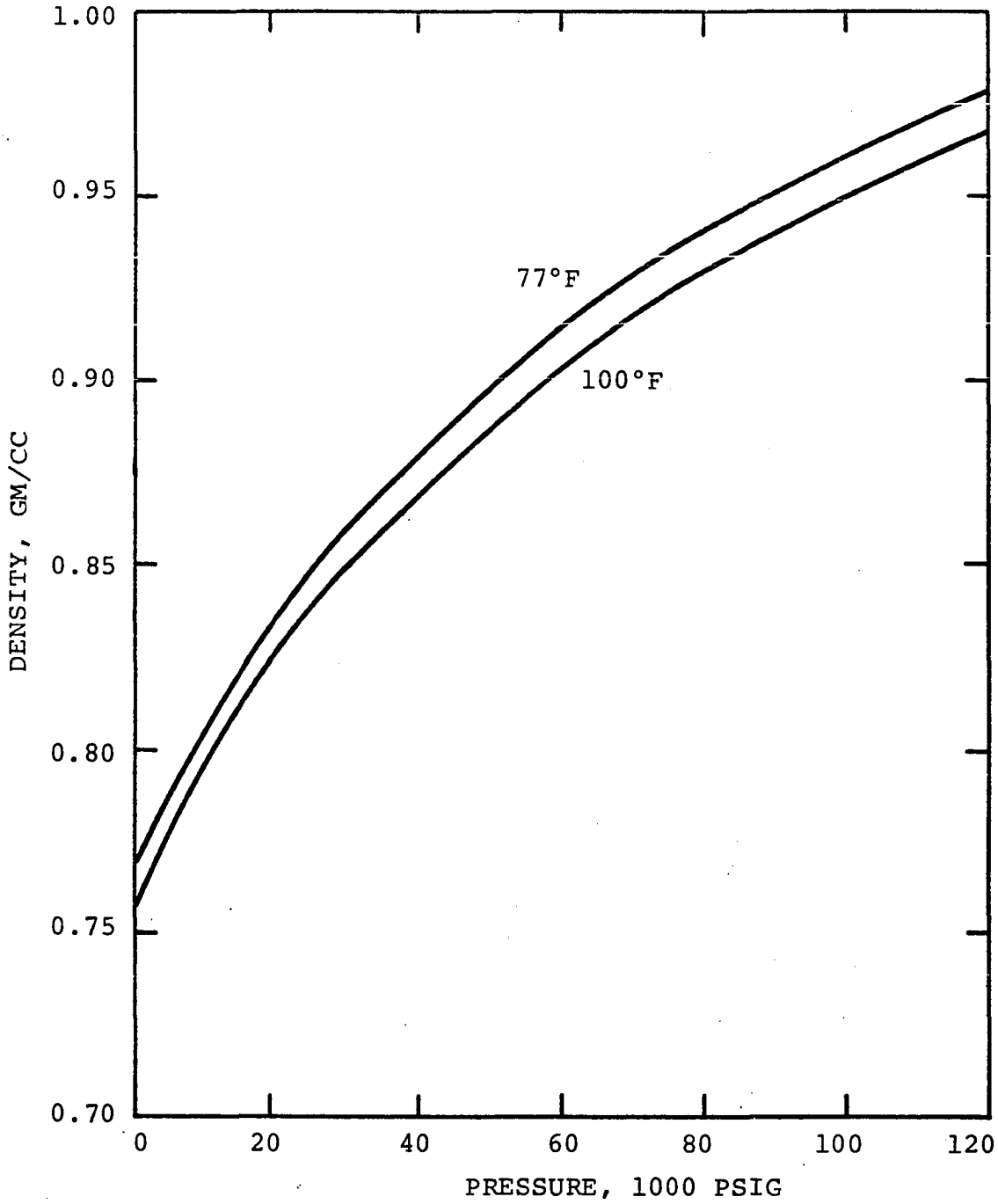

Figure 73. Effect of Pressure and Temperature on the Density of Methyl Cyclohexane.

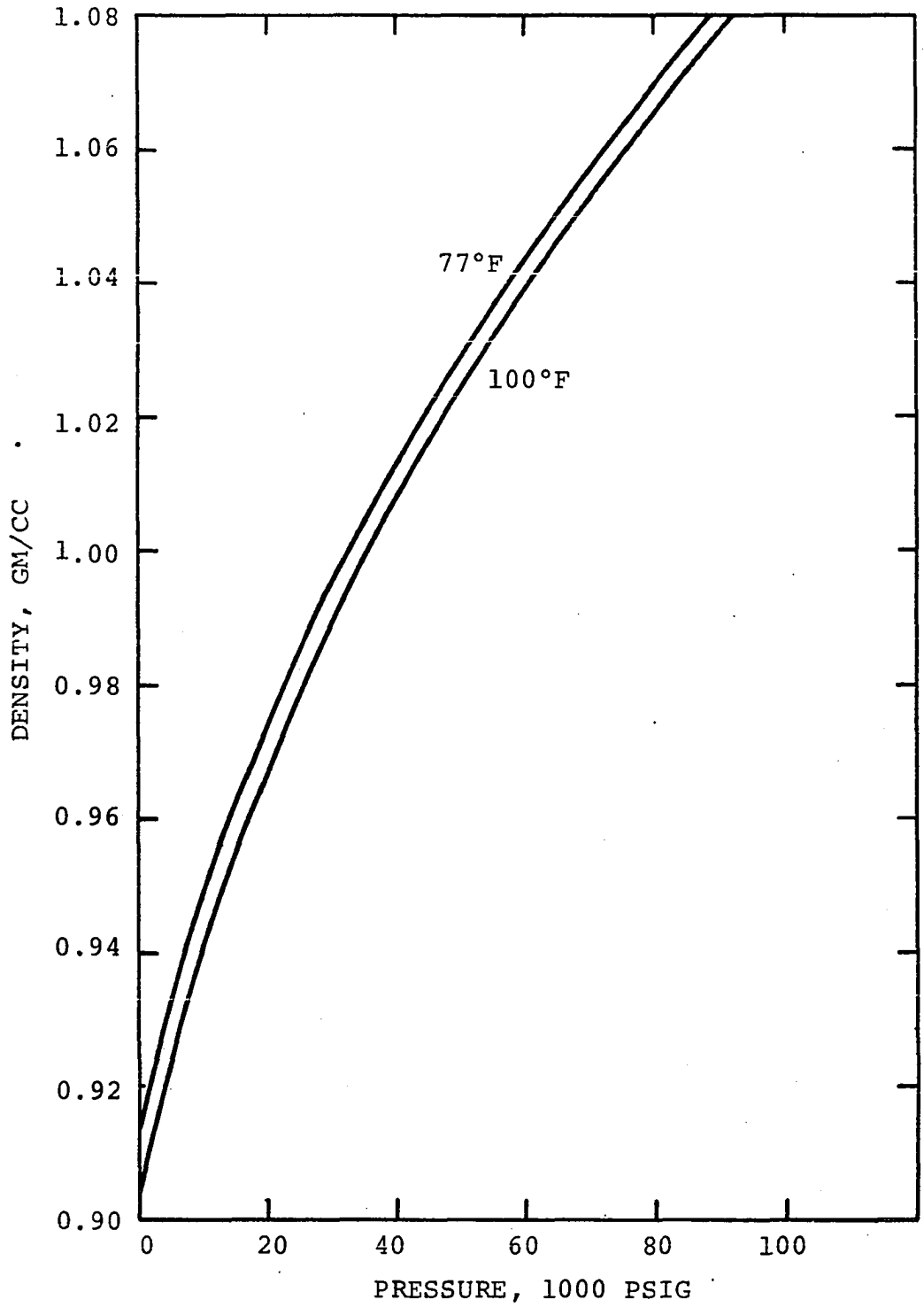

Figure 74. Effect of Pressure and Temperature on the Density of Di(2-Ethylhexyl) Sebacate.

APPENDIX B

VISCOSITY DATA OF CALIBRATION LIQUIDS

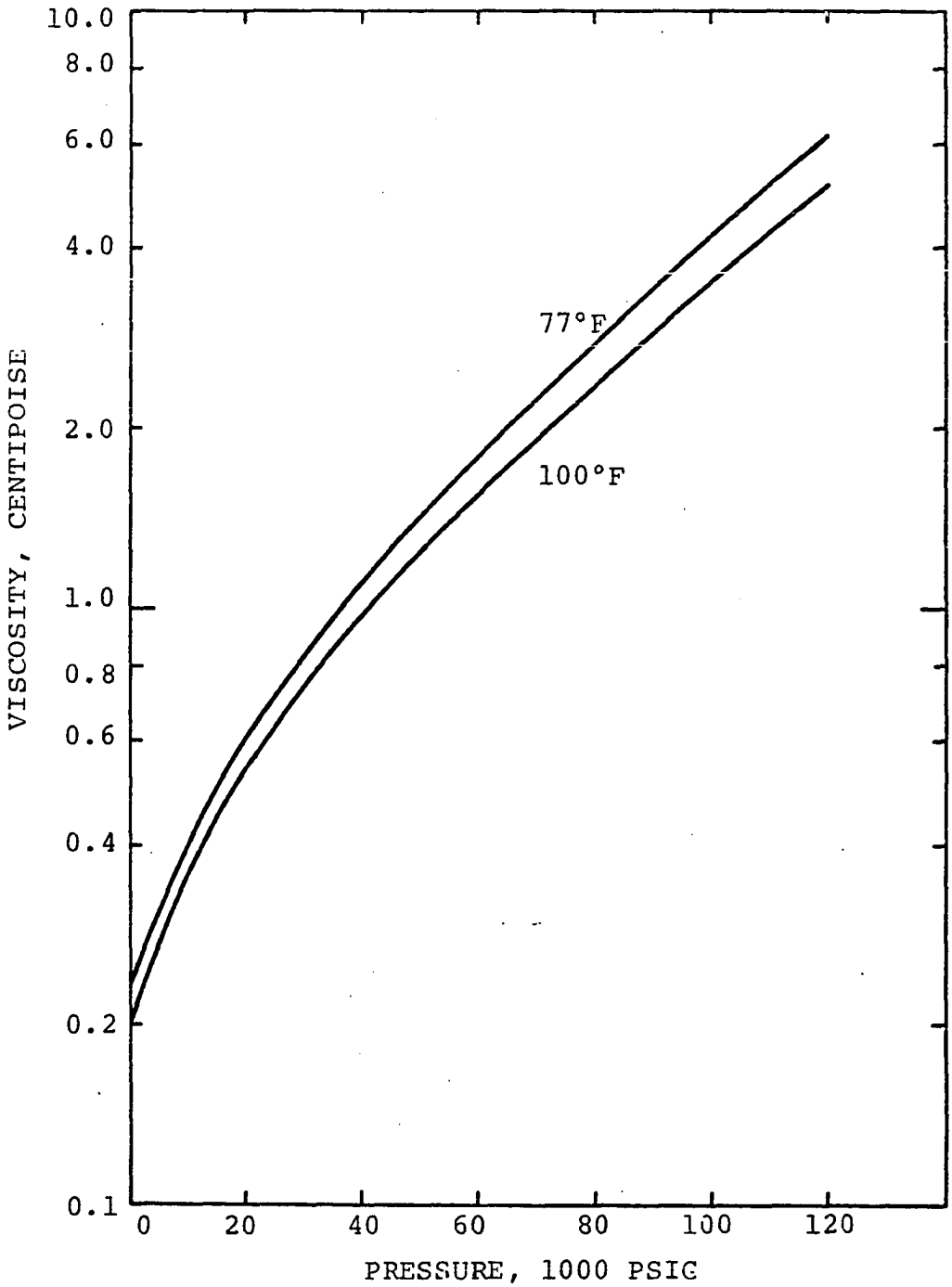

Figure 75. Effect of Pressure and Temperature on the Viscosity of Normal Pentane.

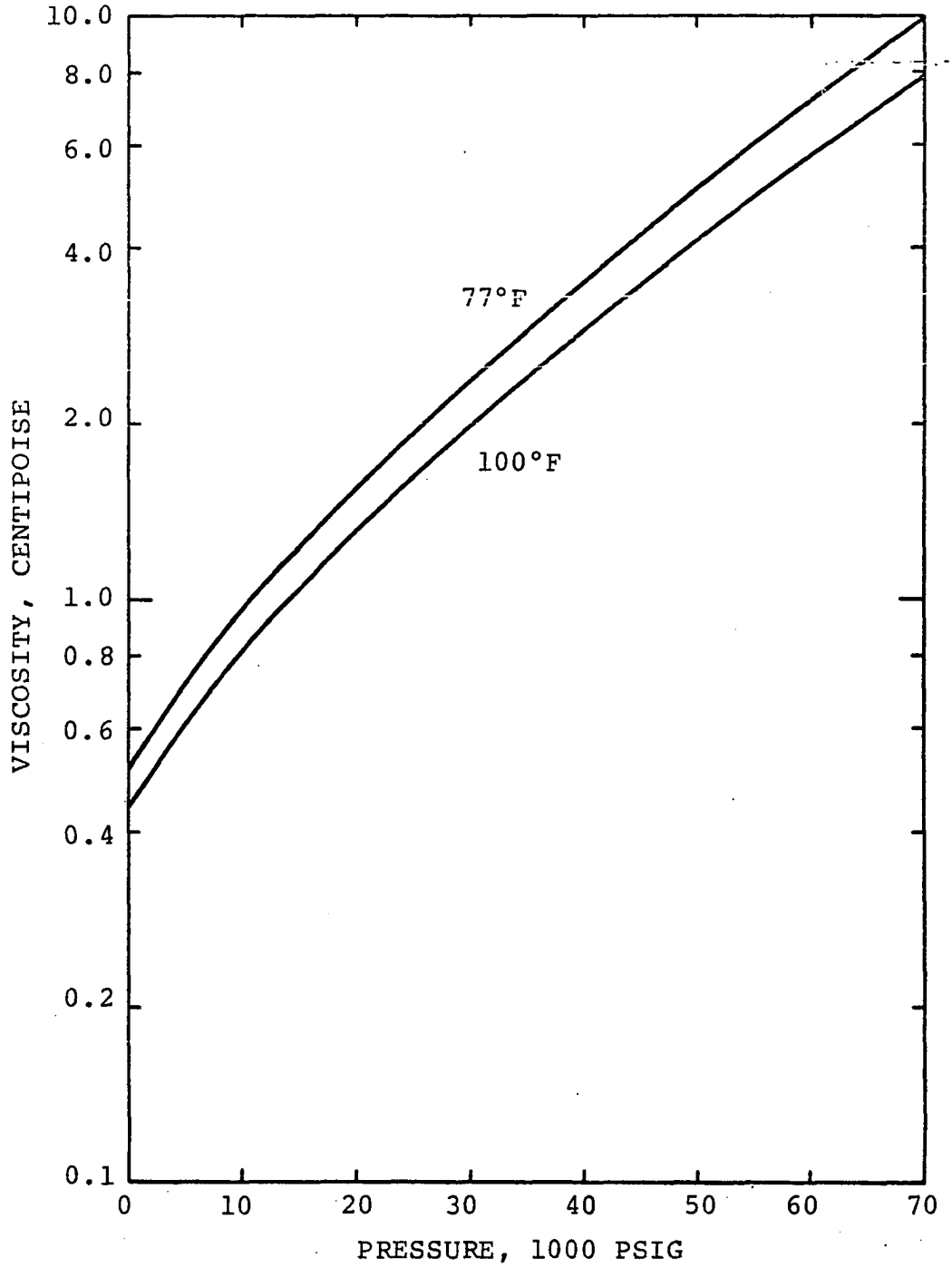

Figure 76. Effect of Pressure and Temperature on the Viscosity of Normal Octane.

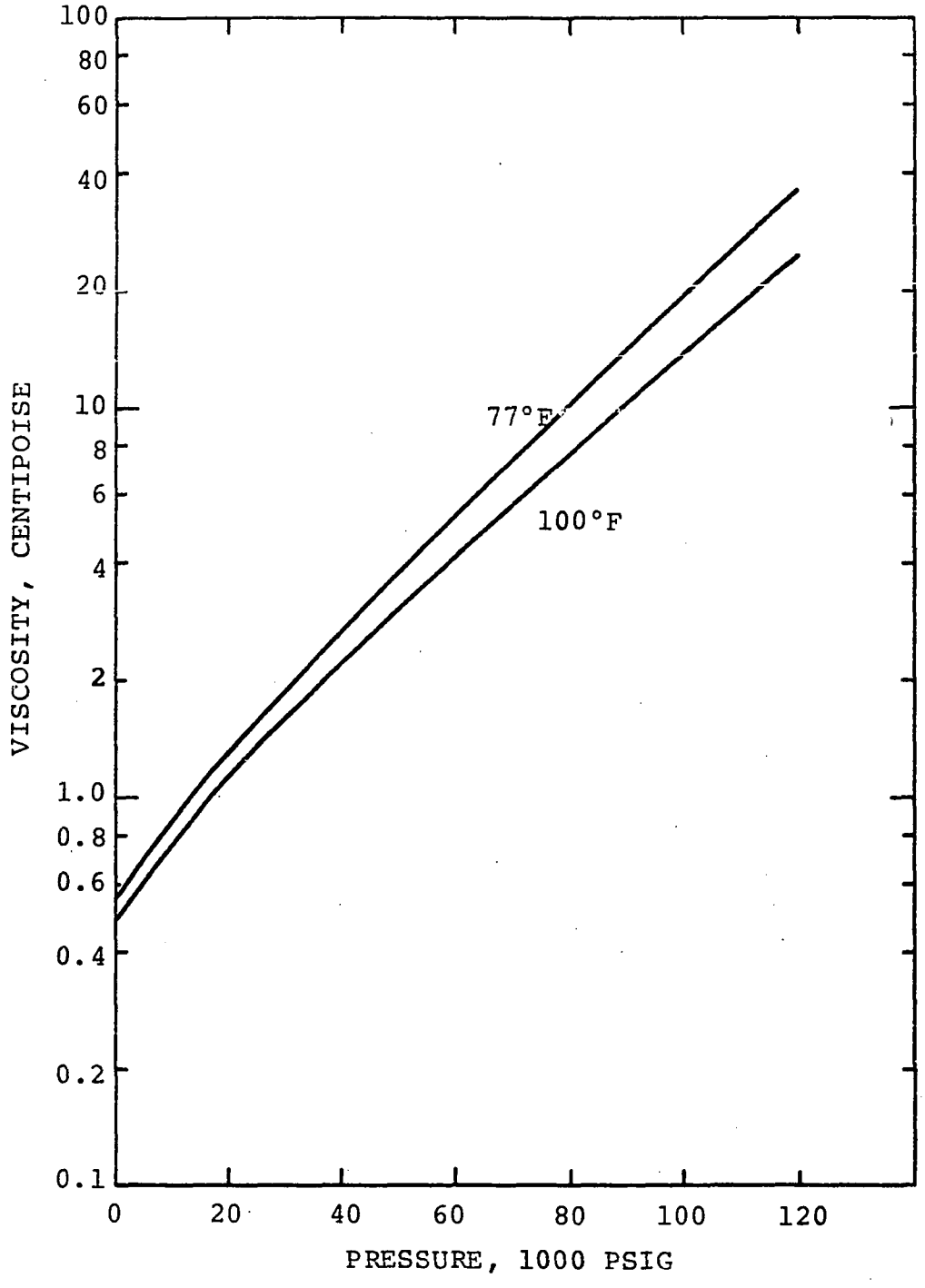

Figure 77. Effect of Pressure and Temperature on the Viscosity of Toluene.

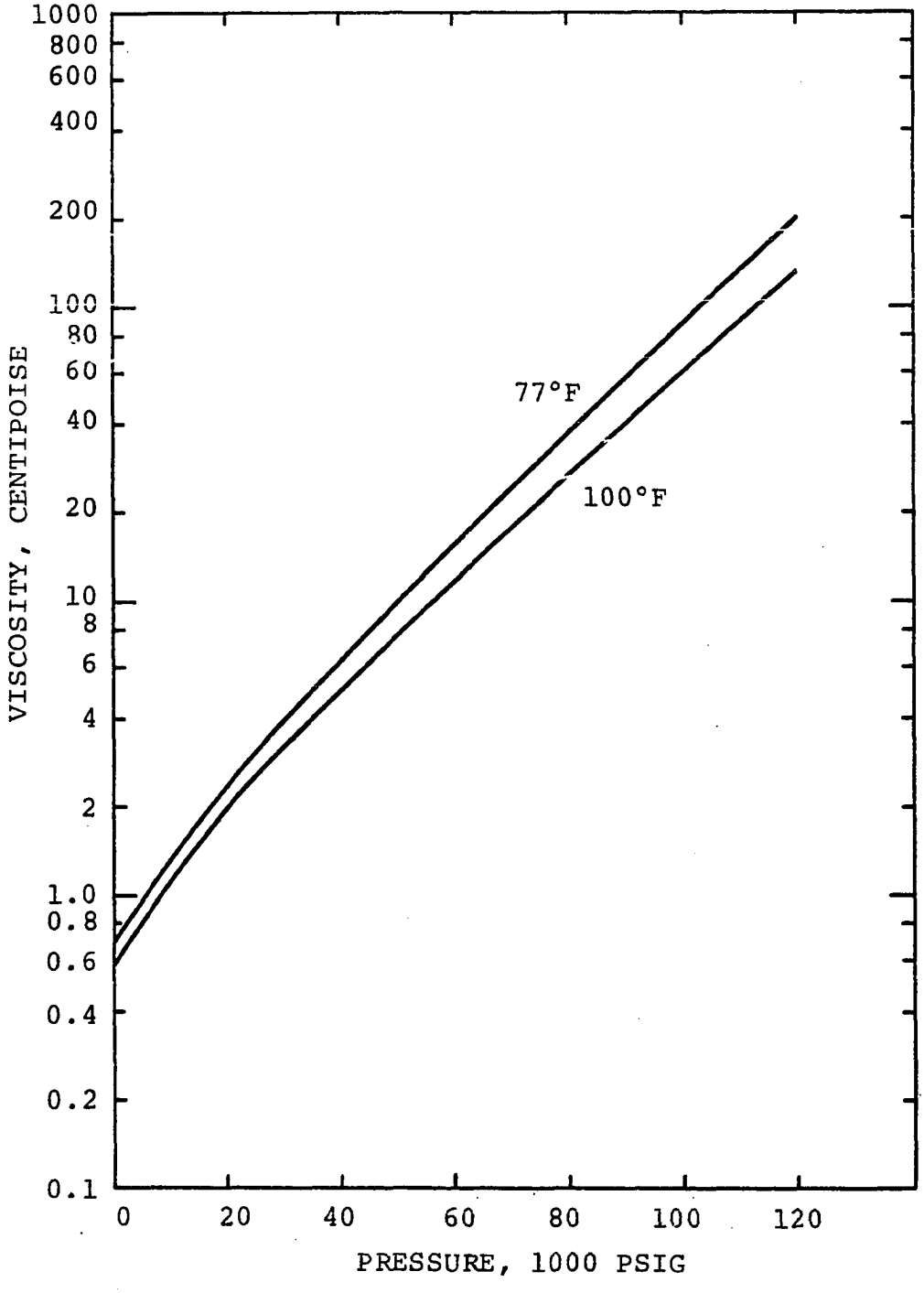

Figure 78. Effect of Pressure and Temperature on the Viscosity of Methyl Cyclohexane.

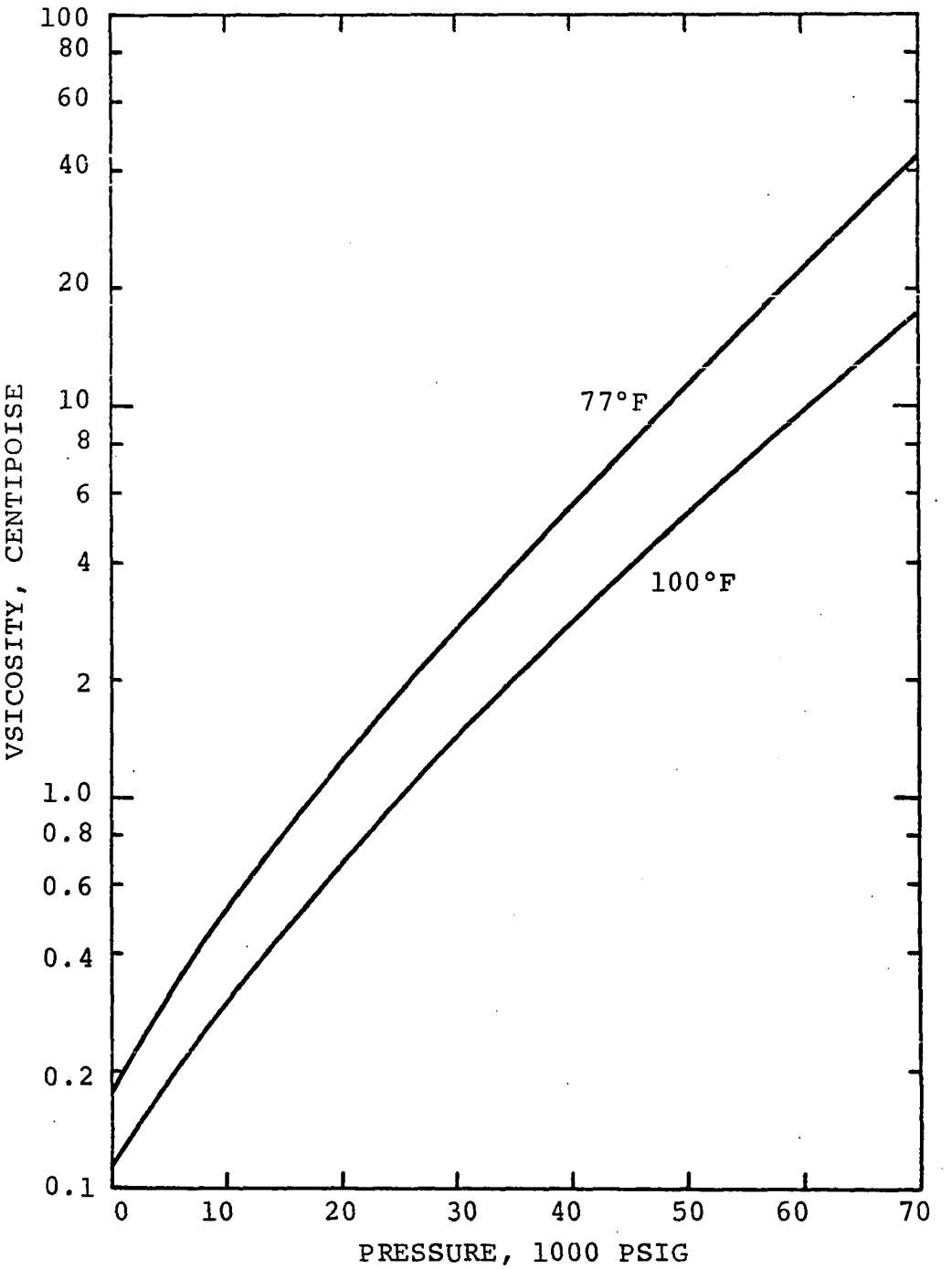

Figure 79. Effect of Pressure and Temperature on the Viscosity of Di(2-Ethylhexyl) Sebacate.

APPENDIX C

REDUCED AND DIMENSIONLESS VISCOELASTIC PROPERTIES OF S-108 AND S-109 POLYSTYRENE SOLUTIONS

TABLE 11

REDUCED AND DIMENSIONLESS VISCOELASTIC PROPERTIES OF
1 PERCENT S-108 POLYSTYRENE IN TOLUENE

Pressure 1000 psig	$a_{T,P}$	ω_r sec^{-1}	$\omega_r \frac{\eta-\eta_s}{cRT} M$	G'_r dyne/cm^2	$G'_r(M/cRT)$	$\eta'_r-\eta_s$ poise	$\frac{\eta'_r-\eta_s}{\eta-\eta_s}$
			AT 77°F				
0	1	3.71×10^5	2.192	822	1.026	0.0043	0.91
10	1.53	5.68×10^5	3.353	197	0.247	0.0030	0.63
20	2.167	8.04×10^5	4.749	338	0.422	0.00325	0.69
30	2.968	1.1×10^6	6.507	717	0.895	0.0026	0.56
50	5.743	2.13×10^6	12.592	913	1.14	0.0022	0.47
70	10.866	4.03×10^6	23.83	2,233	2.787	0.0019	0.39
90	19.814	7.36×10^6	43.46	9,344	11.66	0.0017	0.35
110	38.417	1.43×10^7	84.28	10,188	12.715	0.0012	0.25
120	53.911	2.0×10^7	118.28	8,249	10.30	0.0010	0.20
			AT 100°F				
0	0.866	3.22×10^5	1.899	543	0.678	0.0044	0.929
10	1.31	4.86×10^5	2.872	993	1.24	0.0042	0.895
20	11.85	6.87×10^5	4.058	667	0.833	0.0028	0.589
30	2.506	9.30×10^5	5.494	1,058	1.32	0.0032	0.676
50	4.595	1.71×10^6	10.076	2,526	3.152	0.0024	0.515
70	8.237	3.06×10^6	18.068	4,305	5.373	0.0015	0.312
90	14.803	5.5×10^6	32.475	3,604	4.498	0.0018	0.372
110	26.578	9.87×10^6	58.32	5,388	6.725	0.0015	0.312
120	35.681	1.33×10^7	78.304	7,482	9,338	0.0011	0.242

TABLE 12

REDUCED AND DIMENSIONLESS VISCOELASTIC PROPERTIES OF 2 PERCENT S-108 POLYSTYRENE IN TOLUENE

Pressure 1000 psig	$a_{T,P}$	ω_r sec^{-1}	$\omega_r \frac{\eta-\eta_s}{cRT} M$	G'_r dyne/cm^2	$G'_r(M/cRT)$	$\eta'_r-\eta_s$ poise	$\frac{\eta'_r-\eta_s}{\eta-\eta_s}$
			AT 77°F				
0	1.00	3.71×10^5	2.906	1,038	0.648	0.0107	0.857
10	1.530	5.68×10^5	4.446	1,213	0.757	0.0074	0.587
20	2.167	6.37×10^5	4.991	3,277	2.045	0.0059	0.471
30	2.968	1.10×10^6	8.629	4,534	2.83	0.0049	0.394
50	5.743	2.13×10^6	16.698	6,054	3.78	0.0037	0.297
70	10.866	4.03×10^6	31.597	8,547	5.33	0.0040	0.319
90	19.814	7.36×10^6	57.63	21,382	13.34	0.0046	0.369
110	38.417	1.43×10^7	111.75	26,769	16.71	0.0036	0.291
120	53.911	2.0×10^7	156.83	19,724	12.31	0.0031	0.247
			AT 100°F				
0	0.854	3.17×10^5	2.482	836	0.522	0.0081	0.644
10	1.291	4.79×10^5	3.754	1,983	1.237	0.0093	0.741
20	1.825	6.77×10^5	5.305	3,048	1.902	0.0064	0.508
30	2.470	9.17×10^5	7.181	3,781	2.359	0.0080	0.641
50	4.529	1.68×10^6	13.169	5,620	3.507	0.0061	0.483
70	8.119	3.02×10^6	23.614	5,832	3.639	0.047	0.375
90	14.591	5.42×10^6	42.448	9,840	6.141	0.0033	0.259
110	26.198	9.73×10^6	76.233	20,845	13.008	0.0025	0.196
120	35.171	1.31×10^7	102.35	23,479	14.652	0.0021	0.165

TABLE 13

REDUCED AND DIMENSIONLESS VISCOELASTIC PROPERTIES OF
3 PERCENT S-108 POLYSTYRENE IN TOLUENE

Pressure 1000 psig	$a_{T,P}$	ω_r sec^{-1}	$\omega_r \frac{\eta-\eta_s}{cRT} M$	G'_r dyne/cm^2	$G'_r(M/cRT)$	$\eta'_r-\eta_s$ poise	$\frac{\eta'_r-\eta_s}{\eta-\eta_s}$
			AT 77°F				
0	1.00	3.71×10^5	3.512	1,837	0.764	0.0157	0.69
10	1.530	5.68×10^5	5.373	3,540	1.473	0.0133	0.58
20	2.167	8.04×10^5	7.611	3,822	1.590	0.0120	0.53
30	2.968	1.1×10^6	10.427	5,751	2.393	0.0113	0.46
50	5.743	2.13×10^6	20.18	8,763	3.645	0.0085	0.37
70	10.866	4.03×10^6	38.184	16,782	6.982	0.0066	0.29
90	19.814	7.36×10^6	69.64	26,964	11.218	0.0059	0.26
110	38.417	1.43×10^7	135.05	42,094	17.51	0.0050	0.22
120	53.911	2.0×10^7	189.52	47,605	19.8	0.0045	0.20
			AT 100°F				
0	0.823	3.05×10^5	2.89	1,817	0.756	0.0179	0.788
10	1.244	4.62×10^5	4.377	3,614	1.503	0.0150	0.66
20	1.758	6.53×10^5	6.176	4,587	1.908	0.0127	0.559
30	2.38	8.83×10^5	8.360	5,137	2.137	0.0126	0.555
50	4.364	1.62×10^6	15.333	7,344	3.055	0.0099	0.435
70	7.822	2.90×10^6	27.49	11,187	4.654	0.0081	0.358
90	14.057	5.22×10^6	49.42	18,564	7.723	0.0064	0.280
110	25.939	9.38×10^6	88.74	31,611	13.15	0.0057	0.250
120	33.883	1.26×10^7	119.15	36,792	15.306	0.0047	0.208

TABLE 14

REDUCED AND DIMENSIONLESS VISCOELASTIC PROPERTIES OF
1 PERCENT S-109 POLYSTYRENE IN TOLUENE

Pressure 1000 psig	$a_{T,P}$	ω_r sec^{-1}	$\omega_r \frac{\eta-\eta_s}{cRT} M$	G'_r dyne/cm^2	$G'_r(M/cRT)$	$\eta'_r-\eta_s$ poise	$\frac{\eta'_r-\eta_s}{\eta-\eta_s}$
			AT 77°F				
0	1.00	3.71×10^5	1.356	2,044	2.55	0.00071	0.176
20	2.167	8.04×10^5	2.917	2,580	3.22	0.0023	0.574
30	2.968	1.10×10^6	3.996	1,743	2.176	0.0027	0.675
50	5.743	2.13×10^6	7.733	3,612	4.509	0.0016	0.40
70	10.866	4.03×10^6	14.633	6,746	8.419	0.0015	0.385
90	10.814	7.36×10^6	26.689	8,118	10.132	0.0016	0.393
110	38.417	1.43×10^7	51.756	8,606	10.741	0.0012	0.309
120	53.911	2.00×10^7	72.63	7,019	8,761	0.0015	0.366
			AT 100°F				
0	0.831	3.08×10^5	1.118	597	0.538	0.0031	0.776
10	1.256	4.66×10^5	--	--	--	--	--
20	1.775	6.59×10^5	2.39	3,066	2.766	0.0062	1.53
30	2.403	8.92×10^5	3.236	3,063	2.764	0.0044	1.09
50	4.407	1.64×10^6	5.934	3,086	2.784	0.0071	1.775
70	7.900	2.93×10^6	10.64	4,527	4.084	0.0029	0.727
90	14.197	5.27×10^6	19.126	4,198	3.788	0.0021	0.51
110	25.489	9.47×10^6	34.348	9,065	8.178	0.0013	0.300
120	34.219	1.27×10^7	46.118	11,968	10.797	0.0011	0.282

TABLE 15

REDUCED AND DIMENSIONLESS VISCOELASTIC PROPERTIES OF 2 PERCENT S-109 POLYSTYRENE IN TOLUENE

Pressure 1000 psig	$a_{T,P}$	ω_r sec^{-1}	$\omega_r \frac{\eta-\eta_s}{cRT} M$	G'_r dyne/cm^2	$G'_r(M/cRT)$	$\eta'_r-\eta_s$ poise	$\frac{\eta'_r-\eta_s}{\eta-\eta_s}$
			AT 77°F				
0	1.00	3.71×10^5	1.576	2,833	1.768	0.0043	0.46
10	1.530	5.68×10^5	2.411	3,116	1.944	0.0078	0.83
20	2.167	8.04×10^5	3.415	7,330	4.6	0.0076	0.81
30	2.968	1.10×10^6	4.678	6,295	3.93	0.0067	0.71
50	5.743	2.13×10^6	9,053	9,994	6.24	0.0052	0.56
70	10.866	4.03×10^6	17.131	12,638	7.887	0.0042	0.45
90	19.814	7.36×10^6	31.245	15,272	9.53	0.0034	0.36
110	38.417	1.43×10^7	60.591	15,216	9.495	0.0025	0.27
120	53.911	2.0×10^7	85.027	16,299	10.171	0.0028	0.30
			AT 100°F				
0	0.830	3.08×10^5	1.308	953	0.43	0.0276	2.927
10	1.255	4.66×10^5	1.978	4,583	2.067	0.0125	1.324
20	1.774	6.58×10^5	2.795	1,866	0.842	0.0093	0.990
30	2.401	8.91×10^5	3.784	4,528	2.042	0.0089	0.95
50	4.403	1.63×10^6	6.941	6,222	2.807	0.0059	0.629
70	7.892	2.93×10^6	12.444	4,880	2.201	0.0053	0.564
90	14.183	5.27×10^6	22.371	10,637	4.798	0.0032	0.345
110	25.465	$9,46 \times 10^6$	40.175	19,663	8.87	0.0026	0.278
120	34.188	1.27×10^7	53.941	22,857	10.31	0.0024	0.251

TABLE 16

REDUCED AND DIMENSIONLESS VISCOELASTIC PROPERTIES OF
3 PERCENT S-109 POLYSTYRENE IN TOLUENE

Pressure 1000 psig	$a_{T,P}$	ω_r sec^{-1}	$\omega_r \frac{\eta-\eta_s}{cRT} M$	G'_r dyne/cm^2	$G'_r(M/cRT)$	$\eta'_r-\eta_s$ poise	$\frac{\eta'_r-\eta_s}{\eta-\eta_s}$
			AT 77°F				
0	1.00	3.71×10^5	1 871	1,595	0.664	0.0133	0.795
20	2.167	8.04×10^5	4.054	7,032	2.925	0.0180	1.07
30	2.968	1.10×10^6	5.554	7,336	3.052	0.0111	0.661
50	5.743	2.13×10^6	10.749	9,747	4.055	0.0073	0.434
70	10.866	4.03×10^6	20.34	15,292	6.362	0.0058	0.348
90	19.814	7.36×10^6	37.10	24,053	10.007	0.0039	0.234
110	38.417	1.43×10^7	71.94	34,156	14.21	0.0040	0.230
120	53.911	2.00×10^7	100.955	33,827	14.07	0.00385	0.230
			AT 100°F				
0	0.809	$2\ 99 \times 10^5$	1.51	3,464	1.04	0.026	1.556
10	1.22	4.53×10^5	2.283	3,471	1.04	0.0139	0.928
20	1.724	6.40×10^5	3.227	7,299	2.19	0.0086	0.511
30	2.334	8.66×10^5	4.367	9,071	2.73	0.0133	0.793
50	4.279	1.59×10^6	8.01	11,943	3.59	0.011	0.657
70	7.671	2.85×10^6	14.362	12,400	3.73	0.0074	0.44
80	10.321	3.83×10^6	19.326	15,263	4.59	0.006	0.359
100	18.701	6.95×10^6	35.037	21,641	6.51	0.0045	0.266
120	33.23	1.23×10^7	62.25	36,736	11.047	0.0039	0.234

APPENDIX D

VISCOELASTIC PROPERTIES OF S-108 AND S-109 POLYSTYRENE SOLUTIONS AS PREDICTED BY ROUSE AND ZIMM THEORIES

TABLE 17

VISCOELASTIC PROPERTIES OF 1 PERCENT S-108 POLYSTYRENE IN TOLUENE
AS A FUNCTION OF ANGULAR FREQUENCY at 77°F.
PREDICTED BY ROUSE & ZIMM THEORIES

Zimm Theory					Rouse Theory				
ω sec^{-1}	$\frac{\eta'-\eta_s}{\eta-\eta_s}$	$\eta'-\eta_s$ poise	G'(M/cRT)	G' $dyne/cm^2$	ω sec^{-1}	$\frac{\eta'-\eta_s}{\eta-\eta_s}$	$\eta'-\eta_s$ poise	G'(M/cRT)	G' $dyne/cm^2$
4.01×10^4	1.00	0.00473	1.148×10^{-2}	9.2	2.78×10^4	1.00	0.00473	1.07×10^{-2}	8.58
6.36×10^4	1.00	0.00473	2.818×10^{-2}	2.26×10^1	4.41×10^4	0.9772	0.00462	2.63×10^{-2}	2.11×10^1
1.01×10^5	0.977	0.00462	6.918×10^{-2}	5.54×10^1	7.00×10^4	0.9550	0.00452	6.46×10^{-2}	5.17×10^1
1.60×10^5	0.933	0.00441	1.622×10^{-1}	1.30×10^2	1.11×10^5	0.912	0.00431	1.48×10^{-1}	1.18×10^2
2.53×10^5	0.871	0.00412	3.467×10^{-1}	2.78×10^2	1.76×10^5	0.8318	0.00393	3.16×10^{-1}	2.53×10^2
4.01×10^5	0.776	0.00367	6.456×10^{-1}	5.17×10^2	2.78×10^5	0.6918	0.00327	5.75×10^{-1}	4.61×10^2
6.36×10^5	0.661	0.00313	1.047	8.39×10^2	4.41×10^5	0.5495	0.0026	8.91×10^{-1}	7.14×10^2
1.01×10^6	0.562	0.00266	1.585	1.27×10^3	7.00×10^6	0.4266	0.0020	1.26	1.01×10^3
1.60×10^6	0.490	0.00232	2.291	1.84×10^3	1.11×10^6	0.3388	0.0016	1.70	1.36×10^3
2.53×10^6	0.420	0.00198	3.236	2.59×10^3	1.76×10^6	0.2692	0.0013	2.29	1.83×10^3
4.01×10^6	0.355	0.00168	4.467	3.59×10^3	2.78×10^6	0.2138	0.0010	3.02	2.42×10^3
6.36×10^7	0.308	0.00146	6.310	5.06×10^3	4.41×10^6	0.1698	0.0008	3.89	3.12×10^3
1.01×10^7	0.263	0.00124	8.710	6.98×10^3	7.00×10^6	0.1349	0.0006	5.01	4.02×10^3
1.60×10^7	0.224	0.00106	1.202×10^1	9.63×10^3	1.11×10^7	0.1072	0.0005	6.46	5.17×10^3
2.53×10^7	0.195	0.00 92	1.622×10^1	1.30×10^4	1.76×10^7	0.0851	0.0004	8.32	6.66×10^3
4.01×10^7	00166	0.00078	2.239×10^1	1.79×10^4	2.78×10^7	0.0676	0.0003	1.05×10^1	8.39×10^3

TABLE 18

VISCOELASTIC PROPERTIES OF 2 PERCENT S-108 POLYSTYRENE IN TOLUENE
AS A FUNCTION OF ANGULAR FREQUENCY AT 77°F.
PREDICTED BY ROUSE & ZIMM THEORIES.

Zimm Theory					Rouse Theory				
ω sec^{-1}	$\frac{\eta'-\eta_s}{\eta-\eta_s}$	$\eta'-\eta_s$ poise	G'(M/cRT)	G' $dyne/cm^2$	ω sec^{-1}	$\frac{\eta'-\eta_s}{\eta-\eta_s}$	$\eta'-\eta_s$ poise	G'(M/cRT)	G' $dyne/cm^2$
3.02×10^4	1.00	0.01255	1.148×10^{-2}	1.84×10^1	2.10×10^4	1.00	0.01255	1.07×10^{-2}	1.717×10^1
4.79×10^4	1.00	0.01255	2.818×10^{-2}	4.52×10^1	3.33×10^4	0.9772	0.01226	2.63×10^{-2}	4.125×10^1
7.60×10^4	0.977	0.0123	6.917×10^{-2}	1.11×10^2	5.28×10^4	0.9550	0.01199	6.46×10^{-2}	1.035×10^2
1.20×10^5	0.433	0.0117	1.622×10^{-1}	2.60×10^2	8.36×10^4	0.912	0.01145	1.48×10^{-1}	2.37×10^2
1.91×10^5	0.871	0.0109	3.467×10^{-1}	5.56×10^2	1.325×10^5	0.8318	0.0104	3.16×10^{-1}	5.067×10^2
3.02×10^5	0.776	0.00974	6.456×10^{-1}	1.03×10^3	2.10×10^5	0.6918	0.0087	5.75×10^{-1}	9.22×10^2
4.79×10^5	0.661	0.00829	1.047	1.68×10^3	3.33×10^5	0.5495	0.0069	8.91×10^{-1}	1.428×10^3
7.60×10^5	0.562	0.00706	1.555	2.54×10^3	5.28×10^5	0.4266	0.0054	1.26	2.017×10^3
1.20×10^6	0.490	0.00615	2.291	3.67×10^3	8.36×10^5	0.3388	0.0043	1.70	2.721×10^3
1.91×10^6	0.420	0.00527	3.236	5.19×10^3	1.325×10^6	0.2692	0.0034	2.29	3.671×10^3
3.02×10^6	0.355	0.00445	4.467	7.16×10^3	2.10×10^6	0.2138	0.0027	3.02	4.839×10^3
4.79×10^6	0.309	0.00388	6.310	1.01×10^4	3.33×10^6	0.1698	0.0021	3.89	6.234×10^3
7.60×10^6	0.263	0.0033	8.710	1.40×10^4	5.28×10^6	0.1349	0.0017	5.02	8.031×10^3
1.20×10^7	0.224	0.00281	1.202×10^1	1.93×10^4	8.36×10^6	0.1072	0.0013	6.46	1.0305×10^4
1.91×10^7	0.195	0.00245	1.622×10^1	2.6×10^4	1.325×10^7	0.0851	0.0011	8.32	1.333×10^4
3.02×10^7	0.166	0.00208	2.239×10^1	3.59×10^4	2.10×10^7	0.0676	0.0008	1.05×10^1	1.678×10^4

TABLE 19

VISCOELASTIC PROPERTIES OF 3 PERCENT 108 POLYSTYRENE IN TOLUENE
AS A FUNCTION OF ANGULAR FREQUENCY AT 77°F.
PREDICTED BY ROUSE & ZIMM THEORIES

Zimm Theory					Rouse Theory				
ω sec^{-1}	$\frac{\eta'-\eta_s}{\eta-\eta_s}$	$\eta'-\eta_s$ poise	G'(M/cRT)	G' $dyne/cm^2$	ω sec^{-1}	$\frac{\eta'-\eta_s}{\eta-\eta_s}$	$\eta'-\eta_s$ poise	G'(M/cRT)	G' $dyne/cm^2$
2.50×10^4	1.00	0.02275	1.148×10^{-2}	$2.76 \times 10_1$	1.74×10^4	1.00	0.02275	1.07×10^{-2}	2.75×10^1
3.97×10^4	1.00	0.02275	2.818×10^{-2}	6.77×10^2	2.75×10^4	0.9772	0.0222	2.63×10^{-2}	6.32×10^2
6.29×10^4	0.977	0.0222	6.918×10^{-1}	1.66×10^2	4.37×10^4	0.9550	0.0217	6.46×10^{-2}	1.55×10^2
9.96×10^4	0.935	0.0212	1.622×10^{-1}	3.9×10^2	6.92×10^5	0.912	0.0207	1.48×10^{-1}	3.55×10^2
1.58×10^5	0.871	0.0198	3.467×10^{-1}	8.33×10^2	1.10×10^5	0.8318	0.0189	3.16×10^{-1}	7.60×10^2
2.50×10^5	0.776	0.0177	6.456×10^{-1}	1.55×10^3	1.74×10^5	0.6918	0.0157	5.75×10^{-1}	1.38×10^3
3.97×10^5	0.661	0.0150	1.047	2.52×10^3	2.75×10^5	0.5495	0.0125	8.91×10^{-1}	2.14×10^3
6.29×10^5	0.562	0.0128	1.585	3.81×10^3	4.37×10^5	0.4266	0.0097	1.26	3.03×10^3
9.96×10^6	0.490	0.0111	2.291	5.51×10^3	6.92×10^5	0.3388	0.0077	1.70	4.08×10^3
1.58×10^6	0.420	0.00955	3.236	7.78×10^3	1.10×10^6	0.2692	0.0061	2.29	5.51×10^3
2.50×10^6	0.355	0.00807	4.467	1.07×10^4	1.74×10^6	0.2138	0.0049	3.02	7.26×10^3
3.97×10^6	0.309	0.00703	6.310	1.52×10^4	2.75×10^6	0.1698	0.0039	3.89	9.35×10^3
6.29×10^6	0.263	0.00598	8.710	2.09×10^4	4.37×10^6	0.1349	0.0031	5.02	1.205×10^4
9.96×10^7	0.224	0.00509	1.202×10^1	2.89×10^4	6.92×10^7	0.1072	0.0024	6.46	1.55×10^4
1.58×10^7	0.195	0.00444	1.622×10^1	3.90×10^4	1.10×10^7	0.0851	0.0019	8.32	2.00×10^4
2.50×10^7	0.166	0.00378	2.239×10^1	5.38×10^4	1.74×10^7	0.0676	0.0015	1.04×10^1	2.52×10^4

TABLE 20

VISCOELASTIC PROPERTIES OF 1 PERCENT S-109 POLYSTYRENE IN TOLUENE
AS A FUNCTION OF ANGULAR FREQUENCY AT 77°F.
PREDICTED BY ROUSE & ZIMM THEORIES

Zimm Theory					Rouse Theory				
ω sec^{-1}	$\frac{\eta'-\eta_s}{\eta-\eta_s}$	$\eta'-\eta_s$ poise	G'(M/cRT)	G' $dyne/cm^2$	ω sec^{-1}	$\frac{\eta'-\eta_s}{\eta-\eta_s}$	$\eta'-\eta_s$ poise	G'(M/cRT)	G' $dyne/cm^2$
6.53×10^4	1.00	0.00402	1.148×10^{-2}	1.27×10^1	4.53×10^4	1.00	0.00402	1.07×10^{-2}	1.19×10^1
1.03×10^5	1.00	0.00402	2.818×10^{-2}	3.12×10^1	7.19×10^4	0.9772	0.0039	2.63×10^{-2}	2.92×10^1
1.64×10^5	0.977	0.0039	6.918×10^{-2}	7.67×10^1	1.14×10^5	0.9550	0.0038	6.46×10^{-2}	7.151×10^1
2.6×10^5	0.435	0.0038	1.622×10^{-1}	1.8×10^2	1.81×10^5	0.912	0.0037	1.48×10^{-1}	1.64×10^2
4.12×10^5	0.871	0.0035	3.467×10^{-1}	3.84×10^2	2.86×10^5	0.8318	0.0033	3.16×10^{-1}	3.51×10^2
6.53×10^5	0.776	0.0031	6.456×10^{-1}	7.16×10^2	4.53×10^5	0.6918	0.0027	5.75×10^{-1}	6.30×10^2
1.03×10^6	0.661	0.0027	1.047	1.16×10^3	7.19×10^5	0.5495	0.0022	8.91×10^{-1}	9.88×10^2
1.64×10^6	0.562	0.0023	1.585	1.76×10^3	1.14×10^6	0.4266	0.0017	1.26	1.40×10^3
2.6×10^6	0.490	0.0020	2.291	2.54×10^3	1.81×10^6	0.3388	0.0014	1.70	1.88×10^3
4.12×10^6	0.420	0.0017	3.236	3.59×10^3	2.86×10^6	0.2692	0.0011	2.29	2.54×10^3
6.53×10^6	0.355	0.0014	4.467	4.95×10^3	4.53×10^6	0.2138	0.00086	3.02	3.35×10^3
1.03×10^7	0.309	0.0012	6.310	6.99×10^3	7.19×10^6	0.1698	0.00068	3.89	4.31×10^3
1.64×10^7	0.263	0.0011	8.710	9.65×10^3	1.14×10^7	0.1349	0.00054	5.02	5.55×10^3
2.6×10^7	0.224	0.0009	1.202×10^1	1.33×10^4	1.81×10^7	0.1072	0.00043	6.46	7.16×10^3
4.12×10^7	0.195	0.00078	1.622×10^1	1.80×10^4	2.86×10^7	0.851	0.00034	8.32	9.22×10^3
6.53×10^7	0.166	0.00067	2.239×10^1	2.48×10^4	4.53×10^7	0.0676	0.00027	1.05×10^1	1.16×10^4

TABLE 21

VISCOELASTIC PROPERTIES OF 2 PERCENT S-109 POLYSTYRENE IN TOLUENE
AS A FUNCTION OF ANGULAR FREQUENCY AT 77°F
PREDICTED BY ROUSE & ZIMM THEORIES

Zimm Theory					Rouse Theory				
ω sec^{-1}	$\frac{\eta'-\eta_s}{\eta-\eta_s}$	$\eta'-\eta_s$ poise	G'(M/cRT)	G' $dyne/cm^2$	ω sec^{-1}	$\frac{\eta'-\eta_s}{\eta-\eta_s}$	$\eta'-\eta_s$ poise	G'(M/cRT)	G' $dyne/cm^2$
5.58×10^4	1.00	0.0094	1.148×10^{-2}	2.55×10^4	3.87×10^4	1.00	0.0094	1.07×10^{-2}	2.37×10^1
8.84×10^4	1.00	0.0094	2.818×10^{-2}	6.25×10^2	6.14×10^4	0.9772	0.0092	2.63×10^{-2}	5.83×10^2
1.4×10^5	0.977	0.0092	6.918×10^{-2}	1.53×10^2	9.73×10^4	0.9550	0.0090	6.46×10^{-2}	1.43×10^2
2.22×10^5	0.933	0.0088	1.622×10^{-1}	3.60×10^2	1.54×10^5	0.912	0.0086	1.48×10^{-1}	3.28×10^2
3.52×10^5	0.871	0.0082	3.467×10^{-1}	7.69×10^2	2.44×10^5	0.8318	0.0078	3.16×10^{-1}	7.01×10^2
5.58×10^5	0.776	0.0073	6.456×10^{-1}	1.43×10^3	3.87×10^5	0.6918	0.0064	5.75×10^{-1}	1.28×10^3
8.84×10^5	0.661	0.0062	1.047	2.32×10^3	6.14×10^5	0.5495	0.0052	8.91×10^{-1}	1.97×10^3
1.4×10^6	0.562	0.0053	1.585	3.51×10^3	9.73×10^5	0.4266	0.0040	1.26	2.79×10^3
2.22×10^6	0.490	0.0046	2.291	5.08×10^3	1.54×10^6	0.3388	0.0032	1.70	3.76×10^3
3.52×10^6	0.420	0.0039	3.236	7.17×10^3	2.44×10^6	0.2692	0.0025	2.29	5.08×10^3
5.58×10^6	0.355	0.0033	4.467	9.90×10^3	3.87×10^6	0.2138	0.0020	3.02	6.69×10^3
8.84×10^6	0.309	0.0029	6.310	1.4×10^4	6.14×10^6	0.1698	0.0016	3.89	8.62×10^3
1.4×10^7	0.263	0.0025	8.710	1.93×10^4	9.73×10^6	0.1349	0.0013	5.02	1.11×10^4
2.22×10^7	0.224	0.0021	1.202×10^1	2.67×10^4	1.54×10^7	0.1072	0.0010	6.46	1.43×10^4
3.52×10^7	0.195	0.0018	1.622×10^1	3.6×10^4	2.44×10^7	0.0851	0.0008	8.32	1.84×10^4
5.58×10^7	0.166	0.0016	2.239×10^1	4.96×10^4	3.87×10^7	0.0676	0.00064	1.05×10^1	2.32×10^4

TABLE 22

VISCOELASTIC PROPERTIES OF 3 PERCENT S-109 POLYSTYRENE IN TOLUENE
AS A FUNCTION OF ANGULAR FREQUENCY AT 77°F.
PREDICTED BY ROUSE & ZIMM THEORIES

Zimm Theory					Rouse Theory				
ω sec^{-1}	$\frac{\eta'-\eta_s}{\eta-\eta_s}$	$\eta'-\eta_s$ poise	G'(M/cRT)	G' $dyne/cm^2$	ω sec^{-1}	$\frac{\eta'-\eta_s}{\eta-\eta_s}$	$\eta'-\eta_s$ poise	G'(M/cRT)	G' $dyne/cm^2$
4.7×10^4	1.00	0.0168	1.148×10^{-2}	3.82×10^1	3.26×10^4	1.00	0.0168	1.07×10^{-2}	3.56×10^1
7.45×10^4	1.00	0.0168	$2.8o8 \times 10^{-2}$	9.37×10^1	5.17×10^4	0.9772	0.0164	2.63×10^{-2}	8.75×10^1
1.18×10^5	0.977	0.0164	6.918×10^{-2}	2.3×10^2	8.20×10^4	0.9550	0.0160	6.46×10^{-2}	2.15×10^2
1.87×10^5	0.933	0.0156	1.622×10^{-1}	5.39×10^2	1.30×10^5	0.912	0.0153	1.48×10^{-1}	4.92×10^2
2.96×10^5	0.871	0.0146	3.467×10^{-1}	1.15×10^3	2.06×10^5	0.8318	0.0139	3.16×10^{-1}	1.05×10^3
4.7×10^5	0.776	0.0130	6.456×10^{-1}	2.15×10^3	3.26×10^5	0.6918	0.0116	5.75×10^{-1}	1.91×10^3
7.45×10^5	0.661	0.0111	1.047	3.48×10^3	5.17×10^5	0.5495	0.0092	8.91×10^{-1}	2.96×10^3
1.18×10^6	0.562	0.0094	1.585	5.27×10^3	8.20×10^5	0.4266	0.0072	1.26	4.19×10^3
1.87×10^6	0.490	0.0082	2.291	7.62×10^3	1.30×10^6	0.3388	0.0057	1.70	5.65×10^3
2.96×10^6	0.420	0.0070	3.236	1.08×10^4	2.06×10^6	0.2692	0.0045	2.29	7.62×10^3
4.7×10^6	0.355	0.0059	4.467	1.49×10^4	3.26×10^6	0.2138	0.0036	3.02	1.00×10^4
7.45×10^6	0.309	0.0052	6.310	2.10×10^4	5.17×10^6	0.1698	0.0028	3.89	1.29×10^4
1.18×10^7	0.263	0.0044	8.710	2.9×10^4	8.20×10^6	0.1349	0.0023	5.02	1.67×10^4
1.87×10^7	0.224	0.0038	1.202×10^1	4.0×10^4	1.30×10^7	0.1072	0.0018	6.46	2.15×10^4
2.96×10^7	0.195	0.0033	1.622×10^1	5.39×10^4	2.06×10^7	0.0851	0.001[illegible]	8.32	2.77×10^4
4.7×10^7	0.166	0.0028	2.239×10^1	7.44×10^4	3.26×10^7	0.0676	0.0011	1.05×10^1	3.48×10^4